Faculty of Science and Engineering
School of Civil and Mechanical Engineering

Identification of Fluid Excitation in Pipes

Syed Imad ul Haq Haqqi

This thesis is presented for the Degree of
Master of Philosophy
of
Curtin University

March 2016

Declaration

To the best of my knowledge and belief this thesis contains no material previously published by any other person except where due acknowledgement has been made.

This thesis contains no material which has been accepted for the award of any other degree or diploma in any university.

Signature: _____

Date: _____

Abstract

Flow-induced vibrations and noise are of importance in several engineering applications. Piping systems are used to carry fluids from one area to another in any plant whether it is a chemical plant, a storage terminal, or an oil refinery. High levels of radiating noise from piping systems occur when internal turbulent flow resulting from a pipe fitting for example, elbow, tee, valve, etc., separates from the pipe wall. The disturbed flow generates an intense internal sound field, comprising of plane waves and higher order acoustic modes which propagate throughout the piping system. These acoustic modes excite the pipe wall vibrations, which in turn generate external sound. Vibrations of pipe wall at any point in a system can be associated with the wall pressure fluctuations due to one, some, or all of the excitation as given below [2]:

1. Non-propagating local fluid dynamic and acoustic wall pressure fluctuations associated with the internal flow disturbances.

2. Fully developed turbulent pipe flow wall pressure fluctuations associated with undisturbed straight pipe flow.

3. Propagating internal acoustic field associated with internal flow disturbances.

The research literature during the review phase of this project has confirmed the potential of Computational Fluid Dynamics (CFD) as a dependable tool to predict flows in pipes and associated fittings. The general applicability of CFD in understanding fluid flow in all piping configurations during the design phase is limited due to the fact that it requires intensive computational resources and the time these resources take to resolve an issue. Hence, the Engineers working in the piping design consultancies cannot use these lengthy and costly computational practices for every system unless they want to address a specific problem that has occurred during the normal plant operations.

Also, it was not found anywhere in the literature if the method adopted in this research has been used to understand the excitation of frequency in pipe sections which are downstream of 90^0 bends and tee junctions. These two types of geometries

are integral in any piping system and this is the reason why these geometries have been used in this project.

Keeping in view the fact that the Engineers working in the industry prefer using rules of thumb for timely and effective solutions rather than doing academic research, this study is conducted to provide a general understanding of the fluid flow conditions which exist in pipes when flow passes through discontinuities like 90^0 bends and tee junctions and the frequency excitation that happens as a result of turbulence and the changed fluid flow conditions.

Hence, the first objective of this research was to model the fluid flow using CFD to understand the flow conditions that exist in the pipe sections downstream of a bend and a tee and determine if the fluid flow behaviour is same in both cases or different. The second reason behind this study was to understand the frequency excitation in the pipe wall in the downstream sections after the flow has changed its direction at the mitred bend and bifurcated at a tee and highlight the differences in the nature of excitation if any.

To reach these objectives, two geometries are considered during this project; in the first geometry, two pipes are connected to each other via a 90^0 mitred joint. In the second geometry, one pipe is connected to the second in the centre thus forming a tee junction. Incompressible air flow is modelled at three different speeds using Large Eddy Simulation in OpenFOAM. The wall pressure field obtained from the simulations is imposed on the pipe structural wall to determine the displacements using Transient Analysis. Fast Fourier Transforms are performed on fluid pressure data and the structural displacements data to determine which fluid frequencies present in the fluid flow contribute to the excitation of frequencies in the pipe shell wall and which of these frequencies can be a source of resonance.

This research is novel and important because it identifies the difference in the fluid flow in pipe sections downstream of a 90^0 bend against a tee junction. It has also identified that the frequency excitation in both geometries is different to each other. This research has added value to the existing knowledge of flow conditions that exist in pipes after the fluid flow has come across discontinuities and has enhanced the present understanding of vibrations in piping systems as a result of the turbulence caused by these discontinuities.

Acknowledgments

The best of all praises for Allah the Almighty who provided me the vision, courage, and opportunities to progress this research to its desired objective.

Most importantly, I would like to acknowledge the contribution of my supervisor Dr Andrew King who constantly encouraged and supported me. I would like to attribute my success to his guidance, support, and large amount of patience. I found him to be the best supervisor in my academic life.

I would also like to acknowledge the efforts made by Dr Gareth Forbes and Dr Ian Howard. Their advice helped me in some of the critical aspects of the project.

I would like to make a special mention of Bruce Loneragan of SVT who first proposed to me the project upon my initial contact via an email. I am equally thankful to Andrew Campbell of Worley Parsons as he was the person who seconded this project.

I am much obliged to Ansys support team who advised me during different stages of the project. Epic supercomputer of The Pawsey Centre, formerly iVec, was used extensively throughout this project and without which the massive computations performed in this project could not have been possible.

I would like to dedicate this work to my wife and parents who always prayed and extended moral support for my success.

Contents

List of Tables

List of Figures

List of Abbreviations

CFD	Computational Fluid Dynamics
PISO	Pressure Implicit Splitting of Operators
DFT	Discrete Fourier Transform
FFT	Fast Fourier Transform
LES	Large Eddy Simulation
DNS	Direct Numerical Simulation
RANS	Reynolds Averaged Navier Stokes
SGS	Sub Grid Scale
FEA	Finite Element Analysis

1

INTRODUCTION

In industrial applications, vibrations in piping systems where fluid is flowing at high velocities can cause problems at places where flow discontinuities due to pipe fittings like elbows and tees, orifice plates, and valves exist. These discontinuities result in localized or dispersed disturbances which can cause unsteady loading on the pipe wall and excite it. The pipe surface in turn emits acoustic energy into the surroundings [2]. This unsteady loading may cause fatigue or permanent deformation of the pipe resulting in failure of the system.

Elbows, mitred joints, tees, and other types of pipe fittings are commonly used in industry. Research literature is available on understanding flow in elbows for different conditions; however, this research is novel due to the fact that the frequencies excited in the pipe wall as a result of flow discontinuities present in pipe geometries such as mitred joints and tees are investigated. During literature review, it was not found anywhere that LES (Large Eddy Simulation) was used to capture fluid frequencies downstream of flow discontinuities which were a source of vibrations. This work has provided a data of the frequencies excited by air flowing at different velocities in pipes downstream of a mitred bend and a tee. It has also identified the

differences in frequency excitation between the two geometric configurations. Two pipe geometries were considered to carry out the investigation, one in which two pipes were connected at 90^0 to each other, thus making a mitred bend. Flow coming in from the inlet pipe section experienced a change in direction at the sharp bend. In the second geometry, one pipe was connected to the middle of a longer pipe to form a tee junction. Flow coming from the centre inlet pipe was split in both directions. It is important to understand the frequencies that exist in pipe geometries once the flow has encountered a discontinuity due to a change in the direction or flow bifurcation for different flow conditions. Piping design engineers can use this understanding to optimise the design and mitigate the impact effectively.

In a straight pipe run without any discontinuities, pressure fluctuations present are one of the chief characteristics of turbulent flows. These fluctuations cause structural vibrations which in turn release acoustic energy. “This random wall pressure field is statistically uniform both circumferentially and axially and extends over complete pipe lengths and cannot be removed from the flow; it represents a minimum excitation level always present within the pipe”[1]. However, with pipe fittings which are an integral part of the system, pipe-wall excitation levels can become challenging to tackle. In order to avoid issues related to cracks or complete rupture, it is important to develop a basic understanding of the mechanisms that cause vibrations and their propagation in pipes.

The analysis of this phenomenon requires an understanding of fluid dynamics, structural vibrations and their interaction [2]. It is done in two steps:

1. Determine the wall pressure fluctuations at equal time intervals throughout the surface.

2. Use fluid pressure data as an input to the structural model in a finite element solver to determine the transient response of a pipe due to imposed dynamic loading.

Piping systems vibrate differently at different frequencies. This vibrational response may be lateral along the whole length which is the case at low frequencies; at higher frequencies, it may be radial across its cross section which is normally referred to as the “breathing” mode as if all points are vibrating in phase. As frequencies increase,

neighbouring pipe wall segments may start to vibrate out of phase with each other in radial directions causing a sine wave to develop around the circumference. These are circumferential mode of vibrations [4].

A plane wave is generated when pipe diameter is small compared to the wavelength. Cross-wall modes or higher order modes are acoustic natural frequencies generated due to wave propagation at an angle inside a pipe. This type of wave behaviour is due to the fact that the wavelengths of waves may be smaller as compared to pipe diameter resulting in its propagation at an angle and creation of interference patterns instead of staying in one plane like a plane wave [4].

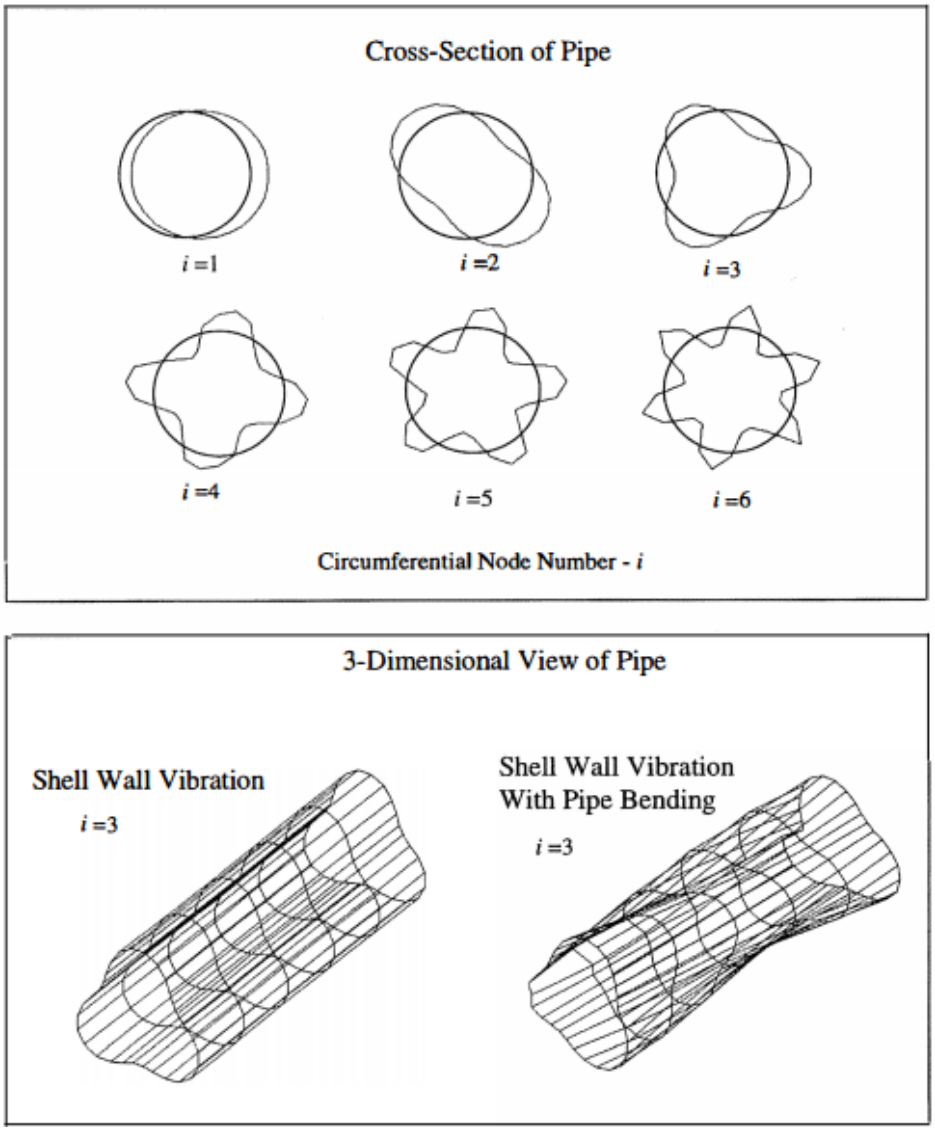

Figure 1.1: Piping Shell Wall Mode Shapes (Price & Smith [4])

1.1 Objective and Significance

The objective of this study was to understand the vibrational frequencies excited by the fluid flowing inside the pipe geometries. These frequencies may cause damage to the piping system either immediately or in the long operational run. These frequencies were recorded at fixed distances called probe locations. The frequencies that were excited in fluid flow and structural wall and demonstrated peaks together were captured as shown in Figure 1.2.

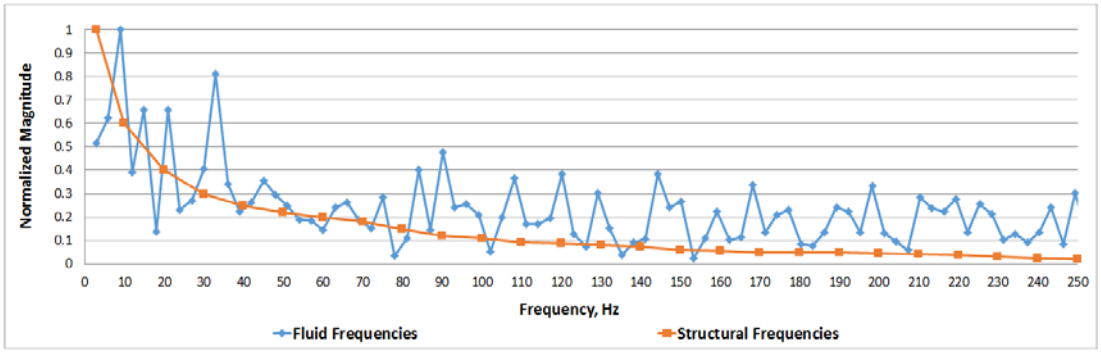

Figure 1.2a: No excitation - Corresponding peaks in fluid and structural frequencies not visible

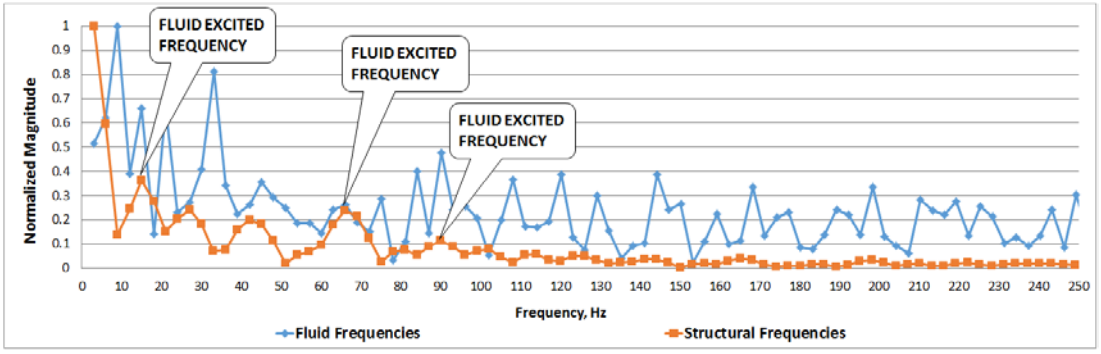

Figure 1.2b: Excitation - Corresponding peaks in fluid and structural frequencies visible

Figure 1.2: Demonstration of Fluid Excited Vibrations in Pipe

1.2 Approach

Flows in tees are three dimensional requiring numerical and experimental techniques to determine their behaviour. Modern CFD techniques have reached a maturity level where actual conditions can be simulated with confidence. According to M. A. Leschziner [5], “three-dimensional and recirculating flows of direct industrial relevance and realistic geometry are now well within the scope of CFD capabilities”. This argument is further supported by the research works reviewed in Chapter 2. This project was completely computational; geometry and mesh preparation were

completed using Ansys Workbench tools, DesignModeler and Meshing. The mesh was then converted into OpenFOAM format and flow was modelled using Large Eddy Simulation technique. Once the flow had reached a pseudo steady state, it was allowed to run for more time after to gather enough pressure data required to perform a Fast Fourier Transform (FFT) that could capture all critical frequencies present in the flow at all probe locations. The wall surface pressure data at successive time steps was extracted and imposed on the structural model. After performing the transient analysis of the structural model, data of the pipe wall displacements at all probe locations were obtained at successive time steps. Probe locations on the structural model were coincident with the fluid model so that the frequencies obtained at probe locations in both models can be plotted together and the fluid frequencies which excited structural frequencies could be identified. Fast Fourier Transforms were performed on the fluid pressure data and structural displacements to obtain frequency spectrums. Graphs for the frequencies present in fluid and structure were prepared to determine which frequencies excited in both, fluid and structure simultaneously. Modal analyses were performed to determine the natural frequencies of the system. These natural frequencies were plotted on the same graphs to determine which fluid excited frequencies could be a source of resonance.

1.3 Thesis Outline

This thesis is organised into six chapters, which are further divided into sub-sections.

i) ***Chapter 1*** outlines the background of the problem and objective of the project. It explains the method adopted to carry out this research.

ii) ***Chapter 2*** provides the literature review on turbulence, computational fluid dynamics, vibration analysis, and fluid structure interaction.

iii) ***Chapter 3*** presents the theory of turbulence, computational fluid dynamics, structural analysis, Discrete Fourier Transform, Nyquist Frequency, OpenFOAM and Ansys Workbench environments.

iv) ***Chapter 4*** provides information on the geometry building, initial and boundary conditions, and numerical technique to perform the fluid simulations. It defines the arrangement of pipe supports on structural geometry and discusses modal and transient structural analyses.

v) ***Chapter 5*** document velocity profiles in both geometries, figures depicting velocity distribution in pipes obtained from CFD simulations, natural frequencies obtained from Modal analyses, and data and graphs of frequencies obtained from fluid and structural simulations. It also gives a comprehensive discussion of the obtained results.

vi) ***Chapter 6*** documents the summary of findings and conclusion.

2

LITERATURE REVIEW

2.1 Fluid Structure Interaction and Vibrations

Fluid structure interaction is a major subject of study. According to Païdoussis [45], flow induced vibrations are caused by "non-resonant buffeting, response to flow periodicity, fluid-elastic instability, and acoustic resonance". He discussed various issues arising as a result of flow induced vibrations and their solutions. Moussou et al. [42] reviewed problems arising as a result of fluid structure interaction in piping systems. These problems included excessive vibrations due to operation of pumps in partial flow regimes, water hammer, cavitation, and vortex shedding. They discussed the drawbacks of not integrating the vibrational and noise aspects when designing piping systems and reflected on the fact that a field engineer has limited knowledge, experience and time to solve these issues. They stressed on the need for a framework to be incorporated in codes and standards to consider these points during the early design phase.

Rattaya et al [43] provided a mathematical analysis to predict vibrations in pipes containing turbulent flow using a correlation function. They studied the amplification

of pipe wall response resulting from the coincidence effects in a pipe in which the air was flowing at a high speed.

Bull et al. [47] studied the higher order acoustic modes produced as a result of flow disturbances in a pipe to determine the pipe wall vibrations and the acoustic radiation into the fluid surrounding the pipe. They found that the effects of these internal disturbances were maximum and restricted to the cut-off frequencies of the higher order acoustic modes and stated the reasons behind this phenomenon. Bull et al. [48] concluded that the nature of vibrations of pipe wall depended on whether the frequency was above or below the cut-off frequency of the lowest high order acoustic mode which is (1,0). If the frequency was above the cut-off frequency, higher order acoustic modes propagated. If the frequency was below, only plane acoustic waves propagated. Pittard et al. [64] observed that the pressure fluctuations on the pipe wall behaved under a near quadratic relationship with the flow rate. They concluded that there was a relationship between the flow rate and pipe vibrations. White et al. [23] discussed the transmission and interaction of energy and described how the acoustic and vibration energy propagated in the piping systems carrying fluid.

Analytical studies have been carried out in cylindrical vibrations by different researchers. El-Raheb [49] developed an analytical method to calculate vibrational response of a finite length pipe system with elbows and straight pipe runs. Nieves et al. [44] conducted an analytical study on axisymmetric standing waves in isotropic, linear and elastic cylinders and concluded that the cylinders vibrate in pure longitudinal and radial axisymmetric modes provided Poisson's ratio was equal to zero. Stepanishen [46] developed a general solution to determine vibrational response of a fluid loaded finite cylindrical shell excited by harmonic force. Fuller [50] studied the transmission of flexural waves in cylindrical shells with discontinuities. He discussed transmission losses associated with these waves and their dependency on poor wave coupling due to the ratio between extensional phase speeds of the materials. Rumerman et al. [51] developed a method of calculating natural frequencies of finite circular cylinders in axially symmetric longitudinal vibrations. They evaluated natural frequencies for solid cylinders with free ends having free and with fixed lateral surfaces.

Fuller and Brevart [54] derived the ratio of energy distribution between the fluid and shell vibrations in an infinite elastic cylinder and developed dispersion curves for convection, both upstream and downstream. They discovered that the convection effects are highest near cut-on frequencies of higher order branches and near coincidence points between shell and fluid type waves where system is resonating. Fuller and Fahy [55] studied dispersion and energy distributions in fluid-filled cylindrical shells and described behaviour of individual branches for different parameters. They discovered free wave behaviour to be dependent on the thickness of the shell wall and on the ratio of density of the shell wall to that of the fluid. Fung et al. [56] discussed cylindrical vibrations and found that Reissner's treatment was sufficient to obtain the lowest modes and frequencies of thin cylinders.

Williams [59] derived the structural intensity vector using Flügge's equations and expressions for total energy density. He concluded that the longitudinal power flow carried acoustic radiation in the fluid and far field. Heckl [60] derived the formulas for modal density, resonance frequencies, and point impedance of cylinders, and experimentally verified them. Junger and Rosato [61] studied elastic waves propagating in shell walls of the cylinders. They discovered that at high frequencies, two modes exist; one corresponding to flexural waves and the other to longitudinal waves.

Arnold et al. [53] conducted a theoretical and experimental examination of thin cylinder vibrations and discovered that some modes of vibrations have higher frequencies than those associated with complex vibrations i.e. complexity of mode of vibration has no relation to natural frequency.

Mason [58] conducted an experimental study of the sound propagating in cylindrical section of a wind tunnel. He discussed three methods of detecting the frequencies and observed that the interference of two or more acoustic modes caused variations in sound pressure levels at different positions.

Other researchers have studied methods to evaluate and reduce vibrations.

Koo et al. [52] studied the effect of arranging pipe supports at equal distances. They confirmed that the periodic arrangement of supports can help in reducing vibrations in piping systems. Huang et al. [57] proposed a matrix method to evaluate vibrations

of fluid carrying curved pipes supported by spring supports. This method is less time consuming as compared to finite element techniques.

Qing et al. [65] studied the orifice-induced wall pressure fluctuations and resulting pipe vibrations. They developed equations of the power spectral density of the wall pressure fluctuations and mathematical models of the cross-spectral density using experimental data. The response of pipe vibrations was obtained using acceptance integral method. Lee et al. [69] studied a piping arrangement connected to a rotary compressor. They derived a procedure to derive the fluid force from pulsating fluid.

Other than the academics, piping vibrations have been discussed by many industrial experts. Wachel et al. [37] developed plots for frequency factors, deflection stress factors, and velocity stress factors for variable aspect ratios of steel piping with different configurations. They provided a table of correction factors based on real-life pipe installations which can be used to correct theoretical calculations of beam natural frequencies. They discussed mechanisms behind vibrations in pipes, described forces of excitation relevant to each of the mechanisms, the response of pipe system and typical issues that can develop as a result of these forces. Price et al. [4] have discussed high-order acoustical modes, energy generated by these modes, and calculation of natural frequencies. They also gave an overview of preventing high-order acoustic modes using industrial devices and discussed case histories where these devices solved real world problems. Wachel [67] developed a nomogram to compare measured natural frequency against the calculated one to evaluate vibration induced stresses. He discussed trouble shooting procedures for excessive vibrations in a running plant [68]. Saha [70] discussed a method to provide the foundation for a proper piping system design.

2.2 Turbulence and Large Eddy Simulation (LES)

Experimental and numerical investigation on turbulence is a subject of constant research. Avila et al. [24] investigated the turbulence in pipe flow and the mechanisms that sustained turbulence. Bull [62] studied wall pressure fluctuations in a turbulent boundary layer flow in a subsonic rectangular duct and confirmed that the pressure sources contributed towards the development of wall pressure field in the boundary layer with a wide range of convected velocities. Mulhearn [63] calculated pressure and pressure-velocity space correlations for turbulence in a turbulent shear

flow using rapid distortion theory. He concluded that the pressure fluctuations remain correlated over significantly greater distances across the flow than velocity fluctuations. He found reasonable agreement for this postulate after drawing a comparison between the data obtained from experiments and the data evaluated from theory. Lauchle et al. [66] developed a procedure to process the signals of the boundary layer wall pressure inside a pipe. Willmarth [22] discussed pressure fluctuations beneath turbulent boundary layers. He reviewed important papers elucidating the development of the phenomenon.

Ugo Piomelli [39, 40] discussed Large Eddy Simulation and its advantages over Reynolds Averaged Navier Stokes (RANS) calculations in predicting the behaviour of coherent structures and their response to disturbances. He reviewed the works of researchers who studied LES for different types of flows. He suggested that LES should be applied where lower level turbulence models do not provide acceptable results for example, “unsteady or three-dimensional boundary layers, separated flows and flows involving geometries with sharp corners”. He concluded that using LES can increase the understanding of the physics behind turbulence in the above-mentioned flows. Nieuwstadt et al. [10] gave a detailed account of the computational requirements for the rigorous calculations that are involved in running the simulations. He used four LES models to run simulations of the convective atmospheric boundary layer and found that all four models lead to similar results despite the fact that they all had different numerical schemes and boundary conditions and that the numerical results were in agreement with the practical measurements.

Fureby et al. [38] investigated four sub-grid scale (SGS) models to investigate their prediction capabilities in channel flows at different Reynolds number. All models gave reasonable results however the differential stress model was found to give better results than the eddy viscosity models. Fureby concluded that acceptable simulations can be performed without modelling wall by refining the mesh perpendicular to the wall such that anisotropy in the near-wall turbulence can be captured. Boris et al. [41] discussed LES and its issues and the requirements for a sub-grid model to be ideal.

An area in which Large eddy simulation has shown success is thermal mixing tees in nuclear power plants. Researchers like Lin-Wen Hu et al. [11], Tingzhen Ming et al. [12], Naik-Nimbalkar et al. [13] carried out studies on mixing tees using LES.

Nimbalkar [13] conducted his experiments to investigate thermal mixing phenomenon in T-junction and validated his results using CFD simulations. The predicted mean velocities and temperatures were in good agreement with the measurements. Similarly, Lin-Wen Hu demonstrated that LES can accurately study the temperature fluctuations in a tee junction in the turbulent mixing flows with a high Reynolds number. Zhu et al. [14] also simulated the thermal fluctuations in a mixing tee junction using LES and Smagorinsky-Lilly sub-grid scale (SGS) model and found results to be acceptable.

2.3 Summary

This chapter discussed fluid structure interaction in pipes, vibrations analysis, and turbulence modelling using LES. During the design process in industry, quasi-static stress analysis is performed and vibrations and noise impacts are not looked into unless the line is connected to machinery like pumps, compressors, or turbines. Some authors raised these concerns and advised the methods to reduce the levels of vibrations. Analytical and experimental studies both have been conducted in this regard. Turbulence and its modelling using Computational Fluid Dynamics were discussed. Many authors have proved that Large Eddy Simulation provided excellent results for their studies on turbulence. Hence, LES was used in this project to model the turbulent flow and to obtain pressure fluctuations at the probe monitor points.

3

THEORETICAL REVIEW

This chapter discusses the fundamental fluid flow equations, theoretical aspects of computational fluid dynamics (CFD), turbulence modelling using CFD, simulation methods and mathematical model used in this project. It details information on the software and solver used to run CFD simulations called OpenFOAM and pisofoam respectively.

It also discusses the theory of modal and transient structural analysis and the software used to perform these analyses, Ansys. Theory on fluid structure interaction, Nyquist frequency and Fast Fourier Transform (FFT) is also presented.

3.1 Governing Equations of Fluid Flow

Continuity equation and the Navier-Stokes equations together provide complete explanation of the motion of a Newtonian fluid at any moment in time. The governing equations for an incompressible fluid flow are as follows:

Continuity Equation:

$$\nabla . \bar{\mathbf{u}} = 0 \tag{3.1}$$

Momentum equations in x, y, and z directions:

$$\rho\left(\frac{\partial\bar{\mathbf{u}}}{\partial \mathrm{t}}+\bar{\mathbf{u}}.\nabla\bar{\mathbf{u}}\right)=-\nabla p+\mu\nabla^{2}\mathbf{u}+\nabla.\sigma_{\mathrm{T}} \qquad (3.2)$$

Where $\bar{\mathbf{u}}$ is the velocity, ρ is the fluid density, μ is the dynamic viscosity, p is the static pressure, and σ_T is the stress tensor.

3.2 Computational Fluid Dynamics

The branch of fluid mechanics which use computer simulations to understand fluid flow and heat transfer by solving governing partial differential equations of fluid dynamics over a geometric domain is called Computational fluid dynamics (CFD). CFD may be employed to understand flow distribution in different piping systems and other associated fittings which may in turn lead to developing an understanding of how fluid flow can cause vibrations [9].

Following are the reasons why CFD is used for solving complex fluid dynamic problems:

1. CFD is economical in terms of money and time as compared to conducting physical experiments.

2. The numerical models of the physical problems have good accuracy and reliability, provided these models have undergone suitable validation.

3.2.1 CFD Methodology

CFD can be used to develop a new design or improve existing design. Results generated by CFD must always be validated against experimental data.

The process of performing a CFD analysis is divided into the following three steps.

1. Pre-processing, which consist of geometry creation and meshing i.e., grid generation, defining initial and boundary conditions, fluid properties, mathematical models, algorithms and numerical schemes for the solver.
2. Solution, which consist of solving governing equations using different iteration procedures under the conditions specified during pre-processing on the generated grid. One of the following three methods can be used for this purpose:

a) Finite difference

b) Finite element

c) Finite volume

Of all the methods mentioned above, Finite Volume is used the most. This method allows the user to model fluid flow by dividing the total volume into small control volumes. The flow inside the domain is then simulated by integration of the governing equations for each control volume, discretization of integral equations into algebraic equations, and solution of the algebraic equations using iterative methods.

3. Post-processing i.e., visualizing the results in a post processor. Post processors are used to visualize specific regions of interest within the domain, scalar variables like pressure and temperature, and produce vector plots showing magnitudes and the directions of flow [30].

3.3 Turbulence and Associated Vibrations

In 1937, von Karman gave the following definition of turbulence: “Turbulence is an irregular motion which in general makes its appearance in fluids, gaseous or liquid, when they flow past solid surfaces or even when neighbouring streams of the same fluid flow past or over one another” [20]. Transition of flows from laminar to turbulence is due to the instability occurring at high Reynolds number. Turbulence is characterized by the presence of an eddy motion. Due to vortex stretching, large eddies are produced which have both velocity and kinetic energy. These large eddies can be of different length scales and constantly break to produce smaller eddies and transfer their kinetic energy to the smaller eddies. This phenomenon is called turbulent energy cascade [21]. Turbulence is also caused by a change in direction of the flow at elbows and tees. These discontinuities create an acoustic field as well as a strong pressure field which is locally concentrated and hydrodynamic in nature. The turbulent boundary layer creates another hydrodynamics pressure field on the interior of the pipe wall. This pressure field is propagating and not locally concentrated. Hence turbulence can be considered to be many random waves travelling with different velocities [23].

3.4 Kolmogorov Microscales

Kolmogorov micro-scales are the smallest scales any turbulent flow can have. For these scales, inertia and viscous effects in a turbulent flow are equal. These micro-scales are mathematically expressed as:

Length scale: $\eta = \left(\frac{\nu^3}{\varepsilon} \right)^{1/4}$ (3.4a)

Time scale: $\tau_\eta = \left(\frac{\nu}{\varepsilon} \right)^{1/2}$ (3.4b)

Velocity scale: $u_\eta = (\nu\varepsilon)^{1/4}$ (3.4c)

ε is the average rate of dissipation of turbulence kinetic energy per unit mass,

and v is the kinematic viscosity of the fluid [28].

3.5 Turbulence Modelling

Turbulence is modelled using Direct Numerical Simulation and turbulence models. There are five main categories of turbulence models out of which one is Large Eddy Simulation and four are covered under Reynolds Averaged Navier Stokes (RANS) models.

1. Large Eddy Simulation

Reynolds Averaged Navier Stokes Models

2. Algebraic (First order closures)
3. One-Equation (First order closures)
4. Multiple-Equation (First order closures)
5. Reynolds-stress models (Second order closures)

3.5.1 Direct Numerical Simulation (DNS)

The complete behaviour of a turbulent flow can be determined by solving Navier-Stokes equations without using any turbulence models. This type of solution is called Direct Numerical Simulation (DNS). It computes Navier-Stokes equations on spatial grids that are fine enough to resolve Kolmogorov length scales with small time steps. DNS can only be used for simple flows. It requires extensive computational resources as the range of length and time scales increase with an increase in Reynolds number. Requirement for these resources depend on the complexity of geometry and Reynolds number.

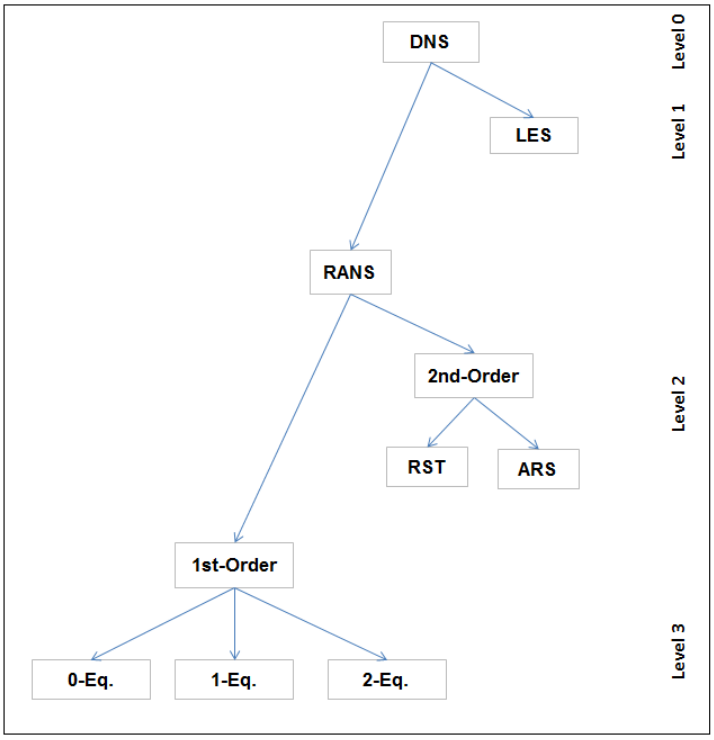

Figure 3.1: Hierarchy of Turbulence Modeling (Adapted from J. Blazek [27])

DNS:	Direct Numerical Simulation
LES:	Large-Eddy Simulation
RANS:	Reynolds-Averaged Navier-Stokes Equations
1st-order:	First order closures
2nd-order:	Second order closures
RST:	Reynolds-Stress Transport models
ARS:	Algebraic Reynolds-Stress models
0-, 1-, 2-Eq:	Zero- (algebraic), one-, two-equation models

3.5.2 Reynolds Averaged Navier-Stokes Modelling (RANS)

Reynolds Averaged Navier-Stokes (RANS) is a time averaging technique to study turbulent flows. In this method the exact solution u splits into the sum of its statistical average $\mathbf{U}$ and a fluctuation $\mathbf{u'}$.

$$u = \mathbf{U} + u' \tag{3.5.2a}$$

The splitting is shown below:

$$u = U + u' \qquad v = V + v' \qquad w = W + w' \tag{3.5.2b}$$

Taking time average and applying the rules of fluctuating properties, we get continuity equation and three momentum equations which are given below:

$$div\,\mathbf{U} = 0 \tag{3.3}$$

$$\frac{\partial U}{\partial t} + div(U\mathbf{U}) = -\frac{1}{\rho}\frac{\partial P}{\partial x} + \nu\, div\, grad\, U + \left[-\frac{\partial \overline{u'^2}}{\partial x} - \frac{\partial \overline{u'v'}}{\partial y} - \frac{\partial \overline{u'w'}}{\partial z} \right] \tag{3.4}$$

$$\frac{\partial V}{\partial t} + div(V\mathbf{U}) = -\frac{1}{\rho}\frac{\partial P}{\partial y} + \nu\, div\, grad\, V + \left[-\frac{\partial \overline{u'v'}}{\partial x} - \frac{\partial \overline{v'^2}}{\partial y} - \frac{\partial \overline{v'w'}}{\partial z} \right] \tag{3.5}$$

$$\frac{\partial U}{\partial t} + div(W\mathbf{U}) = -\frac{1}{\rho}\frac{\partial P}{\partial z} + \nu\, div\, grad\, W + \left[-\frac{\partial \overline{u'w'}}{\partial x} - \frac{\partial \overline{v'w'}}{\partial y} - \frac{\partial \overline{w'^2}}{\partial z} \right] \tag{3.6}$$

Set of these four equations are called Reynolds-averaged Navier-Stokes equations. The three momentum equations result in six additional stresses, three shear and three normal, which are called Reynolds stresses.

$$\tau_{xx} = -\rho u'^2 \qquad \tau_{yy} = -\rho v'^2 \qquad \tau_{zz} = -\rho w'^2 \tag{3.5.2d}$$

$$\tau_{xy} = \tau_{yx} = -\rho\overline{u'v'} \qquad \tau_{xz} = \tau_{zx} = -\rho\overline{u'w'} \qquad \tau_{7} = \tau_{zy} = -\rho\overline{v'w'} \tag{3.5.2e}$$

3.5.3 Large Eddy Simulation (LES)

Large Eddy Simulation compute instantaneous velocity and pressure fluctuations using fewer resources as compared to DNS. This technique lies intermediate between the DNS and RANS. LES is used to separate large eddies from scales present inside the turbulent flows using a filtering operation. Mathematically it is given as:

$$\overline{\phi}(\mathrm{x}, t) = \int_{-\infty}^{\infty}\int_{-\infty}^{\infty}\int_{-\infty}^{\infty} G(\mathrm{x}, \mathrm{x}', \Delta)\phi(\mathrm{x}', t)\mathrm{d}x'_1\, \mathrm{d}x'_2\, \mathrm{d}x'_3 \tag{3.7}$$

where $\overline{\phi}(\mathrm{x}, t)$ is the filtered function, $\phi(\mathrm{x}', t)$ is the unfiltered function, Δ is the filter cutoff width and is taken as $\Delta = \sqrt[3]{\Delta x \Delta y \Delta z}$ [15].

In LES, the equations are filtered spatially to the size of the grid for larger eddies. These large eddies are large structures carrying energy for which momentum and energy transfer are computed exactly. Two scales are used in LES, Grid and Subgrid. Grid Scale (GS) is the length scale of the size of the grid and resolves large eddies which are flow-dependent or anisotropic. Proper grid sizing is important in

computing total turbulent kinetic energy which is mostly contained in the large eddies. Sub-grid scales (SGS) are length scales of eddies smaller than the grid. These small scales are more universal or isotropic and less affected by the boundary conditions than the large ones. These small scales react more rapidly to flow disturbances and recover equilibrium quickly. Smaller eddies containing residual amounts of kinetic energy are resolved using SGS models [39, 40]. An important formula by Batchelor in turbulence modelling is given below:

$$\varepsilon = \frac{u^3}{l} \tag{3.8}$$

Where u is velocity and l is the length scale of eddies containing energy in a fully turbulent flow. It means that energy containing scales determine the rate of energy dissipation. It infers that if the largest energy containing scales of motion are computed with numerical techniques, a refined model of dissipative scales becomes unnecessary if the model for these scales can adjust to the dissipation rate ε set by large scales [19].

3.6 One Eddy Equation Model

One Equation Eddy Model by Akira Yoshizawa [26] was used in this project. The transport equation for SGS turbulent kinetic energy is:

$$\frac{\partial}{\partial t}(k) + \frac{\partial}{\partial x_i}(U_i k) - \frac{\partial}{\partial x_i}\left(\nu_{eff}\,\frac{\partial}{\partial x_i}(k)\right) = -BL - \frac{c_e k^{\frac{3}{2}}}{\Delta} \tag{3.9}$$

Terms on left side of the equation represent the following:

$\frac{\partial}{\partial t}(k)$ is the change of turbulent sub-grid kinetic energy with respect to time,

$\frac{\partial}{\partial x_i}(U_i k)$ represents convection, and $\frac{\partial}{\partial x_i}\left(\nu_{eff}\,\frac{\partial}{\partial x_i}(k)\right)$ models diffusion.

Terms on the right are defined as follows:

–BL is the turbulence decay from resolved scales to the sub-grid scales via energy cascade. $\frac{C_e k^{\frac{3}{2}}}{\Delta}$ is the turbulent dissipation at the smallest scales; its behaviour is that of a sink for turbulent energy.

3.7 Pressure Implicit with Splitting of Operators (PISO) Algorithm

PisoFOAM is a transient solver in OpenFOAM for incompressible flow which uses PISO algorithm developed by Issa. PISO is a non-iterative procedure for handling pressure-velocity coupling of implicitly discretised fluid flow equations [36].

Following are the steps of procedure in PISO [21]:

1. Guess initially p^* at initial time step t_1
2. Solution of discretized momentum equations results in u^*, v^*, w^* at t_1
3. Solution of pressure equations resulting in p' at t_1
4. Correction of pressure and velocities, p^{**}, u^{**}, v^{**}, w^{**} at t_1
5. Solution of second pressure correction equation at t_1
6. Correction of pressure and velocities, p^{***}, u^{***}, v^{***}, w^{***} at t_1
7. Setting up $p = p^{***}$, $u = u^{***}$, $v = v^{***}$, $w = w^{***}$ at t_1
8. Solution of all discretized transport equations at t_1
9. This whole procedure is repeated using the corrected values to be initial guess at second time step t_2 i.e.,

$$p^* = p; \qquad u^* = u, \qquad v^* = v, \qquad w^* = w, \qquad \phi^* = \phi$$

The difference in time step is written as $\Delta t = t_2 - t_1$. The solution continues to run till it has reached the final time step and the user is satisfied that the flow developed inside the geometry is well past the initial errors and that the flow conditions will not change with more time steps. In this project, once flow had reached pseudo steady state, it was allowed to run for more time to gather enough samples to obtain a dense frequency data.

3.8 OpenFOAM

OpenFOAM is a free source code and solves governing fluid flow equations using the finite volume method. OpenFOAM is a C++ library and hence creates applications that are categorized as solvers and utilities. Solvers compute a problem in computational continuum mechanics and utilities execute pre and post-processing tasks. During a solution run, each solution directory written at a particular time step has the name of that time step appended to it [34].

3.9 Transient Structural Analysis

For a structural dynamics system, the equation of motion is given by:

$$[M]\{\ddot{u}(t)\}+[C]\{\dot{u}(t)\}+[K]\{u(t)\}=\{F^a(t)\} \quad (3.10)$$

Where $[M]$ is the structural mass matrix, $[C]$ is the structural damping matrix, $[K]$ is the structural stiffness matrix, $\ddot{u}(t)$ is the nodal acceleration vector, $\dot{u}(t)$ is the nodal velocity vector, $u(t)$ is the nodal displacement vector, and F^a is the applied load vector [25].

3.10 Modal Analysis

Modal analysis was used to determine the natural frequencies and mode shapes of the pipe geometries without any fluid loading. The equations of motion are:

General Equations of Motion:

$$[M]\{\ddot{u}\}+[C]\{\dot{u}\}+[K]\{u\}=F(t) \quad (3.11)$$

For free vibrations without damping, above equation becomes

$$[M]\{\ddot{u}\}+[K]\{u\}=0 \quad (3.12)$$

Free vibrations are harmonic of the form $\{u\}=\{\phi\}_i \mathrm{Sin}(\omega_i t)$, therefore equation 3.11 can be written as

$$\left([K]-\omega_i{}^2[M]\right)\{\phi_i\}=0 \quad (3.13)$$

The roots of this equation are ω_i^2. These roots are called eigenvalues, where *i* range from 1 to the number of degree of freedoms. The corresponding eigenvectors $\{\phi_i\}$ represent the mode shapes; the shapes assumed by the structure when vibrating at frequency f_i. The square roots of the eigenvalues are ω_i, which are natural circular frequencies (radians/sec) of the structure. Natural frequencies are calculated by $f_i=\omega/2\pi$ (cycles/sec). The term Mode Extraction describes the calculation of eigenvalues ω_i^2 and eigenvectors $\{\phi_i\}$. Block Lanczos method is used for mode

extraction which is capable of extracting large number of modes in most models in a large frequency range [35].

3.11 Discrete Fourier Transform (DFT)

For frequency analysis, Discrete Fourier Transform (DFT) is used to obtain an estimate of frequency components of a signal. Consider a finite length sequence $x[n]$ of length N samples such that $x[n]=0$ outside the range $0 \le n \le N-1$. A periodic sequence can be associated with each finite length sequence of length N. Mathematically, it is $\tilde{x}[n]=\sum_{r=-\infty}^{\infty} x[n-rN]$. To recover the finite length $x[n]$ from $\tilde{x}[n]$, following equation is used:

$$x[n]=\begin{cases}\tilde{x}[n], & 0 \le n \le N-1, \\ 0, & \text{otherwise.}\end{cases} \tag{3.14}$$

The Discrete Fourier Series (DFS) coefficients of $\tilde{x}[n]$ are samples of the Fourier transform of $x[n]$ that are spaced in frequency by $2\pi/N$. There is no overlap between the terms $x[n-rN]$ for different values of r as $x[n]$ is assumed to have a finite length N. The DFS coefficients $\tilde{X}[k]$ of the periodic sequence $\tilde{x}[n]$ is itself a periodic sequence with period N. The Fourier coefficients associated with a finite-duration sequence $X[k]$, also called the Discrete Fourier Transform (DFT), are chosen such that these correspond to a finite-duration sequence to one period of $\tilde{X}[k]$. The DFT $X[k]$ is associated with the DFS coefficients $\tilde{X}[k]$ by

$$X[k]=\begin{cases}\tilde{X}[k], & 0 \le k \le N-1, \\ 0, & \text{otherwise.}\end{cases} \tag{3.15}$$

To compute an N-point DFT, N samples of the Fourier transform are computed at N equally spaced frequencies $\omega_k = 2\pi k/N$, i.e., at N points on the unit circle in the z-plane. The algorithms for the digital computation of the N-point DFT are called Fast Fourier Transform (FFT) algorithms. To achieve the highest efficiency, the FFT algorithms must compute all N values of the DFT [31].

3.12 Nyquist Frequency

Nyquist Sampling Theorem states that if $x_c(t)$ is a bandlimited signal with

$$X_c(j\Omega) = 0 \qquad \text{for} \left| \Omega \right| \geq \Omega_N \tag{3.12a}$$

$x_c(t)$ is determined by its samples $x[n] = x_c(nT), n = 0, \pm 1, \pm 2, ...,$ if

$$\Omega_s = \frac{2\pi}{T} \geq 2\Omega_N \tag{3.12b}$$

The frequency Ω_N is called Nyquist frequency and the frequency $2\Omega_N$ that must be exceeded by the sampling frequency is called the Nyquist rate [33].

3.13 Ansys Workbench

Natural frequencies of pipe geometries were obtained using Ansys Modal and transient analyses were performed using Ansys Transient Structural Module in Workbench. Transient analyses were performed to calculate the time history response of the pipe structural geometries subjected to random loads fluctuating with time. Ansys performs transient analyses by time integration utilizing several algorithms which are normally classified as implicit and explicit. Implicit methods are unconditionally stable i.e., the time step size can be selected without any restrictions. Explicit methods are only stable if the time step size is smaller than a critical time period which typically depends on the largest natural frequency of the structure. Ansys uses different solution methods which are as follows:

• Full Method

• Reduced Method

• Modal Superposition Method

For this project, Full Method was used. The Full Method uses original matrices to solve and does not diminish the problem's dimension. This method considers different nonlinearities, automatic time stepping, and many types of loads can be specified; masses are not presumed to be concentrated at the nodes and results are computed quickly [29].

Mapping of External Data to Ansys

Ansys provides the facility of importing loads from other software using External Data utility in its Component Systems. In this utility, loads are imported in a comma

separated variable (csv) format. One file with coordinates can be used as “Master”, which removes the need to have coordinates in all files.

3.14 Fluid Structure Interaction (FSI)

Fluid structure interaction problems can be solved using monolithic or partitioned methods. Monolithic methods treat interactions at the interface synchronously and solve discretised equations. In a partitioned method, equations for both, fluid and structure are integrated in time alternatingly. The interface conditions are enforced asynchronously [16]. Partitioned methods are further sub-divided in one-way FSI and two-way FSI [17]. If the deformation of the solid model is so small that it does not significantly affect the fluid, one-way FSI can be used. Fluid model is solved separately and fluid loads are applied on the structure. If there is significant deformation in the solid model due to fluid forces and these displacements in turn affect the properties of fluid, two-way FSI is used.

One-way fluid structure interaction can be carried out either as Direct or Indirect computing:

1. Direct computing of One-Way FSI:

In this method, the fluid model is solved separately and forces obtained on the model boundary are transferred to the structural part. Analysis is then performed on the structural part and its response is evaluated.

2. Indirect computing of One-Way FSI:

In this technique, the fluid and solid models are prepared separately. Possibilities exist that the meshes for both models may become incompatible with each other at the interface. Also, control parameters are specified in both models individually, therefore the solution steps for fluid and structural models may not match. Linear interpolation is executed if the fluid forces are not available for a certain time step. If the solution time steps of the solid model exceed those of the fluid model, linear extrapolation is performed to compute the fluid results which will not be available. With the exception of these differences, the operations performed in indirect computing are the same as in direct computing [18].

4

NUMERICAL MODELLING

This chapter describes the geometry and meshing parameters, boundary conditions, and other information regarding simulations in OpenFOAM and Ansys Transient Structural and Modal modules.

4.1 Geometry Building and Meshing for CFD Modelling

Two pipe geometries were considered in this project. One consisted of two pipes, one vertical and the other horizontal, connected to each other at 90^0 making a mitred bend. Pipe inside diameter was 72.54mm; length of the vertical pipe upstream of the bend was 2.8m and that of the downstream pipe section was 5m. Air was modelled to flow vertically upwards and change direction at the 90^0 bend in horizontal pipe.

The second geometry consisted of two pipes, one vertical and the other horizontal, the vertical pipe connected to the centre of the horizontal pipe. Pipe diameter is 72.54mm; length of the vertical pipe upstream of the tee junction was 2.8m and that of the downstream pipe section in each direction was 5m, 10m in total. Air was modelled to flow vertically upwards and split at the tee junction in both directions.

These two geometries were considered as these are the most common piping arrangements in industry. The entrance length of 2.8m for the upstream pipe in both geometries was calculated using the Reynolds entrance length formula so that the flow was fully developed by the time it reached the 90^0 bend and the tee junction. Reynolds entrance length formula for turbulent pipe flow is given by [6]:

$$\frac{L_e}{D} \approx 4.4\,\mathrm{Re}^{1/6} \tag{4.1}$$

Based on the highest velocity i.e., 75m/s (Ma < 0.3), entrance length was calculated and upstream pipe length was decided.

Both geometries were built and meshed using Ansys Workbench modules namely DesignModeler and Meshing respectively. For geometry with the 90^0 mitred joint, fluid mesh had 14039200 cells. For tee geometry, the mesh had 31185478 cells. Complete mesh statistics for both geometries for running LES simulations are given in Appendix B.

For both pipe geometries, wall thickness was taken as 6.35mm and mid-surface option was applied to use shell elements. For geometry with the 90^0 mitred joint, structural mesh had 1536 elements. For tee geometry, the mesh had 2640 elements. Complete mesh statistics for both structural geometries are given in Appendix C.

Material Properties for the pipe structural steel were used from Ansys library and are given in Appendix D. Shell Element 181 was used from Ansys Element Library. This element has four nodes and each node has six degrees of freedom, translations in and rotations about x, y, and z directions. This element is capable of analysing thin to moderately thick shells [7].

4.2 Method of Simulations

All fluid simulations were performed using OpenFOAM. The mesh obtained from Ansys was converted into an OpenFOAM readable mesh. The kinematic viscosity of air (ν) was $1.51\text{x}10^{-5}$ m^2/s. Inlet boundary conditions are tabulated in Table 4.1. Simulations were performed in both geometries at three velocities; 45m/s, 60m/s, and 75m/s. At the highest velocity which was 75m/s and Mach number was 0.218, the air is considered to be incompressible [71]. Therefore, the solver used for these simulations was PisoFOAM which is a transient solver for incompressible flow.

Table 4.1: Initial and Boundary Conditions

Velocity (U) m/s	45	60	75
Reynolds Number (Re)	2.16×10^5	2.88×10^5	3.60×10^5
Turbulence Intensity (I)	0.034	0.033	0.032
Turbulence Length Scale (l) m	0.005	0.005	0.005
Turbulent Kinetic Energy (k) m^2/s^2	3.606	5.966	8.816
Turbulent Dissipation rate (ε) m^2/s^3	221.61	471.57	847.11

Pawsey supercomputer Epic [3] was used to run these simulations. Large Eddy Simulation (LES) was used with One Equation Model. Simulations were allowed to run for some time till the flow reached a pseudo steady condition and pressure fluctuations at monitor points showed small variations in magnitudes. Once the solutions had reached a pseudo steady state, these simulations were continued to run to collect the data on which Fast Fourier Transforms could be performed. Epic was a Hewlett Packard (HP) homogeneous cluster. It had same type of processor across all compute nodes; the Intel Xeon X5660 (Westmere). Each node had two X5660 processors and each X5660 processor had 6 cores. These were referred to as "dual hex-core" nodes. In total, Epic had twelve cores per node providing a total of 9600 cores across the 800 nodes. Each node had 24GB RAM. To resolve the fluid model for geometry with the 90^0 mitred joint, 100 nodes were used. For tee geometry, 200 nodes were used.

Simulations for the pipe geometry with 90^0 mitred joint were performed at a time step of 10^{-6} seconds for all three velocities. Based on the critical frequencies obtained after performing Fast Fourier Transforms of the pressure data at the probe monitor points, surface pressure data was written at a time step of 10^{-5} seconds to capture the critical frequencies which had large magnitudes. The surface pressure loads against these time steps were transferred in the Ansys Transient Structural module to perform fluid structure interaction (FSI). Simulations for the pipe geometry with tee junction were performed at a time step of 10^{-6} seconds for 45m/s and 60m/s. For 75m/s, a time step of 10^{-7} seconds was used due to convergence issues. Based on the frequencies obtained using Fast Fourier Transforms of the pressure data at probe monitor points, surface pressure data was written at a time step of 10^{-5} seconds to

capture the critical frequencies. The surface pressure loads for these time steps were transferred in the structural module for FSI. The coordinates used for gathering pressure data along the wall or probe locations are given in Appendix A.

4.3 Pipe Support Arrangement

In the case of geometry with 90^0 mitred bend, the downstream pipe was simply supported at 0.5m and 3.5m from the bend. In the case of tee geometry, the downstream pipe sections were simply supported at 0.5m and 3.5m on both sides of the tee junction. The reason behind supporting the downstream pipe sections at those locations was to keep the number of supports as minimum as possible while the model stayed fully constrained. When the locations of supports were changed, the values of natural frequencies obtained after performing modal analysis changed with minor variations. Despite these small variations, the ratio of the frequencies obtained from the structural analysis with the natural frequencies obtained from modal analysis was approximately the same.

In the "Simply Supported" boundary condition provided by Ansys, straight and curved edges and vertices were prevented from moving and deforming. Rotations were allowed. These support arrangements are shown for both geometries in Figures 4.1 and 4.2.

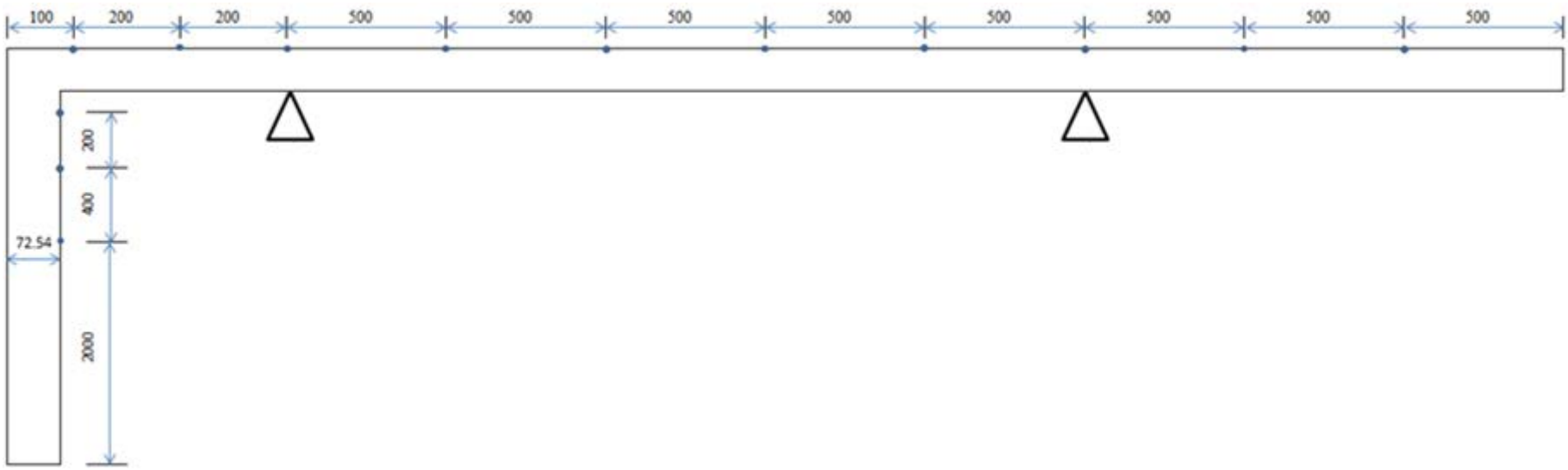

Figure 4.1: Probe Locations and Support Arrangement for Pipe Geometry with 90^0 Mitred Bend

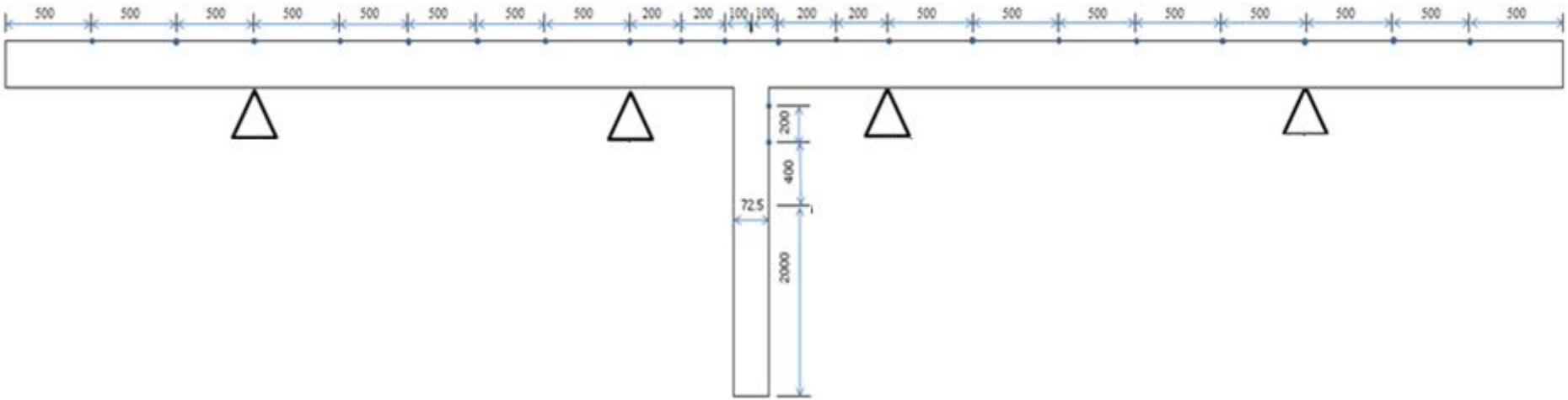

Figure 4.2: Probe Locations and Support Arrangement for Pipe Geometry with Tee Junction

5

RESULTS AND DISCUSSION

The main objective of this study was to determine which frequencies existing in fluid excited those in pipe structural wall and if any of the fluid excited frequencies were a source of resonance.

To achieve this objective, Modal Analyses were performed on both pipe structural geometries and their natural frequencies were obtained. In fluid domain of both geometries, flows were initialized and allowed to run for some time to reach a pseudo steady state. After these simulations had reached a pseudo steady condition, the solutions were allowed to run for a period of time to generate data enough to perform Fast Fourier Transforms (FFT). From the solutions, pressure data for all individual probe locations were obtained and FFT were performed. For geometry with the 90^0 mitred joint, flow reached a pseudo-steady state at 2.5m downstream of the bend for all velocities which can be observed from the pressure data shown in Figures 5.7, 5.8 and 5.9. For geometry with the tee junction, flow reached a pseudo-steady state at 2.5m downstream of the tee junction for all velocities. This can be observed from the pressure data taken in +X direction shown in Figures 5.16, 5.17

and 5.18. Pressure data obtained from CFD for the pipe surface were imported in Ansys Transient Structural module.

To obtain fluid frequencies for all six cases, 333,000 samples of the pressure data were used to perform FFT. To obtain structural frequencies for all six cases, 33,300 samples were used from the results of transient analyses. The reason was that the CFD simulations were run at a time step increment of 10^{-6}s and all critical fluid frequencies were found to be around $5x10^4$ Hz; therefore, structural simulations were performed at 10^{-5}s to capture all such frequencies as dictated by Nyquist Theorem. Hence, the frequency spectrums of structural displacements were obtained at intervals similar to those of the fluid pressure fluctuations. In all cases, magnitudes of the frequencies obtained from FFT were normalized and these normalized magnitudes were then plotted against their respective frequencies.

5.1 Natural Frequencies of Pipe Geometries

Natural frequencies of both geometries were obtained from modal analyses and tabulated in Tables 5.1 and 5.2. Mode Shape 1 at 0Hz in Table 5.1, which tabulates natural frequencies for pipe geometry with the 90^0 mitred bend indicate rigid body behaviour of the geometry.

Table 5.1: Natural Frequencies for Pipe Geometry with 90^0 Mitred Bend

Mode Shape	Natural Frequency ω_0 (Hz)	Mode Shape	Natural Frequency ω_0 (Hz)
1	0 (rigid body)	8	46.864
2	5.8211	9	61.988
3	14.34	10	76.017
4	20.024	11	114.73
5	29.799	12	117
6	33.163	13	121.27
7	44.271	14	149.19

Table 5.2: Natural Frequencies for Pipe Geometry with Tee Junction

Mode Shape	Natural Frequency ω_0 (Hz)	Mode Shape	Natural Frequency ω_0 (Hz)
1	0 (rigid body)	18	122.35
2	8.4257	19	125.73
3	16.394	20	139.34
4	16.963	21	152.99
5	20.049	22	169.33
6	20.073	23	169.73
7	36.957	24	176.2
8	41.613	25	177.78
9	43.148	26	208.25
10	43.833	27	239.34
11	44.65	28	242.33
12	54.147	29	250.58
13	97.568	30	262.08
14	99.943	31	266.66
15	110.08	32	290.1
16	111.75	33	299.38
17	112.05	34	365.68

5.2 Mesh Independence for both Geometries

To achieve mesh independence, several meshes for both geometries were considered. Simulations were run at 75m/s for different mesh sizes until no change in results were observed between subsequent meshes.

L. J. De Chant [8] derived a relationship to obtain the analytical velocity profile. This analytical profile relationship is given as under:

$$u = U_{\max}\left[\sin\left(\frac{\pi}{2}\left(1-\frac{r}{R}\right)^{1/2}\right)\right]^{\frac{1}{2}} \tag{5.1}$$

Where u is the instantaneous velocity, U_{max} is the maximum velocity at the centre of the pipe, r is the distance from the center of the pipe to the location at which the velocity is recorded, and R is the pipe radius.

In the case in which air was modelled to flow at 75m/s, the velocity profile obtained downstream of the 90^0 mitred joint on the mesh selected for the project and the one obtained using Equation 5.1 are compared in Figure 5.1. Velocity profile obtained downstream of the tee junction in the case in which the air was modelled to flow at 75m/s is shown in Figure 5.2.

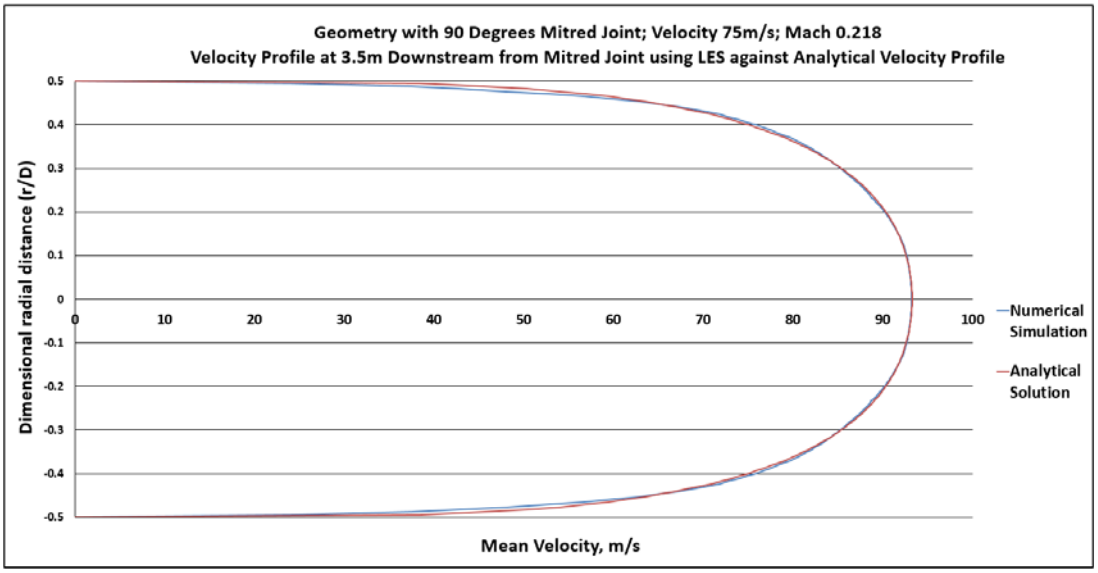

Figure 5.1: Instantaneous Velocity Profile Comparison in Geometry with 90^0 Mitred Joint -Velocity Profile using LES against that obtained from L. J. De Chant's Equation

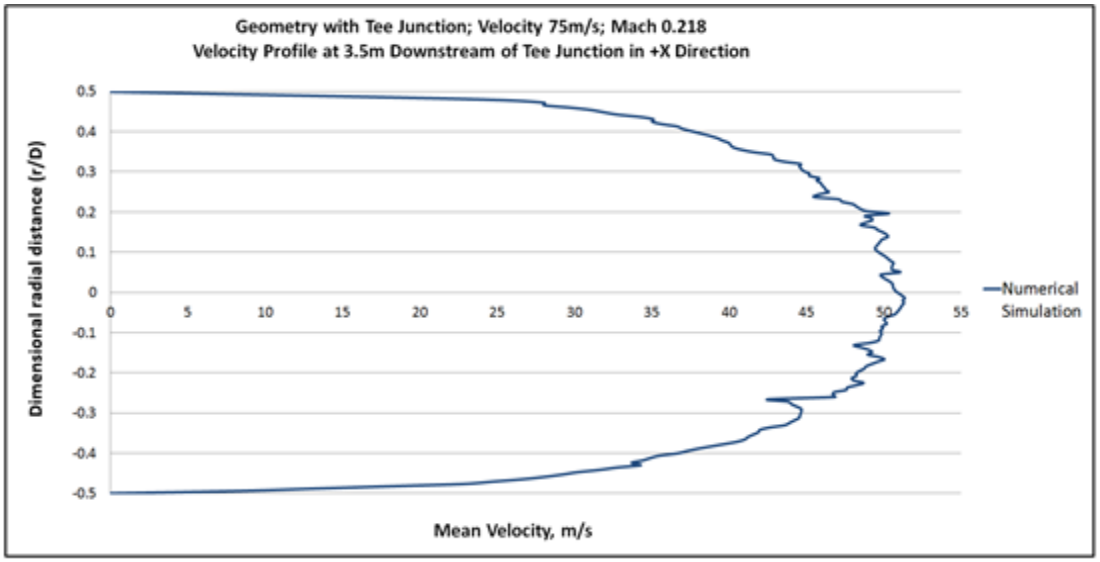

Figure 5.2: Instantaneous Velocity Profile in Geometry with Tee Junction using LES

5.3 Flow Development and Frequencies in the Geometry with 90^0 Mitred Bend for all Velocities

As the flow was initialized for all three velocities, the solutions showed spikes in velocities but as the simulation run time increased, solutions reached a pseudo steady state. Errors present at the time of initialization were reduced and the solution moved towards convergence. For 45m/s, solution reached the pseudo steady condition at approx. 0.12s and after this time, pressure continually fluctuated without showing any major deviation. For 60m/s and 75m/s, solution reached convergence at approx. 0.09s and 0.07s respectively however pressure spikes and drops were visualized even after the solution had reached pseudo steady state. These spikes happened at instances where solution stopped and restarted against a new job. In order to get rid of these spikes and drops, simulations were cancelled numerous times and started fresh but the spikes and drops did not disappear.

As shown in Figures 5.3, 5.4, and 5.5, the flow had fully developed in the upstream pipe before reaching the 90^0 mitred section for all three velocities; 45m/s, 60m/s, and 75m/s. No-slip region was identified at the walls whereas the velocity was highest in the centre. As the flow changed its direction at the bend, separation regions were seen in the downstream pipe. U_{mean} results show increase in velocity due to sudden pressure drop as the fluid changed its direction. As the distance from the mitred section was increased, the velocity decreased.

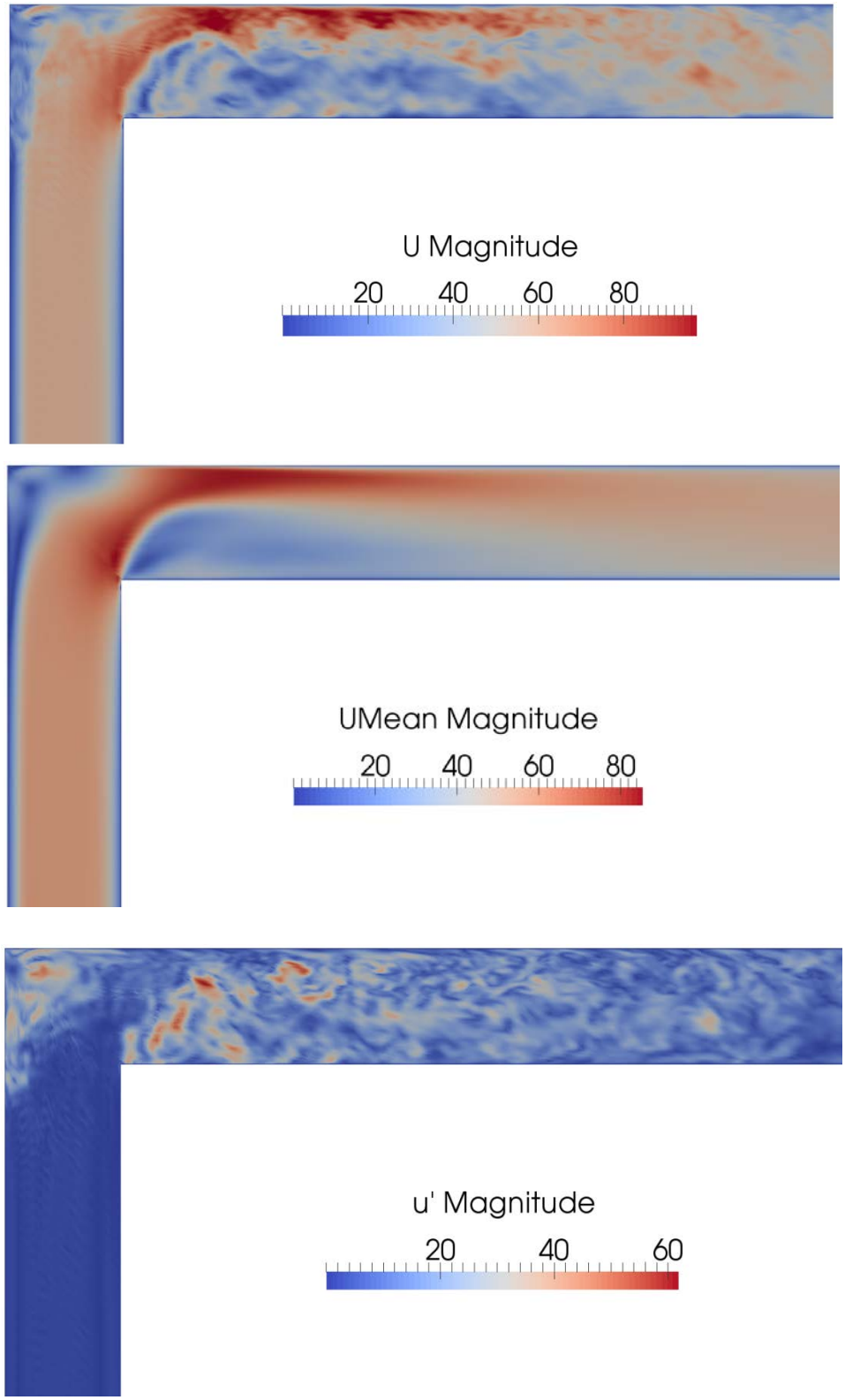

Figure 5.3: Geometry with 90^0 Mitred Joint – Velocity Distribution for flow at 45m/s at 0.513 seconds

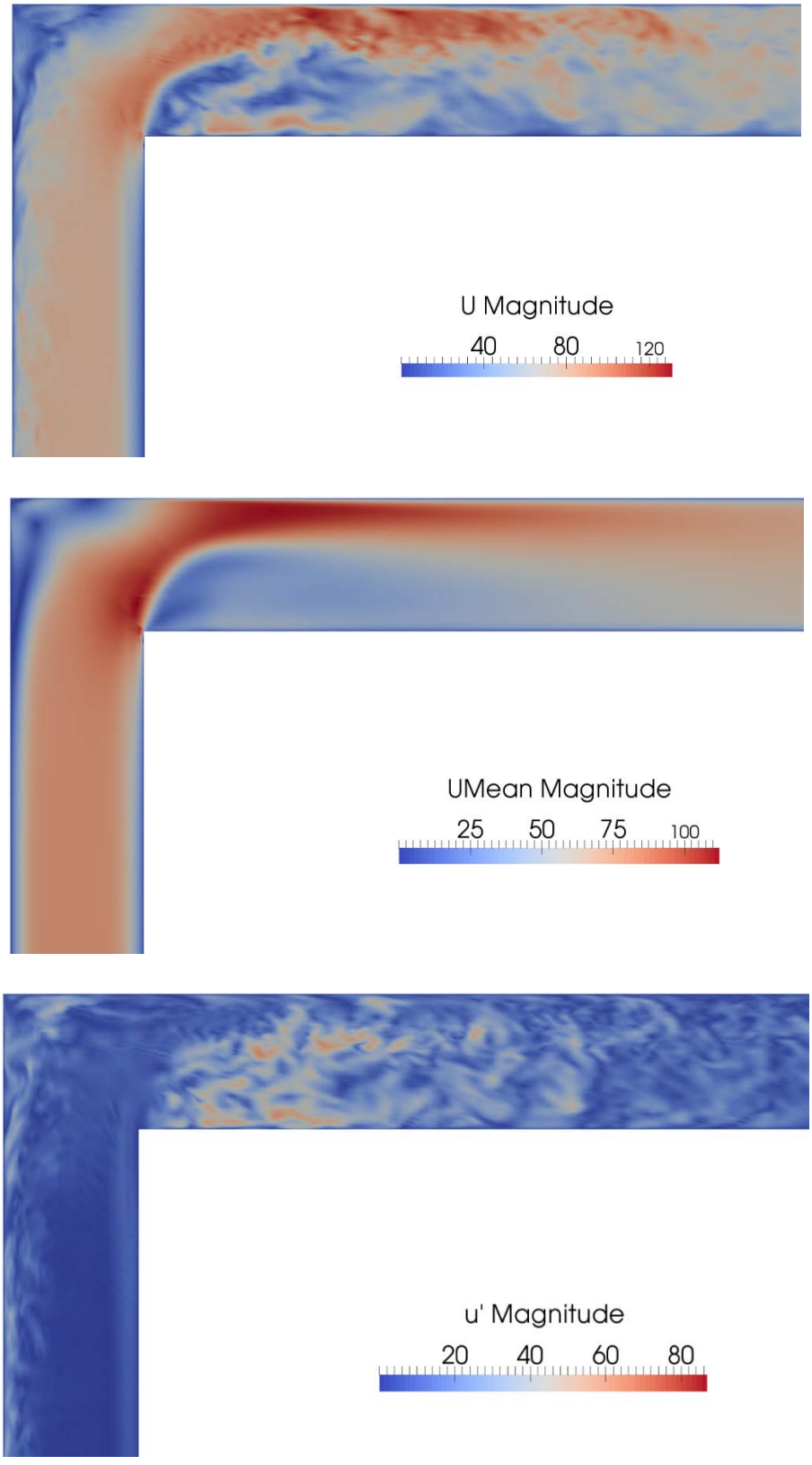

Figure 5.4: Geometry with 90^0 Mitred Joint – Velocity Distribution for flow at 60m/s at 0.513 seconds

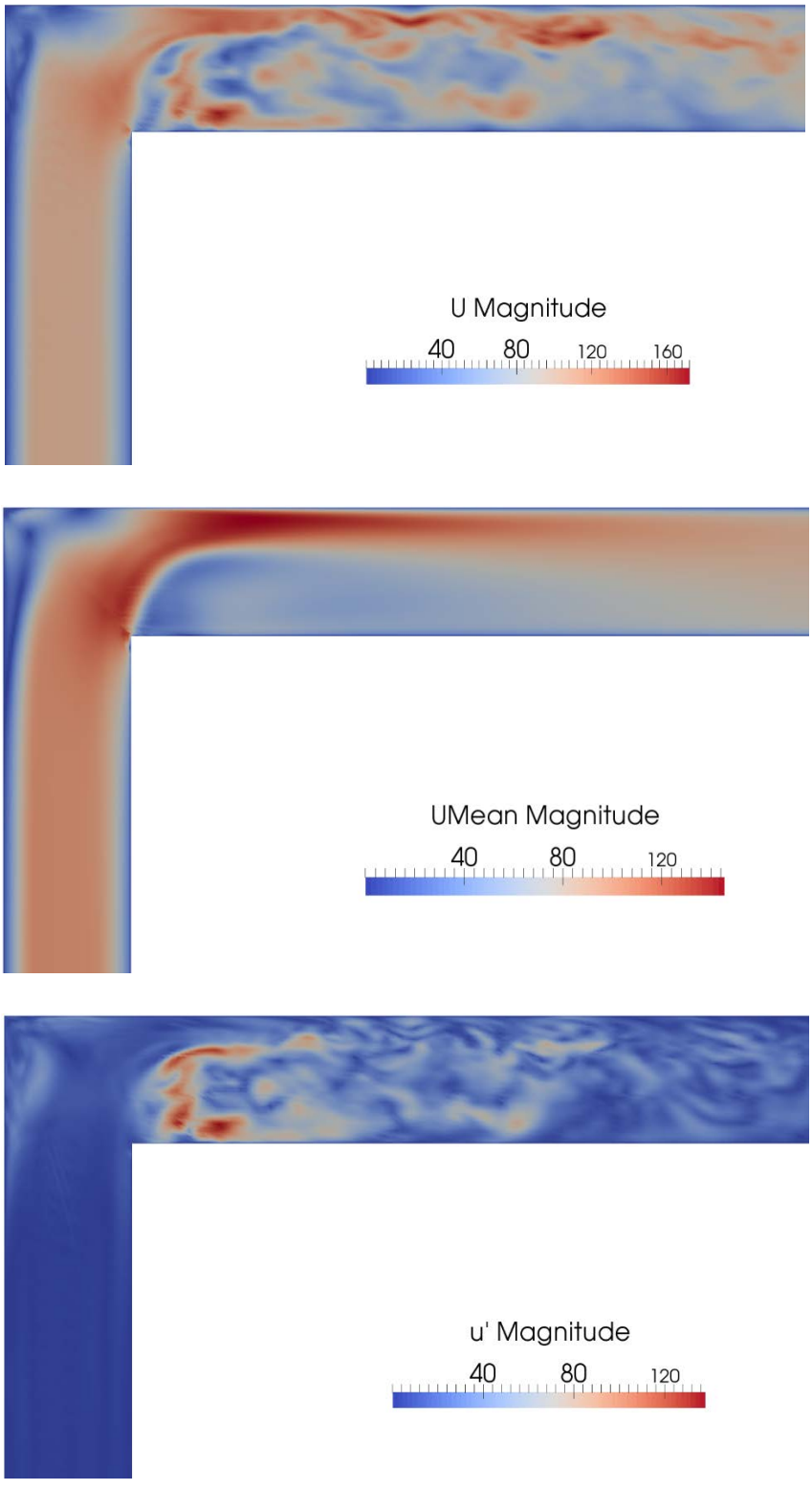

Figure 5.5: Geometry with 90^0 Mitred Joint – Velocity Distribution for flow at 75m/s at 0.513 seconds

After imposing the fluid surface pressure loads on structural geometry and performing transient analyses, data of structural displacements against the defined time steps were obtained and FFT were performed on these data. This discussion is limited to the frequencies below 129Hz. All frequencies higher than 129Hz were ignored due to their small magnitudes as compared to the ones that were lower and exhibited the same characteristics i.e., whether these frequencies excited initially as a structural or fluid mode, they continued to show excitation as the same mode or changed modes from structure to fluid and vice versa at all probe locations along the complete downstream pipe without any defined principle. To demonstrate this phenomenon, Figure 5.6 is given as an example. In this figure, 9Hz changed mode from fluid at probe location 1 to a structural mode at probe location 2. 30Hz changed mode from structural at probe location 1 to a fluid mode at probe location 2. 39Hz excited as fluid mode at both probe locations without changing to structural mode and 87Hz excited as structural mode at both probe locations without changing to fluid mode. These frequencies are listed in Table 5.3.

Pressure fluctuations in mitred bend geometry for all three velocities i.e., 45m/s, 60m/s, and 75m/s are shown in Figures 5.7, 5.8, and 5.9 respectively. All figures have two graphs, one showing the initial time periods in which the transient fluctuations at the start of the simulations start to diminish in magnitude. The other graph shows the time periods in which the solution has reached a pseudo steady state until the end of the simulation. For 45m/s, data was taken from approx. 0.18s till 0.52s to perform Fast Fourier Transforms (FFT) and obtain a frequency spectrum. With air flow of 60m/s, data was taken from approx. 0.28s till 0.62s for FFT. For 75m/s, the data range considered was between approx. 0.42s and 0.79s for FFT. Frequency plots for natural, fluid, and structural frequencies at different probe locations for 45m/s are shown in Figures 5.10 and 5.11. Similar frequency plots for all three velocities at all probe locations are given in Appendices E, F, and G.

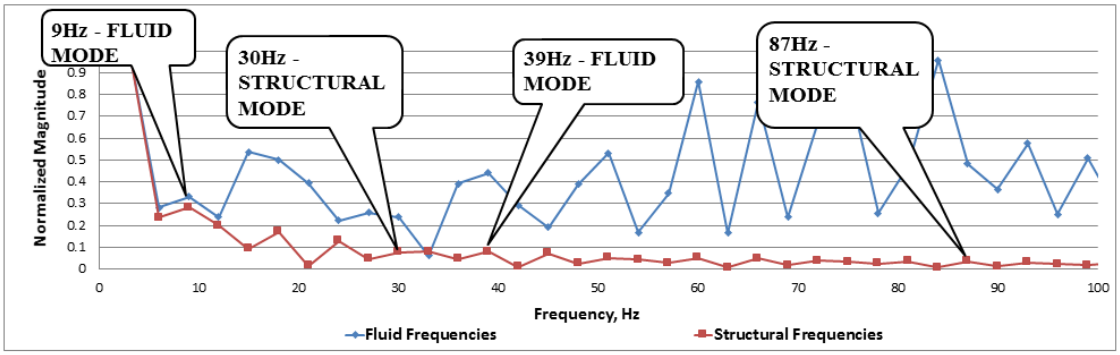

Figure 5.6a: Frequencies Excited at Probe Location 1

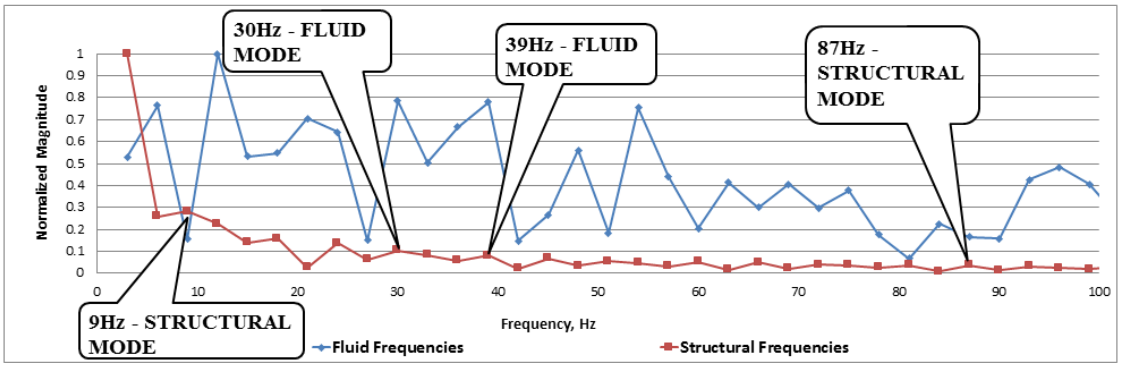

Figure 5.6b: Frequencies Excited at Probe Location 2

Figure 5.6: Frequencies and Their Modes of Excitation

Table 5.3: Sample Table for listing Frequencies at different Probe Location

Frequency (Hz)	Mode	Probe Locations
9	Fluid	Probe Location 1
	Structural	Probe Location 2
30	Fluid	Probe Location 2
	Structural	Probe Location 1
39	Fluid	Probe Location 1, Probe Location 2
	Structural	Not excited
87	Fluid	Not excited
	Structural	Probe Location 1, Probe Location 2

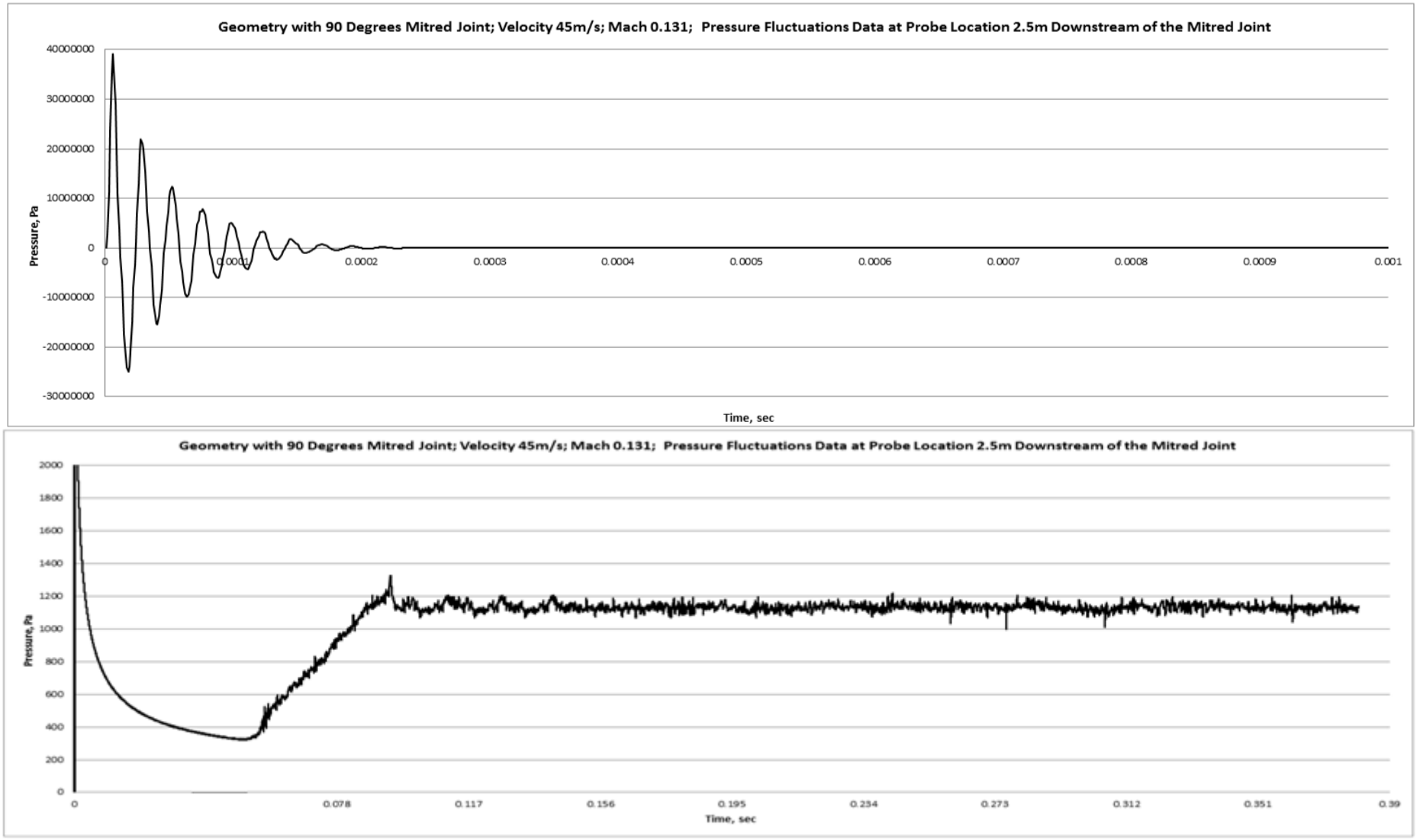

Figure 5.7: Pressure Fluctuations at Probe Location 2.5m Downstream of the Mitred Joint for air flowing with a velocity of 45m/s

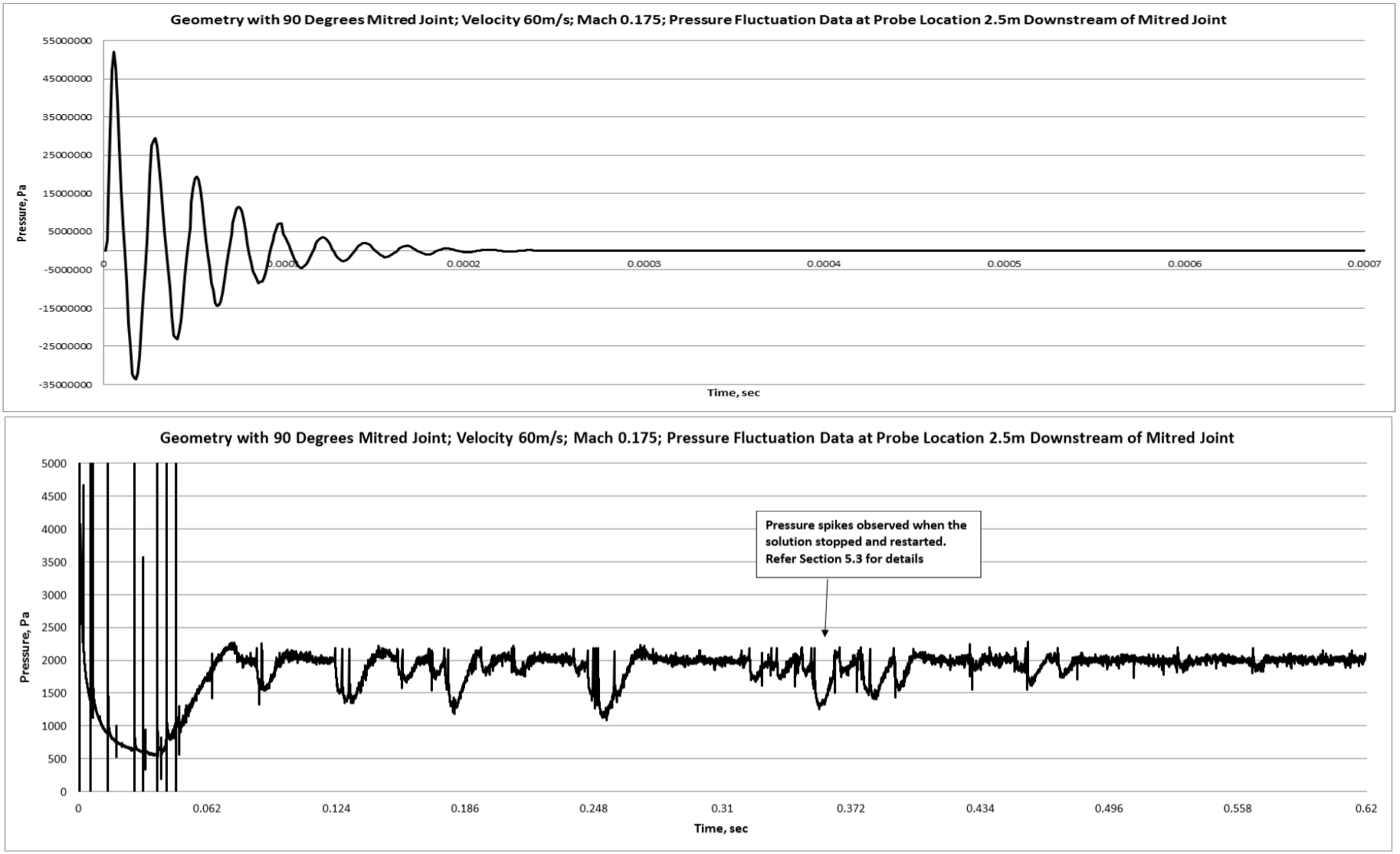

Figure 5.8: Pressure Fluctuations at Probe Location 2.5m Downstream of the Mitred Joint for air flowing with a velocity of 60m/s

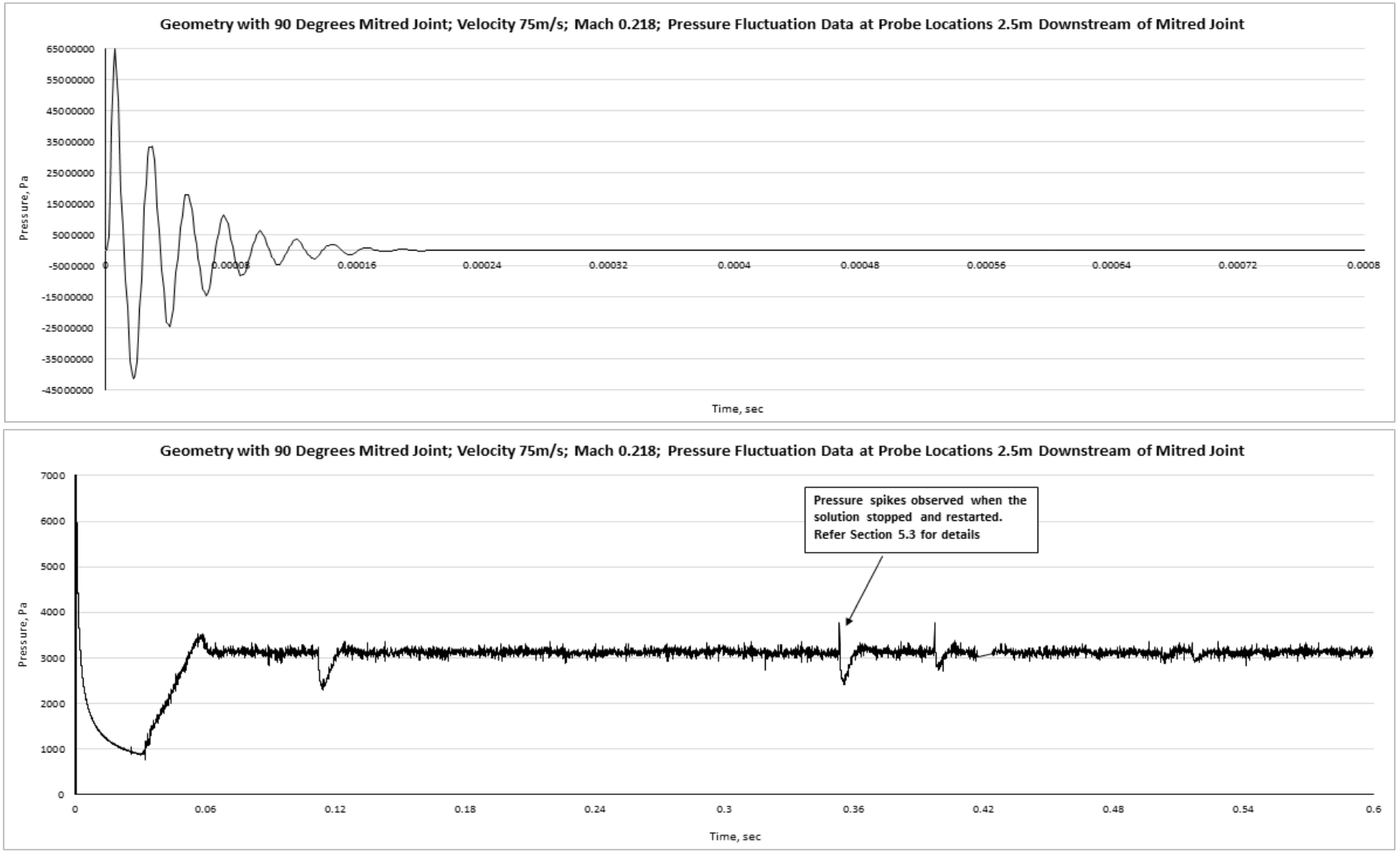

Figure 5.9: Pressure Fluctuations at Probe Location 2.5m Downstream of the Mitred Joint for air flowing with a velocity of 75m/s

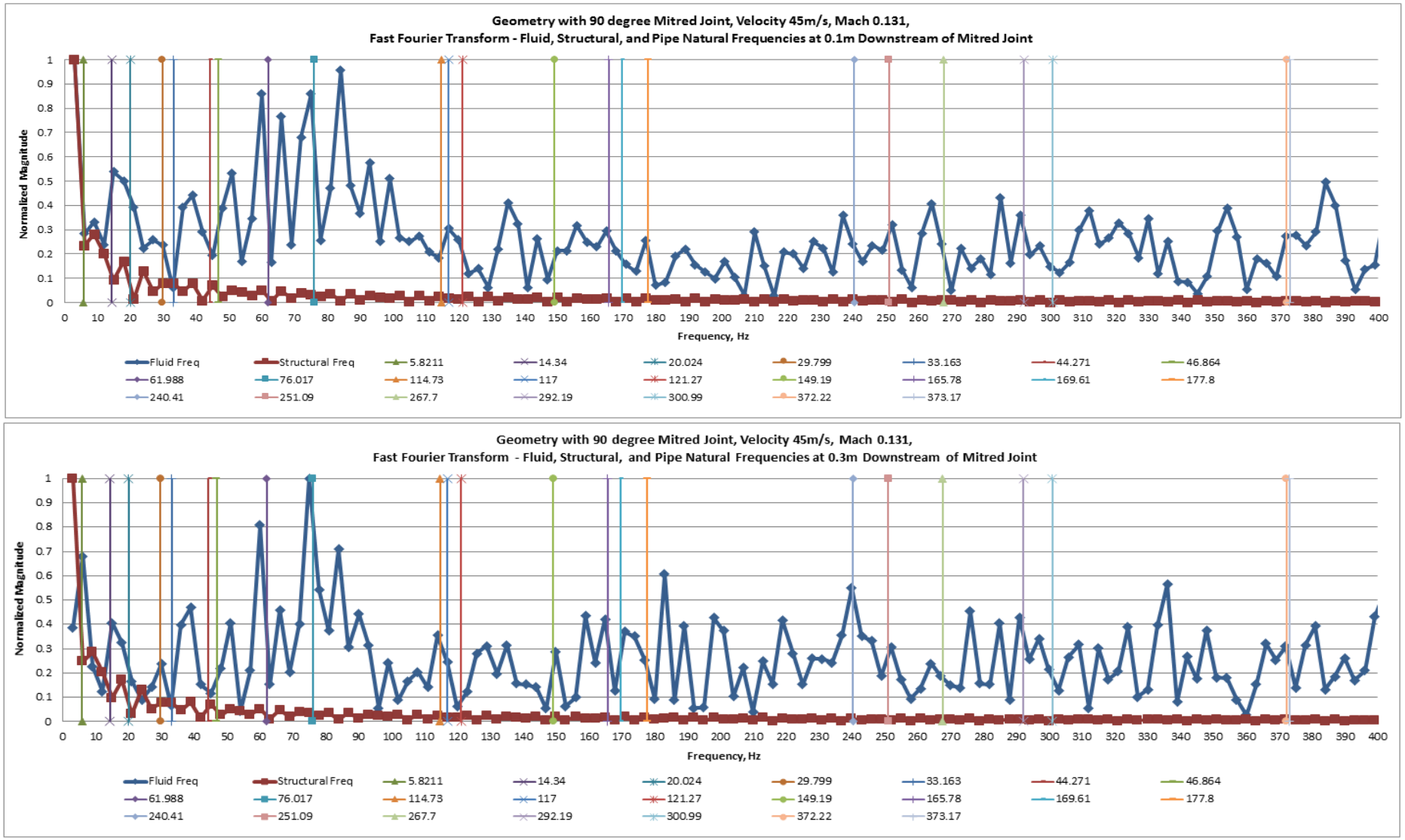

Figure 5.10: Frequency Plots at Probe Locations 0.1m and 0.3m Downstream of the Mitred Joint for air flowing with a velocity of 45m/s

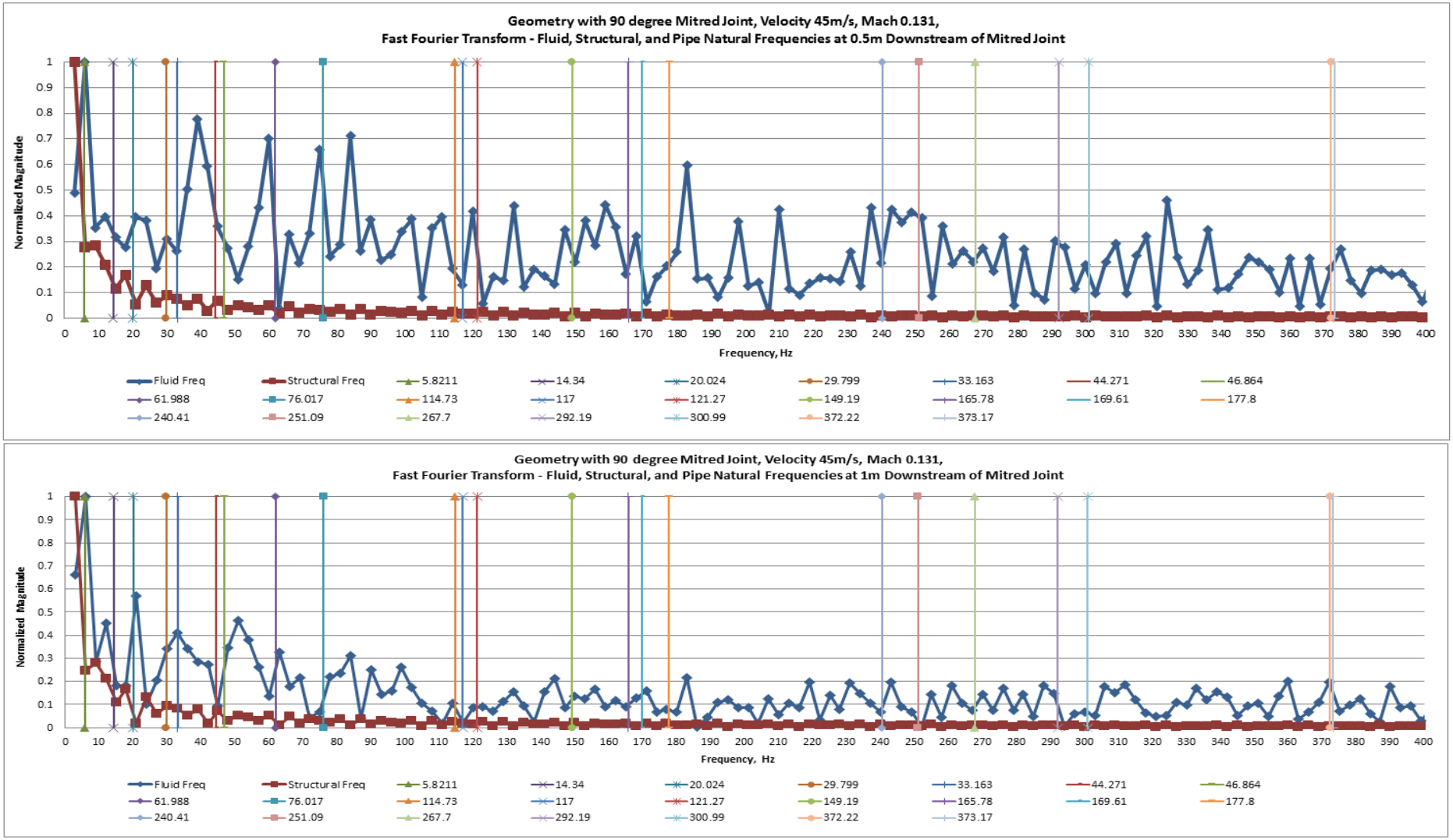

Figure 5.11: Frequency Plots at Probe Locations 0.5m and 1m Downstream of the Mitred Joint for air flowing with a velocity of 45m/s

In the case of air flowing at 45m/s, 39Hz and 66Hz excited as fluid mode at most probes in the pipe downstream of the 90^0 mitred bend. 39Hz excited as fluid mode from 0.1m to 0.5m, from 1.5m to 3.5m, and then at 4.5m on the downstream pipe. At other probe locations, it excited as structural mode. 66Hz appeared as fluid mode from 0.1m to 0.5m, from 1.5 to 3m, and then at 4.5m. After 39Hz and 66Hz, 3Hz, 51Hz, 60Hz, and 108Hz excited as fluid mode at more probe locations than other frequencies present in the system. Of these, 3Hz had the highest magnitude. These frequencies and their respective probe locations at which these were excited are tabulated in Table 5.4 below:

Table 5.4: Frequencies present downstream of the mitred bend for 45m/s showing highest excitation

Frequency (Hz)	Mode	Probe Locations Downstream of Mitred Joint (m)
3	Fluid	0.1, 2.0, 3.0 – 4.5
	Structural	0.3 – 1.5, 2.5
39	Fluid	0.1 – 0.5, 1.5 – 3.5, 4.5
	Structural	1.0, 4.0
51	Fluid	0.1 – 1.0
	Structural	1.5 – 4.5
60	Fluid	0.1 – 0.5
	Structural	1.0 – 4.5
66	Fluid	0.1 – 0.5, 1.5 – 3.0, 4.5
	Structural	1.0, 3.5, 4.0
108	Fluid	0.1, 0.3, 1.5, 3.0, 4.5
	Structural	0.5, 1.0, 2.0, 2.5, 3.5

All fluid excited frequencies in the pipe section downstream of the 90^0 mitred joint and their normalized magnitudes are given in Table 5.5 below:

Table 5.5: Fluid excited frequencies present downstream of the mitred bend for 45m/s

Fluid Excited Frequency in Pipe Wall ω (Hz)	**Natural Frequency ω_0 (Hz)**	**Mode Shape**	$\frac{\omega}{\omega_0}$	**Normalized Magnitude**
3	5.821	2	0.52	1.000
9	5.821	2	0.65	0.282
18	20.024	4	0.90	0.181
24	20.024	4	0.83	0.135
30	29.799	5	0.99	0.104
39	44.271	7	0.88	0.080
45	44.271	7	0.98	0.069
51	46.884	8	0.92	0.053
60	61.988	9	0.97	0.052
66	61.988	9	0.94	0.049
72	76.017	10	0.95	0.038
75	76.017	10	0.99	0.044
81	76.017	10	0.94	0.036
87	76.017	10	0.87	0.035
93	76.017	10	0.82	0.029
102	114.73	11	0.89	0.028
108	114.73	11	0.94	0.030
129	121.27	13	0.94	0.025

For air velocity of 60m/s, 3Hz had the highest magnitude. 3Hz and 69Hz appeared as fluid mode in the complete downstream pipe. 9Hz, 24Hz, and 42Hz excited as structural mode throughout in the downstream pipe without once changing to fluid mode. Frequencies like 30Hz, 78Hz, 90Hz, 111Hz, 117Hz, and 129Hz appeared as fluid mode at different probe locations. All frequencies discussed above are tabulated in Table 5.6 below:

Table 5.6: Frequencies present downstream of the mitred bend for 60m/s showing highest excitation

Frequency (Hz)	Mode	Probe Locations Downstream of Mitred Joint (m)
3	Fluid	0.1 – 4.5
9	Structural	0.1 – 4.5
24	Structural	0.1 – 4.5
30	Fluid	0.3 – 3.5
	Structural	0.1, 4.0, 4.5
42	Structural	0.1 – 4.5
69	Fluid	0.1 – 4.5
78	Fluid	0.3 – 3.5, 4.5
	Structural	0.1, 4.0
90	Fluid	0.1, 0.5, 1.0, 2.5
	Structural	0.3, 1.5, 2.0, 3.0 – 4.5
111	Fluid	0.1 – 3.5
	Structural	4.0, 4.5
117	Fluid	0.1, 0.3, 1.5, 4.5
	Structural	0.5, 1.0, 2.0 – 4.0
129	Fluid	0.5 - 3.0
	Structural	0.1, 0.3, 3.5 – 4.5

All fluid excited frequencies in the pipe section downstream of the 90^0 mitred joint and their normalized magnitudes are given in Table 5.7.

Table 5.7: Fluid excited frequencies present downstream of the mitred bend for 60m/s

Fluid Excited Frequency in Pipe Wall ω (Hz)	**Natural Frequency ω_0 (Hz)**	**Mode Shape**	**$\frac{\omega}{\omega_0}$**	**Normalized Magnitude**
3	5.821	2	0.52	1.000
30	29.799	5	0.99	0.151
36	33.163	6	0.92	0.041
51	46.884	8	0.92	0.070
57	61.988	9	0.92	0.047
63	61.988	9	0.98	0.041
69	76.017	10	0.91	0.039
78	76.017	10	0.97	0.032
84	76.017	10	0.90	0.031
90	76.017	10	0.84	0.036
96	114.73	11	0.84	0.036
111	114.73	11	0.97	0.030
117	117	12	1	0.029
129	121.27	13	0.94	0.021

For air flowing with a velocity of 75m/s, the frequencies which showed highest excitation in the pipe downstream of the 90^0 mitred bend are tabulated in Table 5.8. 3Hz had the highest magnitude. 30Hz and 57Hz excited as fluid mode and 24Hz appeared as structural mode throughout the downstream section. 36Hz and 42Hz initially excited as a structural mode at 0.1m. From 0.3m, both frequencies excited as a fluid mode throughout the downstream pipe. Other frequencies which excited as a fluid mode were 51Hz, 78Hz, 84Hz and 129Hz.

Table 5.8: Frequencies present downstream of the mitred bend at 75m/s showing highest excitation

Frequency (Hz)	Mode	Probe Locations Downstream of Mitred Joint (m)
24	Structural	0.1 – 4.5
30	Fluid	0.1 – 4.5
36	Fluid	0.3 – 4.5
	Structural	0.1
42	Fluid	0.3 – 4.5
	Structural	0.1
51	Fluid	0.1 – 1.0, 2.0 – 3.5, 4.5
	Structural	1.5, 4.0
57	Fluid	0.1 – 4.5
78	Fluid	1.0 – 2.5, 4.0, 4.5
	Structural	0.1 – 0.5, 3.0, 3.5
84	Fluid	0.3 – 2.5, 3.5
	Structural	0.1, 3.0, 4.0, 4.5
129	Fluid	0.1, 1.0 – 4.5
	Structural	0.3, 0.5

All fluid excited frequencies in the pipe section downstream of the 90^0 mitred joint and their normalized magnitudes are given in Table 5.9.

Table 5.9: Fluid excited frequencies present downstream of the mitred bend at 75m/s

Fluid Excited Frequency in Pipe Wall ω (Hz)	Natural Frequency ω_0 (Hz)	Mode Shape	$\frac{\omega}{\omega_0}$	Normalized Magnitude
3	5.821	2	0.52	1.000
9	5.821	2	0.65	0.030
15	14.34	3	0.96	0.379
30	29.799	5	0.99	0.137
36	33.163	6	0.92	0.104
42	44.271	7	0.95	0.076
51	46.884	8	0.92	0.070
57	61.988	9	0.92	0.068
63	61.988	9	0.98	0.061
69	76.017	10	0.91	0.051
78	76.017	10	0.97	0.044
84	76.017	10	0.90	0.035
102	114.73	11	0.89	0.024
129	121.27	13	0.94	0.027

Mode Shape 2 for the geometry with 90^0 bend is illustrated in Figure 5.12 below.

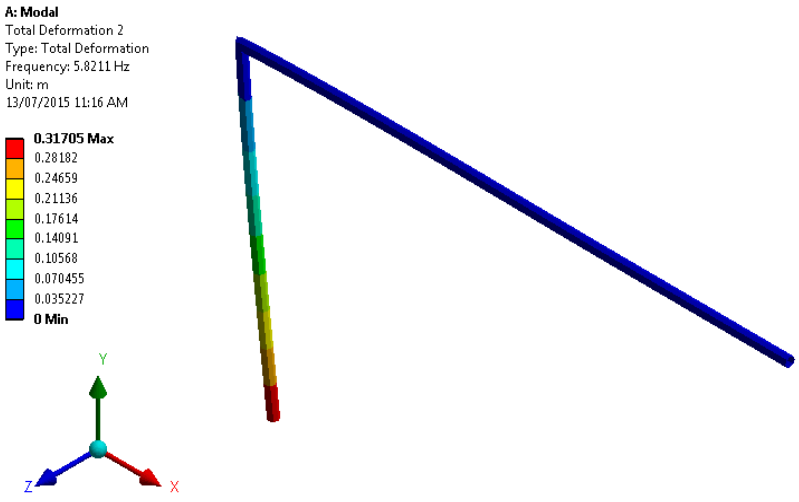

Figure 5.12: Geometry with 90^0 Mitred Bend - Mode Shape 2

5.4 Flow Development and Frequencies in the Geometry with Tee Junction for all Velocities

Like the solutions for flows modelled in the geometry with 90^0 bend, the solutions for the tee geometry exhibited spikes in velocities but as the simulation run time increased, solutions reached a pseudo steady state as these moved towards convergence. For 45m/s, solution became pseudo steady at 0.07s. After this time, pressure continually fluctuated without showing any major deviation. For 60m/s and 75m/s, solution reached convergence at 0.049s and 0.04s respectively; however, pressure spikes and drops were seen due to solution stops and restarts at new jobs. As previously for mitred joint case, these could not be avoided despite numerous attempts to stop and restart the solution.

Flows were developed in the upstream section before it reached the tee junction as shown in Figures 5.13, 5.14, and 5.15. All figures have two graphs, one showing the initial time periods in which the transient fluctuations at the start of the simulations start to diminish in magnitude. The other graph shows the time periods in which the solution has reached a pseudo steady state until the end of the simulation. No-slip region was identified at the walls whereas velocity was the highest in the centre. As the flow divided at the tee junction, separation regions were observed in the downstream pipes on both sides of the tee. U_{mean} results showed that the inlet fluid velocity was retained to some distance in the downstream pipe near the upper wall before decreasing. In other regions, velocity was not seen to reach this magnitude. Fluctuating velocity component u' demonstrated high magnitudes in the vicinity of tee junction due to the sharp corners in the mitred tee junction.

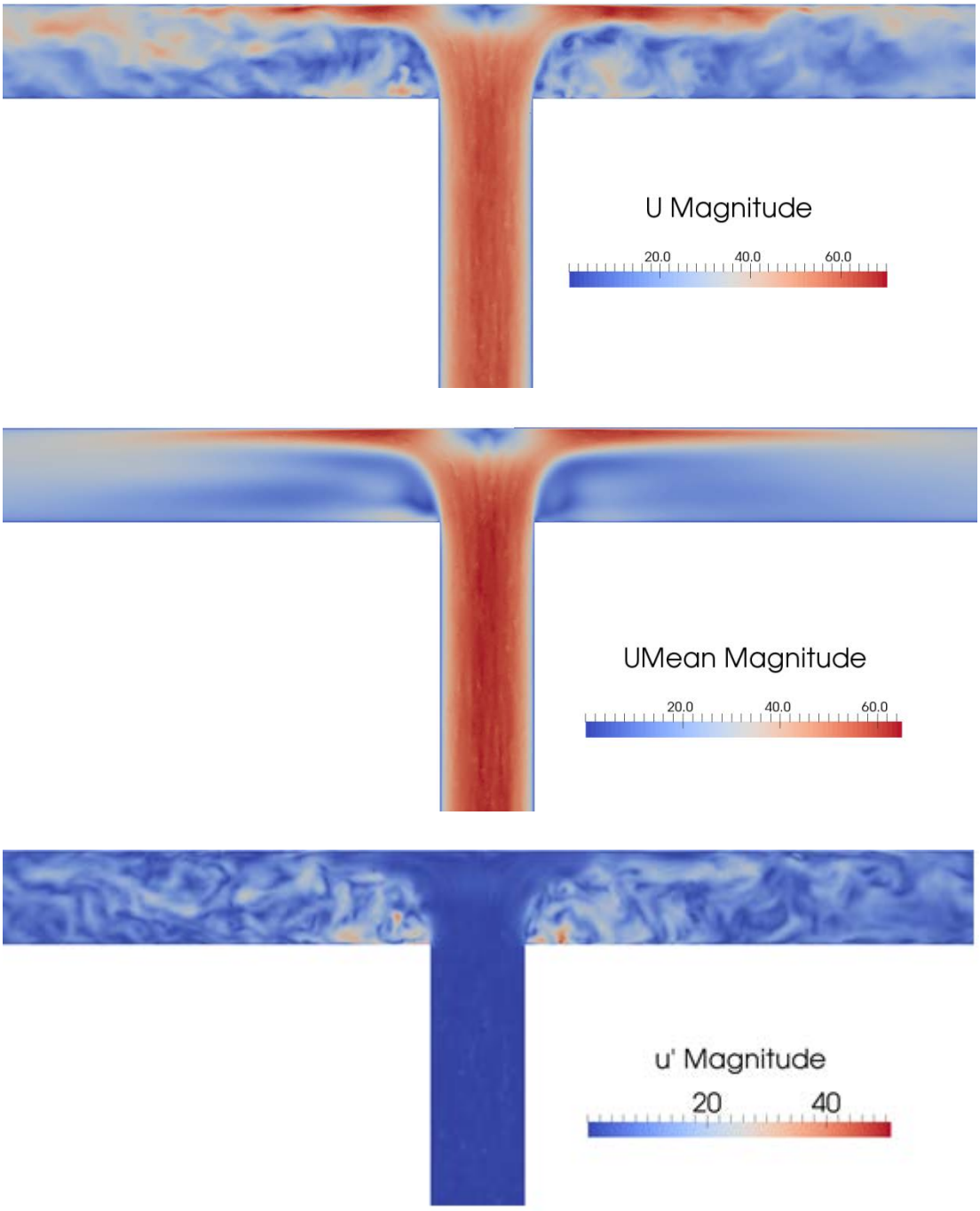

Figure 5.13: Geometry with Tee Junction – Velocity Distribution for flow at 45m/s at 0.513 seconds

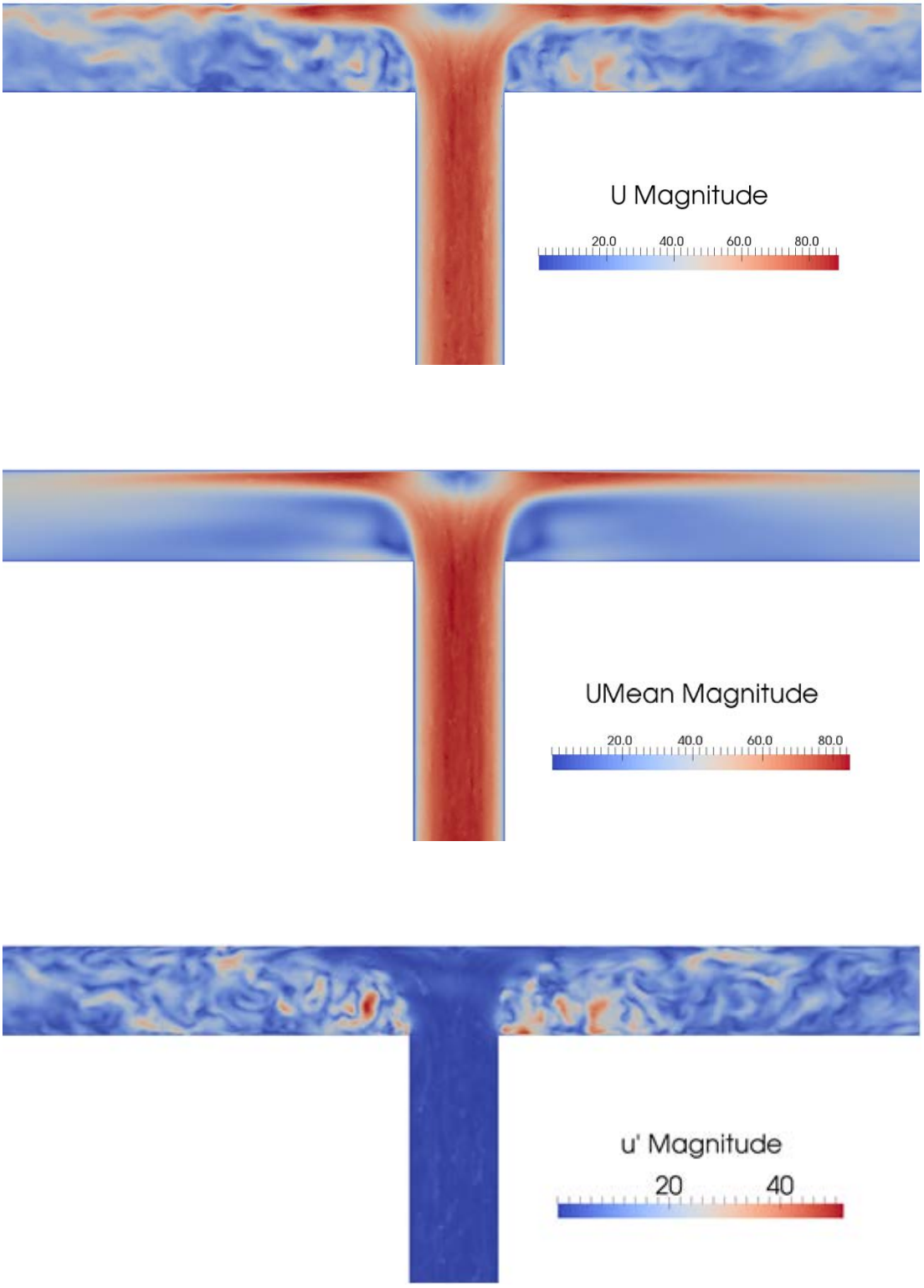

Figure 5.14: Geometry with Tee Junction – Velocity Distribution for flow at 60m/s at 0.464811 seconds

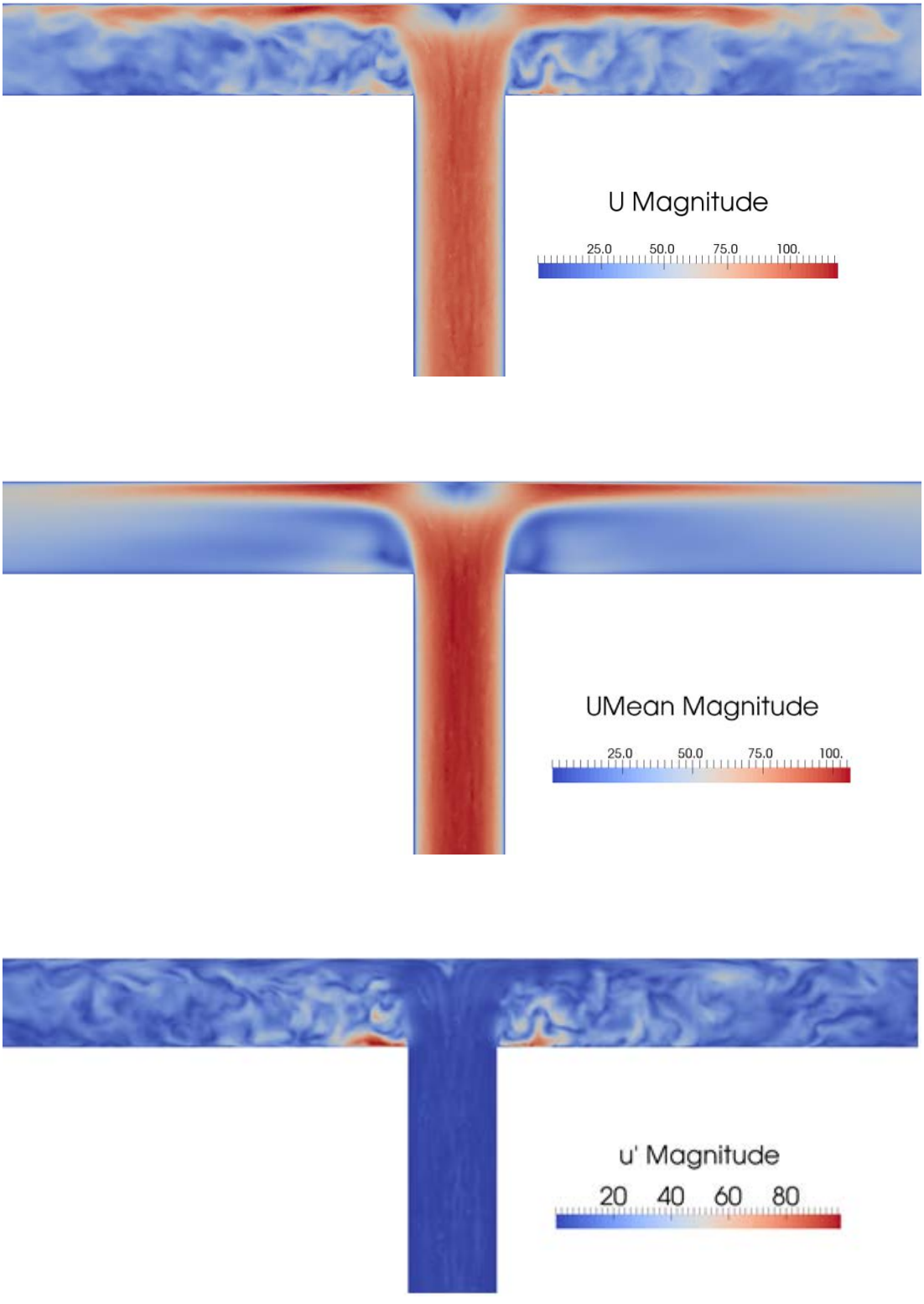

Figure 5.15: Geometry with Tee Junction – Velocity Distribution for flow at 75m/s at 0.3297594 seconds

After the fluid surface pressure loads were imposed on structural geometry and transient analyses were performed, structural displacements were obtained for all probe locations defined on pipe wall and a FFT was performed on these data of displacements. For 45m/s, data for Fast Fourier Transforms (FFT) was taken from approximately 0.38s to 0.71s. For air flow of 60 m/s, data taken for FFT ranged from approx. 0.15s to 0.49s. For 75m/s, data for FFT lied in between approx. 0.08s to 0.42s.

In pipe shell wall, 3Hz had the highest magnitude. After the flow had split and changed directions at the tee junction, frequencies present in the fluid on either side of the tee junction in the downstream pipe sections exhibited spectrums that were completely different to each other. In structural shell wall, frequencies were almost a mirror image of each other. A general discussion of the frequencies excited in the pipe wall in the downstream sections is as follows:

From 0.1m to 0.5m, the frequencies that had high magnitudes were 3Hz, 15Hz, 24Hz, 36Hz, 45Hz, 54Hz, 66Hz, 75Hz, 87Hz, 102Hz, 126Hz, 138Hz, and 150Hz. Frequencies higher than 150Hz were extremely small in magnitude as observed at 0.5m; however from 1m, these frequencies demonstrated a change in magnitudes. From 1m, 78Hz, 162Hz, 189Hz, 201Hz, 228Hz, and 249Hz excited with a higher magnitude and displayed peaks. 45Hz, 102Hz, and 126Hz increased in magnitudes. 102Hz and 46Hz excited with the highest magnitudes at 1m and 2m respectively. From 2.5m, 147Hz, 162Hz, 174Hz, 189Hz, 201Hz, 216Hz, 228Hz, 255Hz, 276Hz, 309Hz, 333Hz, and 354Hz excited with an increase in their peak magnitudes.

Pressure fluctuations in the tee geometry for all three velocities i.e., 45m/s, 60m/s, and 75m/s are shown in Figures 5.16, 5.17, and 5.18 respectively.

Frequency plots for natural, fluid, and structural frequencies at different probe locations for 45m/s are shown in Figures 5.19 to 5.22. Similar frequency plots for all three velocities at all probe locations are given in Appendices H, I, and J.

Mode Shape figures for the tee geometry are given in Figures 5.23 to 5.27.

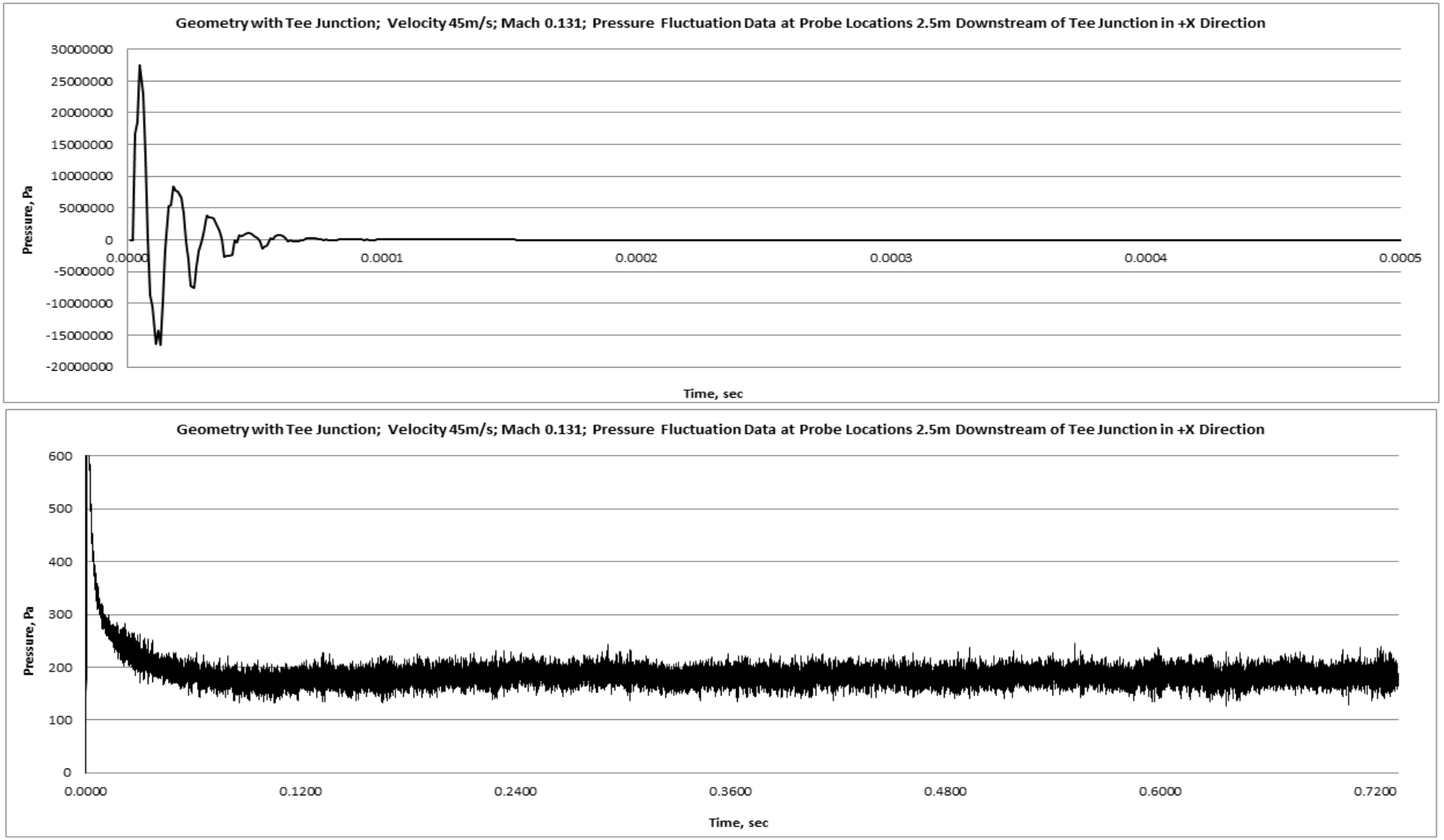

Figure 5.16: Pressure Fluctuations at Probe Location 2.5m Downstream of the Tee Junction in +X Direction for air flowing with a velocity of 45m/s

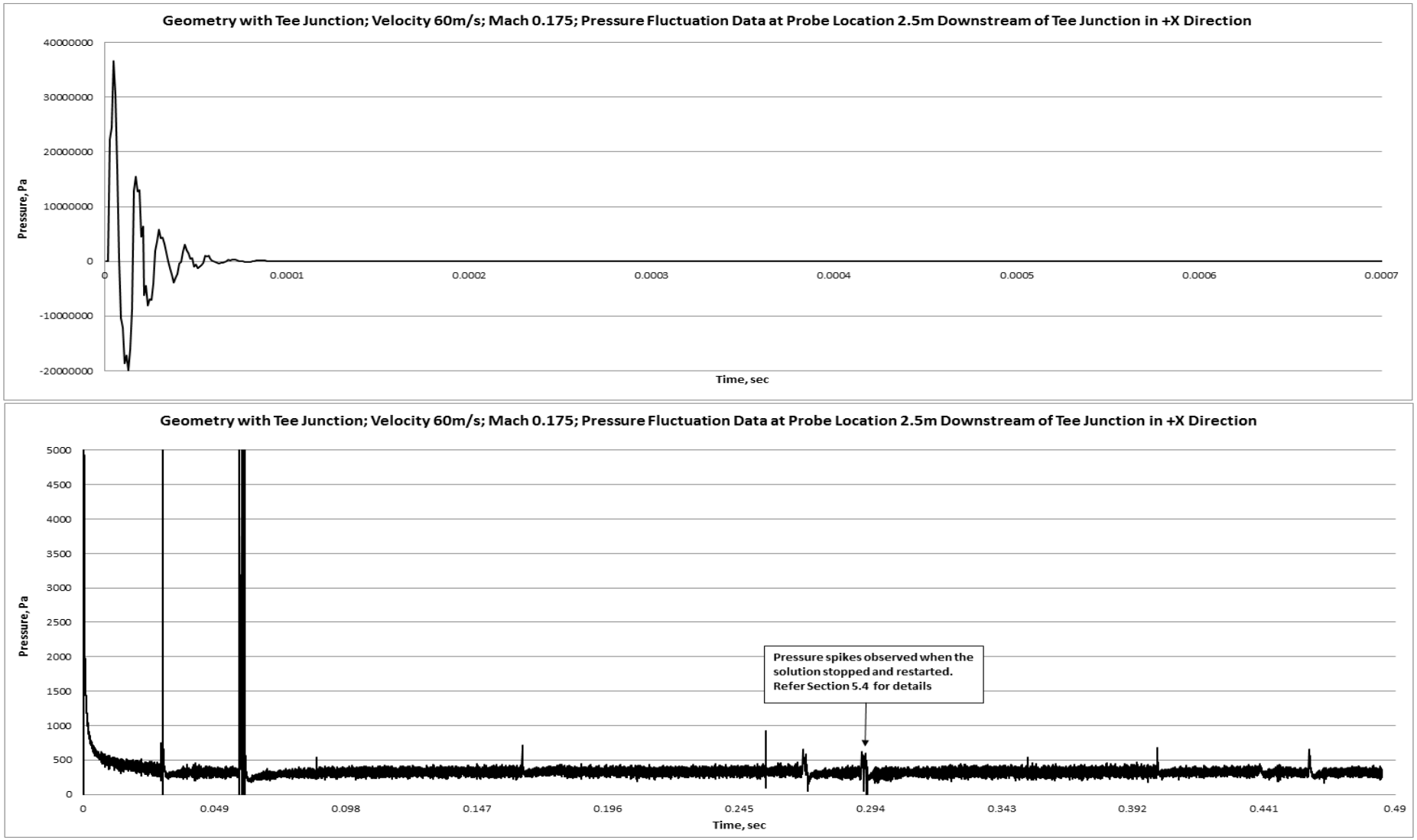

Figure 5.17: Pressure Fluctuations at Probe Location 2.5m Downstream of the Tee Junction in +X Direction for air flowing with a velocity of 60m/s

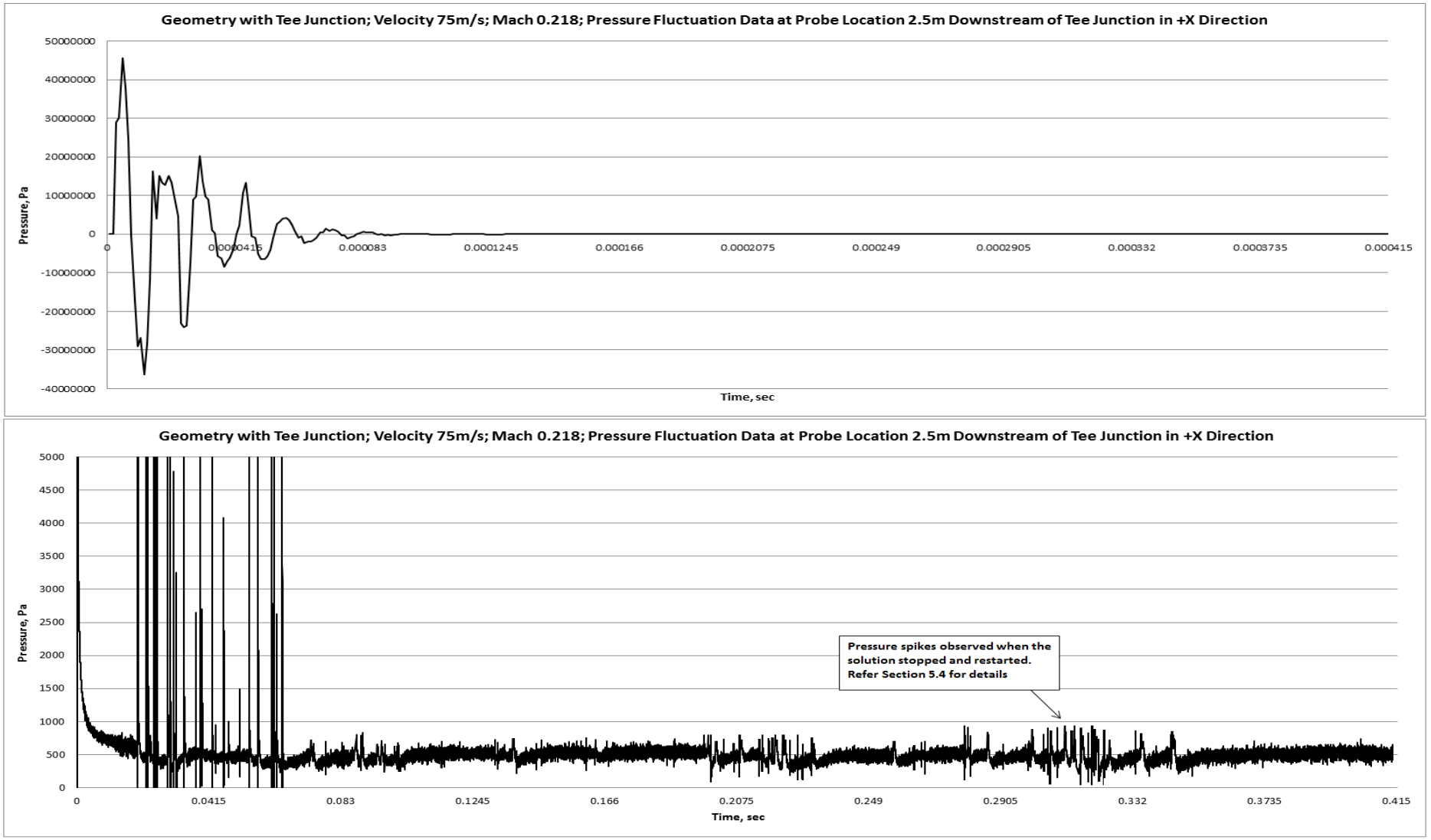

Figure 5.18: Pressure Fluctuations at Probe Location 2.5m Downstream of the Tee Junction in +X Direction for air flowing with a velocity of 75m/s

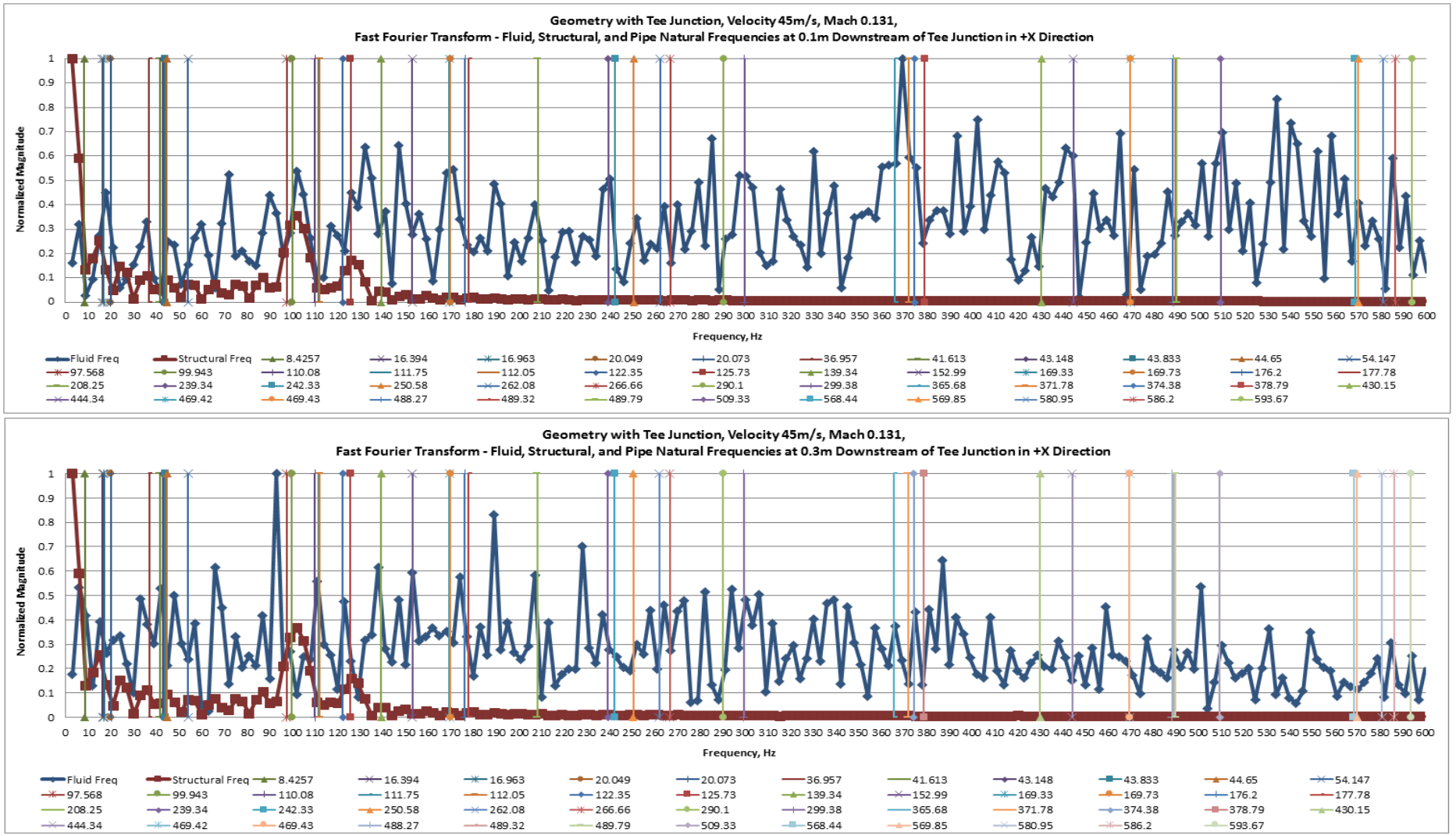

Figure 5.19: Frequency Plots at Probe Locations 0.1m and 0.3m Downstream of the Tee Junction in +X Direction for air flowing with a velocity of 45m/s

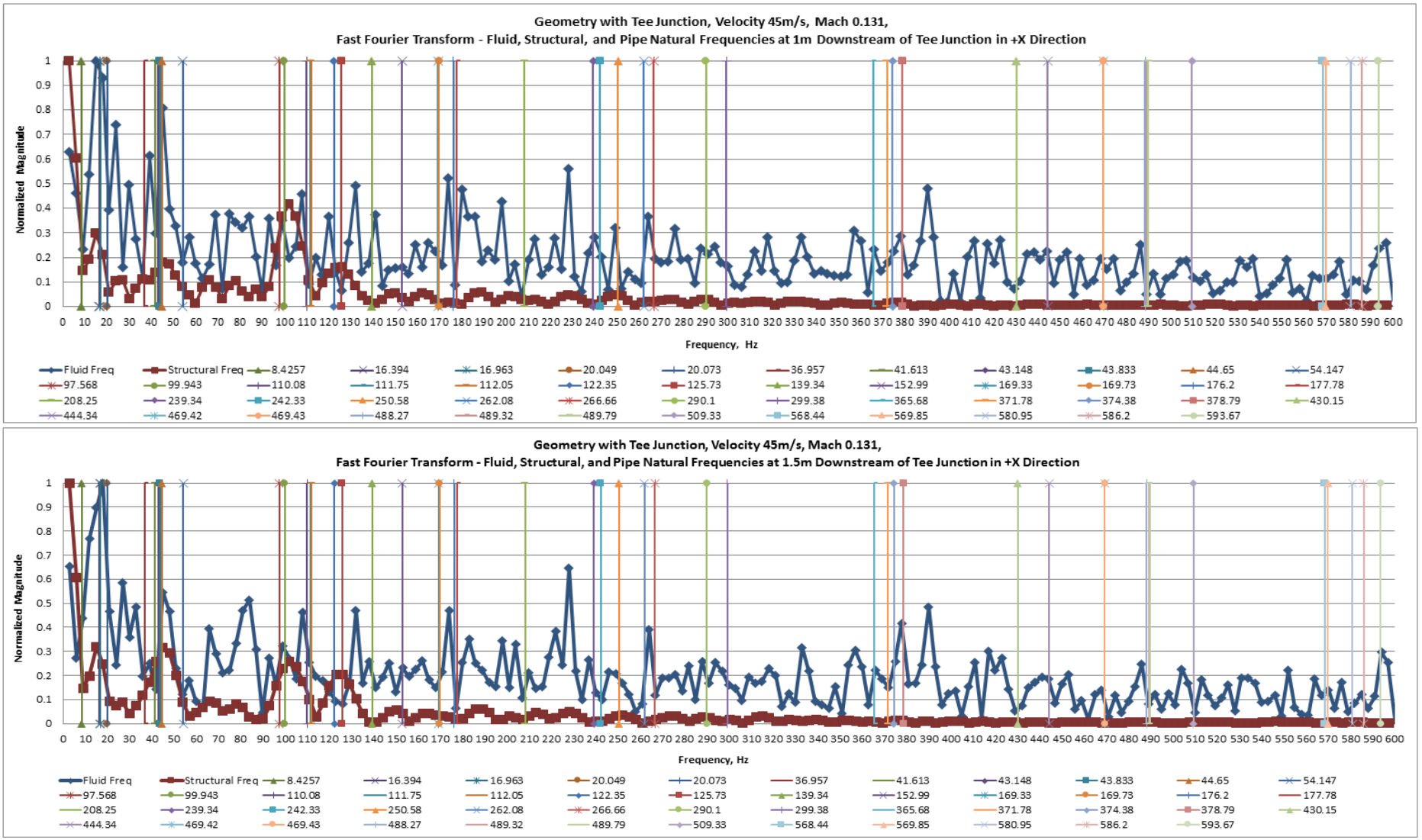

Figure 5.20: Frequency Plots at Probe Locations 1m and 1.5m Downstream of the Tee Junction in +X Direction for air flowing with a velocity of 45m/s

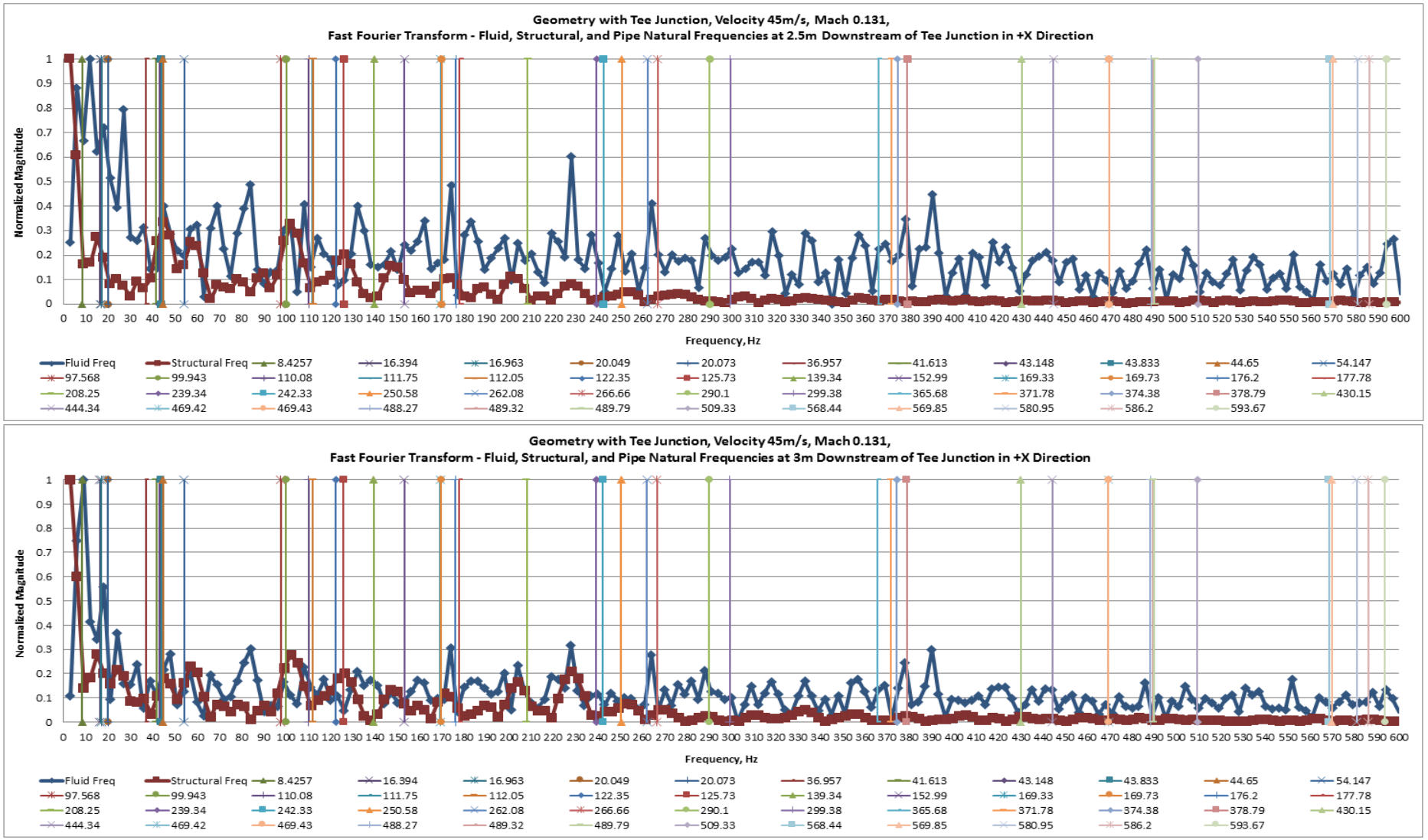

Figure 5.21: Frequency Plots at Probe Locations 2.5m and 3m Downstream of the Tee Junction in +X Direction for air flowing with a velocity of 45m/s

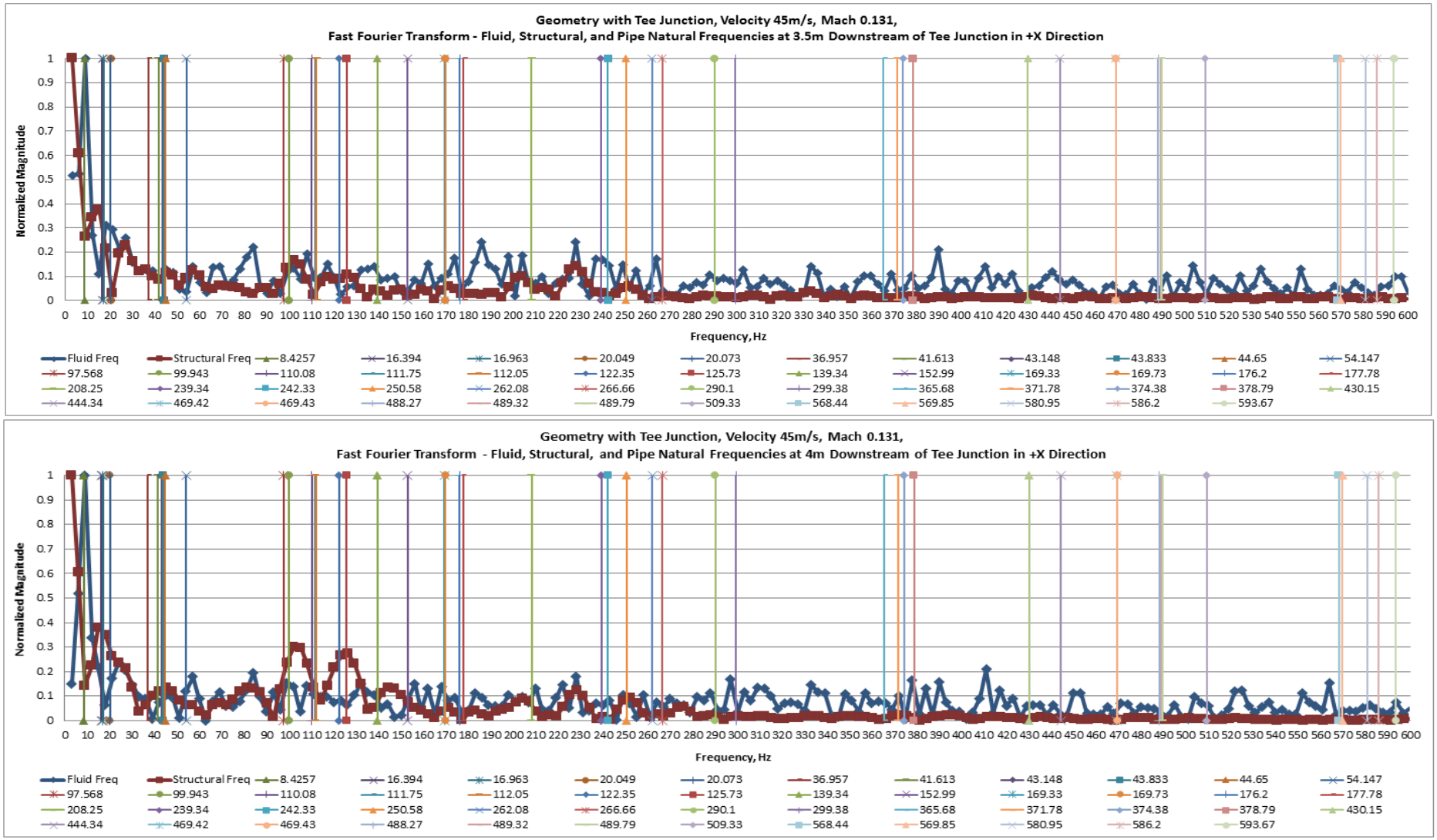

Figure 5.22: Frequency Plots at Probe Locations 3.5m and 4m Downstream of the Tee Junction in +X Direction for air flowing with a velocity of 45m/s

For air flowing at 45m/s, 3Hz had the highest magnitude in the downstream pipe. 3Hz, 24Hz, 45Hz, 228Hz, and 252Hz excited as fluid mode more times than any other frequency. These frequencies and the probe points at which these were excited are tabulated in Table 5.10.

Table 5.10: Frequencies present downstream of the Tee Junction in both directions for 45m/s

Frequency (Hz)	Mode	Probe Locations Downstream of Tee Junction in +X Direction	Probe Locations Downstream of Tee Junction in -X Direction
3	Fluid	1.0, 1.5	3.5
	Structural	0.1 – 0.5, 2.0 – 4.5	0.1 – 3.0, 4.0, 4.5
24	Fluid	0.3, 1.5, 3.0, 3.5	0.1, 0.3
	Structural	0.1, 0.5, 1.0, 2.0, 2.5, 4.0, 4.5	0.5 – 4.5
45	Fluid	0.1, 1.0 – 2.5, 3.5, 4.0	0.1, 0.3, 2.0, 4.0
	Structural	0.3, 0.5, 3.0, 4.5	0.5 – 1.5, 2.5 – 3.5, 4.5
228	Fluid	1.0, 1.5, 2.5 – 4.0	1.0, 1.5, 2.5, 3.0, 3.5
	Structural	0.1 – 0.5, 2.0, 4.5	0.1 – 0.5, 2.0, 4.0, 4.5
252	Fluid	3.0	1.5, 2.5 – 4.0
	Structural	0.1 – 2.5, 3.5 – 4.5	0.1 – 1.0, 2.0, 4.5

Fluid excited frequencies in +X direction are given in Table 5.11 below:

Table 5.11: Fluid excited frequencies present downstream of the Tee Junction in +X Direction for 45m/s

Fluid Excited Frequency in Pipe Wall ω (Hz)	Natural Frequency ω_0 (Hz)	Mode Shape	$\frac{\omega}{\omega_0}$	Normalized Magnitude
3	8.4257	2	0.36	1.000
15	16.394	3	0.91	0.298
18	20.049	5	0.90	0.537

Fluid Excited Frequency in Pipe Wall ω (Hz)	**Natural Frequency ω_0 (Hz)**	**Mode Shape**	$\frac{\omega}{\omega_0}$	**Normalized Magnitude**
24	20.049	5	1.19	0.217
27	20.049	5	1.35	0.106
36	36.957	7	0.97	0.126
45	44.65	11	1.00	0.511
54	54.147	12	1.00	0.075
57	54.147	12	1.05	0.229
66	54.147	12	1.22	0.092
69	54.147	12	1.27	0.071
75	97.568	12	0.77	0.075
87	97.568	13	0.89	0.103
102	99.943	14	0.98	0.355
117	122.35	18	0.96	0.094
126	125.73	19	1.00	0.173
132	139.34	20	0.95	0.044
138	139.34	20	0.99	0.042
144	139.34	20	0.97	0.137
147	152.99	21	0.96	0.047
159	152.99	21	0.96	0.026
162	169.33	22	0.96	0.043
165	169.33	22	0.97	0.023
174	176.2	24	0.99	0.017
183	177.78	25	0.97	0.043
198	208.25	26	0.95	0.020
204	208.25	26	0.98	0.099
213	208.25	26	0.98	0.049
228	239.34	27	0.95	0.207
252	250.58	29	0.99	0.075
270	266.66	31	0.99	0.050
333	365.68	34	0.91	0.049

Fluid excited frequencies in -X direction are given in Table 5.12.

Table 5.12: Fluid excited frequencies present downstream of the Tee Junction in -X Direction for 45m/s

Fluid Excited Frequency in Pipe Wall ω (Hz)	Natural Frequency ω_0 (Hz)	Mode Shape	$\frac{\omega}{\omega_0}$	Normalized Magnitude
3	8.4257	2	0.36	1.000
15	16.394	3	0.91	0.258
24	20.049	5	0.84	0.151
27	20.049	5	0.74	0.122
33	36.957	7	0.89	0.099
45	44.65	11	0.99	0.321
57	54.147	12	0.95	0.285
66	54.147	12	0.82	0.236
69	54.147	12	0.78	0.077
78	97.568	13	0.80	0.107
81	97.568	13	0.83	0.098
102	99.943	14	0.98	0.413
123	122.35	18	0.99	0.050
126	125.73	19	1.00	0.172
132	139.34	20	0.95	0.049
147	152.99	21	0.96	0.173
162	169.33	22	0.96	0.054
174	176.2	24	0.99	0.117
183	177.78	25	0.97	0.028
204	208.25	26	0.98	0.102
213	208.25	26	0.98	0.028
222	208.25	26	0.94	0.022
228	239.34	27	0.95	0.236
252	250.58	29	0.99	0.095
288	290.1	32	0.99	0.029
333	365.68	34	0.91	0.044

In the case of air flowing at a velocity of 60m/s, 3Hz had the highest magnitude in pipe shell wall and excited as a fluid mode at 0.1m and 1m downstream of the tee junction in –X direction. After 3Hz, 36Hz, 69Hz, 90Hz and 102Hz excited as a result of fluid forces more times than other frequencies present in the system. 102Hz was the only frequency which excited as a fluid mode without changing to structural mode once in –X direction.

The above mentioned frequencies and their excitation locations are tabulated in Table 5.13.

Table 5.13: Frequencies present downstream of the Tee Junction in both directions for 60m/s

Frequency (Hz)	Mode	Probe Locations Downstream of Tee Junction in +X Direction	Probe Locations Downstream of Tee Junction in -X Direction
3	Fluid	Not excited	0.1, 1.0
	Structural	0.1 – 4.5	0.3, 0.5, 1.5 – 4.5
36	Fluid	0.5, 3.5	0.1 – 1.0, 3.0 – 4.0
	Structural	0.1, 0.3, 1.0 – 3.0, 4.0, 4.5	2.0, 2.5, 4.5
69	Fluid	Not excited	2.0 – 3.5
	Structural	0.1 – 4.5	0.1 – 1.5, 4.0, 4.5
90	Fluid	2.0 – 3.5, 4.5	2.0, 2.5, 4.5
	Structural	0.1 – 1.5, 4.0	0.1 – 1.5, 3.0 – 4.0
102	Fluid	0.3, 1.5 – 4.0	0.1 – 4.5
	Structural	0.1, 0.5, 4.5	Not excited

Fluid excited frequencies in +X direction are given in Table 5.14.

Table 5.14: Fluid excited frequencies present downstream of the Tee Junction in +X Direction for 60m/s

Fluid Excited Frequency in Pipe Wall ω (Hz)	Natural Frequency ω_0 (Hz)	Mode Shape	$\frac{\omega}{\omega_0}$	Normalized Magnitude
15	16.394	3	0.91	0.295
18	20.049	5	0.90	0.538
24	20.049	5	0.84	0.148
36	36.957	7	0.97	0.126
42	43.148	9	0.97	0.263
54	54.147	12	1.00	0.075
60	54.147	12	0.90	0.152
66	54.147	12	0.82	0.105
75	54.147	12	0.72	0.078
81	97.568	13	0.83	0.136
87	97.568	13	0.89	0.101
90	97.568	13	0.92	0.125
102	99.943	14	0.98	0.366
126	125.73	19	1.00	0.173
129	125.73	19	0.97	0.029
138	139.34	20	0.99	0.042
144	139.34	20	0.97	0.137
150	152.99	21	0.98	0.056
159	152.99	21	0.96	0.069
165	169.33	22	0.97	0.038
180	177.78	25	0.99	0.020
183	177.78	25	0.97	0.043
213	208.25	26	0.98	0.044
252	250.58	29	0.99	0.092
333	365.68	34	0.91	0.049

Fluid excited frequencies in –X direction are given in Table 5.15.

Table 5.15: Fluid excited frequencies present downstream of the Tee Junction in -X Direction for 60m/s

Fluid Excited Frequency in Pipe Wall ω (Hz)	Natural Frequency ω_0 (Hz)	Mode Shape	$\frac{\omega}{\omega_0}$	Normalized Magnitude
3	8.4257	2	0.36	1.000
15	16.394	3	0.91	0.293
24	20.049	5	0.84	0.257
27	20.049	5	0.74	0.111
36	36.957	7	0.97	0.129
42	43.148	9	0.97	0.198
48	44.65	11	0.93	0.129
54	54.147	12	1.00	0.074
60	54.147	12	0.90	0.165
66	54.147	12	0.82	0.074
69	54.147	12	0.78	0.098
75	54.147	12	0.72	0.078
90	97.568	13	0.92	0.130
102	99.943	14	0.98	0.413
114	112.05	17	0.98	0.093
123	122.35	18	0.99	0.065
126	125.73	19	1.00	0.141
129	125.73	19	0.97	0.088
144	139.34	20	0.97	0.103
150	152.99	21	0.98	0.064
159	152.99	21	0.96	0.026
165	169.33	22	0.97	0.049
168	169.33	22	0.99	0.021
174	176.2	24	0.99	0.116
183	177.78	25	0.97	0.036
192	208.25	26	0.92	0.031
198	208.25	26	0.95	0.035
204	208.25	26	0.98	0.178
213	208.25	26	0.98	0.057
228	239.34	27	0.95	0.236

Fluid Excited Frequency in Pipe Wall ω (Hz)	Natural Frequency ω_0 (Hz)	Mode Shape	$\frac{\omega}{\omega_0}$	Normalized Magnitude
237	239.34	27	0.99	0.028
252	250.58	29	0.99	0.095
267	266.66	31	1.00	0.050
309	299.38	33	0.97	0.027
315	299.38	33	0.95	0.031

For 75m/s, the frequencies which were visible as a fluid mode in the downstream pipe at more probe points than other frequencies were 3Hz, 15Hz, 90Hz, 150Hz, and 189Hz.

The above mentioned frequencies and their probe locations are tabulated in Table 5.16.

Table 5.16: Frequencies present downstream of the Tee Junction in both directions at 75m/s

Frequency (Hz)	Mode	Probe Locations Downstream of Tee Junction in +X Direction	Probe Locations Downstream of Tee Junction in -X Direction
3	Fluid	0.1, 0.3	0.1 – 0.5, 1.5 – 4.0
	Structural	0.5 – 4.5	1.0, 4.5
15	Fluid	0.3, 3, 3.5	0.1 – 1.5, 3.0 – 4.5
	Structural	0.1, 0.5 – 2.5, 4.0, 4.5	2.0, 2.5
90	Fluid	2, 2.5, 3.5, 4.5	0.1, 2, 2.5, 3.5, 4.5
	Structural	0.1 – 1.5, 3.0, 4.0	0.3 – 1.5, 3.0, 4.0
150	Fluid	0.3, 1, 1.5, 3.5	0.5 – 1.5
	Structural	0.1, 0.5, 2.0 – 3.0, 4.0, 4.5	2.0 – 4.5
189	Fluid	1.0, 1.5, 2.5, 3.0	0.5 – 1.5, 2.5, 3.0
	Structural	0.1 – 0.5, 2.0, 3.5 – 4.5	0.1, 0.3, 2.0, 3.5 – 4.5

Fluid excited frequencies in +X direction are given in Table 5.17.

Table 5.17: Fluid excited frequencies present downstream of the Tee Junction in +X Direction for 75m/s

Fluid Excited Frequency in Pipe Wall ω (Hz)	Natural Frequency ω_0 (Hz)	Mode Shape	$\frac{\omega}{\omega_0}$	Normalized Magnitude
3	8.4257	2	0.36	1.000
15	16.394	3	0.91	0.375
24	20.049	5	0.84	0.148
33	36.957	7	0.89	0.092
45	44.65	11	0.99	0.091
66	54.147	12	0.82	0.134
75	54.147	12	0.72	0.078
90	97.568	13	0.92	0.125
99	99.943	14	0.99	0.039
102	99.943	14	0.98	0.288
129	125.73	19	0.97	0.099
144	139.34	20	0.97	0.137
150	152.99	21	0.98	0.056
159	152.99	21	0.96	0.069
183	177.78	25	0.97	0.043
189	177.78	25	0.94	0.067
198	208.25	26	0.95	0.020
210	208.25	26	0.99	0.013
213	208.25	26	0.98	0.044
243	242.33	28	1.00	0.014
249	250.58	29	0.99	0.046
255	250.58	29	0.98	0.013
264	266.66	31	0.99	0.026
276	266.66	31	0.97	0.055
288	290.1	32	0.99	0.029
306	299.38	33	0.98	0.029

Fluid excited frequencies in –X direction are given in Table 5.18.

Table 5.18: Fluid excited frequencies present downstream of the Tee Junction in -X Direction for 75m/s

Fluid Excited Frequency in Pipe Wall ω (Hz)	Natural Frequency ω_0 (Hz)	Mode Shape	$\frac{\omega}{\omega_0}$	Normalized Magnitude
3	8.4257	2	0.36	1.000
15	16.394	3	0.91	0.364
24	20.049	5	0.84	0.151
33	36.957	7	0.89	0.099
45	44.65	11	0.99	0.181
48	44.65	11	0.93	0.129
66	54.147	12	0.82	0.236
75	54.147	12	0.72	0.078
90	97.568	13	0.92	0.130
102	99.943	14	0.98	0.363
126	125.73	19	1.00	0.156
129	125.73	19	0.97	0.088
138	139.34	20	0.99	0.041
144	139.34	20	0.97	0.103
150	152.99	21	0.98	0.064
159	152.99	21	0.96	0.056
189	177.78	25	0.94	0.077
198	208.25	26	0.95	0.034
201	208.25	26	0.97	0.027
210	208.25	26	0.99	0.018
249	250.58	29	0.99	0.047
264	266.66	31	0.99	0.021
276	266.66	31	0.97	0.050
288	290.1	32	0.99	0.035
312	299.38	33	0.96	0.023
333	365.68	34	0.91	0.044

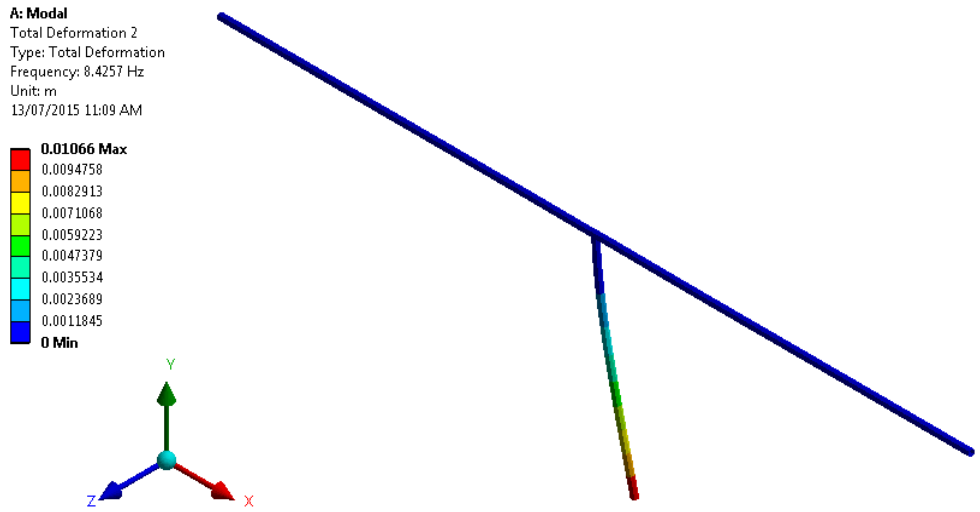

Figure 5.23: Geometry with Tee Junction – Mode Shape 2

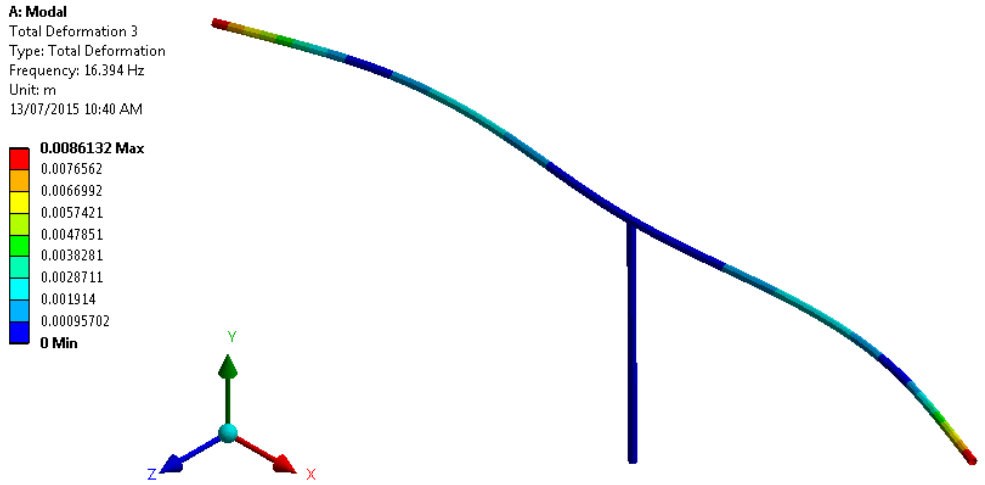

Figure 5.24: Geometry with Tee Junction – Mode Shapes 3

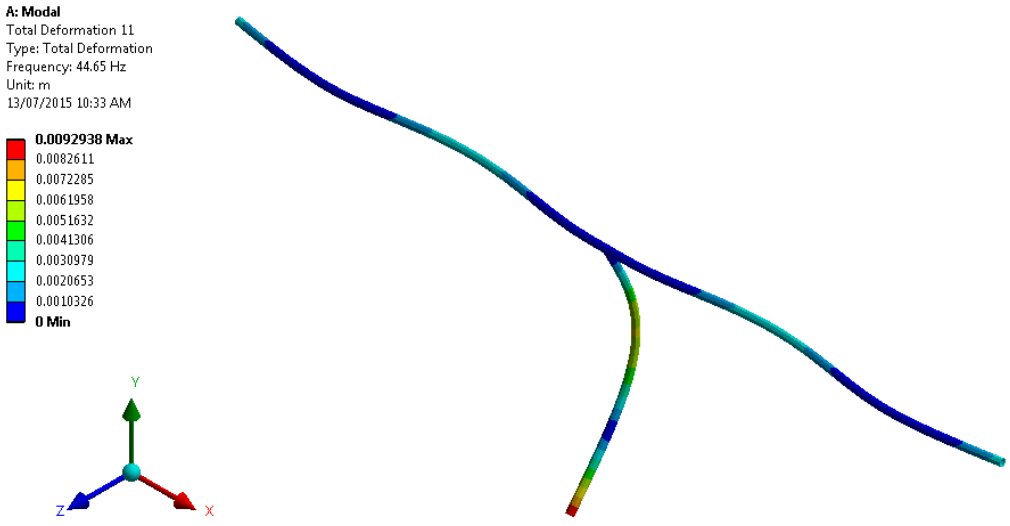

Figure 5.25: Geometry with Tee Junction – Mode Shapes 11

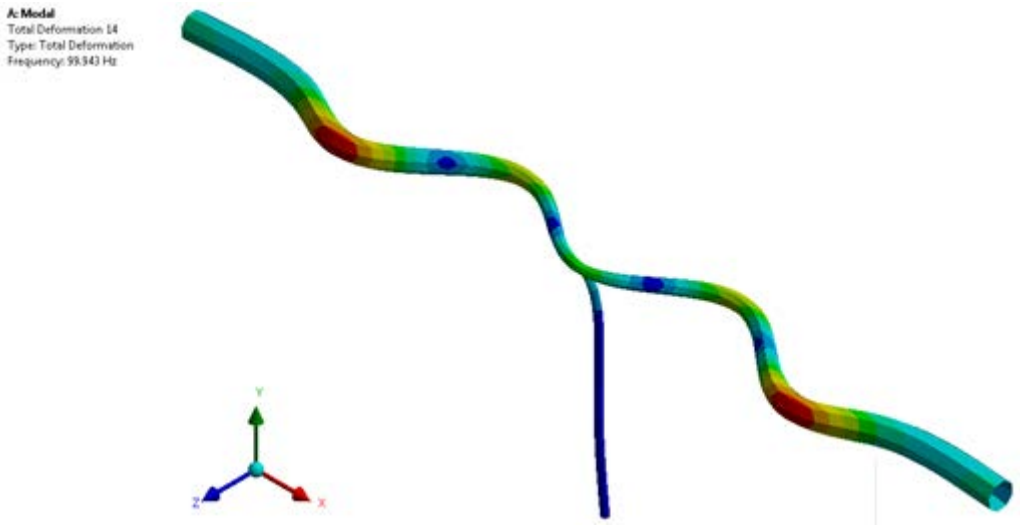

Figure 5.26: Geometry with Tee Junction – Mode Shape 14

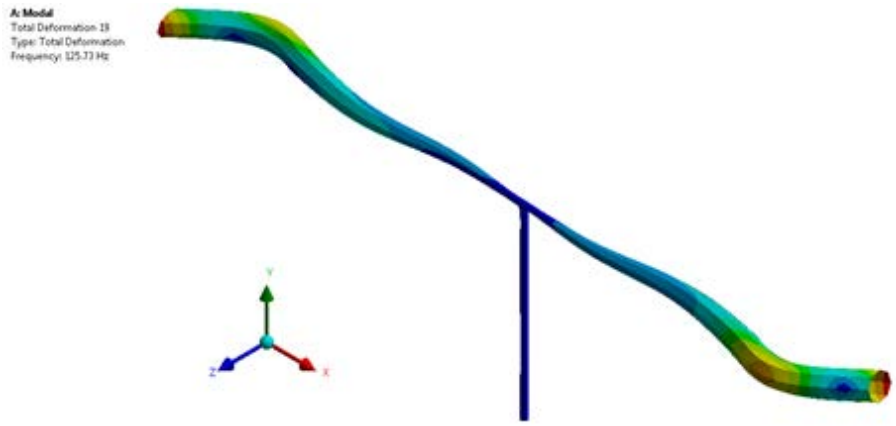

Figure 5.27: Geometry with Tee Junction – Mode Shape 19

5.5 Comparison of Results

For the geometry with 90^0 mitred bend, the velocity profile obtained using LES at a distance of 3.5m downstream from the bend exhibited good agreement with the analytical solution. In the geometry with tee junction, the flow developed but did not reach the fully developed profile in the downstream pipe sections. Also, the flows in the downstream pipe sections of the tee geometry reached a pseudo steady state earlier than the flows in the pipe downstream of the 90^0 mitred bend. This is due to the fact that the flow divided at the tee junction and velocity in downstream pipe sections decreased. In the 90^0 bend, velocity had increased in the immediate vicinity of the bend from what it was after the flow had suffered a change in direction.

For all three velocities in both geometries, 3Hz had the highest magnitude in pipe shell wall. With air flowing through the geometry having 90^0 bend at 45m/s, none of the frequencies

tabulated appeared completely as a fluid mode in the downstream pipe. All frequencies displayed mode changing at different probe locations. At 60m/s, 3Hz and 69Hz excited as fluid mode completely and at 75m/s, 30Hz and 57Hz excited as fluid mode throughout the complete downstream section. In tee geometry, for air flowing at 60m/s, 102Hz was the only frequency that excited completely as a fluid mode in –X direction throughout the downstream section. Since the frequencies excited in fluid or structural mode without any pre-defined principle, excitation may be different for different flow velocities for fluids with different densities flowing in the same geometries. These also depend upon support arrangement. If supports are placed closer or different type of supports are used for example, U-bolts or other structural supports which hold the pipe firmly to the support on which it is resting and the pipe cannot move, magnitudes of frequencies may diminish.

In the geometry with 90^0 mitred bend, after the flows had undergone a change in direction at the bend, frequencies excited initially were of higher magnitudes. These magnitudes decreased as the distance increased from the mitred section as a general trend. While the flow was developing in the downstream pipe, the magnitudes of frequencies were higher. When the flow had developed fully, these magnitudes diminished. Hence, the instability generated at the bend was overcome by the viscous forces present inside the fluid. This study determined that the flow had developed downstream of the 90^0 mitred bend at x/D = 48 against x/D = 53 found by Norton [2] in his experimental study who also used a 90^0 mitred joint. x/D is a dimensionless parameter used by Norton where x is the distance of the probe from the mitred section in the downstream pipe and D is the pipe diameter. For air flowing in the tee geometry, this was not the case. Since the flow did not fully establish in the downstream pipe sections, pipe was not filled with the boundary layer and complete downstream section was considered as hydrodynamic entrance length region. Higher frequencies of higher magnitudes were observed as the distance from the tee junction increased due to the fact that the instabilities produced as a result of flow bifurcation at the tee junction were still present.

For the geometry with 90^0 bend, except for 3Hz and 9Hz, all fluid excited frequencies were within a ratio of 0.8 to 1 with the natural frequencies of the geometry obtained from modal analysis. For tee geometry, except for 3Hz, all frequencies were within a ratio of 0.7 to 1 with the natural frequencies of the geometry obtained from modal analysis. Hence, 15Hz and higher were more likely to cause resonance as they all were in close vicinity of the natural frequencies. Modal analysis of both geometries performed by changing support locations

resulted in small variations in the natural frequencies. However, since those natural frequencies were still in close proximity to the natural frequencies obtained for the geometries with the way these were supported in the project, the ratios of fluid excited frequencies to the natural frequencies may show minor variations or remain same as their existing values.

Frequencies in the mitred bend geometry were evaluated till the natural frequencies associated with Mode Shape 13; whereas, in tee geometry, these were studied till Mode Shape 33, the reason being the fact that higher frequencies excited with an increase in magnitudes as the distance from the tee junction increased.

5.6 Method Evaluation

This method is suitable for determining flow induced vibrations in pipe geometries. The velocity profile provided good conformity with the analytical solution. The flow was established during this study at approximately the same distance as in the experimental study by Norton [2], which supported the fact that flow development was accurately captured. Hence pressure data was used with confidence. One way Fluid Structure Interaction was performed using Direct Computing method, theory of which was explained in Section 3.14. This method was used for this project because the air flow inside the pipe geometries caused extremely small displacements. Displacements of the order of 10^{-6}mm were observed in the pipe downstream of the 90^0 mitred joint. Displacements on either side of the tee junction were between 10^{-9}mm and 10^{-6}mm. Fluid and structural models are solved separately but the time step for running the simulations in structural model was the same as that used to obtain the surface pressure data from CFD. The modes which caused resonance were identified. This method can also be used for compressible flows and identify other higher frequencies which cannot be seen here as density would also play its part.

This method has highlighted the difference in the way frequencies are excited in different pipe geometries. It is resource intensive because of the fact that extremely dense mesh is required to capture the pressure fluctuations on the pipe wall and subsequently map the pressure data on the structural geometry to determine the structural response. The results obtained from this work can be used as a reference for engineers.

Flow entering an elbow or a tee junction may have disturbances imposed on it due to the fact that the inlet of the pipe may be connected to a pump, compressor or a turbine. In this work, these disturbances were ignored.

6

CONCLUSION

This thesis has presented and discussed the frequency response of two pipe geometries by modelling air flow at three speeds; 45m/s, 60m/s, and 75m/s. The first geometry had two pipes connected at 90^0 to each other forming a mitred bend. The second geometry had one vertical pipe connected to a horizontal pipe in the middle, thus forming a tee junction. Mitred bends and tees are commonly used in industry and an understanding of the factors that may contribute to their failure is of fundamental significance. Research literature on the fluid modelling in elbows to understand and optimise process parameters is available however this research is original and novel because Large Eddy Simulation was used for the first time to capture the frequencies present in the fluid that were a source of vibrations in pipe geometries.

Large Eddy Simulation (LES) was used to model the fluid flow in OpenFOAM. LES is resource intensive but due to its success as reviewed in Chapter 2, it was used for this project. One Eddy Equation Model was used for SGS modelling as described in Section 3.6. The models were evaluated for mesh independence. Mesh independence was checked for both geometries using LES at the highest velocity i.e., 75m/s. After several runs, when it was observed that the results did not change between subsequent meshes, final meshes were selected for running the simulations at other speeds. Velocity profile obtained from the

numerical simulations in the pipe downstream of 90^0 mitred bend displayed a similarity to the analytical solution obtained by Chant's equation 5.1.

After resolving the fluid models for all velocities, the obtained surface pressure data was imposed on the pipe structural model to perform a transient analysis. The frequencies present in the flow were then compared with the frequencies excited in the pipe structural model to understand which fluid frequencies contributed to the excitation of structural frequencies in the pipe shell wall. This work provided the reader with an understanding of the fluid flow conditions in pipe geometries once the flow had undergone discontinuities present in pipe geometries such as mitred joints and tees and the differences in the frequency excitation in pipe shell wall.

Key observations identified are:

The distance at which the flow had developed in the pipe downstream of the 90^0 mitred bend is approximately the same as that at which the flow had established in the experimental study conducted by Norton. The flow had developed downstream of the 90^0 mitred joint at x/D = 48 against x/D = 53 found by Norton [2] in his experimental study using different fittings including a 90^0 mitred bend. This difference is due to the fact that the distances between the probe locations selected for this project are different from the locations used by Norton. This study showed that the flow was fully developed at a distance within 10% of the region identified in Norton's experiment. Therefore, this method can be considered as one which can predict turbulence in pipes and confidently used to model pipe flows.

In the pipe downstream of the 90^0 mitred bend, a smooth velocity profile of air flow was obtained, whereas in the pipe sections downstream of the tee junction, the flow profile did not develop completely. This demonstrated that the hydrodynamic entrance region of the flow entering the downstream section of the tee geometry is long as compared to that of the flow entering the pipe downstream of a 90^0 mitred bend. Hydrodynamic entrance region in defined as the region from the point where flow has entered till the point where flow has developed completely. In the pipe sections downstream of the tee junction, despite the fact that Reynolds number had reduced after the flow bifurcated at the tee junction, the entrance length increased and effects of disturbance due to flow bifurcation and change in direction were seen to affect the velocity profile till the end of the

downstream pipe sections. There is a possibility that if a bigger length of pipe was modelled as a downstream, profile could have developed.

In the geometry with 90^0 mitred bend, the first few frequencies had high magnitudes, first being the highest and the remaining frequencies following with reduced magnitudes. In tee geometry, as the distance from the tee junction increased, high frequencies increased in magnitudes till finally diminishing at 4.5m downstream of the tee junction. This insight gives the rule of thumb that that the pipe support immediately after a bend is exposed to low frequency vibrations. In case of a tee, the supports located immediately after a tee are exposed to low frequency vibrations and the supports at some distance away from the tee junction are exposed to high frequency vibrations. Hence, design criteria for the supports should be different as these frequencies may be damaging to the system.

Mode changing was observed for frequencies in both geometries i.e., frequencies changed from a fluid to structural and structural to fluid mode. In case of geometry with the 90^0 bend, some frequencies excited as a fluid mode only when air was modelled to flow at 60m/s and 75m/s. In tee geometry, only one frequency excited completely as a fluid mode in –X direction at 60m/s. This should not be taken as a principle. The number of frequencies resulting from fluid excitation and their values may change with the density and velocity of fluid and the way pipe is supported.

Due to higher frequencies increasing in magnitudes with the increase in distance from the tee junction, mode shapes considered for resonating frequencies were more as compared to those considered for mitred bend geometry. Against the general understanding that due to flow discontinuities in pipes, highest excitation levels are concentrated at low frequencies, typically below 100Hz [32], this research has identified that at high speeds like 45m/s and above, frequencies from 270Hz to 360Hz may also show high excitation in pipes downstream of the tee junctions which may in turn lead to high frequency vibration modes in pipes.

Using this method, circumferential mode of vibrations and their magnitudes can be obtained and regions can be determined where the circumferential modes of a pipe may change to a lateral mode.

This study is novel and significant because a detailed LES was performed to model turbulence and capture pressure fluctuations on the pipe walls. The results from CFD were

coupled with Transient Finite Element Analysis to perform Fluid Structure Interaction in pipe geometries. This method has identified the difference in the excitation of frequencies in pipe sections downstream of a tee junction against a 90^0 mitred bend. In pipe sections downstream of a tee junction, higher frequencies are excited with greater magnitudes as the distance increased from the tee junction. These frequencies may damage the system and should be taken into account when designing the pipe supports.

Due to the significant amount of computational cost involved, this technique is still academic. For this reason, combinations of multiple fittings were not investigated in this thesis. Engineers in industry may use these results to broaden their understanding of fluid flows and vibrations in piping systems and in the presence of a tee junction, should use supports that can isolate vibration levels at higher frequencies for a significant length on each side of the tee. This technique allows the effectiveness of vibration reducing devices to be predicted.

Isolation reduces the transmitted vibration response of a system by rearranging energy so that force is opposed by inertia (mass). Resilient supports (isolators), typically elastomeric, spring, and pneumatic, decouple a system from force inputs, and cause the isolated system to be out of phase with the force inputs. Isolators are sized according to the load on the isolators, the f_n of the isolated system, and the frequency of the force input [72].

Another method is to use U-clamps which fix the pipe firmly to the structural support on which the pipe is resting. A third option may be to add masses at the locations where frequency of the pipes is closer to the natural frequency by adding small pipe pieces welded around the pipe carrying fluid. This will give additional mass to the system at the specific locations and hence the vibration response will be altered.

Future study is possible using this method for single phase or multiphase flow to determine the frequencies and design piping systems and their supports to avoid excessive vibration levels. Further research in flows in piping systems having tee junctions is possible to identify why higher frequencies excited with increased magnitudes as the distance from the tee junction increased and why parabolic velocity profile was not established.

7

REFERENCES

1. M. P. Norton, D. G. Karczub, Fundamentals of Noise and Vibration Analysis for Engineers, 2nd ed. Cambridge Univ. Press, 2003, pp. 442.
2. M. P. Norton, The effects of internal flow disturbances on the vibration response of and the acoustic radiation from pipes, PhD Dissertation, Dept. Mech. Eng., University of Western Australia, 1979.
3. The Pawsey Supercomputing Centre, https://www.pawsey.org.au/
4. S. M. Price, D. R. Smith, Proc. 28th Turbomachinery Symp., Sources and remedies of high-frequency piping vibration and noise, http://turbolab.tamu.edu/proc/turboproc/T28/Vol28019.pdf
5. M. A. Leschziner, Modeling turbulent recirculating flows by finite-volume methods–current status and future directions, Int. J. Heat and Fluid Flow, Vol. 10, Sept. 1989.
6. Bruce R. Munson, Donald F. Young, Theodore H. Okiishi, Fundamentals of Fluid Mechanics, 4th ed. John Wiley & Sons, Inc., 2002, pp. 448.
7. Ansys Element Reference, Release 12.1, Part I – Element Library, 2009, pp. 1173.
8. L. J. De Chant, The venerable 1/7th power law turbulent velocity profile: a classical nonlinear boundary value problem solution and its relationship to stochastic processes, Appl. Math. and Computation, Vol. 161, pp. 463-474, 2005.
9. Energy Institute, Guidelines for the avoidance of Vibrations Induced Fatigue Failure in Process Pipework, 2nd ed. 2008, pp. 125.

10. F. T. M. Nieuwstadt, J. G. M. Eggels, R. J. A. Janssen, M. B. J. M. Pourquie, Direct and large-eddy simulations of turbulence in fluids, Future Generation Comput. Syst., Vol. 10, pp. 189-205, 1994.

11. Lin-Wen Hu, M. S. Kazimi, LES benchmark study of high cycle temperature fluctuations caused by thermal striping in a mixing tee, Int. J. Heat and Fluid Flow, Vol. 27, pp. 54–64, 2006.

12. T. Ming, J. Zhao, Large-eddy simulation of thermal fatigue in a mixing tee, Int. J. Heat and Fluid Flow, Vol. 37, pp. 93–108, 2012.

13. V.S. Naik-Nimbalkar, A.W. Patwardhan, I. Banerjee, G. Padmakumar, G. Vaidyanathan, Thermal mixing in T-junctions, Chemical Eng. Sci., Vol. 65, pp. 5901–5911, 2010.

14. Wei-Yu Zhu, T. Lu, Pei-Xue Jiang, Zhi-Jun Guo, Kui-Sheng Wang, Large eddy simulation of hot and cold fluids mixing in a T-junction for predicting thermal fluctuations, Appl. Math. and Mechanics, Vol. 30(11), pp. 1379–1392, 2009.

15. H. K. Versteeg, and W. Malalasekera, An Introduction to Computational Fluid Dynamics, 2nd ed. Pearson Educ. Limited, 2007, pp. 99-100.

16. C. Michler, S.J. Hulshoff, E.H. van Brummelen, R. de Borst, Monolithic Approach to Fluid-Structure Interaction, Comput. and Fluids, Vol. 33, pp. 839-848, Jun 2004.

17. F. K. Benra, H. J. Dohmen, J. Pei, S. Schuster, and B. Wan, A Comparison of One-Way and Two-Way Coupling Methods for Numerical Analysis of Fluid-Structure Interactions, Journal of Applied Mathematics, Vol. 2011 (2011), Article ID 853560, 16 pages, http://dx.doi.org/10.1155/2011/853560

18. D. Bjurhede, M. Harryson, A comparative study of coupled and uncoupled analysis methods for thermohydraulic loads in piping systems, Masters Dissertation, Dept. Construction Sciences, Structural Mechanics, Lund University, 2012.

19. U. Piomelli, J. R. Chasnov, Large Eddy Simulations: Theory and Applications, Turbulence and Transition Modelling, Vol. 2 of the series ERCOFTAC Series, 1996, pp. 269-336.

20. David C. Wilcox, Turbulence Modeling for CFD, DCW Industries, Inc., 3rd ed. 2006, pp. 5.

21. H. K. Versteeg, and W. Malalasekera, An Introduction to Computational Fluid Dynamics, 2nd ed. Pearson Educ. Limited, 2007, pp. 42-43.

22. W. W. Willmarth, Pressure Fluctuations beneath Turbulent Boundary Layers, Annu. Review of Fluid Mechanics, Vol. 7, 1975, pp. 13-36.

23. P. H. White, R. J. Sawley, Energy Transmisson in Piping Systems and Its Relation to Noise Control, ASME J. Manuf. Sci. and Eng. Vol. 94, Issue 2, pp. 746-751.

24. K. Avila, D. Moxey, A. Lozar, M. Avila, D. Barkley, B. Hof, The Onset of Turbulence in Pipe Flow, SCIENCE, www.science.org, Vol. 333, Jul 2011.

25. Ansys Mechanical APDL Theory Reference, Release 14.5, Chapter 17.2 – Transient Analysis, Chapter 17.2.2.1, 2012, pp. 839.

26. A. Yoshizawa, A Statistically-Derived Subgrid-Scale Kinetic Energy Model for the Large-Eddy Simulation of Turbulent Flows, J. Physical Soc. Japan, 54, No. 8, Aug. 1985, pp. 2834-2839.

27. J. Blazek, Computational Fluid Dynamics: Principles and Applications, Chapter 7, Elsevier, 2001, pp. 226.

28. M. T. Landahl, E. Mollo-Christensen, Turbulence and Random Processes in Fluid Mechanics, 2nd ed. Cambridge Univ. Press, 1992, pp. 10.

29. E. Wang, T. Nelson, CADFEM GmbH, Munich, Germany, Structural Dynamic Capabilities of ANSYS, http://www.ansys.com/staticassets/ANSYS/staticassets/resourcelibrary/confpaper/2002-Int-ANSYS-Conf-200.PDF

30. H. K. Versteeg, and W. Malalasekera, An Introduction to Computational Fluid Dynamics, 2nd ed. Pearson Educ. Limited, 2007, pp. 2-4.

31. Alan V. Oppenheim, Ronald W. Schafer, John R. Buck, Discrete-Time Signal Processing, 2nd ed. Prentice Hall, Inc., 1998, pp. 541-630.

32. Energy Institute, Guidelines for the avoidance of Vibrations Induced Fatigue Failure in Process Pipework, 2nd ed. 2008, pp. 7.

33. Alan V. Oppenheim, Ronald W. Schafer, John R. Buck, Discrete-Time Signal Processing, 2nd ed. Prentice Hall, Inc., 1998, pp. 146.

34. OpenFOAM User Guide: 4.1 File structure of OpenFOAM cases, http://www.openfoam.org/docs/user/case-file-structure.php

35. Ansys Mechanical APDL Theory Reference, Release 14.5, Chapter 17.3 – Mode Frequency Analysis, Section 17.3.2, 2012, pp. 853.

36. R. I. Issa, Solution of the Implicitly Discretised Fluid Flow Equations by Operator-Splitting, J. Computational Physics, Vol. 62, 1985, pp. 40-65.

37. J. C. Wachel, S. J. Morton, K. E. Atkins, Piping Vibration Analysis, Proc. 19th Turbomachinery Symp., 1990, http://www.engdyn.com/images/uploads/57-piping_vibration_analysis_-_jcw&kea.pdf

38. C. Fureby, A. D. Gosman, G. Tabor, H. G. Weller, N. Sandham, M. Wolfshtein,, Large Eddy Simulation of Turbulent Channel Flows, Proc. Turbulent Shear Flows 11, Vol. 3, pp. 28-13, 1997.

39. U. Piomelli, A. Scotti, E. Balaras, Large-Eddy Simulation of Turbulent Flows, from Desktop to Supercomputer, Invited Talk, Vector and Parallel Processing — VECPAR 2000, Vol. 1981 of the series Lecture Notes in Comput. Sci., May 2001, pp. 551-577.

40. U. Piomelli, Large-eddy simulation: achievements and challenges, Progress Aerospace Sciences, Vol. 35, Issue 4, May 1999, pp. 335-362.

41. J. P. Boris, F. F. Grinstein, E. S. Oran, R. L. Kolbe, New Insights into Large Eddy Simulation, Naval Research Laboratory Washington, DC 20375-5000, NRL/MR/4400-92-6979, Apr. 30 1992, http://citeseerx.ist.psu.edu/viewdoc/download?doi=10.1.1.455.1369&rep=rep1&type=pdf

42. P. Moussou, P. Lafon, S. Potapov, L. Paulhiac, A. S, Tijsseling, Industrial cases of FSI due to internal flows, http://www.win.tue.nl/analysis/reports/rana04-04.pdf

43. J. V. Rattayya, M. C. Junger, Flow excitation of cylindrical shells and associated coincidence effects, J. Acoust. Soc. America, Vol. 36, No. 5, May 1964.

44. F. J. Nieves, F. Gascon, A. Bayon, An analytical, numerical and experimental study of the axisymmetric vibrations of a short cylinder, J. Sound and Vibrations, Vol. 313, pp. 617-630, 2008.

45. M. P. Païdoussis, Real-life experiences with flow-induced vibration, J. Fluids and Structures, Vol. 22, pp. 741-755, 2006.

46. P. R. Stepanishen, Modal coupling in the vibration of fluid loaded cylindrical shells, J. Acoust. Soc. America, Vol. 71, Apr. 1982.

47. M. K. Bull, M. P. Norton, The proximity of coincidence and acoustic cut-off frequencies in relation to acoustic radiation from pipes with disturbed internal turbulent flow, J. Sound and Vibration Vol. 69(1), pp. 1-11, 1980.

48. M. K. Bull, M. P. Norton, Mechanisms of the generation of external acoustic radiation from pipes due to internal flow disturbances, J. Sound and Vibration, Vol. 94(1), pp. 105-146, 1984.

49. M. El-Raheb, Vibrations of three dimensional pipe systems with acoustic coupling, J. Sound and Vibration, Vol. 78(1), pp. 39-67, 1981.

50. C. R. Fuller, The Effects of Wall discontinuities on the propagation of flexural waves in cylindrical shells, J. Sound and Vibration Vol. 75(2), pp. 207-228, 1981.

51. M. Rumerman, S. Raynor, Natural Frequencies Of Finite Circular Cylinders In Axially Symmetric Longitudinal Vibration, J. Sound and Vibration, Vol. 15(4), pp. 529-543, 1971.

52. G. H. Koo, Y. S. Park, Vibration Reduction by using Periodic supports in a piping system, J. Sound and Vibration, Vol. 210(1), pp. 53-68, 1998.

53. R. N. Arnold, G. B. Warburton, Flexural Vibrations Of The Walls Of Thin Cylindrical Shells Having Freely Supported Ends, Proc. Royal Soc. London, Series A, Math. Physical Sci., Vol.197, Issue 1049, pp. 238-256, 1948.

54. B. J. Brevart, C. R. Fuller, Effect of an Internal Flow on the Distribution of Vibrational Energy in an Infinite Fluid-Filled Thin Cylindrical Elastic Shell, J. Sound and Vibration, Vol. 167(1), pp. 149-163, 1993.

55. C. R. Fuller, F. J. Fahy, Characteristics Of Wave Propagation And Energy Distributions In Cylindrical Elastic Shells Filled With Fluid, J. Sound and Vibration Vol. 81(4), pp. 501-518, 1982.

56. Y. C. Fung, A. Kaplan, E. E. Sechler, On the Vibration of Thin Cylindrical Shells under Internal Pressure, The Ramo-Woolridge Corporation Report No. AM 5-8, October 14, 1955. http://www.dtic.mil/dtic/tr/fulltext/u2/607517.pdf

57. Y. Huang, G. Zeng, F. Wei, A New Matric Method for Solving Vibration and Stability of Curved Pipes Conveying Fluid, J. Sound and Vibration, Vol. 251(2), pp. 215-225, 2002.

58. V. Mason, Some Experiments On The Propagation Of Sound Along A Cylindrical Duct Containing Flowing Air, J. Sound and Vibration, Vol. 10(2), pp. 228-226, 1969.

59. E. G. Williams, Structural intensity in thin cylindrical shells, J. Acoust. Soc. America, Vol. 89, Number 4, Pt. 1, Apr. 1991.

60. M. Heckl, Vibrations of Point-Driven Cylindrical Shells, J. Acoust. Soc. America, Vol. 34, No. 10, Oct. 1962.

61. M. C. Junger, F. J. Rosato, The Propagation of Elastic Waves in Thin-Walled Cylindrical Shells, J. Acoust. Soc. America, Vol. 26, No. 5, Sept. 1954.

62. M. K. Bull, Wall-pressure fluctuations associated with subsonic turbulent boundary layer flow, J. Fluid Mechanics, Vol. 28, Part 4, pp. 719-754, 1967.

63. P. J. Mulhearn, On the structure of pressure fluctuations in turbulent shear flow, J. Fluid Mechanics, Vol. 71, Part 4, pp. 801-813, 1975.

64. M. T. Pittard, R. P. Evans, R. D. Maynes, J. D. Blotter, Experimental and numerical investigation of turbulent flow induced pipe vibration in fully developed flow, Review of Scientific Instruments 75, 2393, 2004.

65. Qing, M., Jinghui, Z., Orifice-induced Wall Pressure Fluctuations and Pipe Vibrations: Theory and Modeling of Fluid Excitations, Flow Turbulence And Combustion, 2007, Vol.79(1), pp.25-40.

66. G. C. Lauchle, M. A. Daniels, Wall pressure fluctuations in turbulent pipe flow, Phys. Fluids, Vol. 30, pp. 3019-3024, 1987.

67. J. C. Wachel, Displacement Method for determining acceptable piping vibration amplitudes, PVP Vol. 313-2, Int. Pressure Vessels and Piping Codes and Standards: Volume 2 – Current Perspectives ASME 1995, http://www.engdyn.com/images/uploads/72-displacement_method_for_determining_acceptable_piping_vibration_amplitudes_-_jcw.pdf

68. J. C. Wachel, D. R. Smith, Vibration Troubleshooting of Existing Piping Systems, July 1991, http://www.engdyn.com/images/uploads/59-vibration_troubleshooting_of_existing_piping_systems_-_drs&jcw.pdf

69. S. H. Lee, S. M. Ryu, W. B. Jeong, Vibration analysis of compressor piping system with fluid pulsation, J. Mech. Sci. and Technology 26 (12), pp. 3903-3909, 2012.

70. S. Saha, A Time History Method for Analyzing Operational Piping Vibrations, World J. Mechanics, 2, pp. 325-333, 2012.

71. Stephen R. Turns, Thermodynamics: Concepts and Applications, Volume 1, Cambridge University Press, 6 Mar. 2006. pp. 442.

72. Andrew K. Costain, J Michael Robichaud, Bretech Engineering Ltd., Practical Methods for Vibration Control of Industrial Equipment, http://www.bretech.com/reference/Practical%20Methods%20for%20Vibration%20Control%20of%20Industrial%20Equipment.pdf

Appendix A

Probe Locations

Geometry with 90^0 Mitred Joint Probe Locations (x,y,z) mm	**Geometry with Tee Joint Probe Locations (x,y,z) mm**
(36.27, 2000, 0)	(36.27, 2000, 0)
(36.27, 2400, 0)	(36.27, 2400, 0)
(36.27, 2600, 0)	(36.27, 2600, 0)
(100, 2798, 0)	(100, 2798, 0)
(300, 2798, 0)	(300, 2798, 0)
(500, 2798, 0)	(500, 2798, 0)
(1000, 2798, 0)	(1000, 2798, 0)
(1500, 2798, 0)	(1500, 2798, 0)
(2000, 2798, 0)	(2000, 2798, 0)
(2500, 2798, 0)	(2500, 2798, 0)
(3000, 2798, 0)	(3000, 2798, 0)
(3500, 2798, 0)	(3500, 2798, 0)
(4000, 2798, 0)	(4000, 2798, 0)
(4500, 2798, 0)	(4500, 2798, 0)
	(-100, 2798, 0)
	(-300, 2798, 0)
	(-500, 2798, 0)
	(-1000, 2798, 0)
	(-1500, 2798, 0)
	(-2000, 2798, 0)
	(-2500, 2798, 0)
	(-3000, 2798, 0)
	(-3500, 2798, 0)
	(-4000, 2798, 0)
	(-4500, 2798, 0)

Appendix B

Mesh Statistics of Fluid Volumes of Project Geometries

	Final Mesh for Geometry with 90^0 Mitred Joint	**Final Mesh for Geometry with Tee Junction**
Points	14385936	7728062
Faces	42461414	66317594
Internal Faces	41768186	64998018
Cells	14039200	31185478
Boundary Patches	3	4
Face Zones	1	1
Cell Zones	1	1
Overall number of cells of each type		
Hexahedra	14033600	6573700
Prisms	5600	24611778
Geometry		
Overall domain	(-0.03627 0 -0.03627)	(-5 0 -0.03627)
bounding box	(4.96373 2.8 0.03627)	(5 2.79999 0.03627)
Max cell openness	5.083×10^{-16}	4.746×10^{-16}
Max aspect ratio	28.1551	11.7523
Minimum face area	1.068×10^{-07}	2.199×10^{-7}
Maximum face area	9.616×10^{-06}	9.336×10^{-6}
Min volume	6.441×10^{-10}	8.406×10^{-11}
Max volume	3.096×10^{-08}	5.333×10^{-9}
Total volume	0.0319273	0.0525906
Mesh non-orthogonality		
Max	54.994	72.113
Average	24.404	14.828
Max skewness	2.483	2.330
Patch Topology		
Outlet		
Faces	5014	1640 (for both
Points	5136	1109 outlets)
Inlet		
Faces	5014	1556
Points	5136	1043
Wall		
Faces	683200	1314740
Points	683444	657509

Appendix C

Mesh Statistics of Structural Geometries

Sizing	
Use Advanced Size Function	On: Proximity and Curvature
Curvature Normal Angle	10.90^0
Proximity Accuracy	0.5
Min Size	8.3789×10^{-3} m
Proximity Min Size	8.3789×10^{-3} m
Max Face Size	4.1894×10^{-2} m
Minimum Edge Length	6.196×10^{-2} m
Statistics	
Nodes	4624
Elements	1536

Mesh Data for Pipe Structural Geometry with 90^0 Mitred Bend

Sizing	
Use Advanced Size Function	On: Curvature
Curvature Normal Angle	Default (30^0)
Min Size	8.095×10^{-3} m
Max Face Size	4.0475×10^{-2} m
Minimum Edge Length	6.196×10^{-2} m
Statistics	
Nodes	2651
Elements	2640

Mesh Data for Pipe Structural Geometry with Tee Junction

Appendix D

Structural Material Properties (Ansys Library)

Structural Steel - Constants

Density	7850 kg m^{-3}
Coefficient of Thermal Expansion	$1.2x10^{-5}$ C^{-1}
Specific Heat	434 J kg^{-1} C^{-1}
Thermal Conductivity	60.5 W m^{-1} C^{-1}
Resistivity	$1.7x10^{-7}$ ohm m
Compressive Yield Strength (Pa)	$2.50x10^{8}$
Tensile Yield Strength (Pa)	$2.50x10^{8}$
Tensile Ultimate Strength (Pa)	$4.60x10^{8}$

Structural Steel - Strain-Life Parameters

Strength Coefficient (Pa)	$9.20x10^{8}$
Strength Exponent	-0.106
Ductility Coefficient	0.213
Ductility Exponent	-0.47
Cyclic Strength Coefficient (Pa)	$1.00x10^{9}$
Cyclic Strain Hardening Exponent	0.2

Structural Steel - Isotropic Elasticity

Young's Modulus (Pa)	$2.00x10^{11}$
Poisson's Ratio	0.3
Bulk Modulus (Pa)	$1.67x10^{11}$
Shear Modulus (Pa)	$7.69x10^{10}$
Isotropic Relative Permeability	10000

Appendix E

Pressure Fluctuations and Frequency Plots for Geometry with 90^0 Mitred Bend for Fluid Velocity modelled at 45m/s, Mach 0.131 at Probe Locations

Distance	Fluid Excited Frequencies Downstream of 90 Degree Mitred Bend
0.1	3, 9, 39, 51, 60, 66, 93, 108, 135
0.3	39, 51, 60, 66, 108, 129, 135
0.5	30, 39, 60, 66, 102
1	51, 114, 123
1.5	39, 45, 66, 108
2.5	30, 39, 66, 114
3	3, 39, 66, 75, 108, 123
3.5	3, 39, 75, 81, 87, 93, 102
4	3, 18, 24
4.5	3, 9, 18, 30, 39, 66, 72, 102, 108, 135

Table E.1: Fluid excited frequencies downstream of the 90 Degree Mitred Bend for 45m/s

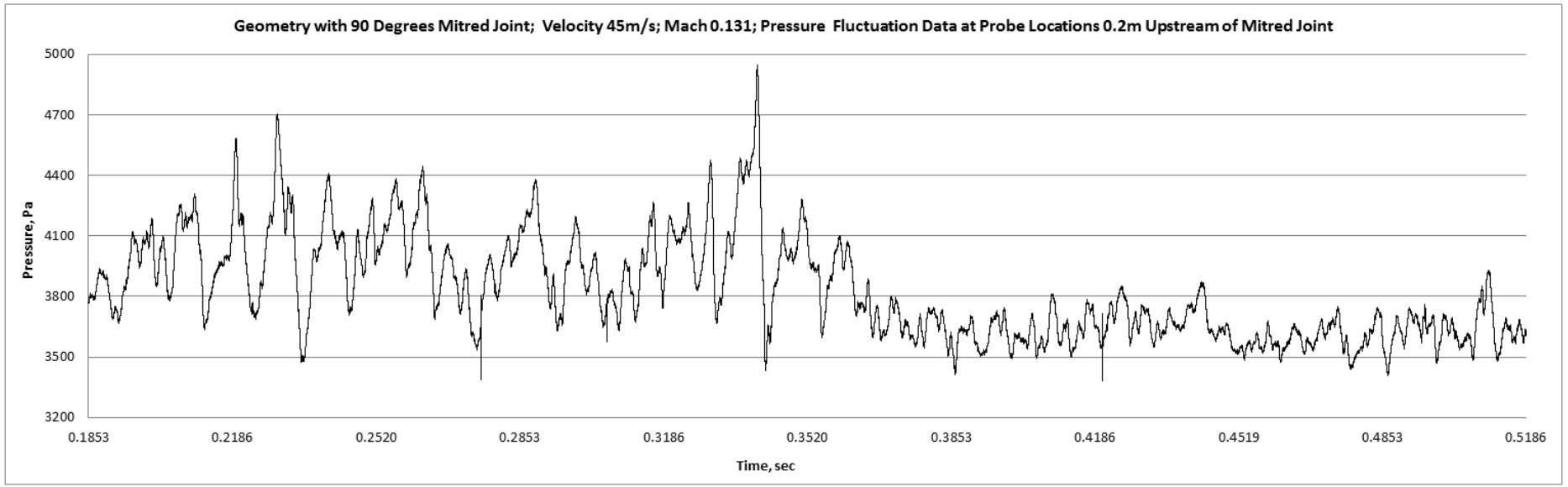
Geometry with 90 Degrees Mitred Joint; Velocity 45m/s; Mach 0.131; Pressure Fluctuation Data at Probe Locations 0.2m Upstream of Mitred Joint
Pressure, Pa
5000
4700
4400
4100
3800
3500
3200
0.1853
0.2186
0.2520
0.2853
0.3186
0.3520
0.3853
0.4186
0.4519
0.4853
0.5186
Time, sec

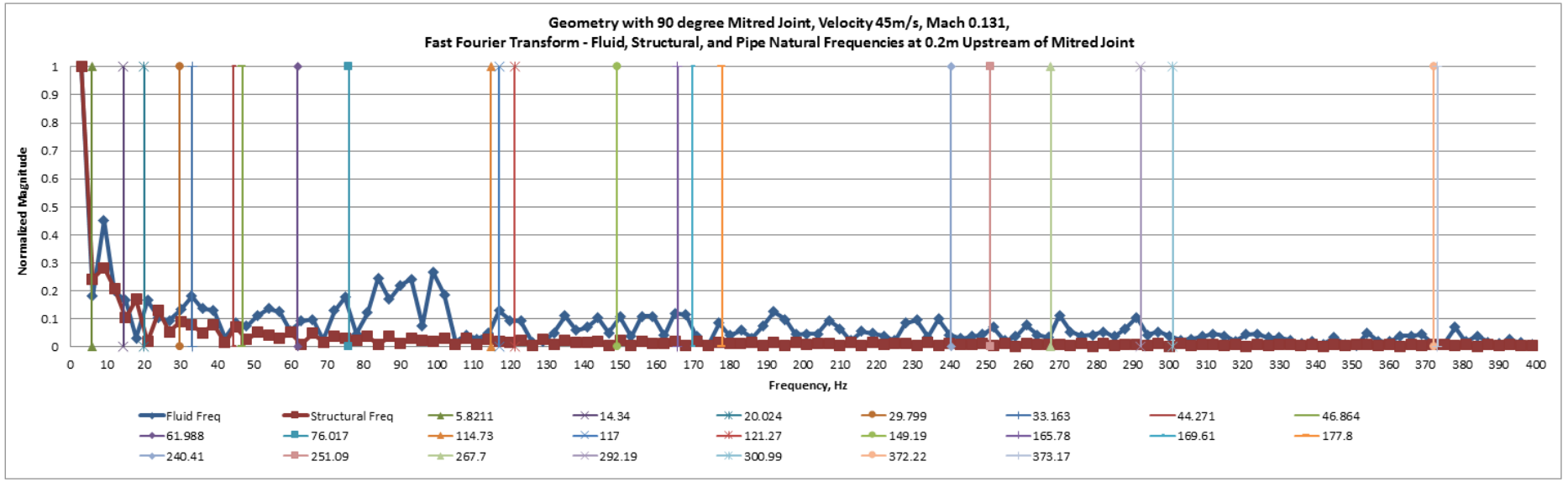
Geometry with 90 degree Mitred Joint, Velocity 45m/s, Mach 0.131,
Fast Fourier Transform - Fluid, Structural, and Pipe Natural Frequencies at 0.2m Upstream of Mitred Joint
Normalized Magnitude
1
0.9
0.8
0.7
0.6
0.5
0.4
0.3
0.2
0.1
0
0 10 20 30 40 50 60 70 80 90 100 110 120 130 140 150 160 170 180 190 200 210 220 230 240 250 260 270 280 290 300 310 320 330 340 350 360 370 380 390 400
Frequency, Hz
Fluid Freq
Structural Freq
5.8211
14.34
20.024
29.799
33.163
44.271
46.864
61.988
76.017
114.73
117
121.27
149.19
165.78
169.61
177.8
240.41
251.09
267.7
292.19
300.99
372.22
373.17

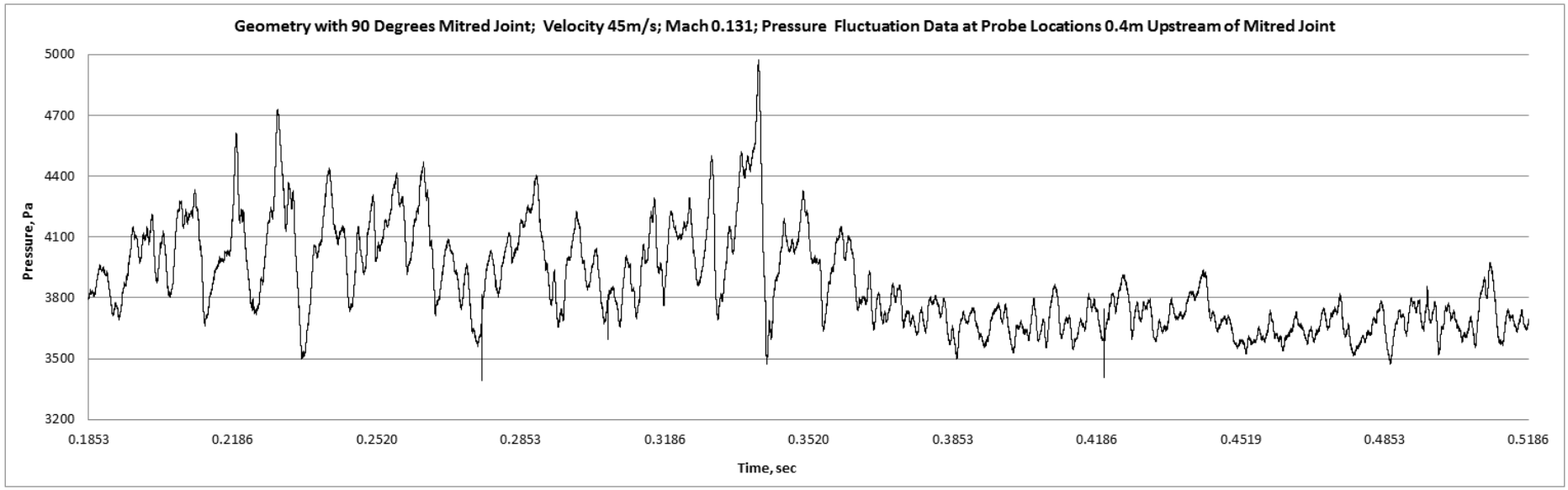
Geometry with 90 Degrees Mitred Joint; Velocity 45m/s; Mach 0.131; Pressure Fluctuation Data at Probe Locations 0.4m Upstream of Mitred Joint
Pressure, Pa
5000
4700
4400
4100
3800
3500
3200
0.1853
0.2186
0.2520
0.2853
0.3186
0.3520
0.3853
0.4186
0.4519
0.4853
0.5186
Time, sec

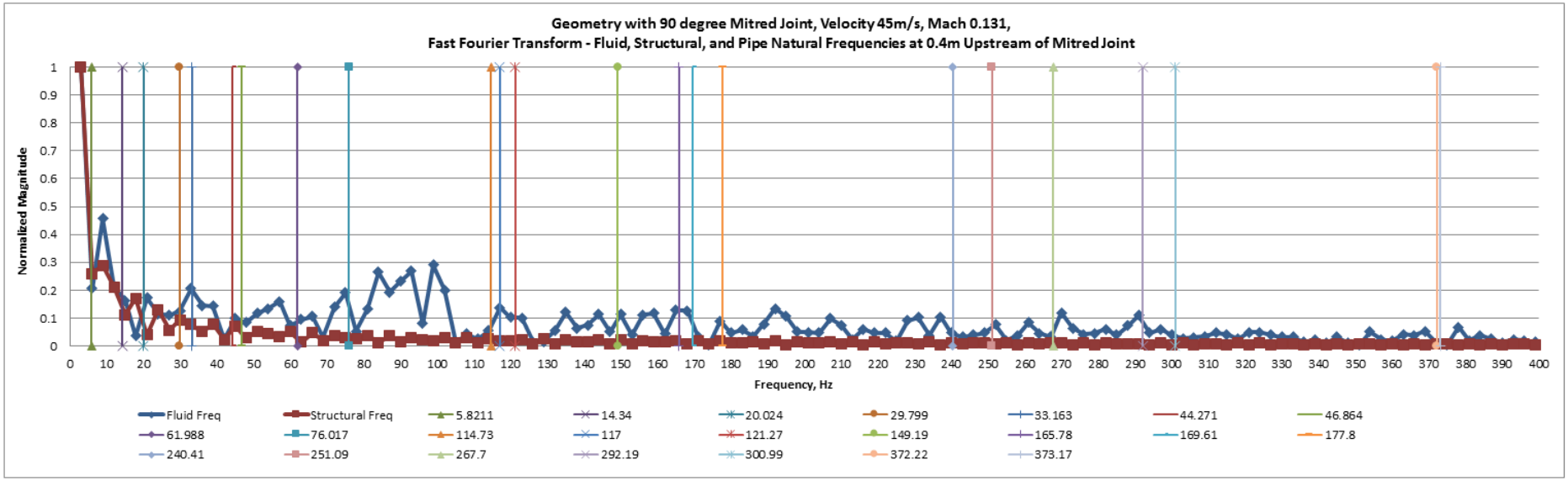
Geometry with 90 degree Mitred Joint, Velocity 45m/s, Mach 0.131,
Fast Fourier Transform - Fluid, Structural, and Pipe Natural Frequencies at 0.4m Upstream of Mitred Joint
Normalized Magnitude
Frequency, Hz
Fluid Freq
Structural Freq
5.8211
14.34
20.024
29.799
33.163
44.271
46.864
61.988
76.017
114.73
117
121.27
149.19
165.78
169.61
177.8
240.41
251.09
267.7
292.19
300.99
372.22
373.17

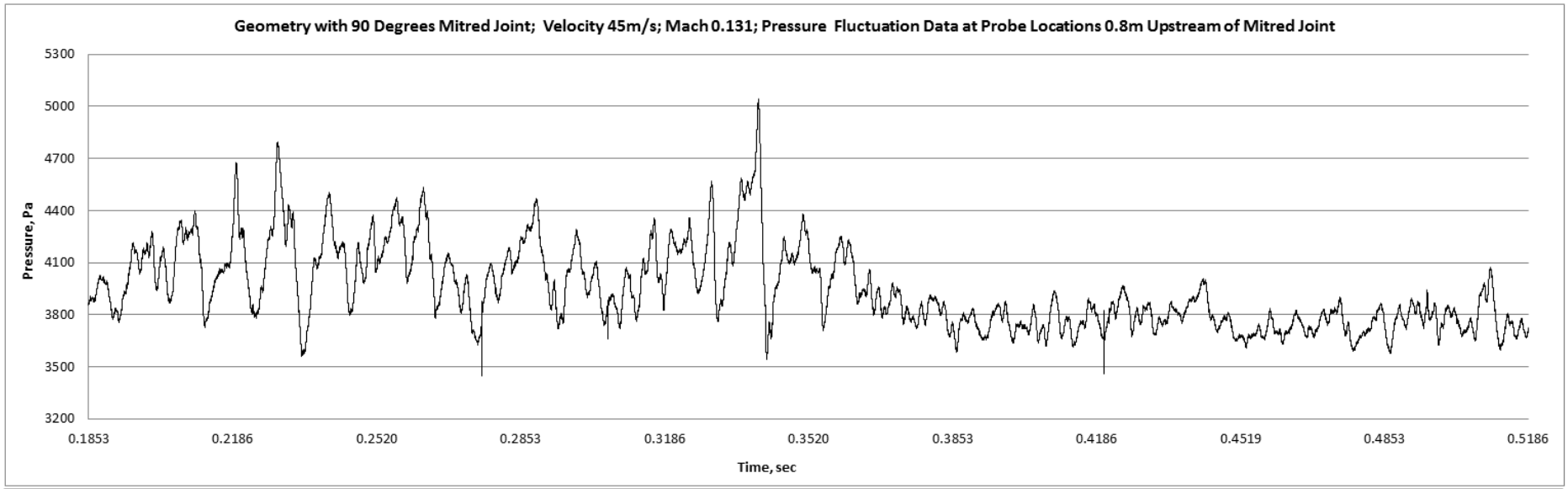
Geometry with 90 Degrees Mitred Joint; Velocity 45m/s; Mach 0.131; Pressure Fluctuation Data at Probe Locations 0.8m Upstream of Mitred Joint
Pressure, Pa
5300
5000
4700
4400
4100
3800
3500
3200
0.1853
0.2186
0.2520
0.2853
0.3186
0.3520
0.3853
0.4186
0.4519
0.4853
0.5186
Time, sec

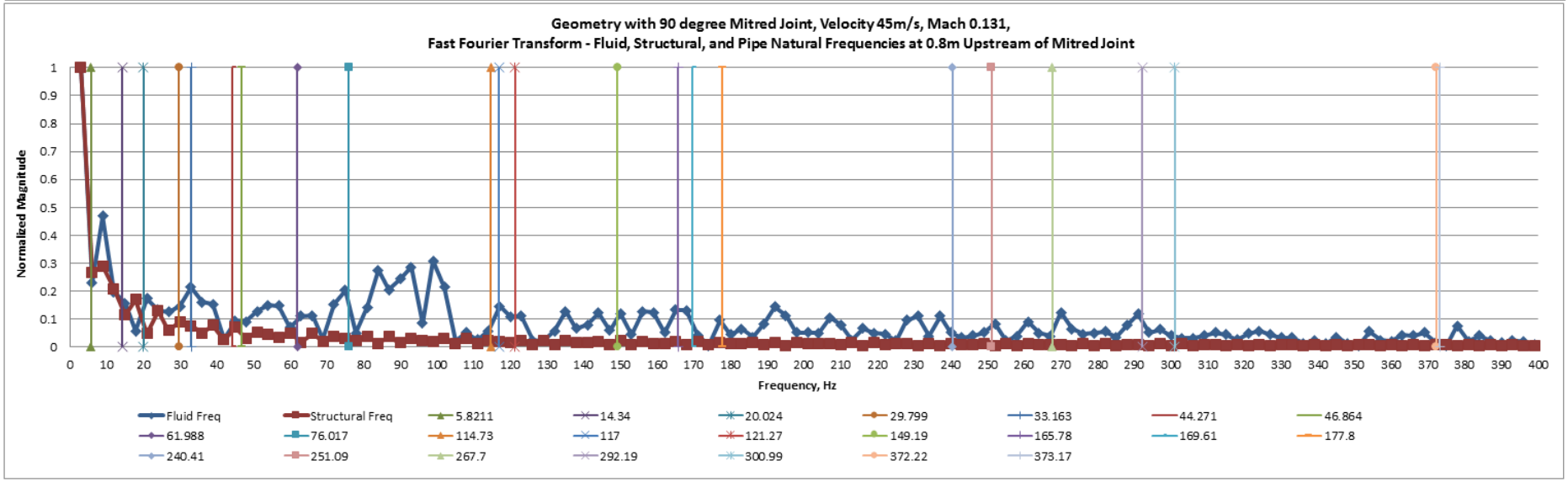
Geometry with 90 degree Mitred Joint, Velocity 45m/s, Mach 0.131,
Fast Fourier Transform - Fluid, Structural, and Pipe Natural Frequencies at 0.8m Upstream of Mitred Joint
Normalized Magnitude
Frequency, Hz
Fluid Freq
Structural Freq
5.8211
14.34
20.024
29.799
33.163
44.271
46.864
61.988
76.017
114.73
117
121.27
149.19
165.78
169.61
177.8
240.41
251.09
267.7
292.19
300.99
372.22
373.17

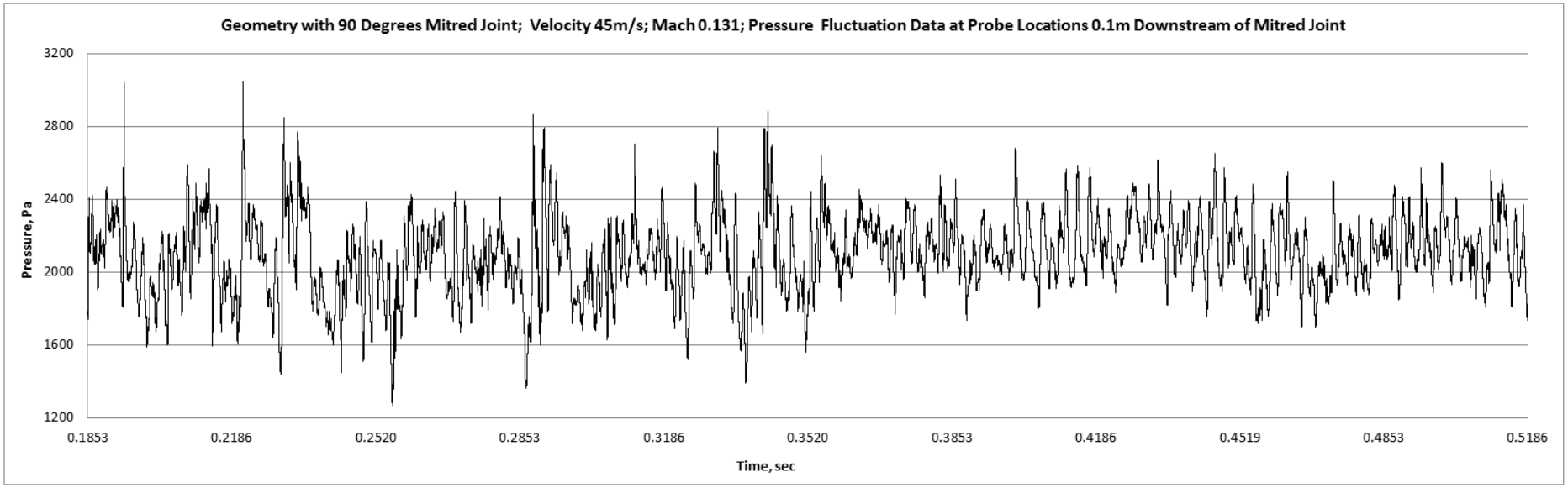
Geometry with 90 Degrees Mitred Joint; Velocity 45m/s; Mach 0.131; Pressure Fluctuation Data at Probe Locations 0.1m Downstream of Mitred Joint
Pressure, Pa
3200
2800
2400
2000
1600
1200
0.1853
0.2186
0.2520
0.2853
0.3186
0.3520
0.3853
0.4186
0.4519
0.4853
0.5186
Time, sec

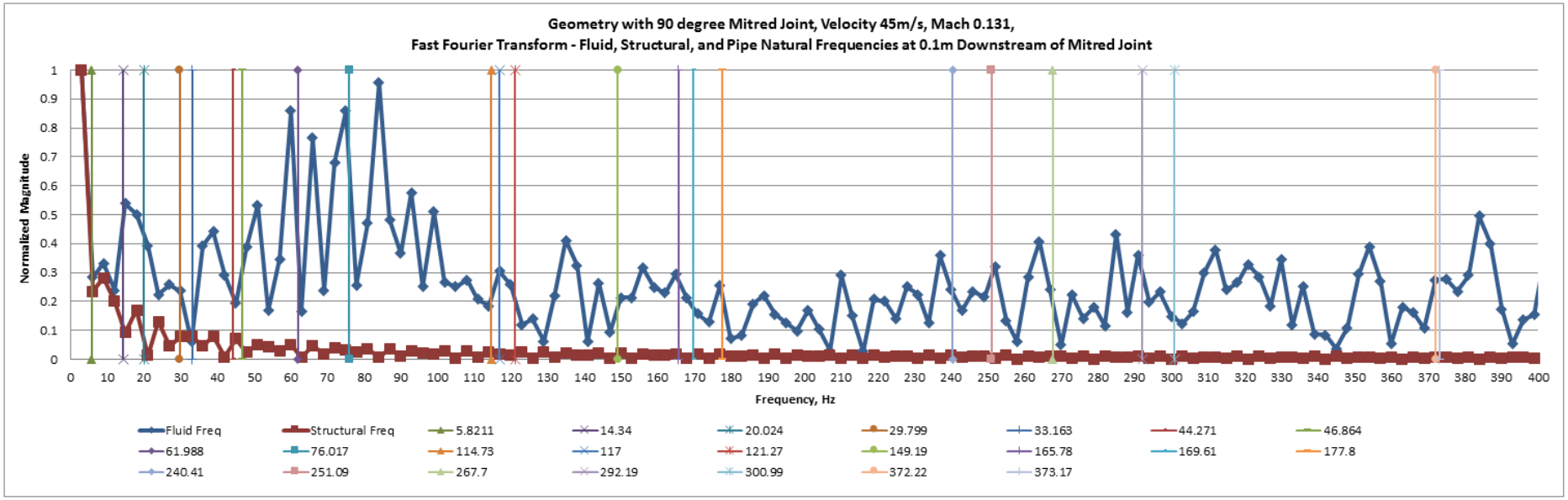
Geometry with 90 degree Mitred Joint, Velocity 45m/s, Mach 0.131,
Fast Fourier Transform - Fluid, Structural, and Pipe Natural Frequencies at 0.1m Downstream of Mitred Joint
Normalized Magnitude
Frequency, Hz
Fluid Freq
Structural Freq
5.8211
14.34
20.024
29.799
33.163
44.271
46.864
61.988
76.017
114.73
117
121.27
149.19
165.78
169.61
177.8
240.41
251.09
267.7
292.19
300.99
372.22
373.17

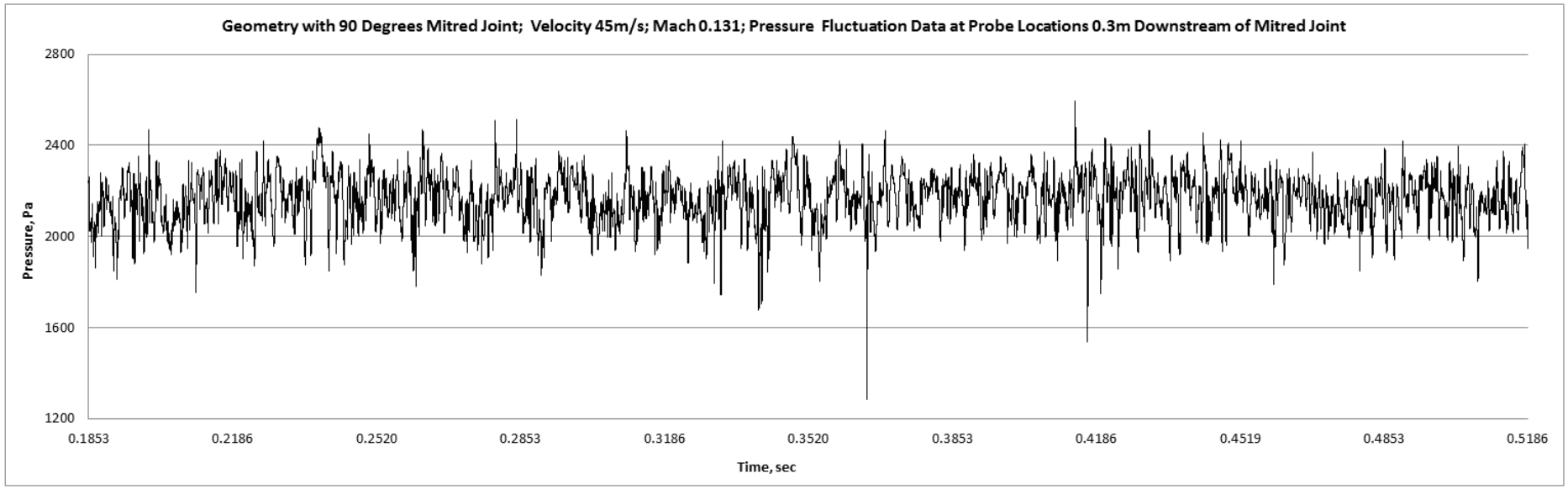
Geometry with 90 Degrees Mitred Joint; Velocity 45m/s; Mach 0.131; Pressure Fluctuation Data at Probe Locations 0.3m Downstream of Mitred Joint
Pressure, Pa
2800
2400
2000
1600
1200
0.1853
0.2186
0.2520
0.2853
0.3186
0.3520
0.3853
0.4186
0.4519
0.4853
0.5186
Time, sec

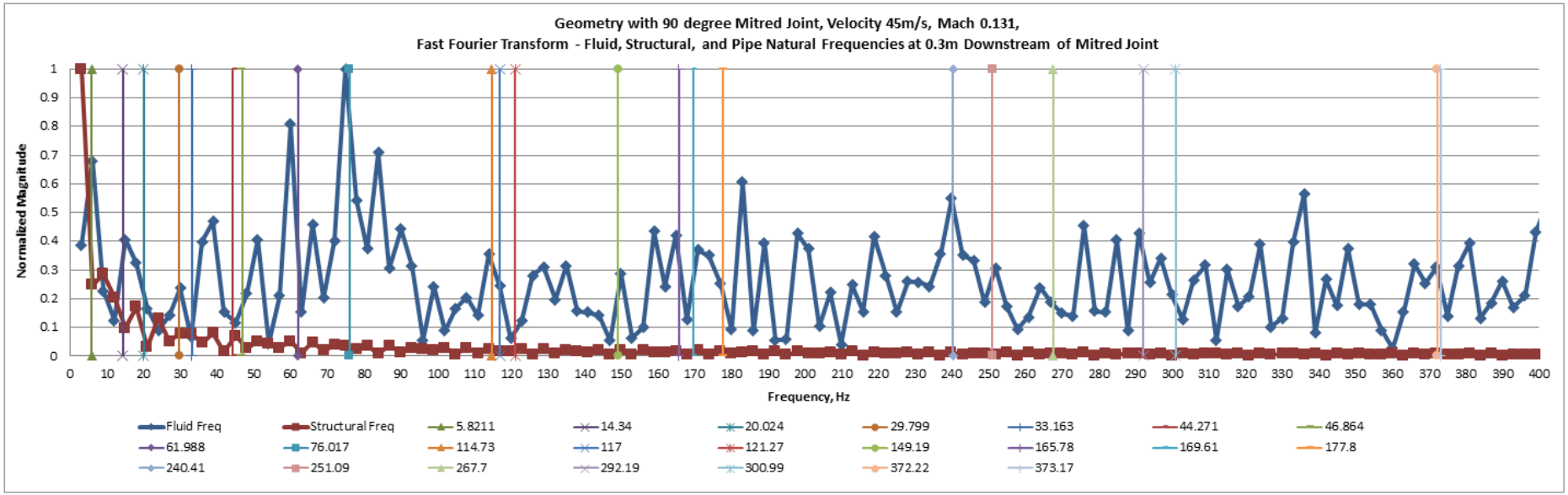
Geometry with 90 degree Mitred Joint, Velocity 45m/s, Mach 0.131,
Fast Fourier Transform - Fluid, Structural, and Pipe Natural Frequencies at 0.3m Downstream of Mitred Joint
Normalized Magnitude
Frequency, Hz
Fluid Freq
Structural Freq
5.8211
14.34
20.024
29.799
33.163
44.271
46.864
61.988
76.017
114.73
117
121.27
149.19
165.78
169.61
177.8
240.41
251.09
267.7
292.19
300.99
372.22
373.17

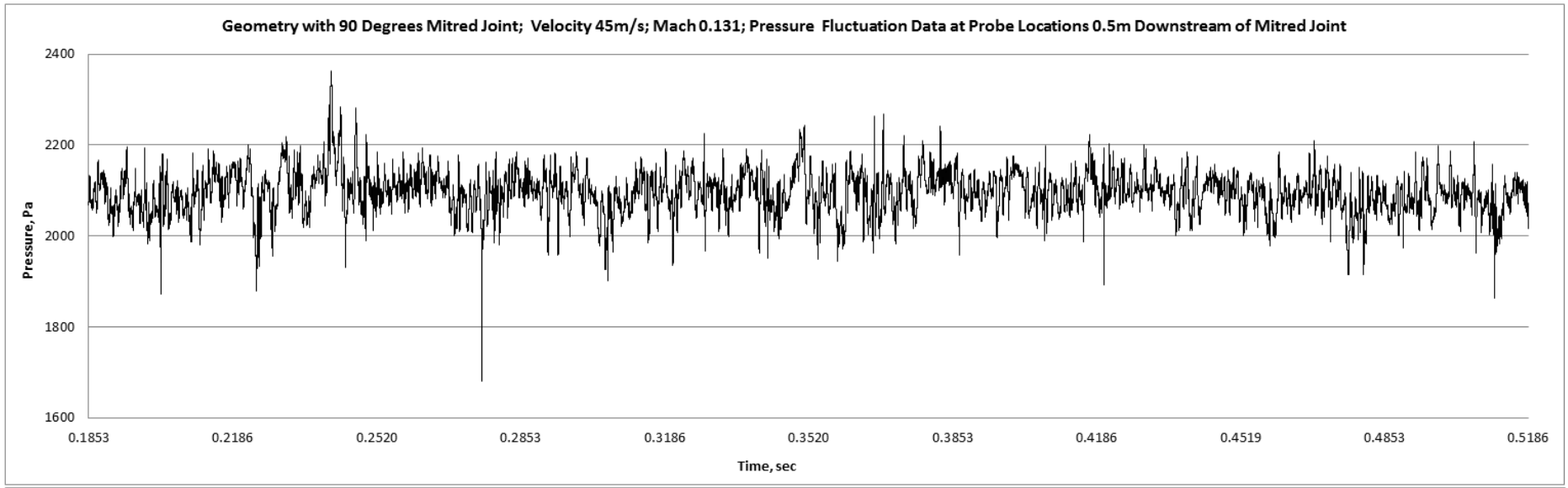
Geometry with 90 Degrees Mitred Joint; Velocity 45m/s; Mach 0.131; Pressure Fluctuation Data at Probe Locations 0.5m Downstream of Mitred Joint
Pressure, Pa
2400
2200
2000
1800
1600
0.1853
0.2186
0.2520
0.2853
0.3186
0.3520
0.3853
0.4186
0.4519
0.4853
0.5186
Time, sec

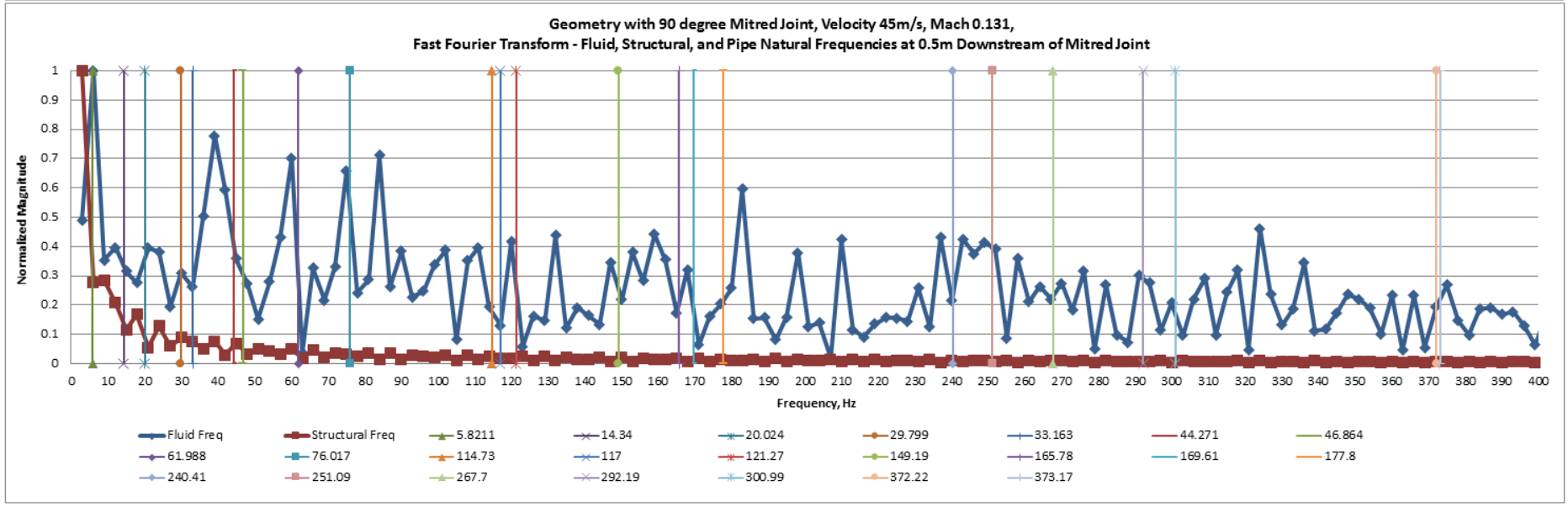
Geometry with 90 degree Mitred Joint, Velocity 45m/s, Mach 0.131,
Fast Fourier Transform - Fluid, Structural, and Pipe Natural Frequencies at 0.5m Downstream of Mitred Joint
Normalized Magnitude
Frequency, Hz
Fluid Freq
Structural Freq
5.8211
14.34
20.024
29.799
33.163
44.271
46.864
61.988
76.017
114.73
117
121.27
149.19
165.78
169.61
177.8
240.41
251.09
267.7
292.19
300.99
372.22
373.17

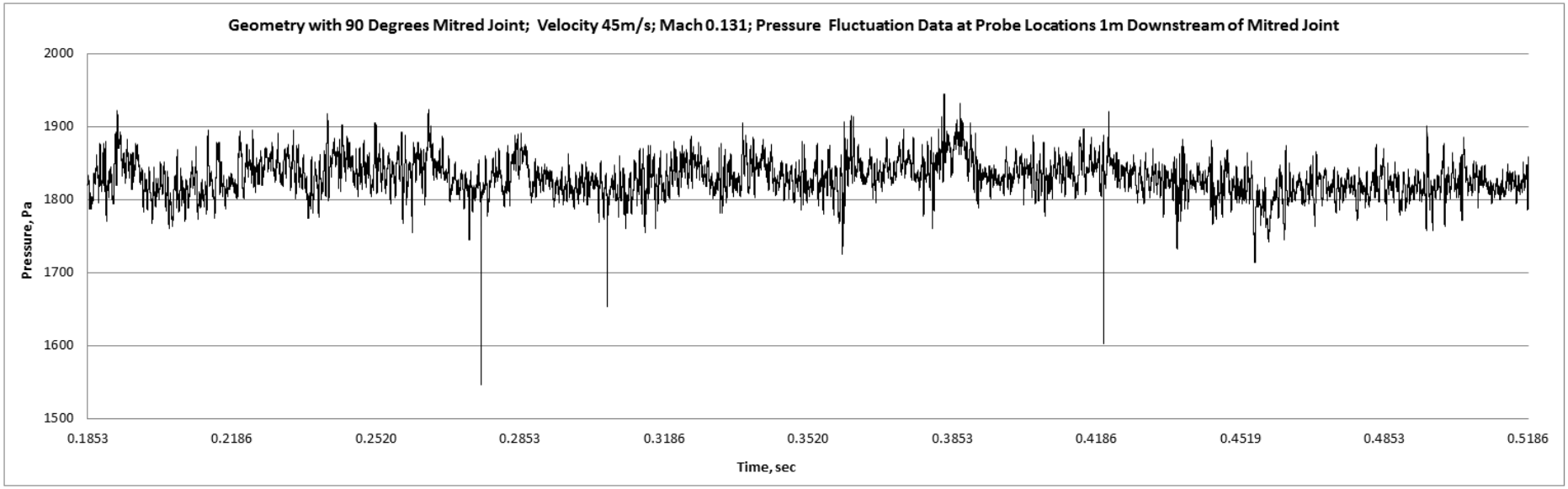
Geometry with 90 Degrees Mitred Joint; Velocity 45m/s; Mach 0.131; Pressure Fluctuation Data at Probe Locations 1m Downstream of Mitred Joint
Pressure, Pa
2000
1900
1800
1700
1600
1500
0.1853
0.2186
0.2520
0.2853
0.3186
0.3520
0.3853
0.4186
0.4519
0.4853
0.5186
Time, sec

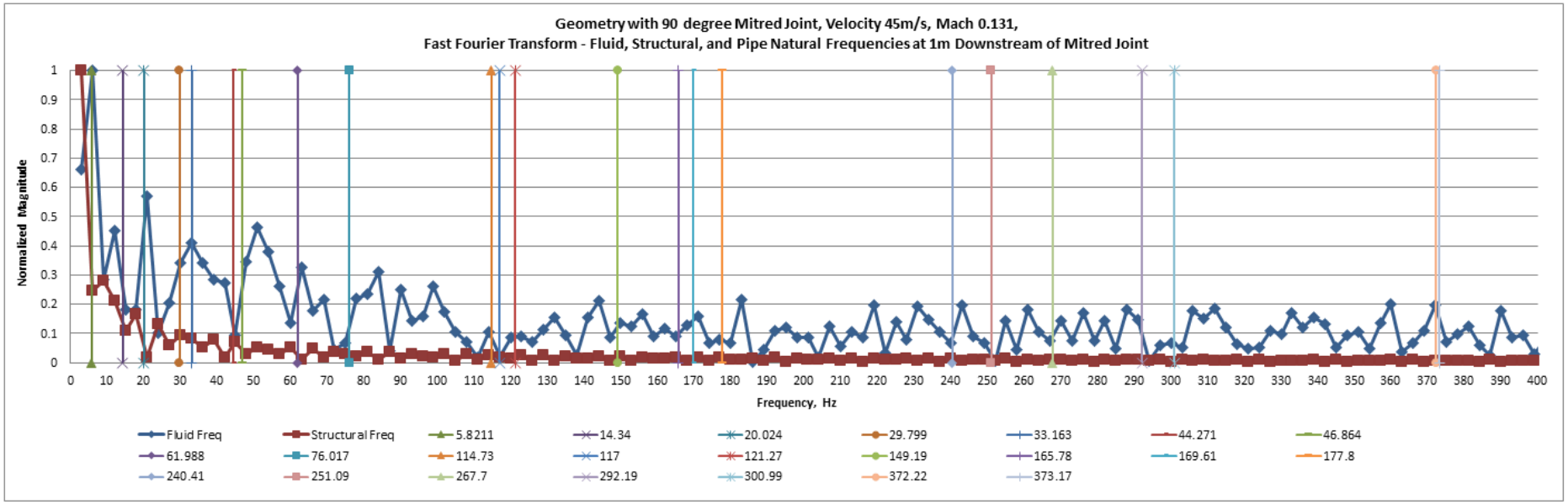
Geometry with 90 degree Mitred Joint, Velocity 45m/s, Mach 0.131,
Fast Fourier Transform - Fluid, Structural, and Pipe Natural Frequencies at 1m Downstream of Mitred Joint
Normalized Magnitude
Frequency, Hz
Fluid Freq
Structural Freq
5.8211
14.34
20.024
29.799
33.163
44.271
46.864
61.988
76.017
114.73
117
121.27
149.19
165.78
169.61
177.8
240.41
251.09
267.7
292.19
300.99
372.22
373.17

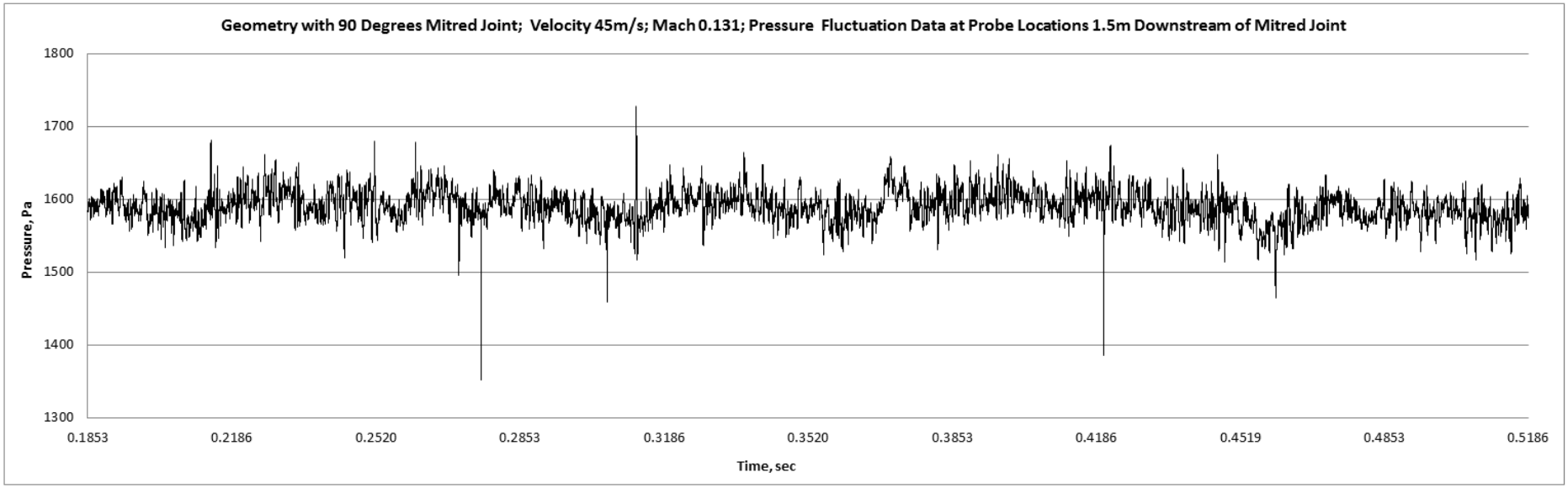
Geometry with 90 Degrees Mitred Joint; Velocity 45m/s; Mach 0.131; Pressure Fluctuation Data at Probe Locations 1.5m Downstream of Mitred Joint
Pressure, Pa
1800
1700
1600
1500
1400
1300
0.1853
0.2186
0.2520
0.2853
0.3186
0.3520
0.3853
0.4186
0.4519
0.4853
0.5186
Time, sec

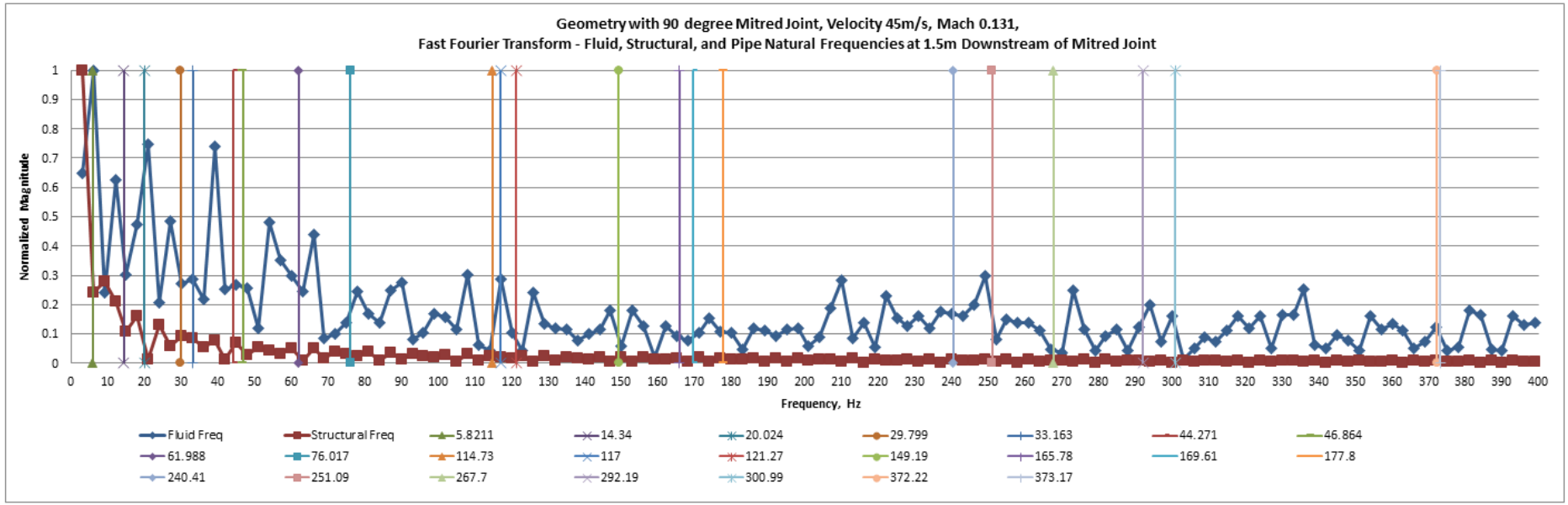
Geometry with 90 degree Mitred Joint, Velocity 45m/s, Mach 0.131,
Fast Fourier Transform - Fluid, Structural, and Pipe Natural Frequencies at 1.5m Downstream of Mitred Joint
Normalized Magnitude
Frequency, Hz
Fluid Freq
Structural Freq
5.8211
14.34
20.024
29.799
33.163
44.271
46.864
61.988
76.017
114.73
117
121.27
149.19
165.78
169.61
177.8
240.41
251.09
267.7
292.19
300.99
372.22
373.17

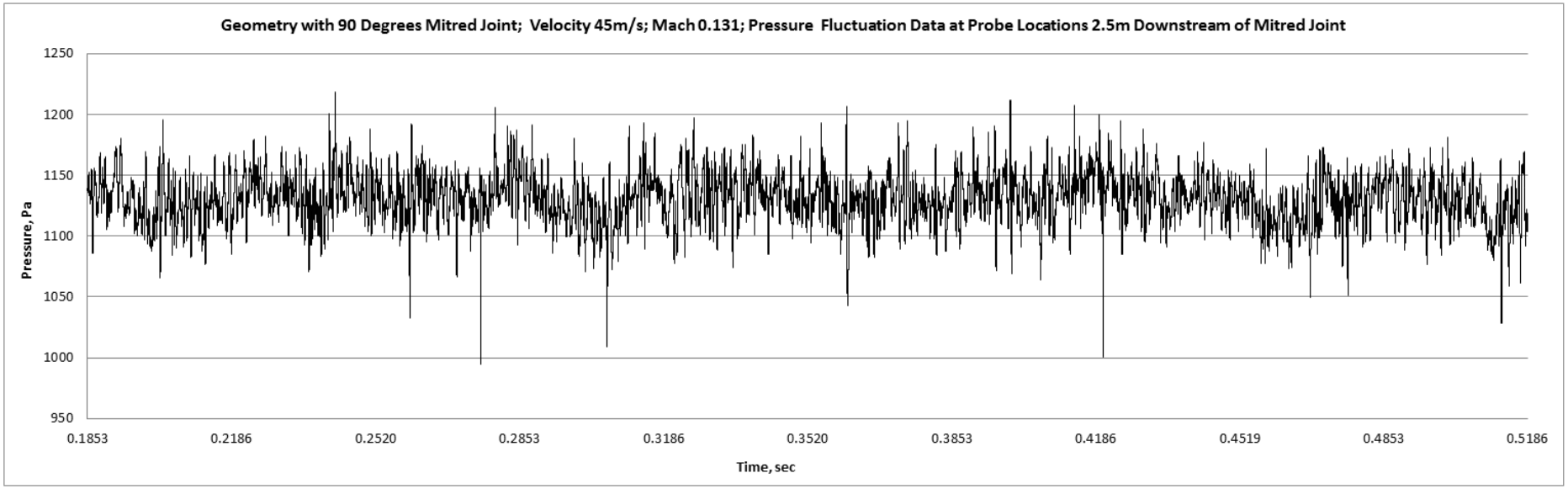
Geometry with 90 Degrees Mitred Joint; Velocity 45m/s; Mach 0.131; Pressure Fluctuation Data at Probe Locations 2.5m Downstream of Mitred Joint
Pressure, Pa
1250
1200
1150
1100
1050
1000
950
0.1853
0.2186
0.2520
0.2853
0.3186
0.3520
0.3853
0.4186
0.4519
0.4853
0.5186
Time, sec

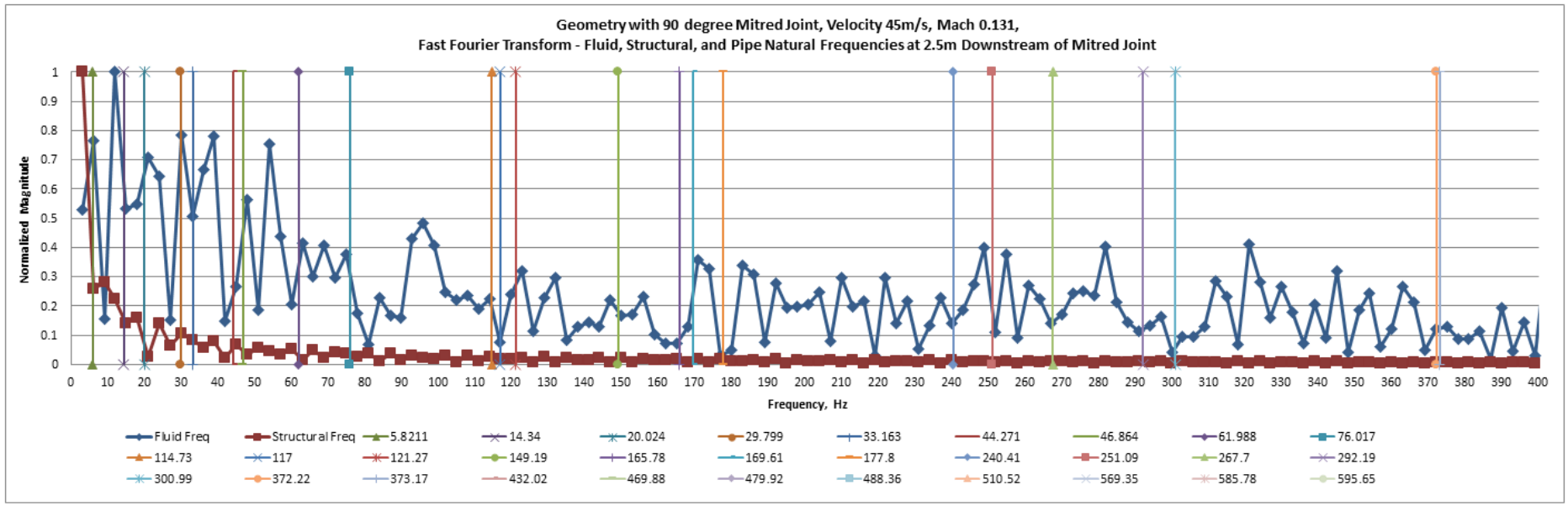
Geometry with 90 degree Mitred Joint, Velocity 45m/s, Mach 0.131,
Fast Fourier Transform - Fluid, Structural, and Pipe Natural Frequencies at 2.5m Downstream of Mitred Joint
Normalized Magnitude
Frequency, Hz
Fluid Freq
Structural Freq
5.8211
14.34
20.024
29.799
33.163
44.271
46.864
61.988
76.017
114.73
117
121.27
149.19
165.78
169.61
177.8
240.41
251.09
267.7
292.19
300.99
372.22
373.17
432.02
469.88
479.92
488.36
510.52
569.35
585.78
595.65

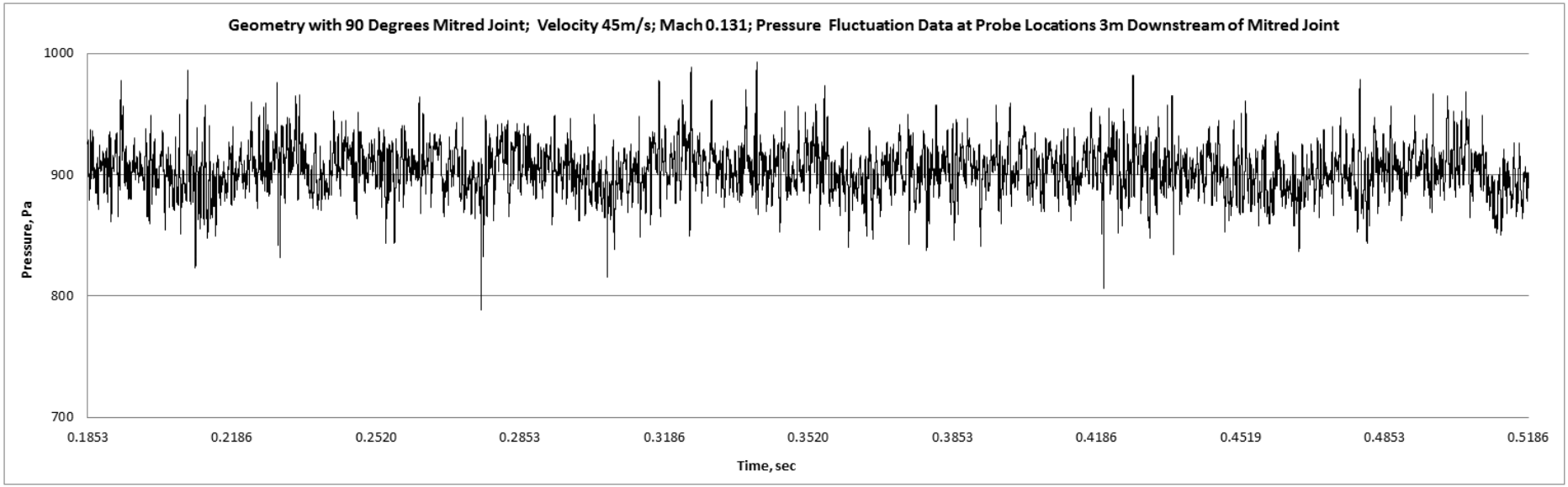
Geometry with 90 Degrees Mitred Joint; Velocity 45m/s; Mach 0.131; Pressure Fluctuation Data at Probe Locations 3m Downstream of Mitred Joint
Pressure, Pa
1000
900
800
700
0.1853
0.2186
0.2520
0.2853
0.3186
0.3520
0.3853
0.4186
0.4519
0.4853
0.5186
Time, sec

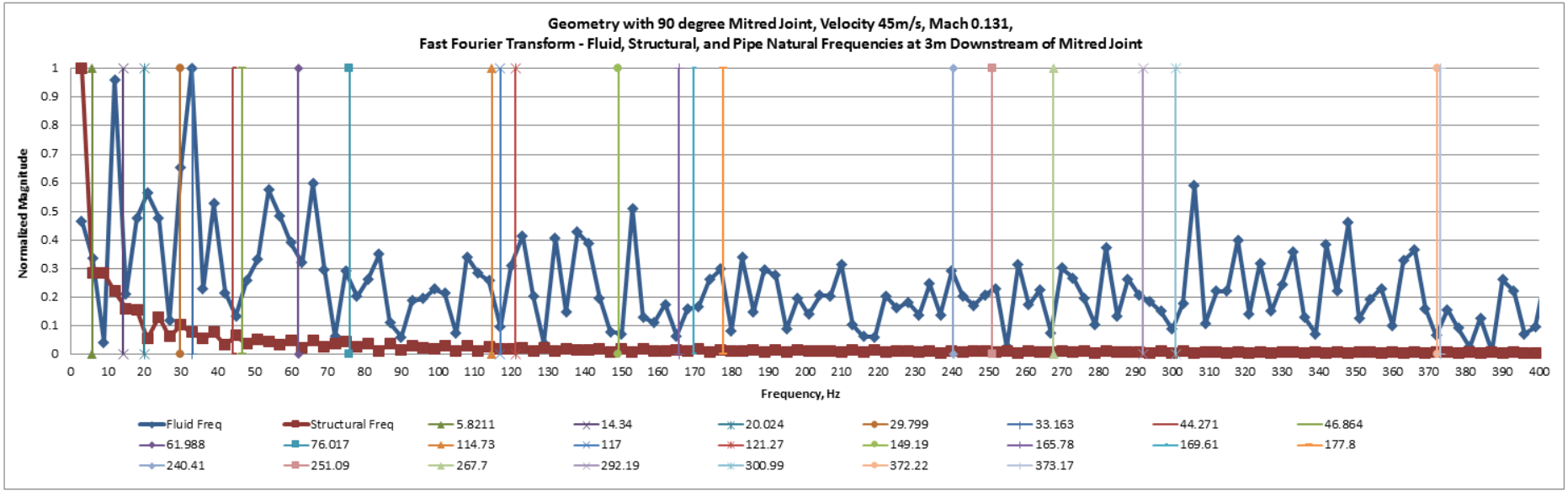
Geometry with 90 degree Mitred Joint, Velocity 45m/s, Mach 0.131,
Fast Fourier Transform - Fluid, Structural, and Pipe Natural Frequencies at 3m Downstream of Mitred Joint
Normalized Magnitude
Frequency, Hz
Fluid Freq
Structural Freq
5.8211
14.34
20.024
29.799
33.163
44.271
46.864
61.988
76.017
114.73
117
121.27
149.19
165.78
169.61
177.8
240.41
251.09
267.7
292.19
300.99
372.22
373.17

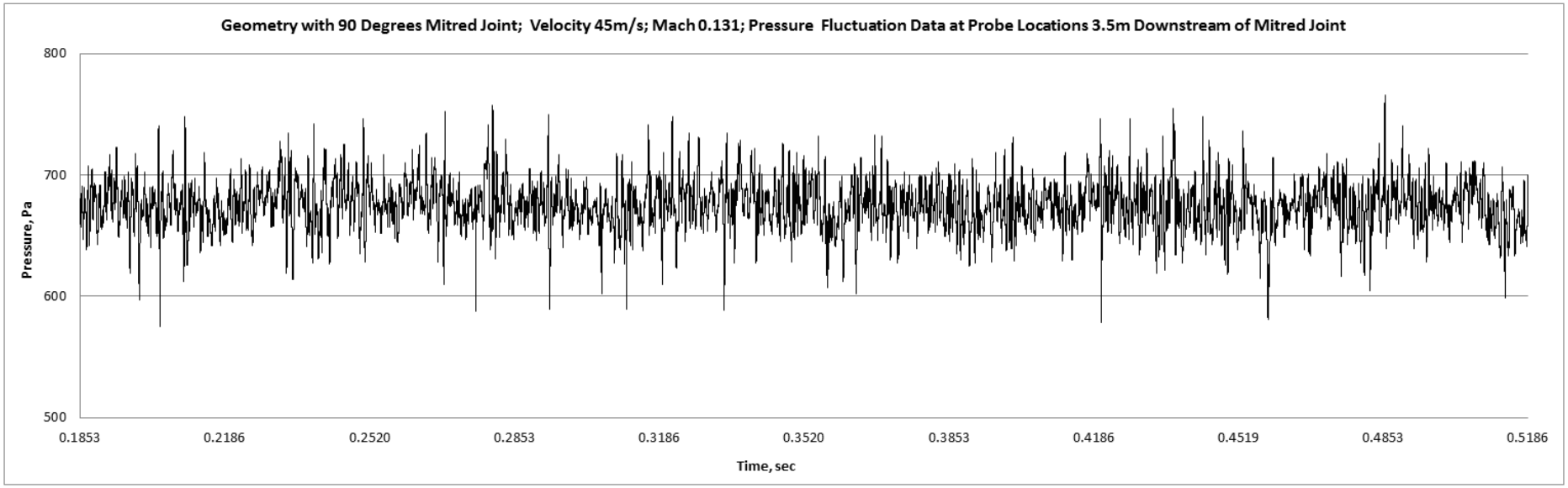
Geometry with 90 Degrees Mitred Joint; Velocity 45m/s; Mach 0.131; Pressure Fluctuation Data at Probe Locations 3.5m Downstream of Mitred Joint
Pressure, Pa
800
700
600
500
0.1853
0.2186
0.2520
0.2853
0.3186
0.3520
0.3853
0.4186
0.4519
0.4853
0.5186
Time, sec

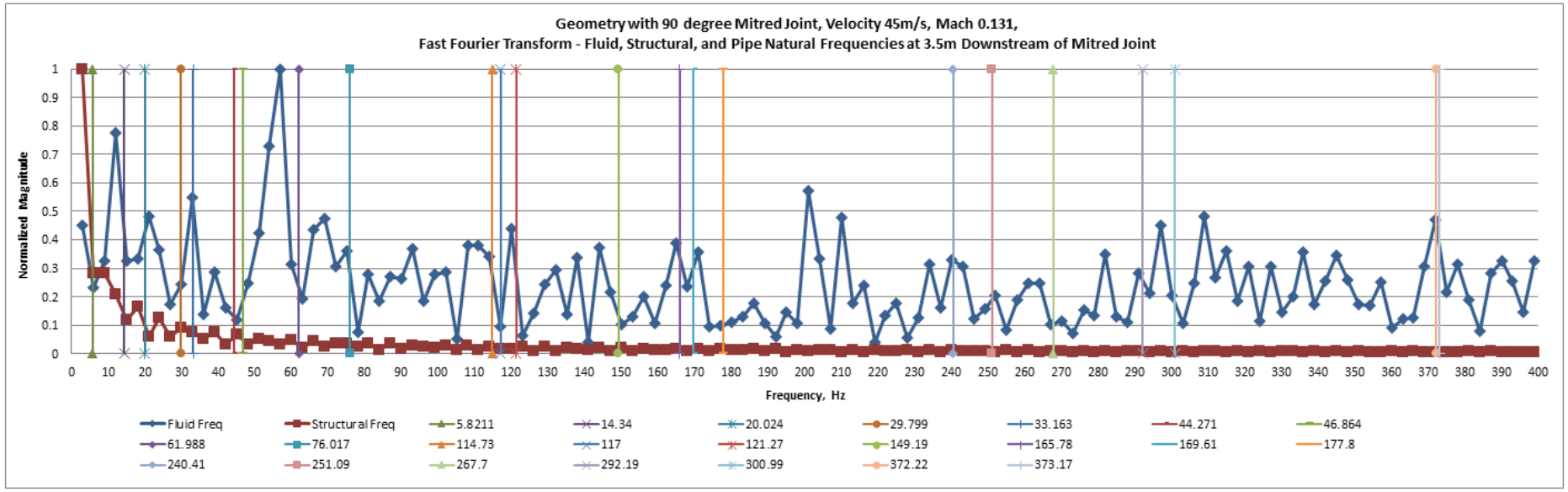
Geometry with 90 degree Mitred Joint, Velocity 45m/s, Mach 0.131,
Fast Fourier Transform - Fluid, Structural, and Pipe Natural Frequencies at 3.5m Downstream of Mitred Joint
Normalized Magnitude
Frequency, Hz
Fluid Freq
Structural Freq
5.8211
14.34
20.024
29.799
33.163
44.271
46.864
61.988
76.017
114.73
117
121.27
149.19
165.78
169.61
177.8
240.41
251.09
267.7
292.19
300.99
372.22
373.17

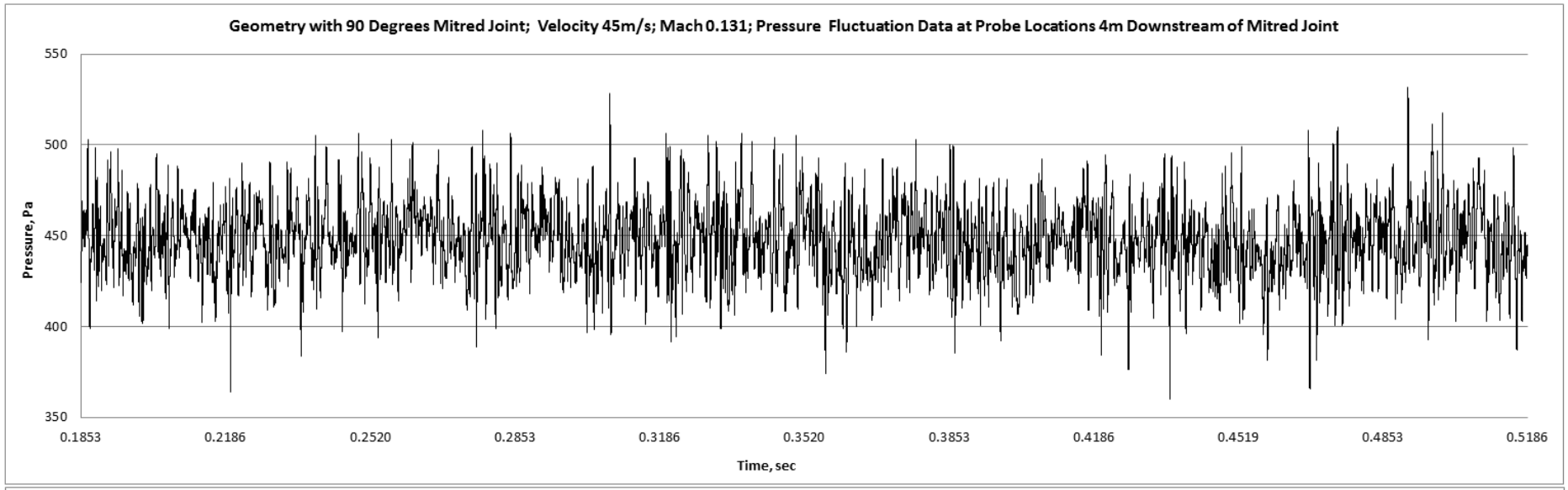
Geometry with 90 Degrees Mitred Joint; Velocity 45m/s; Mach 0.131; Pressure Fluctuation Data at Probe Locations 4m Downstream of Mitred Joint
Pressure, Pa
550
500
450
400
350
0.1853
0.2186
0.2520
0.2853
0.3186
0.3520
0.3853
0.4186
0.4519
0.4853
0.5186
Time, sec

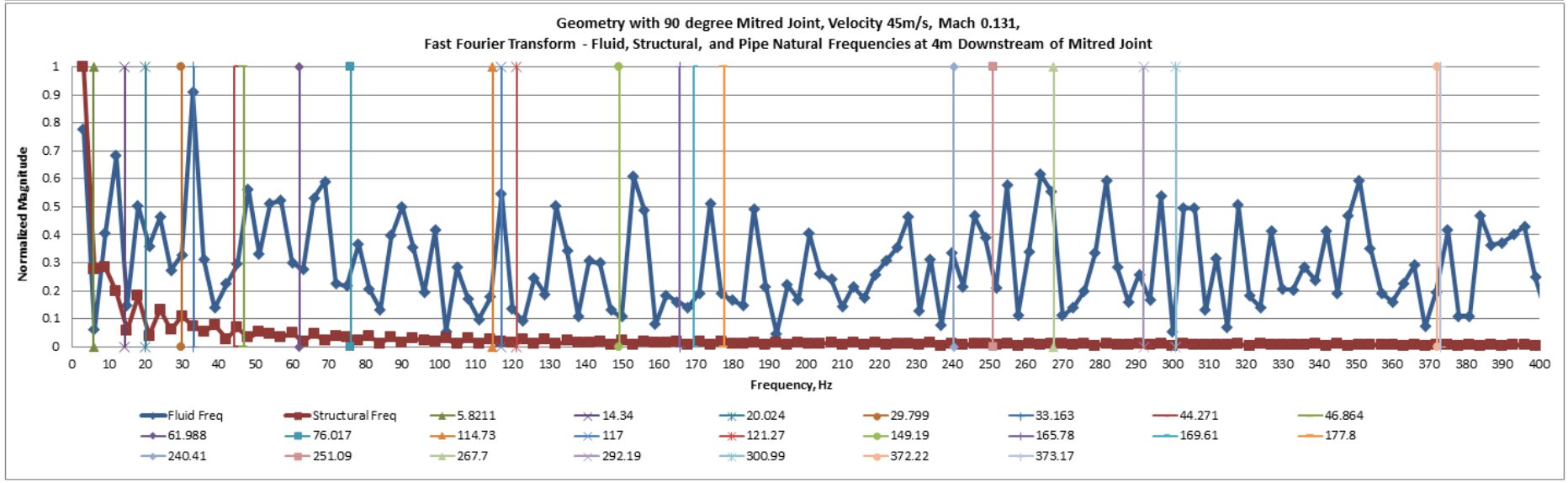
Geometry with 90 degree Mitred Joint, Velocity 45m/s, Mach 0.131,
Fast Fourier Transform - Fluid, Structural, and Pipe Natural Frequencies at 4m Downstream of Mitred Joint
Normalized Magnitude
Frequency, Hz
Fluid Freq
Structural Freq
5.8211
14.34
20.024
29.799
33.163
44.271
46.864
61.988
76.017
114.73
117
121.27
149.19
165.78
169.61
177.8
240.41
251.09
267.7
292.19
300.99
372.22
373.17

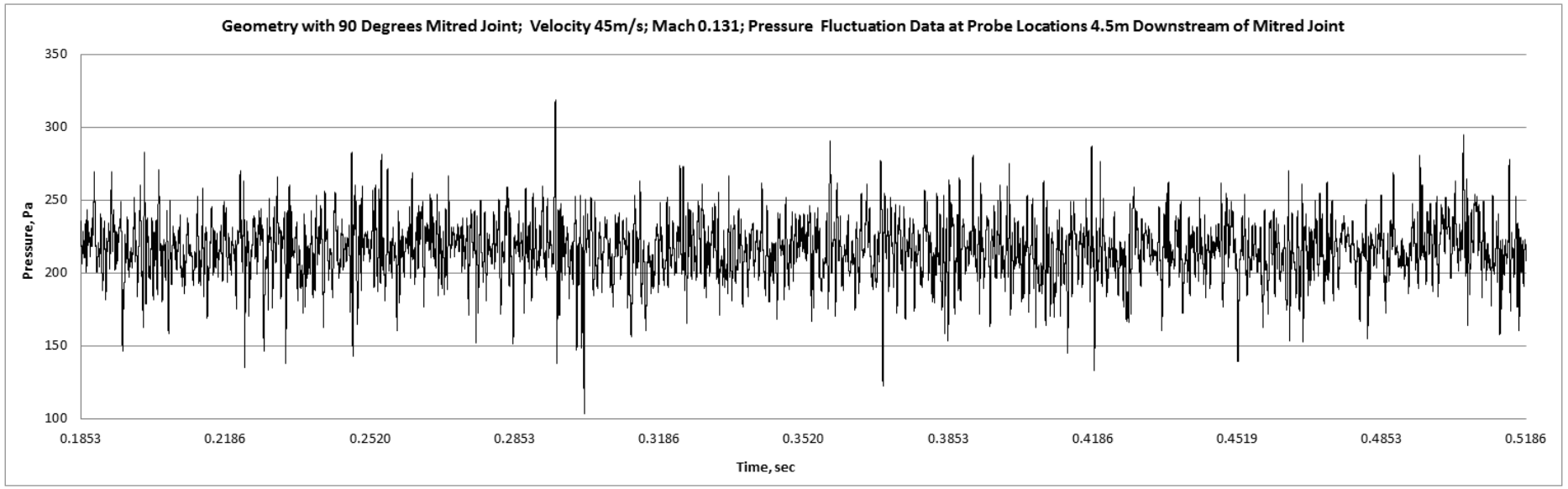
Geometry with 90 Degrees Mitred Joint; Velocity 45m/s; Mach 0.131; Pressure Fluctuation Data at Probe Locations 4.5m Downstream of Mitred Joint
Pressure, Pa
350
300
250
200
150
100
0.1853
0.2186
0.2520
0.2853
0.3186
0.3520
0.3853
0.4186
0.4519
0.4853
0.5186
Time, sec

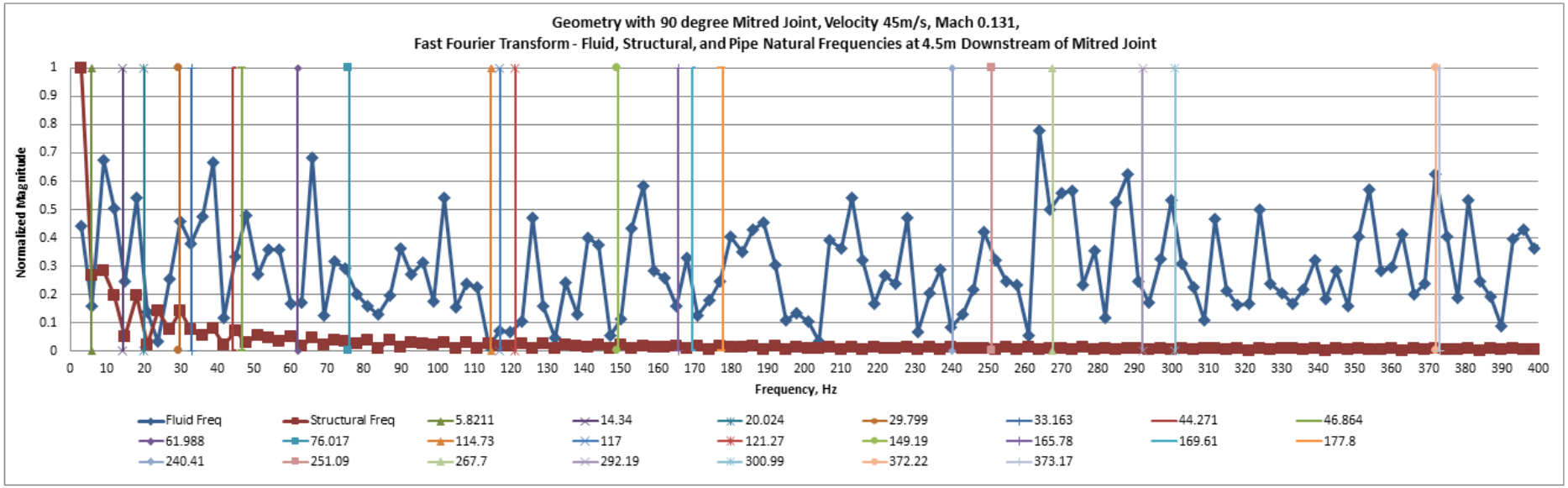
Geometry with 90 degree Mitred Joint, Velocity 45m/s, Mach 0.131,
Fast Fourier Transform - Fluid, Structural, and Pipe Natural Frequencies at 4.5m Downstream of Mitred Joint
Normalized Magnitude
Frequency, Hz
Fluid Freq
Structural Freq
5.8211
14.34
20.024
29.799
33.163
44.271
46.864
61.988
76.017
114.73
117
121.27
149.19
165.78
169.61
177.8
240.41
251.09
267.7
292.19
300.99
372.22
373.17

Appendix F

Frequency Plots for Geometry with 90^0 Mitred Bend for Fluid Velocity modelled at 60m/s, Mach 0.175 at Probe Locations

Distance	Fluid Excited Frequencies Downstream of 90 Degree Mitred Bend
0.1	3, 51, 57, 63, 69, 84, 90, 111, 117, 138
0.3	3, 30, 63, 69, 78, 90, 111, 117
0.5	3, 30, 69, 78, 90, 99, 111, 129
1	3, 30, 69, 78, 90, 111, 129
1.5	3, 30, 51, 69, 78, 111, 117, 129
2.5	3, 30, 69, 78, 90, 111, 129
3	3, 30, 51, 69, 78, 96, 111, 123, 129
3.5	3, 30, 69, 78, 111
4	3, 69, 129
4.5	3, 36, 69, 78, 96, 117

Table F.1: Fluid excited frequencies downstream of the 90 Degree Mitred Bend for 60m/s

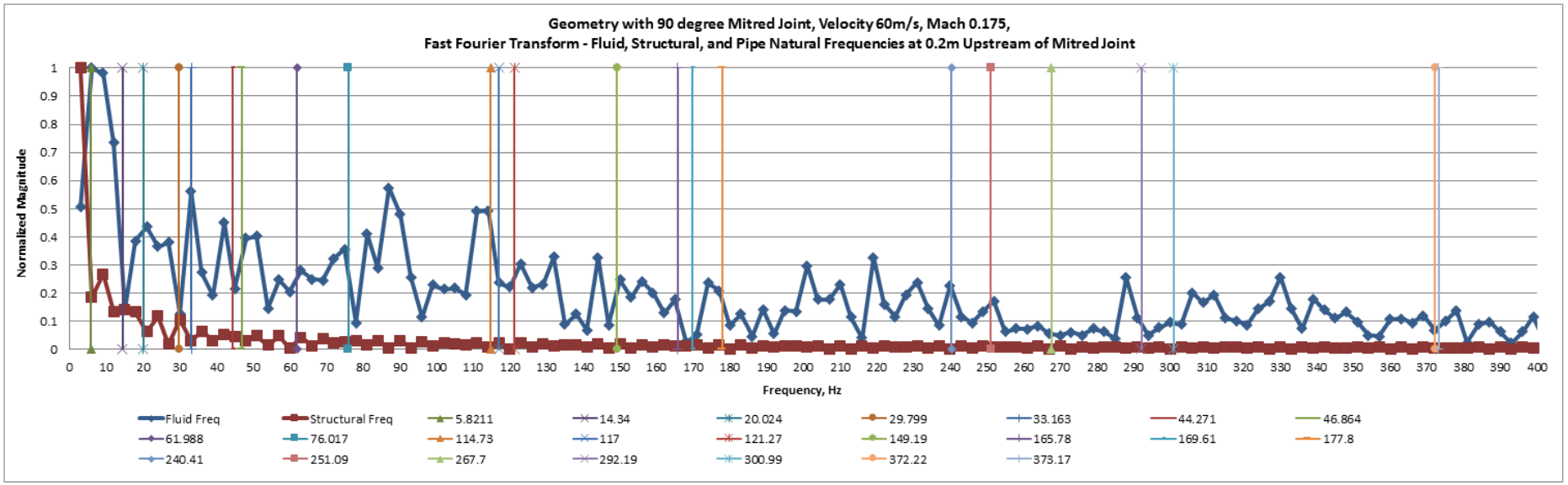
Geometry with 90 degree Mitred Joint, Velocity 60m/s, Mach 0.175,
Fast Fourier Transform - Fluid, Structural, and Pipe Natural Frequencies at 0.2m Upstream of Mitred Joint
Normalized Magnitude
Frequency, Hz
Fluid Freq
Structural Freq
5.8211
14.34
20.024
29.799
33.163
44.271
46.864
61.988
76.017
114.73
117
121.27
149.19
165.78
169.61
177.8
240.41
251.09
267.7
292.19
300.99
372.22
373.17

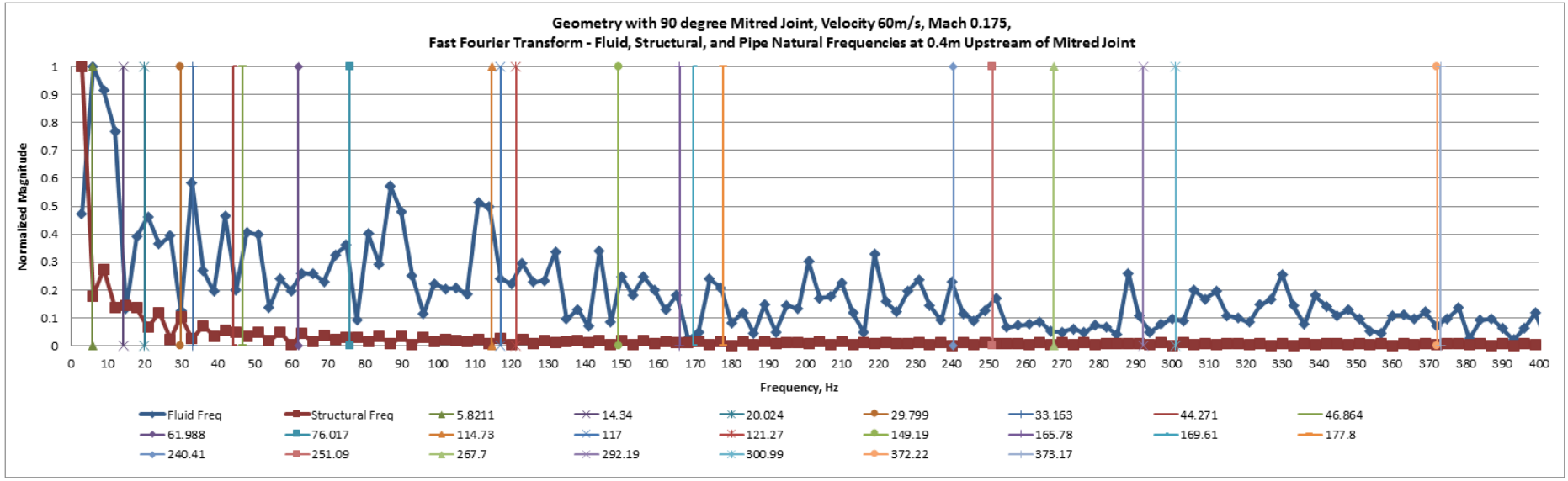
Geometry with 90 degree Mitred Joint, Velocity 60m/s, Mach 0.175,
Fast Fourier Transform - Fluid, Structural, and Pipe Natural Frequencies at 0.4m Upstream of Mitred Joint
Normalized Magnitude
Frequency, Hz
Fluid Freq
Structural Freq
5.8211
14.34
20.024
29.799
33.163
44.271
46.864
61.988
76.017
114.73
117
121.27
149.19
165.78
169.61
177.8
240.41
251.09
267.7
292.19
300.99
372.22
373.17

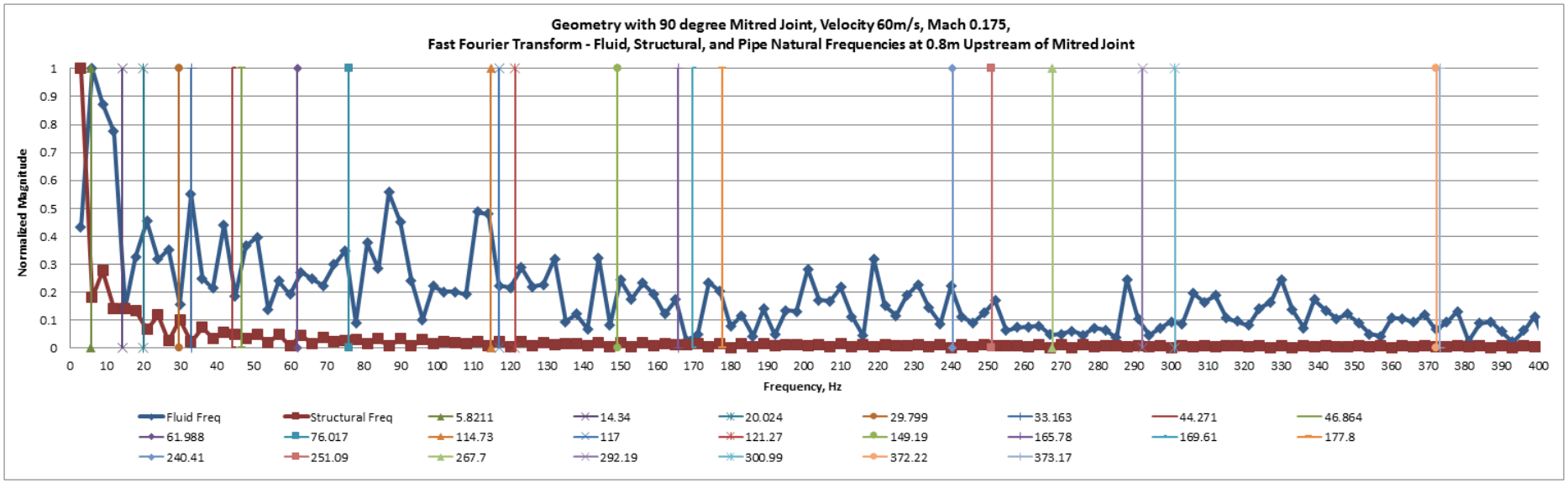
Geometry with 90 degree Mitred Joint, Velocity 60m/s, Mach 0.175,
Fast Fourier Transform - Fluid, Structural, and Pipe Natural Frequencies at 0.8m Upstream of Mitred Joint
Normalized Magnitude
Frequency, Hz
Fluid Freq
Structural Freq
5.8211
14.34
20.024
29.799
33.163
44.271
46.864
61.988
76.017
114.73
117
121.27
149.19
165.78
169.61
177.8
240.41
251.09
267.7
292.19
300.99
372.22
373.17

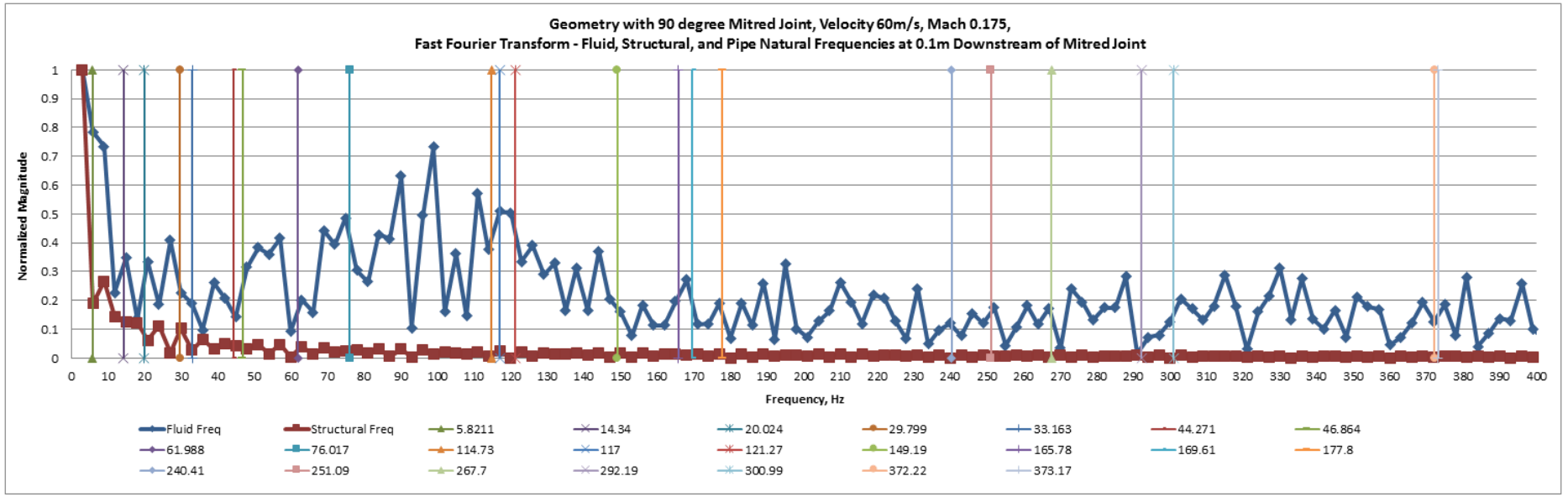
Geometry with 90 degree Mitred Joint, Velocity 60m/s, Mach 0.175,
Fast Fourier Transform - Fluid, Structural, and Pipe Natural Frequencies at 0.1m Downstream of Mitred Joint
Normalized Magnitude
Frequency, Hz
Fluid Freq
Structural Freq
5.8211
14.34
20.024
29.799
33.163
44.271
46.864
61.988
76.017
114.73
117
121.27
149.19
165.78
169.61
177.8
240.41
251.09
267.7
292.19
300.99
372.22
373.17

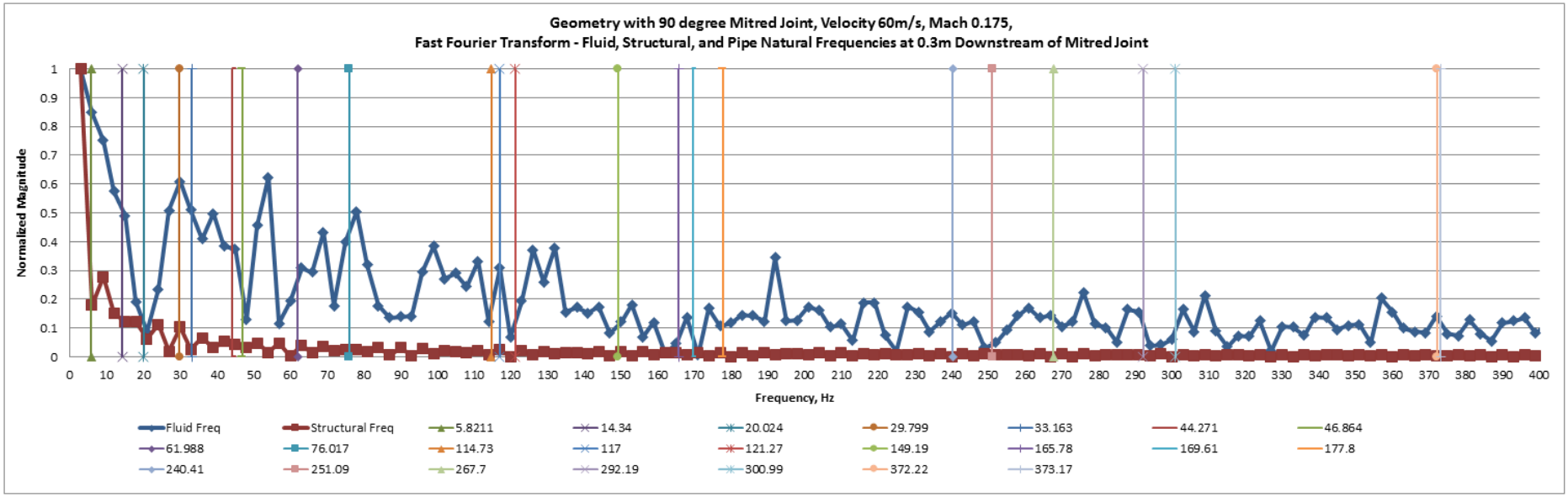
Geometry with 90 degree Mitred Joint, Velocity 60m/s, Mach 0.175,
Fast Fourier Transform - Fluid, Structural, and Pipe Natural Frequencies at 0.3m Downstream of Mitred Joint
Normalized Magnitude
Frequency, Hz
Fluid Freq
Structural Freq
5.8211
14.34
20.024
29.799
33.163
44.271
46.864
61.988
76.017
114.73
117
121.27
149.19
165.78
169.61
177.8
240.41
251.09
267.7
292.19
300.99
372.22
373.17

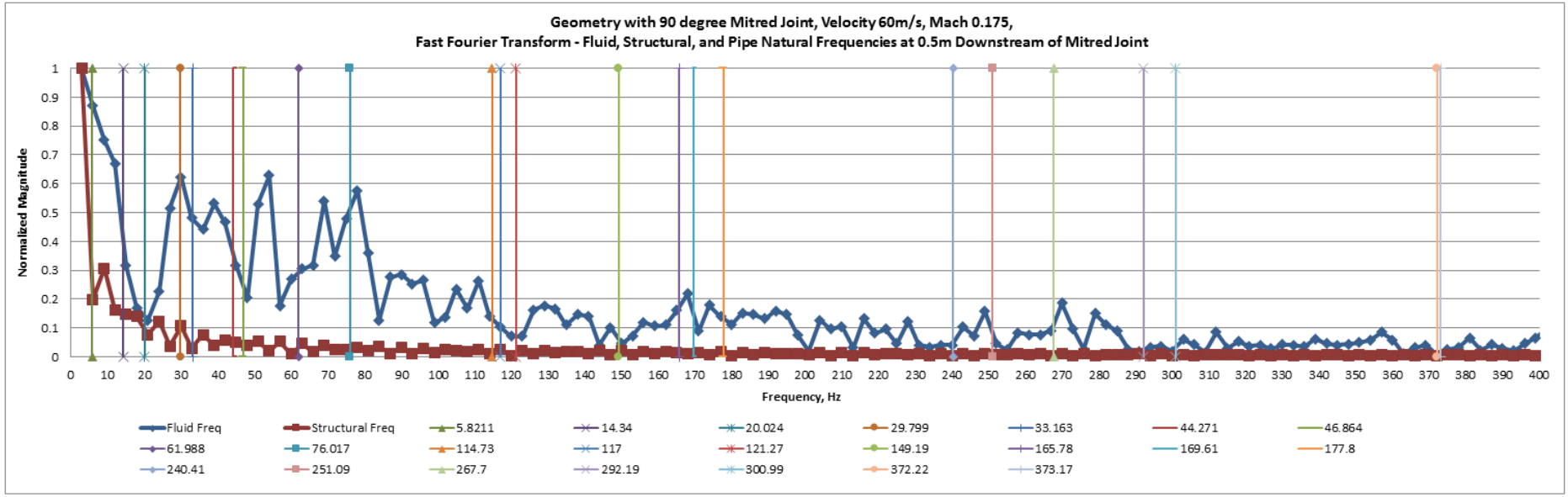
Geometry with 90 degree Mitred Joint, Velocity 60m/s, Mach 0.175,
Fast Fourier Transform - Fluid, Structural, and Pipe Natural Frequencies at 0.5m Downstream of Mitred Joint
Normalized Magnitude
Frequency, Hz
Fluid Freq
Structural Freq
5.8211
14.34
20.024
29.799
33.163
44.271
46.864
61.988
76.017
114.73
117
121.27
149.19
165.78
169.61
177.8
240.41
251.09
267.7
292.19
300.99
372.22
373.17

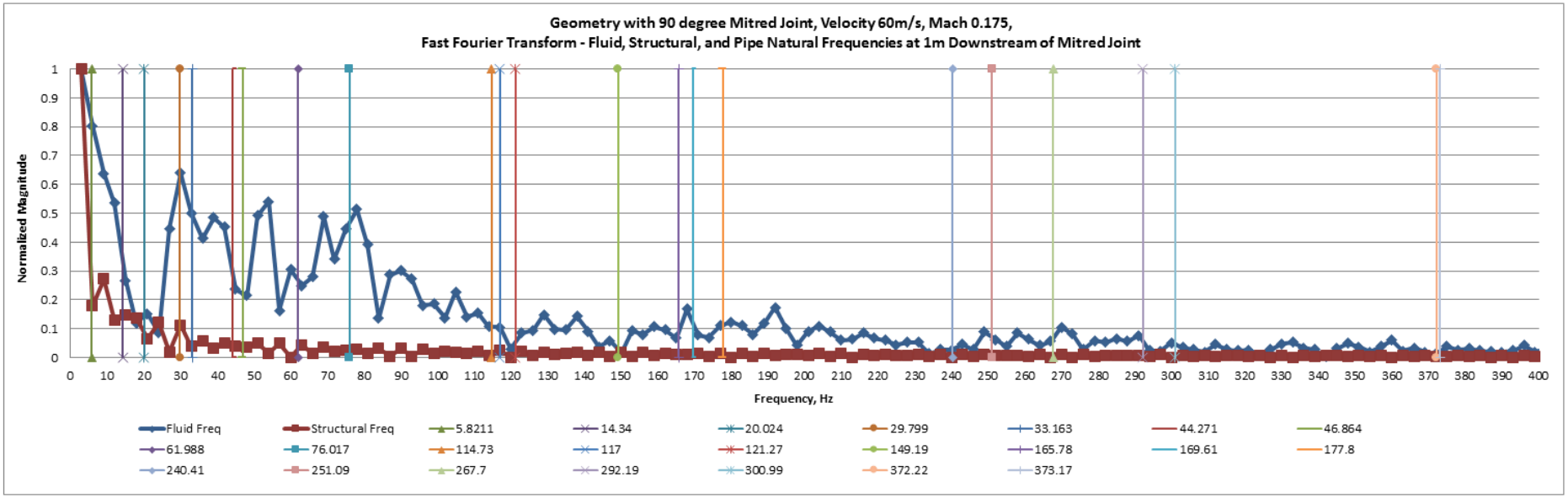
Geometry with 90 degree Mitred Joint, Velocity 60m/s, Mach 0.175,
Fast Fourier Transform - Fluid, Structural, and Pipe Natural Frequencies at 1m Downstream of Mitred Joint
Normalized Magnitude
Frequency, Hz
Fluid Freq
Structural Freq
5.8211
14.34
20.024
29.799
33.163
44.271
46.864
61.988
76.017
114.73
117
121.27
149.19
165.78
169.61
177.8
240.41
251.09
267.7
292.19
300.99
372.22
373.17

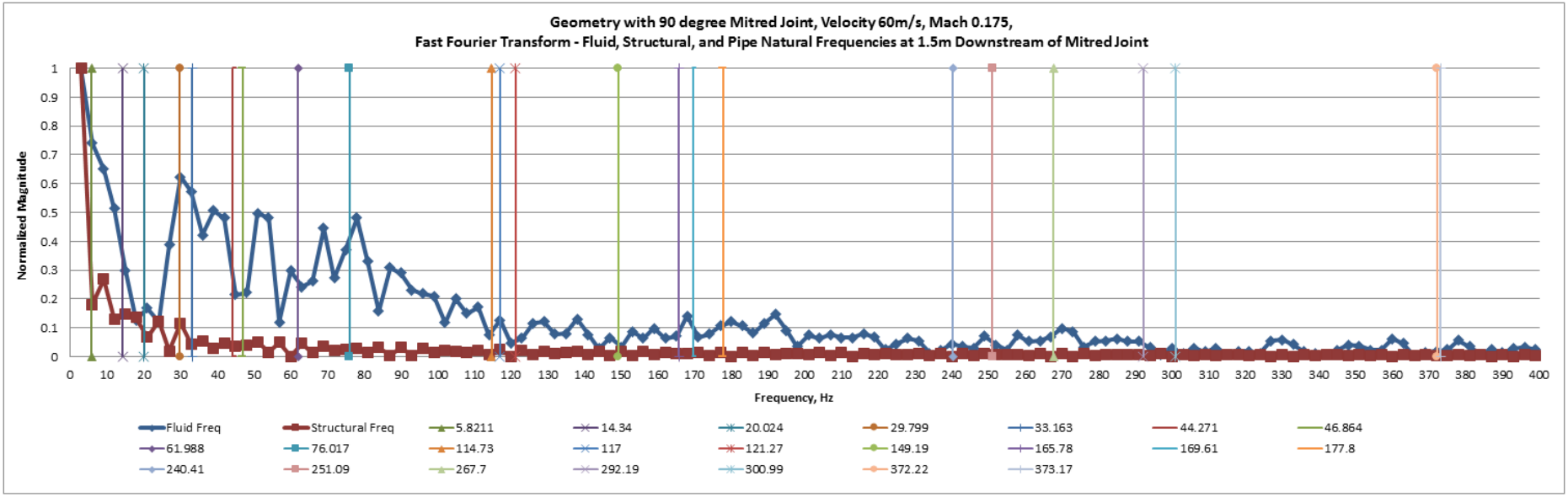
Geometry with 90 degree Mitred Joint, Velocity 60m/s, Mach 0.175,
Fast Fourier Transform - Fluid, Structural, and Pipe Natural Frequencies at 1.5m Downstream of Mitred Joint
Normalized Magnitude
Frequency, Hz
Fluid Freq
Structural Freq
5.8211
14.34
20.024
29.799
33.163
44.271
46.864
61.988
76.017
114.73
117
121.27
149.19
165.78
169.61
177.8
240.41
251.09
267.7
292.19
300.99
372.22
373.17

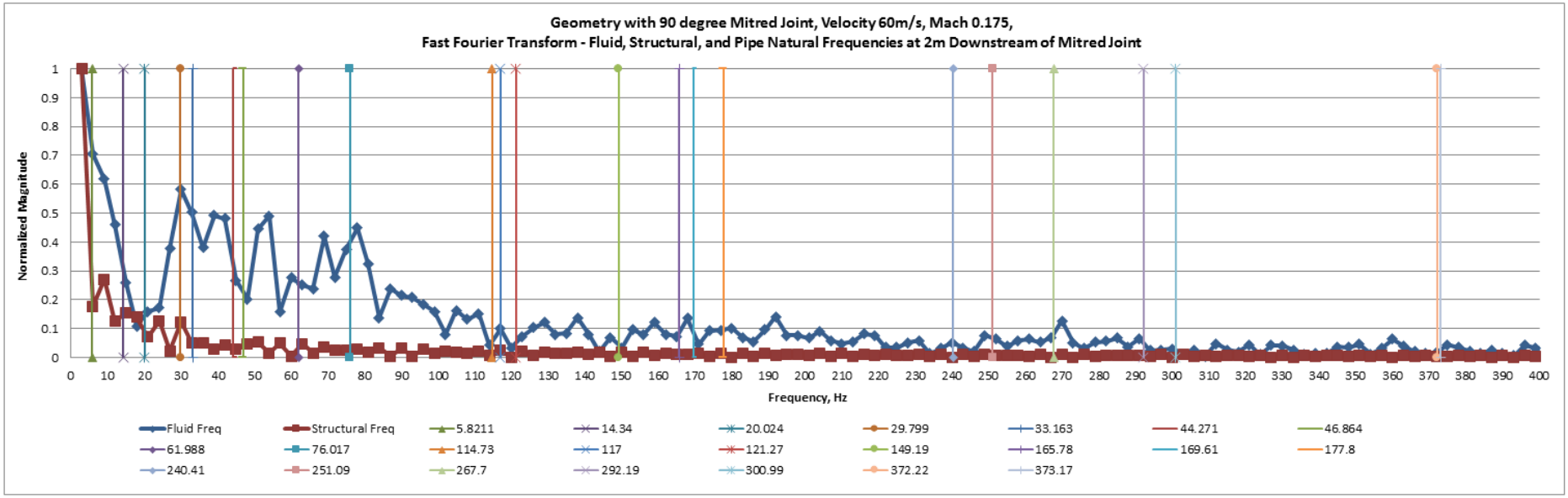
Geometry with 90 degree Mitred Joint, Velocity 60m/s, Mach 0.175,
Fast Fourier Transform - Fluid, Structural, and Pipe Natural Frequencies at 2m Downstream of Mitred Joint
Normalized Magnitude
Frequency, Hz
Fluid Freq
Structural Freq
5.8211
14.34
20.024
29.799
33.163
44.271
46.864
61.988
76.017
114.73
117
121.27
149.19
165.78
169.61
177.8
240.41
251.09
267.7
292.19
300.99
372.22
373.17

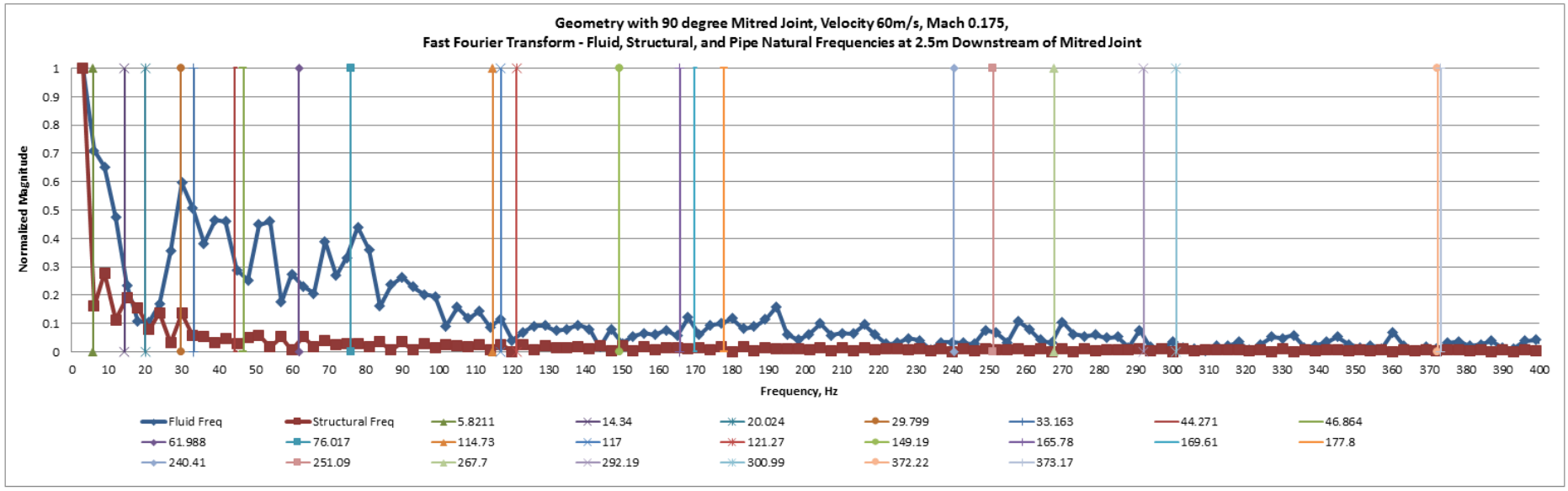
Geometry with 90 degree Mitred Joint, Velocity 60m/s, Mach 0.175,
Fast Fourier Transform - Fluid, Structural, and Pipe Natural Frequencies at 2.5m Downstream of Mitred Joint
Normalized Magnitude
Frequency, Hz
Fluid Freq
Structural Freq
5.8211
14.34
20.024
29.799
33.163
44.271
46.864
61.988
76.017
114.73
117
121.27
149.19
165.78
169.61
177.8
240.41
251.09
267.7
292.19
300.99
372.22
373.17

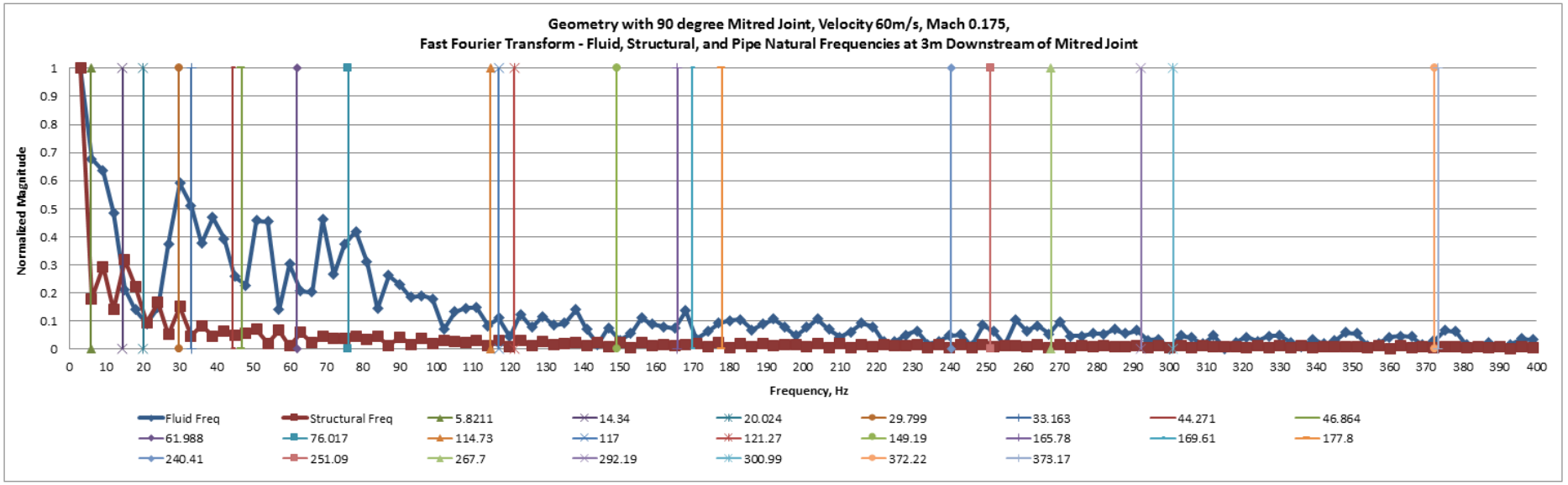
Geometry with 90 degree Mitred Joint, Velocity 60m/s, Mach 0.175,
Fast Fourier Transform - Fluid, Structural, and Pipe Natural Frequencies at 3m Downstream of Mitred Joint
Normalized Magnitude
Frequency, Hz
Fluid Freq
Structural Freq
5.8211
14.34
20.024
29.799
33.163
44.271
46.864
61.988
76.017
114.73
117
121.27
149.19
165.78
169.61
177.8
240.41
251.09
267.7
292.19
300.99
372.22
373.17

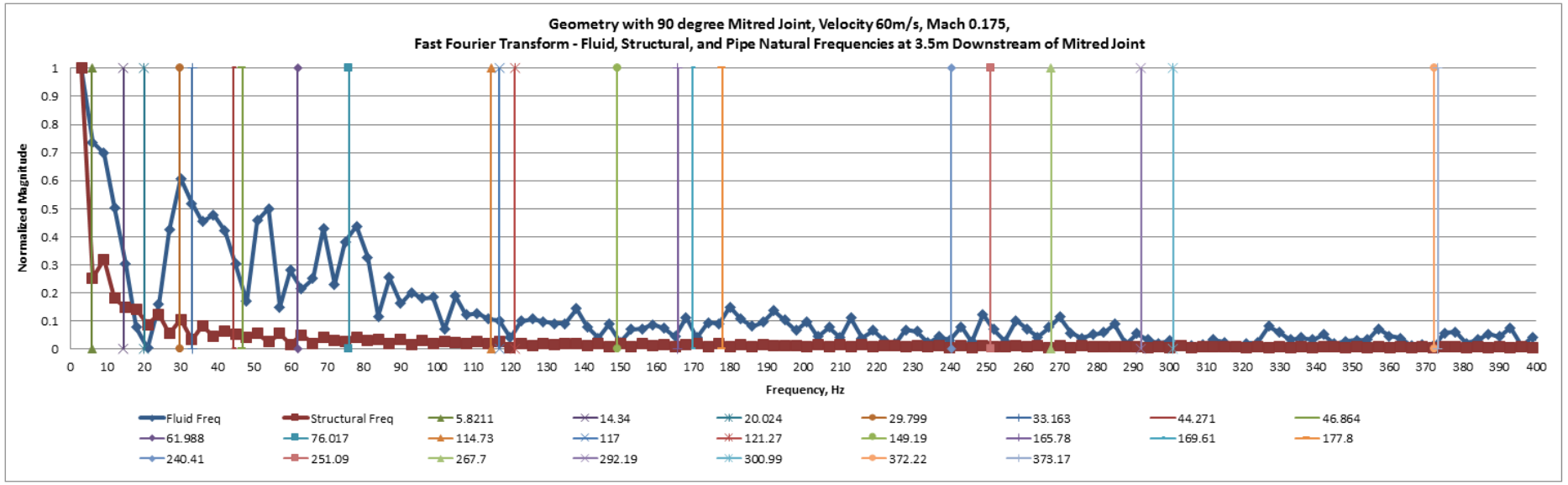
Geometry with 90 degree Mitred Joint, Velocity 60m/s, Mach 0.175,
Fast Fourier Transform - Fluid, Structural, and Pipe Natural Frequencies at 3.5m Downstream of Mitred Joint
Normalized Magnitude
Frequency, Hz
Fluid Freq
Structural Freq
5.8211
14.34
20.024
29.799
33.163
44.271
46.864
61.988
76.017
114.73
117
121.27
149.19
165.78
169.61
177.8
240.41
251.09
267.7
292.19
300.99
372.22
373.17

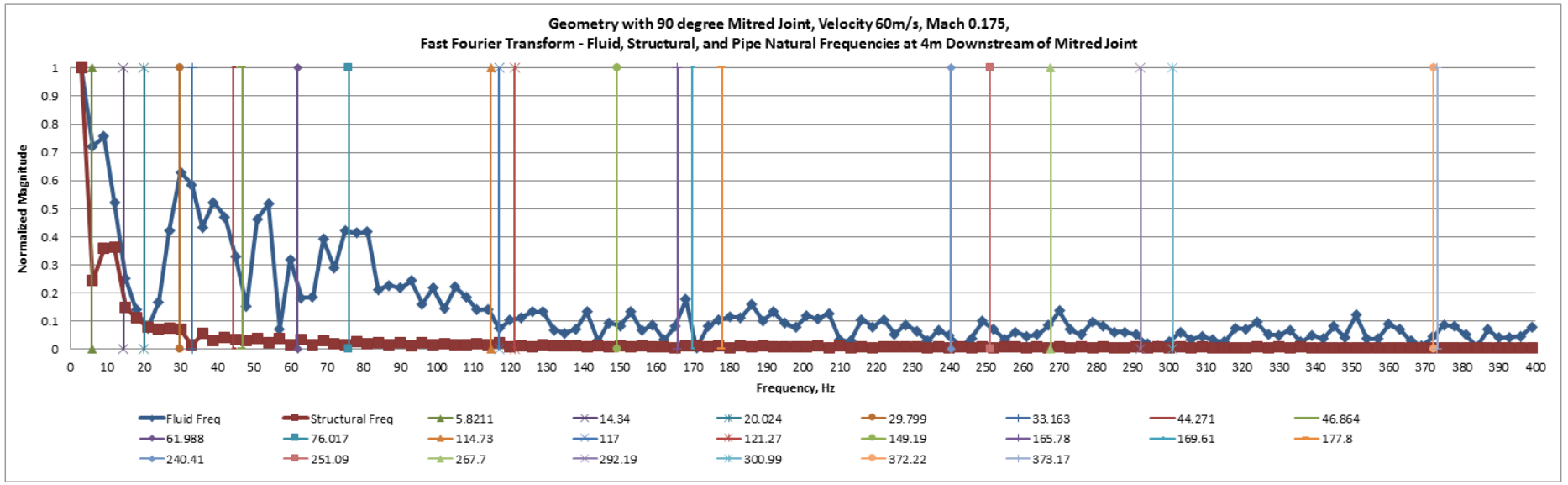
Geometry with 90 degree Mitred Joint, Velocity 60m/s, Mach 0.175,
Fast Fourier Transform - Fluid, Structural, and Pipe Natural Frequencies at 4m Downstream of Mitred Joint
Normalized Magnitude
Frequency, Hz
Fluid Freq
Structural Freq
5.8211
14.34
20.024
29.799
33.163
44.271
46.864
61.988
76.017
114.73
117
121.27
149.19
165.78
169.61
177.8
240.41
251.09
267.7
292.19
300.99
372.22
373.17

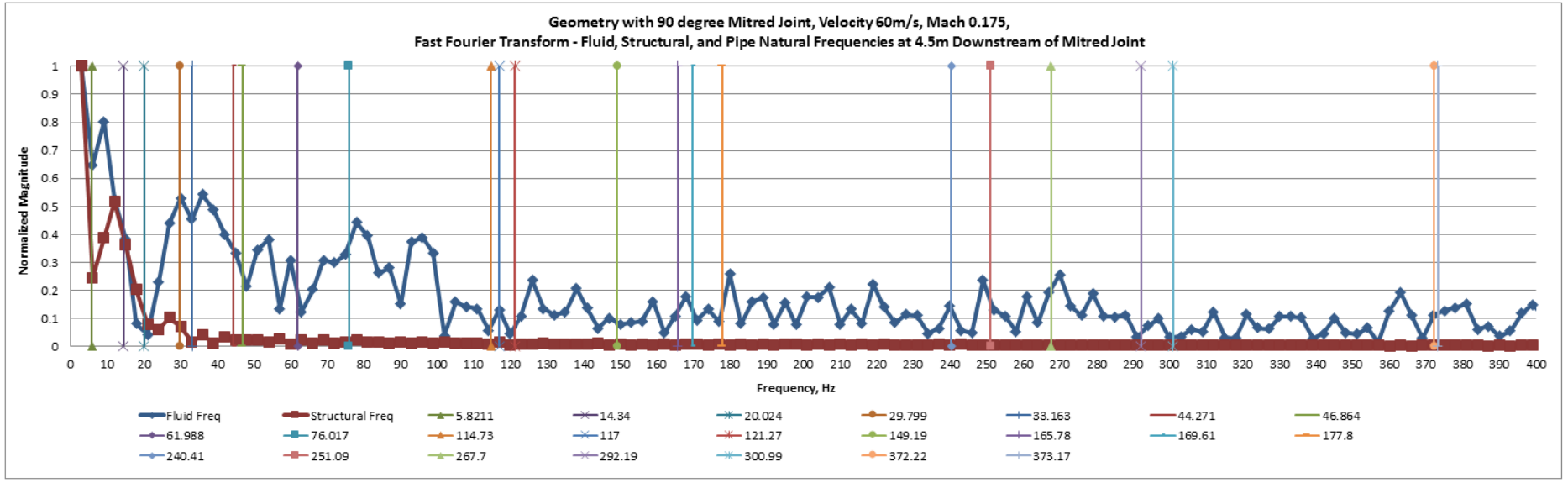
Geometry with 90 degree Mitred Joint, Velocity 60m/s, Mach 0.175,
Fast Fourier Transform - Fluid, Structural, and Pipe Natural Frequencies at 4.5m Downstream of Mitred Joint
Normalized Magnitude
Frequency, Hz
Fluid Freq
Structural Freq
5.8211
14.34
20.024
29.799
33.163
44.271
46.864
61.988
76.017
114.73
117
121.27
149.19
165.78
169.61
177.8
240.41
251.09
267.7
292.19
300.99
372.22
373.17

Appendix G

Frequency Plots for Geometry with 90^0 Mitred Bend for Fluid Velocity modelled at 75m/s, Mach 0.218 at Probe Locations

Distance	Fluid Excited Frequencies Downstream of 90 Degree Mitred Bend
0.1	3, 30, 51, 57
0.3	30, 36, 42, 51, 57, 84, 102
0.5	30, 36, 42, 51, 57, 84
1	30, 36, 42, 51, 57, 78, 84, 129
1.5	30, 36, 42, 57, 78, 84, 129
2.5	30, 36, 42, 51, 57, 78, 84, 129
3	30, 36, 42, 51, 57, 129
3.5	9, 30, 36, 42, 51, 57, 84, 129
4	9, 15, 30, 36, 42, 57, 78, 90, 129
4.5	15, 30, 36, 42, 51, 57, 63, 69, 78, 129

Table G.1: Fluid excited frequencies downstream of the 90 Degree Mitred Bend for 75m/s

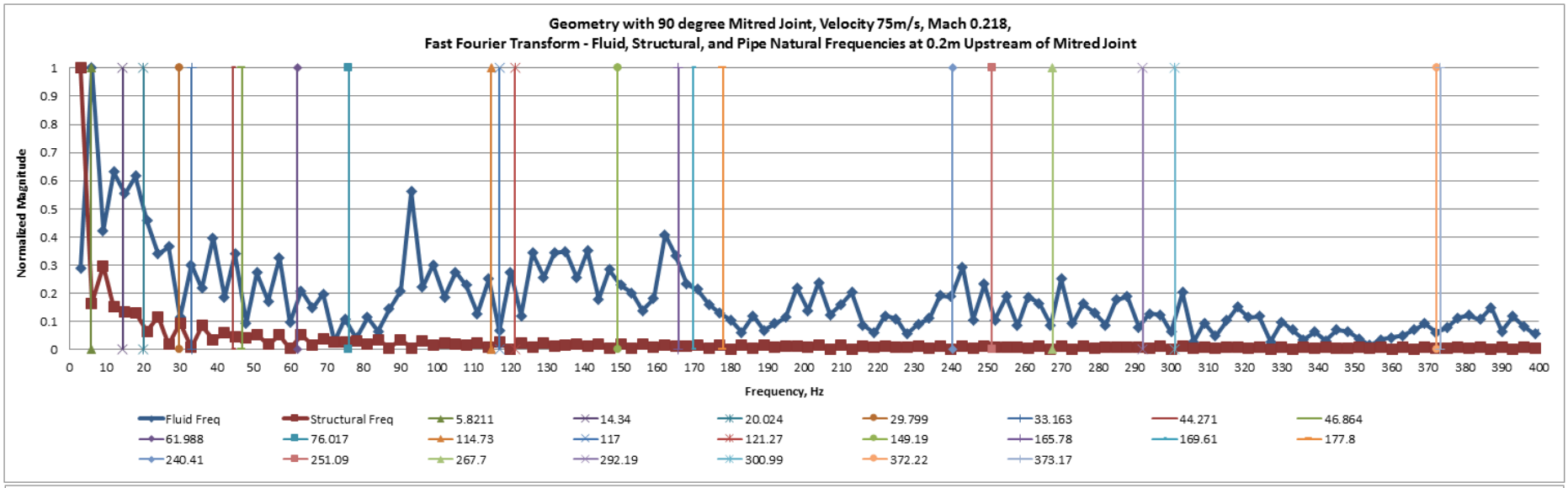
Geometry with 90 degree Mitred Joint, Velocity 75m/s, Mach 0.218,
Fast Fourier Transform - Fluid, Structural, and Pipe Natural Frequencies at 0.2m Upstream of Mitred Joint
Normalized Magnitude
Frequency, Hz
Fluid Freq
Structural Freq
5.8211
14.34
20.024
29.799
33.163
44.271
46.864
61.988
76.017
114.73
117
121.27
149.19
165.78
169.61
177.8
240.41
251.09
267.7
292.19
300.99
372.22
373.17

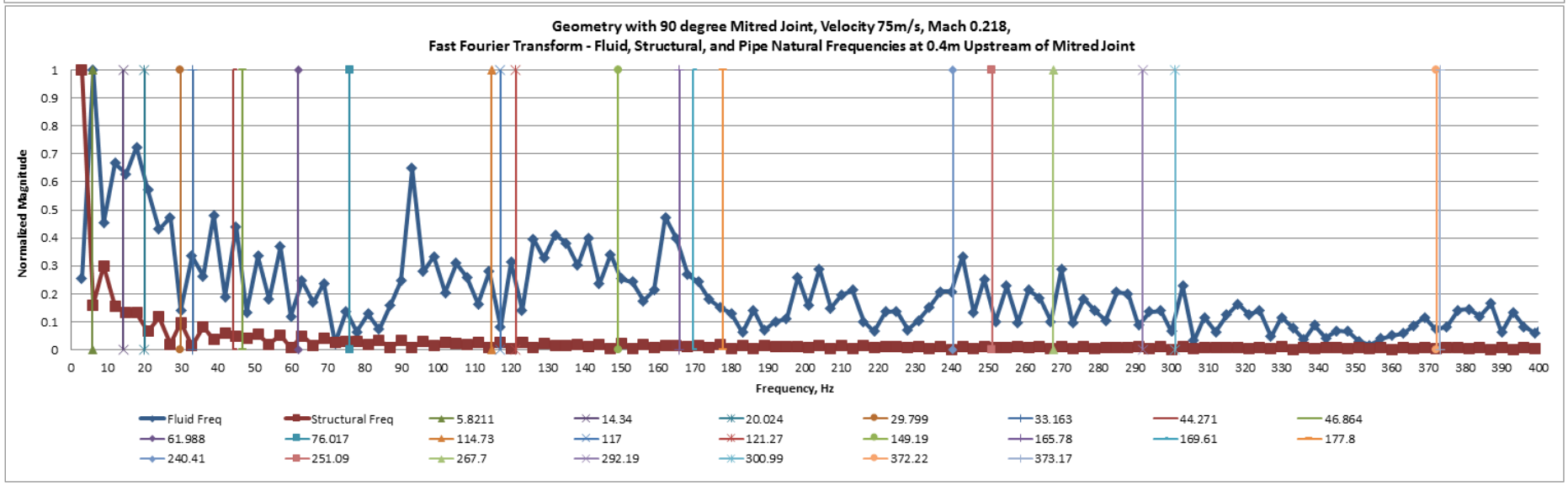
Geometry with 90 degree Mitred Joint, Velocity 75m/s, Mach 0.218,
Fast Fourier Transform - Fluid, Structural, and Pipe Natural Frequencies at 0.4m Upstream of Mitred Joint
Normalized Magnitude
Frequency, Hz
Fluid Freq
Structural Freq
5.8211
14.34
20.024
29.799
33.163
44.271
46.864
61.988
76.017
114.73
117
121.27
149.19
165.78
169.61
177.8
240.41
251.09
267.7
292.19
300.99
372.22
373.17

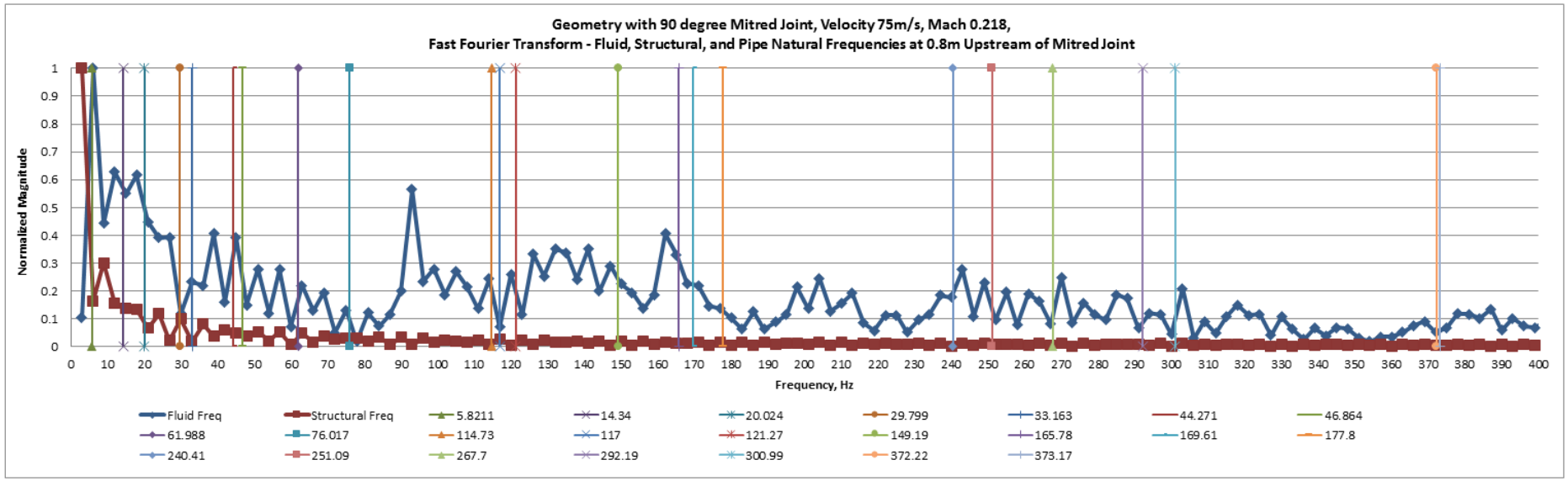
Geometry with 90 degree Mitred Joint, Velocity 75m/s, Mach 0.218,
Fast Fourier Transform - Fluid, Structural, and Pipe Natural Frequencies at 0.8m Upstream of Mitred Joint
Normalized Magnitude
Frequency, Hz
Fluid Freq
Structural Freq
5.8211
14.34
20.024
29.799
33.163
44.271
46.864
61.988
76.017
114.73
117
121.27
149.19
165.78
169.61
177.8
240.41
251.09
267.7
292.19
300.99
372.22
373.17

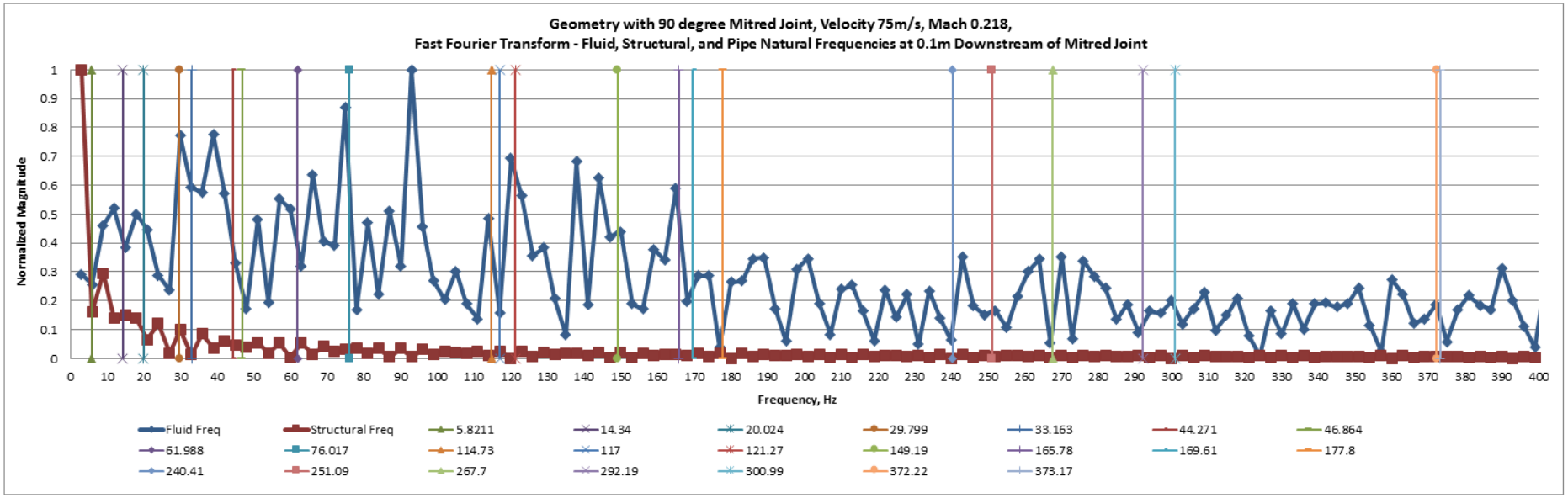
Geometry with 90 degree Mitred Joint, Velocity 75m/s, Mach 0.218,
Fast Fourier Transform - Fluid, Structural, and Pipe Natural Frequencies at 0.1m Downstream of Mitred Joint
Normalized Magnitude
Frequency, Hz
Fluid Freq
Structural Freq
5.8211
14.34
20.024
29.799
33.163
44.271
46.864
61.988
76.017
114.73
117
121.27
149.19
165.78
169.61
177.8
240.41
251.09
267.7
292.19
300.99
372.22
373.17

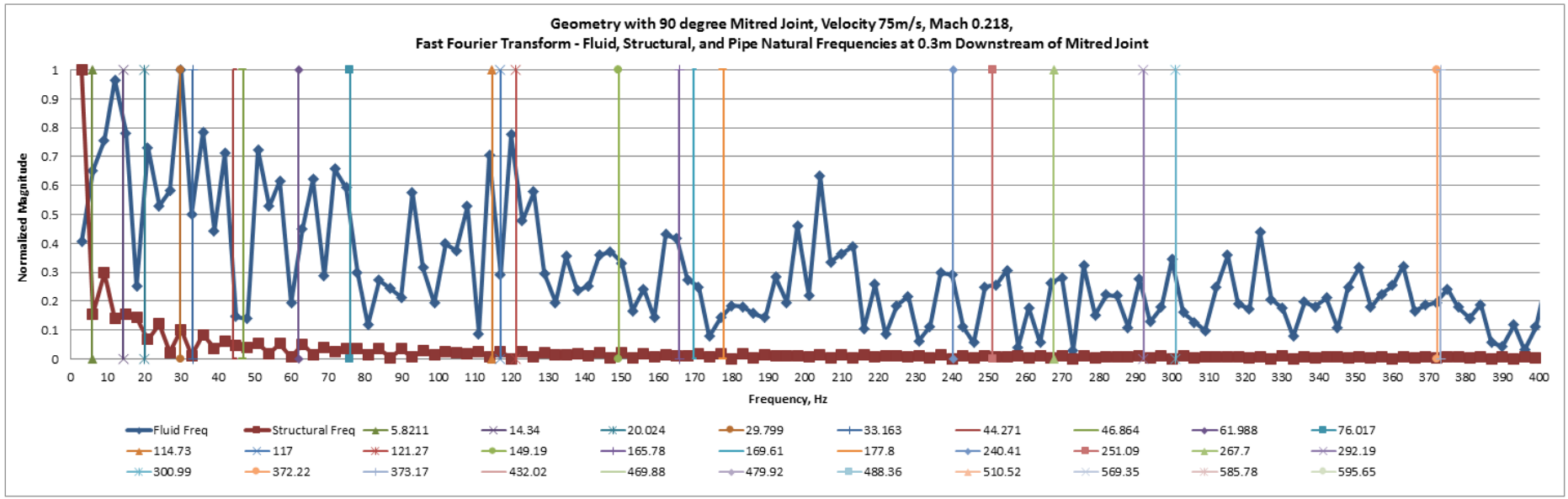
Geometry with 90 degree Mitred Joint, Velocity 75m/s, Mach 0.218,
Fast Fourier Transform - Fluid, Structural, and Pipe Natural Frequencies at 0.3m Downstream of Mitred Joint
Normalized Magnitude
Frequency, Hz
Fluid Freq
Structural Freq
5.8211
14.34
20.024
29.799
33.163
44.271
46.864
61.988
76.017
114.73
117
121.27
149.19
165.78
169.61
177.8
240.41
251.09
267.7
292.19
300.99
372.22
373.17
432.02
469.88
479.92
488.36
510.52
569.35
585.78
595.65

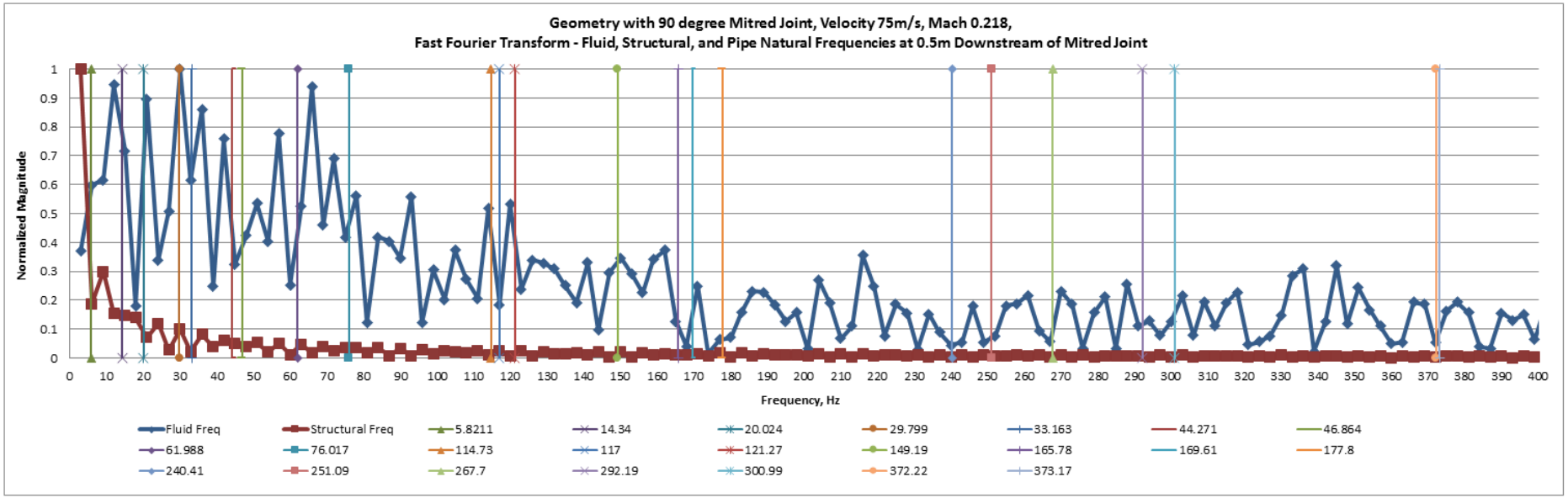
Geometry with 90 degree Mitred Joint, Velocity 75m/s, Mach 0.218,
Fast Fourier Transform - Fluid, Structural, and Pipe Natural Frequencies at 0.5m Downstream of Mitred Joint
Normalized Magnitude
Frequency, Hz
Fluid Freq
Structural Freq
5.8211
14.34
20.024
29.799
33.163
44.271
46.864
61.988
76.017
114.73
117
121.27
149.19
165.78
169.61
177.8
240.41
251.09
267.7
292.19
300.99
372.22
373.17

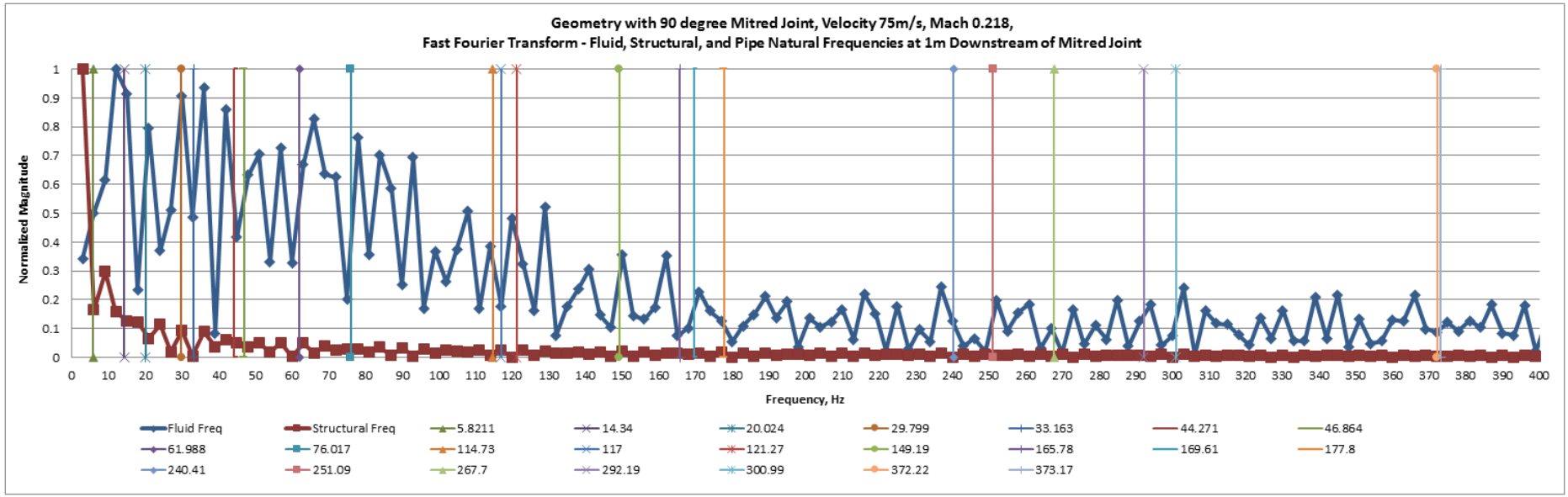
Geometry with 90 degree Mitred Joint, Velocity 75m/s, Mach 0.218,
Fast Fourier Transform - Fluid, Structural, and Pipe Natural Frequencies at 1m Downstream of Mitred Joint
Normalized Magnitude
Frequency, Hz
Fluid Freq
Structural Freq
5.8211
14.34
20.024
29.799
33.163
44.271
46.864
61.988
76.017
114.73
117
121.27
149.19
165.78
169.61
177.8
240.41
251.09
267.7
292.19
300.99
372.22
373.17

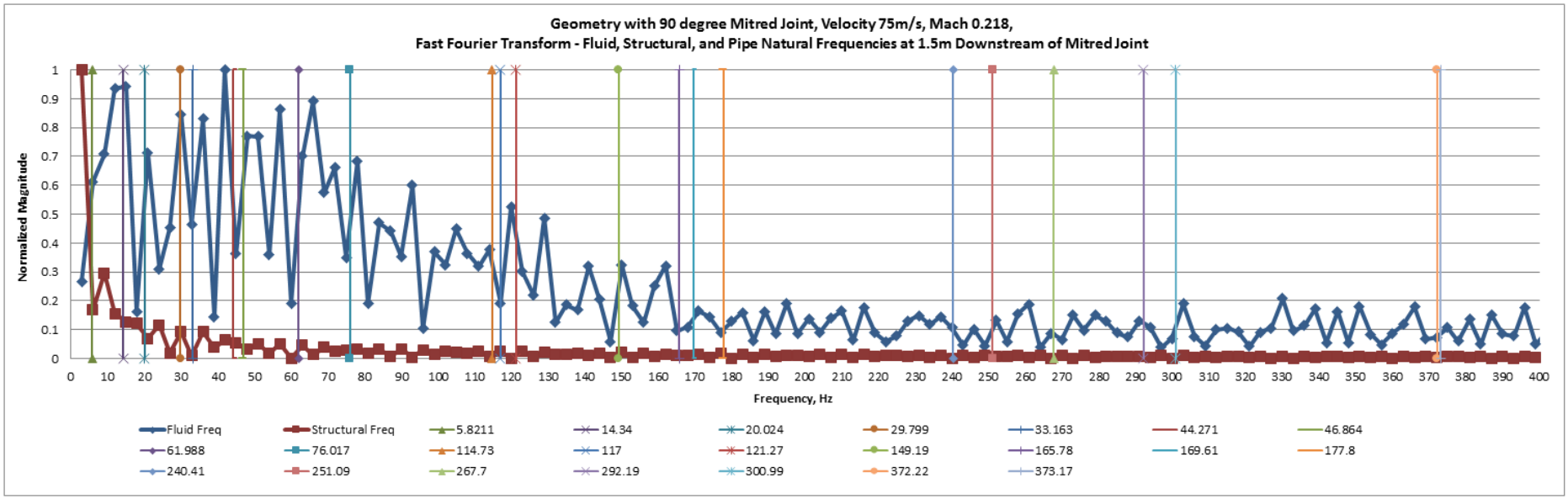
Geometry with 90 degree Mitred Joint, Velocity 75m/s, Mach 0.218,
Fast Fourier Transform - Fluid, Structural, and Pipe Natural Frequencies at 1.5m Downstream of Mitred Joint
Normalized Magnitude
Frequency, Hz
Fluid Freq
Structural Freq
5.8211
14.34
20.024
29.799
33.163
44.271
46.864
61.988
76.017
114.73
117
121.27
149.19
165.78
169.61
177.8
240.41
251.09
267.7
292.19
300.99
372.22
373.17

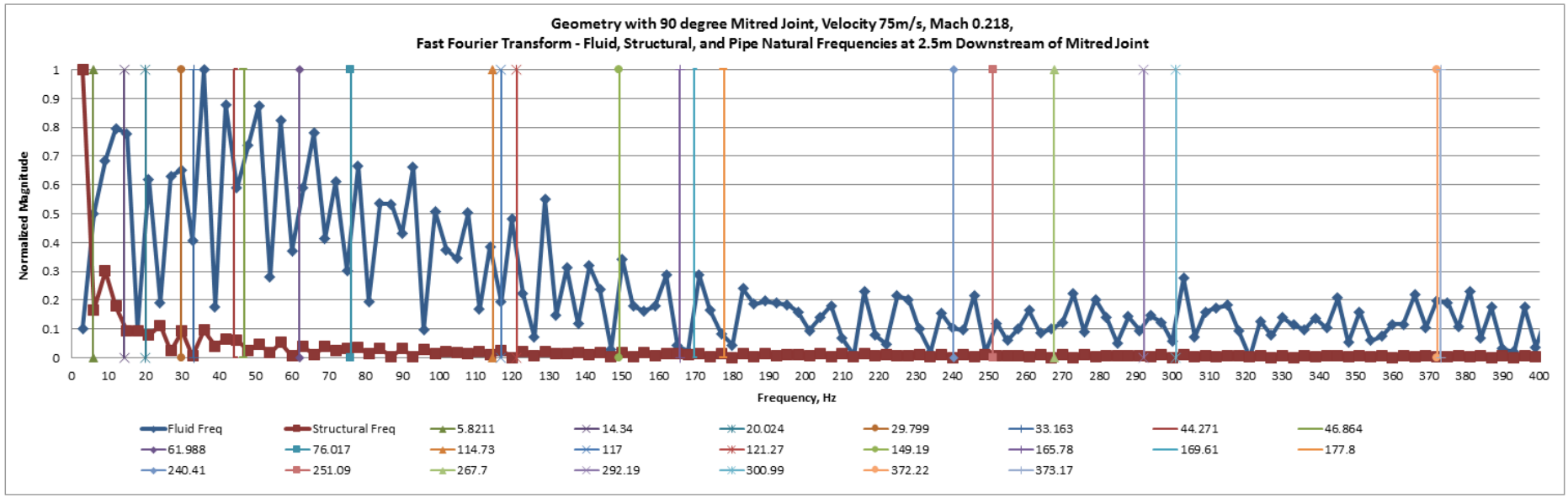
Geometry with 90 degree Mitred Joint, Velocity 75m/s, Mach 0.218,
Fast Fourier Transform - Fluid, Structural, and Pipe Natural Frequencies at 2.5m Downstream of Mitred Joint
Normalized Magnitude
Frequency, Hz
Fluid Freq
Structural Freq
5.8211
14.34
20.024
29.799
33.163
44.271
46.864
61.988
76.017
114.73
117
121.27
149.19
165.78
169.61
177.8
240.41
251.09
267.7
292.19
300.99
372.22
373.17

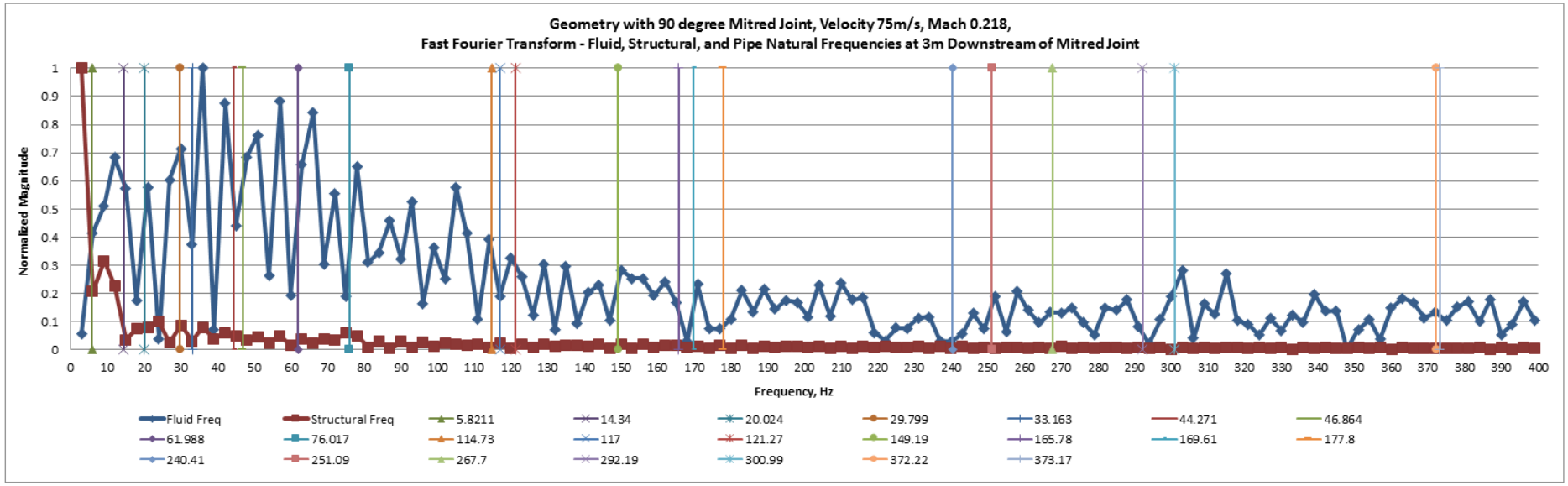
Geometry with 90 degree Mitred Joint, Velocity 75m/s, Mach 0.218,
Fast Fourier Transform - Fluid, Structural, and Pipe Natural Frequencies at 3m Downstream of Mitred Joint
Normalized Magnitude
Frequency, Hz
Fluid Freq
Structural Freq
5.8211
14.34
20.024
29.799
33.163
44.271
46.864
61.988
76.017
114.73
117
121.27
149.19
165.78
169.61
177.8
240.41
251.09
267.7
292.19
300.99
372.22
373.17

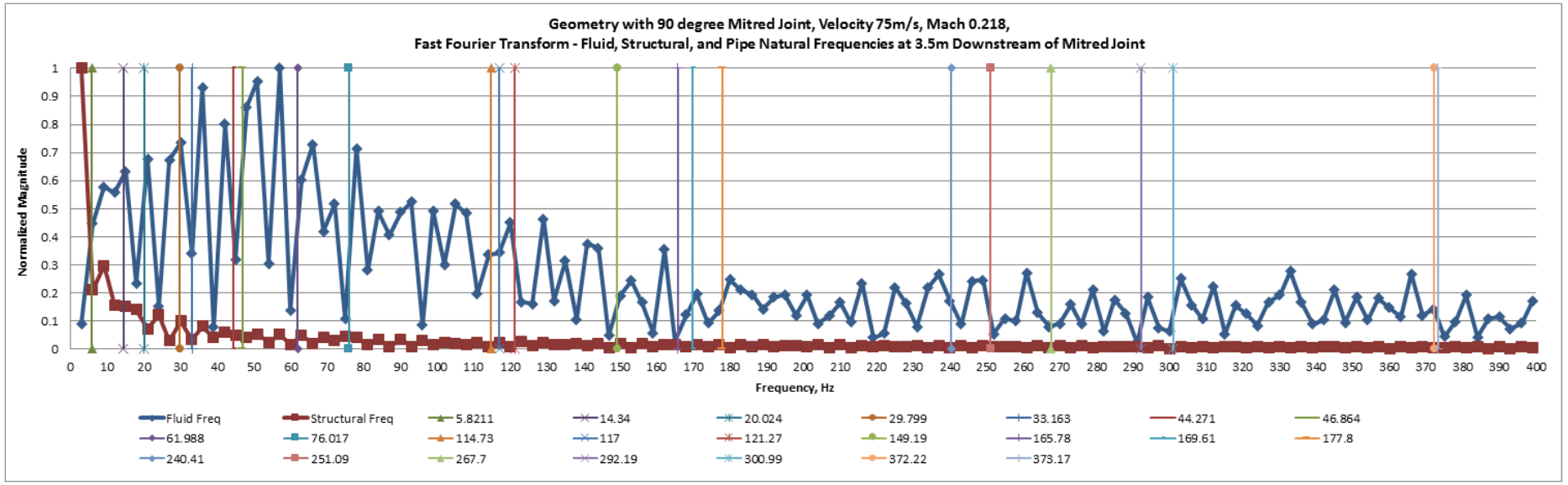
Geometry with 90 degree Mitred Joint, Velocity 75m/s, Mach 0.218,
Fast Fourier Transform - Fluid, Structural, and Pipe Natural Frequencies at 3.5m Downstream of Mitred Joint
Normalized Magnitude
Frequency, Hz
Fluid Freq
Structural Freq
5.8211
14.34
20.024
29.799
33.163
44.271
46.864
61.988
76.017
114.73
117
121.27
149.19
165.78
169.61
177.8
240.41
251.09
267.7
292.19
300.99
372.22
373.17

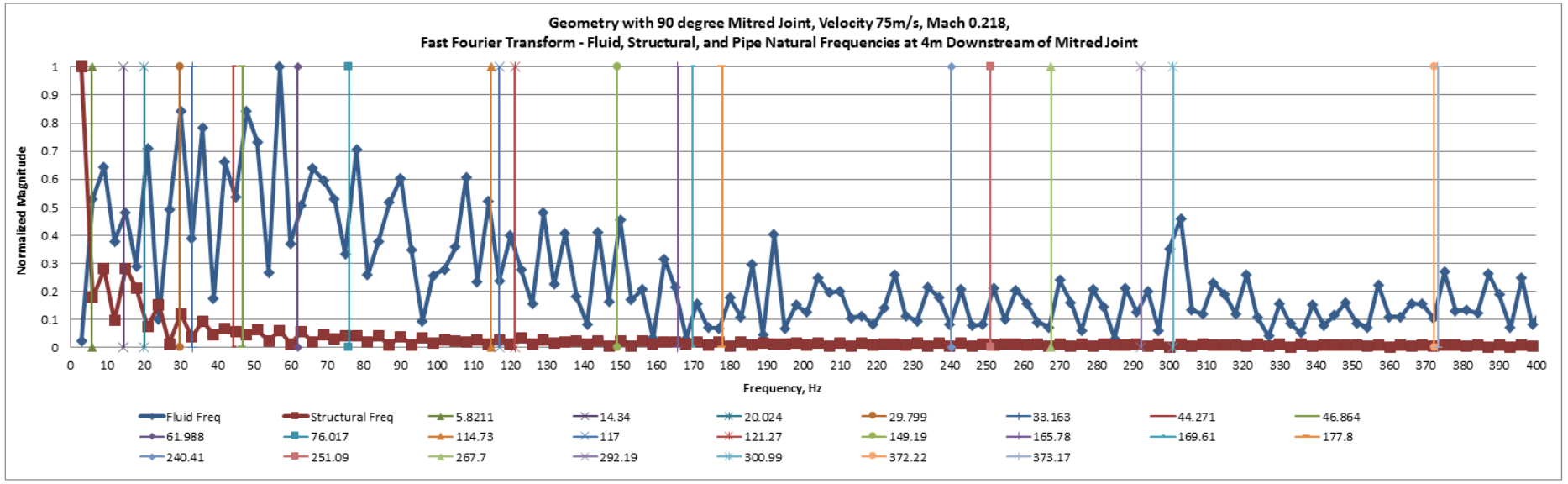
Geometry with 90 degree Mitred Joint, Velocity 75m/s, Mach 0.218,
Fast Fourier Transform - Fluid, Structural, and Pipe Natural Frequencies at 4m Downstream of Mitred Joint
Normalized Magnitude
Frequency, Hz
Fluid Freq
Structural Freq
5.8211
14.34
20.024
29.799
33.163
44.271
46.864
61.988
76.017
114.73
117
121.27
149.19
165.78
169.61
177.8
240.41
251.09
267.7
292.19
300.99
372.22
373.17

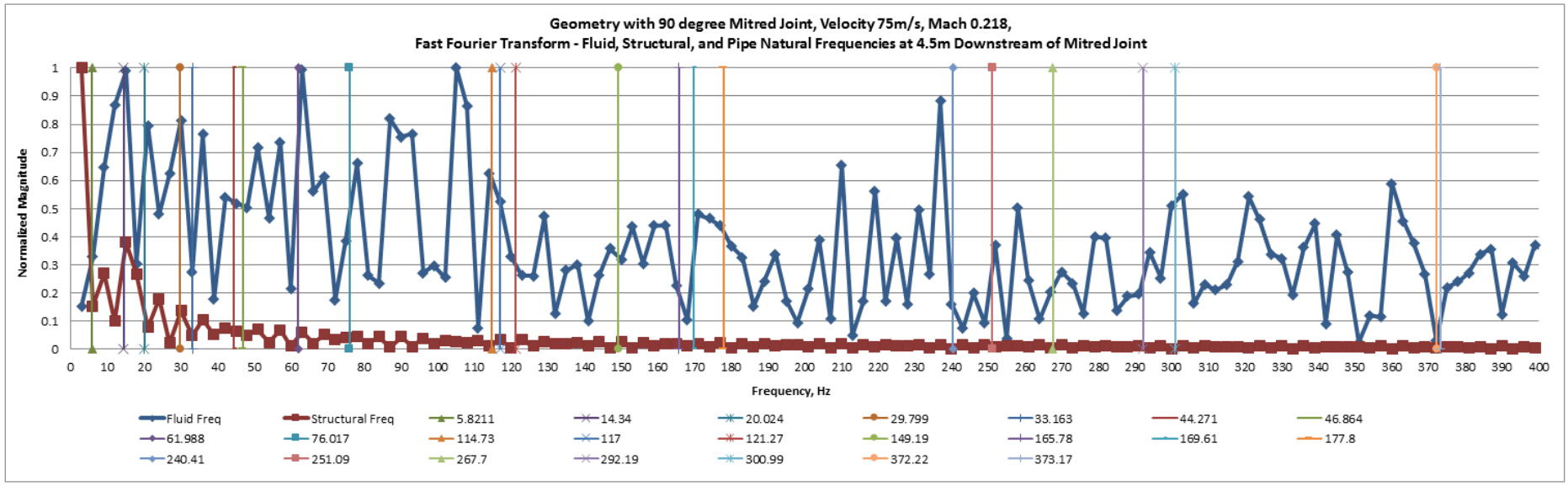
Geometry with 90 degree Mitred Joint, Velocity 75m/s, Mach 0.218,
Fast Fourier Transform - Fluid, Structural, and Pipe Natural Frequencies at 4.5m Downstream of Mitred Joint
Normalized Magnitude
Frequency, Hz
Fluid Freq
Structural Freq
5.8211
14.34
20.024
29.799
33.163
44.271
46.864
61.988
76.017
114.73
117
121.27
149.19
165.78
169.61
177.8
240.41
251.09
267.7
292.19
300.99
372.22
373.17

Appendix H

Pressure Fluctuations and Frequency Plots for Geometry with Tee Junction for Fluid Velocity modelled at 45m/s, Mach 0.131 at Probe Locations

Distance	Fluid Excited Frequencies Downstream of Tee Junction in +X Direction	Fluid Excited Frequencies Downstream of Tee Junction in -X Direction
0.1	36, 45, 102, 126	15, 24, 126
0.3	15, 24, 66, 75, 87, 138	15, 24, 126
0.5	54, 159	Only structural frequencies are present
1	15, 45, 174, 228	3, 27, 66, 78, 102, 162, 213, 228
1.5	3, 27, 45, 66, 162, 228	45, 228, 252, 288
2	45, 102, 132, 147, 183	15, 27, 132, 147, 183
2.5	45, 102, 174, 228	33, 57, 174, 228, 252
3	24, 57, 204, 228, 252, 270, 333	69, 81, 147, 228, 252, 333
3.5	24, 36, 45, 57, 69, 102, 117, 138, 204, 213, 228	228, 252
4	45, 69, 144, 183, 204, 228	15, 204, 252
4.5	18, 165, 198	66, 123, 222

Table H.1: Fluid excited frequencies downstream of the Tee Junction for 45m/s

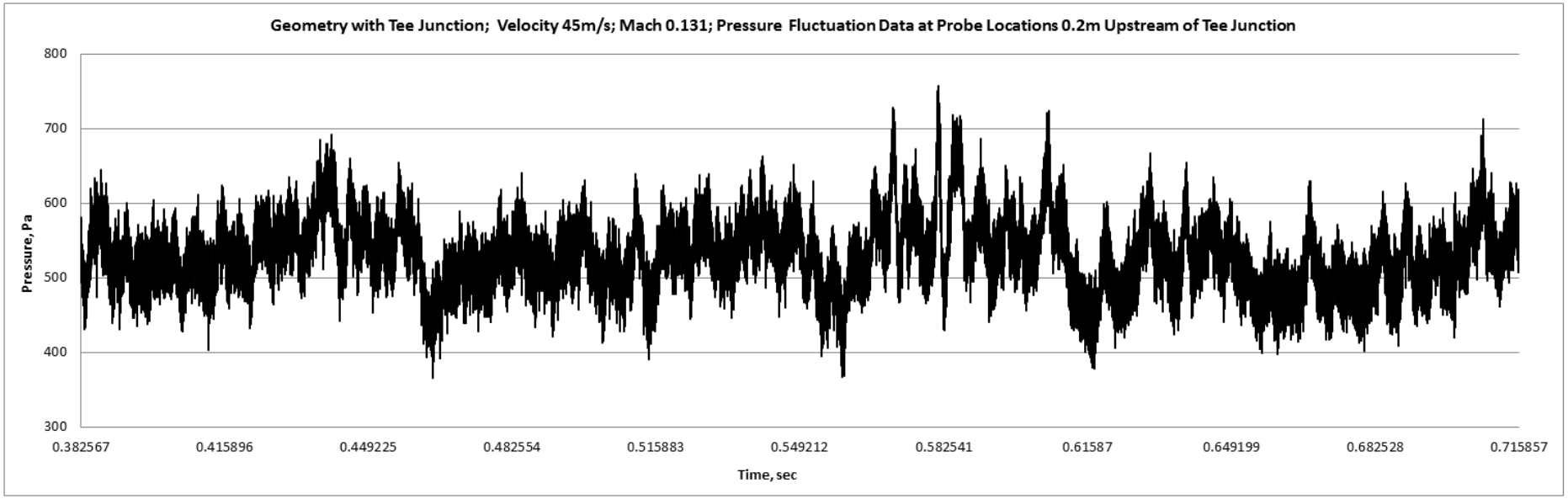
Geometry with Tee Junction; Velocity 45m/s; Mach 0.131; Pressure Fluctuation Data at Probe Locations 0.2m Upstream of Tee Junction
Pressure, Pa
800
700
600
500
400
300
0.382567
0.415896
0.449225
0.482554
0.515883
0.549212
0.582541
0.61587
0.649199
0.682528
0.715857
Time, sec

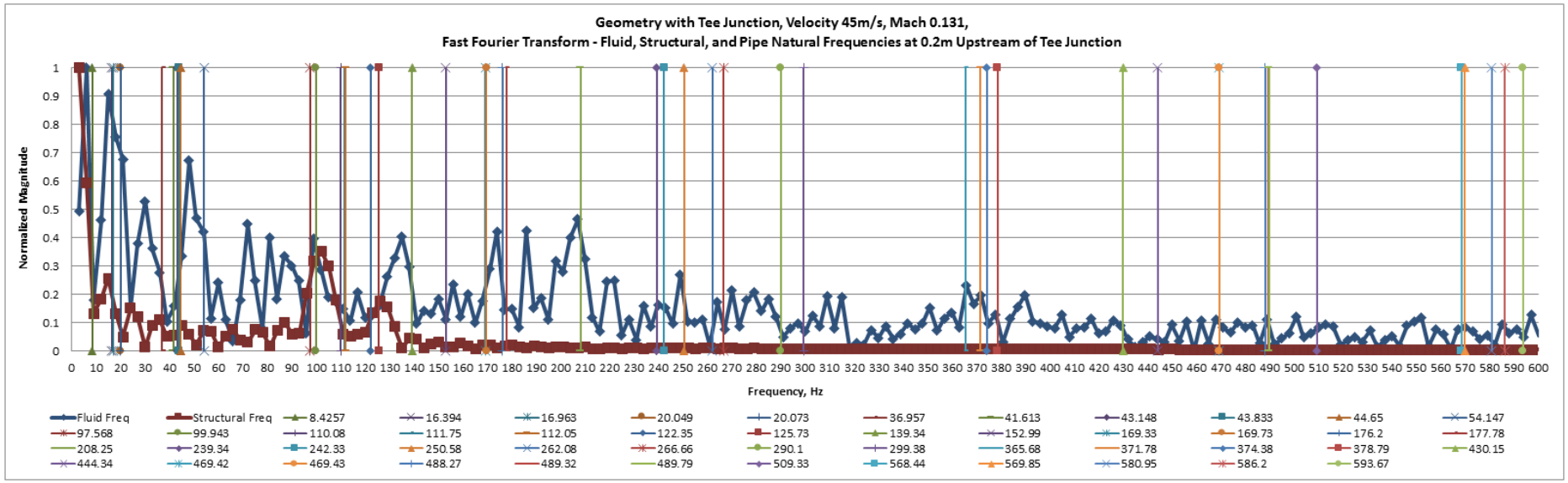
Geometry with Tee Junction, Velocity 45m/s, Mach 0.131,
Fast Fourier Transform - Fluid, Structural, and Pipe Natural Frequencies at 0.2m Upstream of Tee Junction
Normalized Magnitude
Frequency, Hz
Fluid Freq
Structural Freq
8.4257
16.394
16.963
20.049
20.073
36.957
41.613
43.148
43.833
44.65
54.147
97.568
99.943
110.08
111.75
112.05
122.35
125.73
139.34
152.99
169.33
169.73
176.2
177.78
208.25
239.34
242.33
250.58
262.08
266.66
290.1
299.38
365.68
371.78
374.38
378.79
430.15
444.34
469.42
469.43
488.27
489.32
489.79
509.33
568.44
569.85
580.95
586.2
593.67

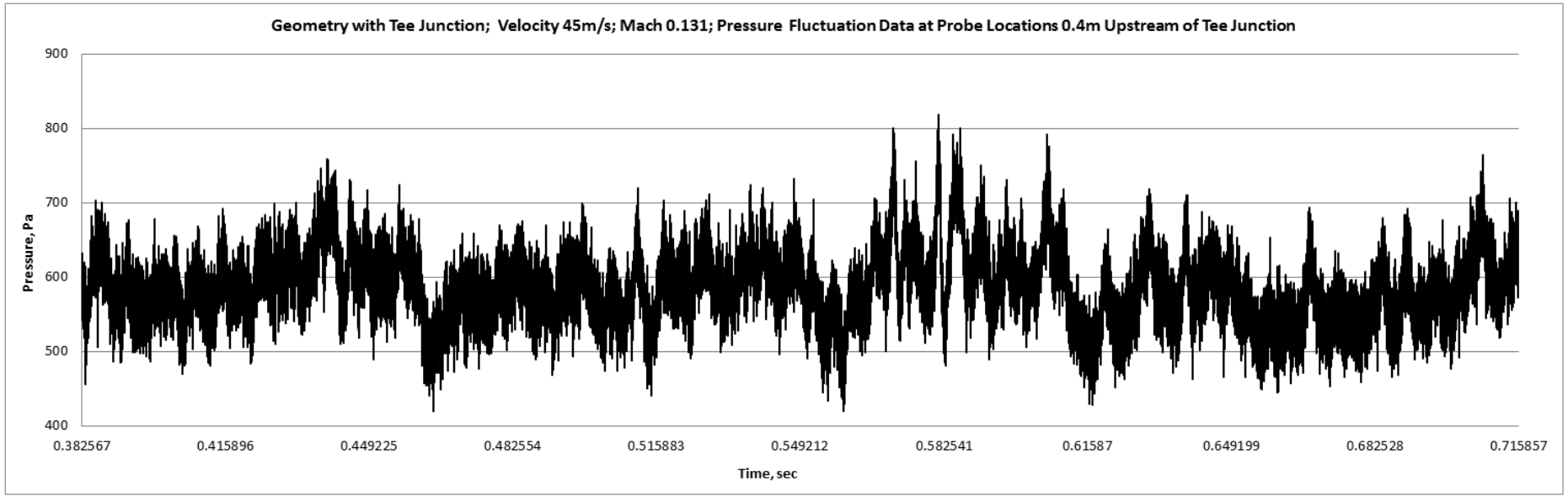
Geometry with Tee Junction; Velocity 45m/s; Mach 0.131; Pressure Fluctuation Data at Probe Locations 0.4m Upstream of Tee Junction
Pressure, Pa
900
800
700
600
500
400
0.382567
0.415896
0.449225
0.482554
0.515883
0.549212
0.582541
0.61587
0.649199
0.682528
0.715857
Time, sec

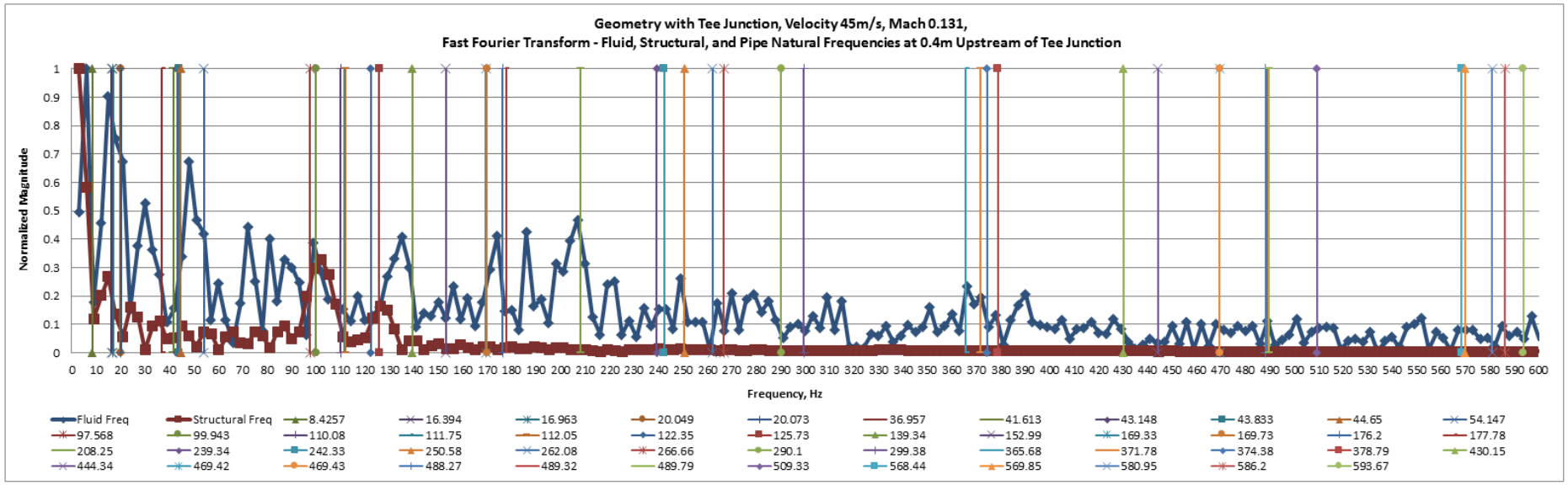
Geometry with Tee Junction, Velocity 45m/s, Mach 0.131,
Fast Fourier Transform - Fluid, Structural, and Pipe Natural Frequencies at 0.4m Upstream of Tee Junction
Normalized Magnitude
Frequency, Hz
Fluid Freq
Structural Freq
8.4257
16.394
16.963
20.049
20.073
36.957
41.613
43.148
43.833
44.65
54.147
97.568
99.943
110.08
111.75
112.05
122.35
125.73
139.34
152.99
169.33
169.73
176.2
177.78
208.25
239.34
242.33
250.58
262.08
266.66
290.1
299.38
365.68
371.78
374.38
378.79
430.15
444.34
469.42
469.43
488.27
489.32
489.79
509.33
568.44
569.85
580.95
586.2
593.67

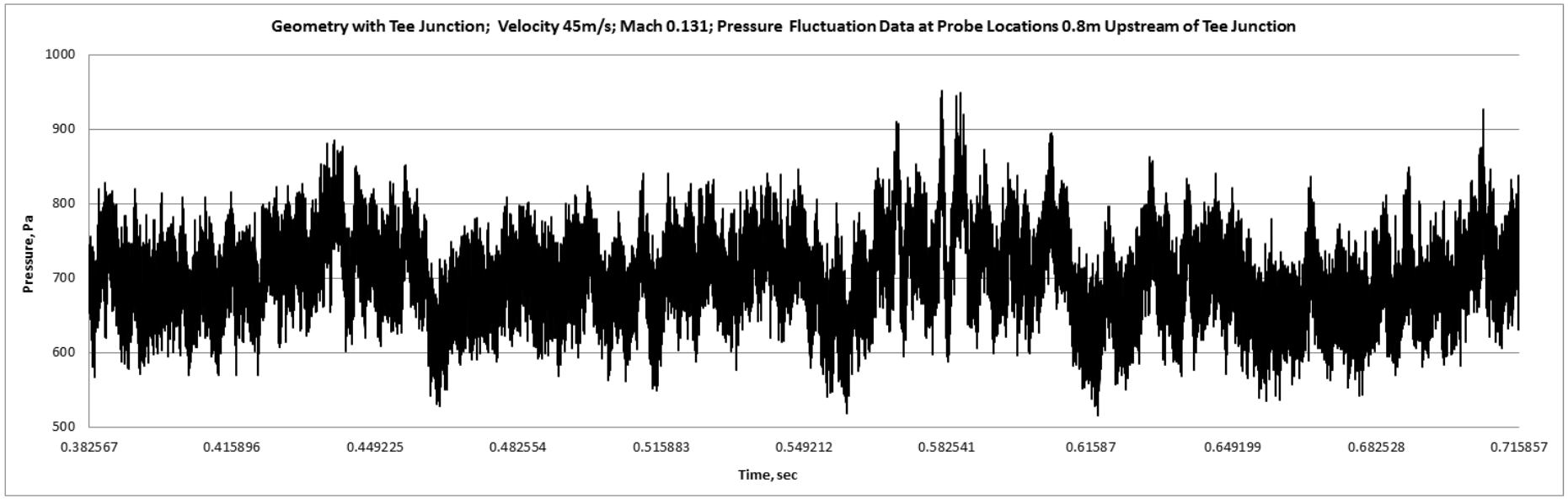
Geometry with Tee Junction; Velocity 45m/s; Mach 0.131; Pressure Fluctuation Data at Probe Locations 0.8m Upstream of Tee Junction
Pressure, Pa
1000
900
800
700
600
500
0.382567
0.415896
0.449225
0.482554
0.515883
0.549212
0.582541
0.61587
0.649199
0.682528
0.715857
Time, sec

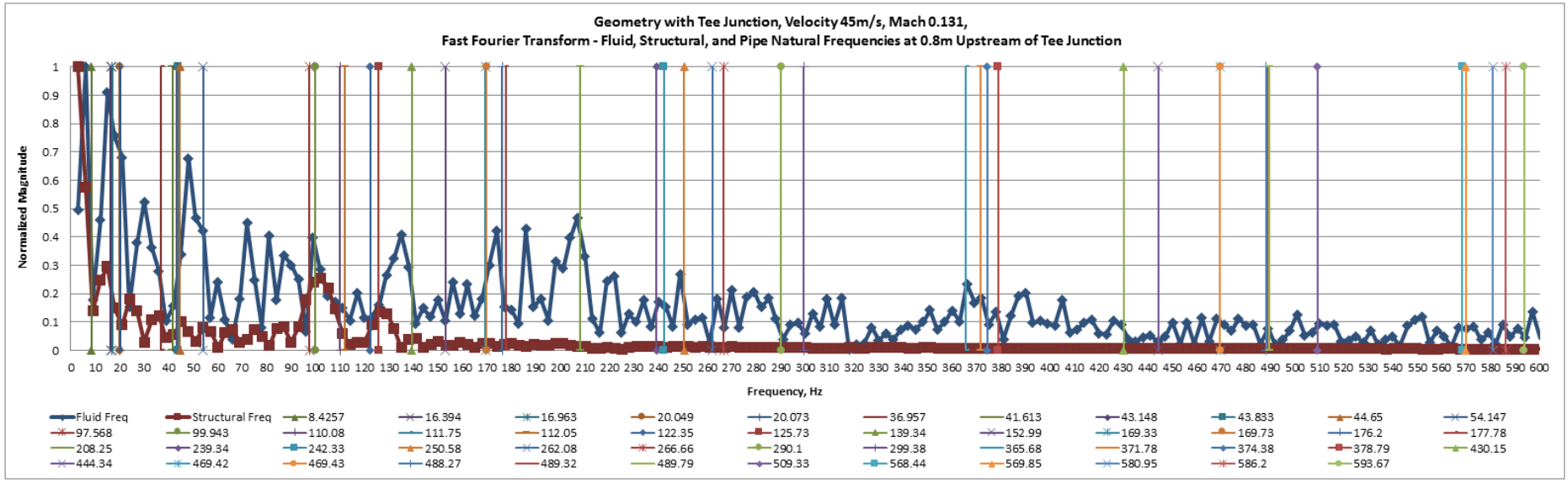
Geometry with Tee Junction, Velocity 45m/s, Mach 0.131,
Fast Fourier Transform - Fluid, Structural, and Pipe Natural Frequencies at 0.8m Upstream of Tee Junction
Normalized Magnitude
Frequency, Hz
Fluid Freq
Structural Freq
8.4257
16.394
16.963
20.049
20.073
36.957
41.613
43.148
43.833
44.65
54.147
97.568
99.943
110.08
111.75
112.05
122.35
125.73
139.34
152.99
169.33
169.73
176.2
177.78
208.25
239.34
242.33
250.58
262.08
266.66
290.1
299.38
365.68
371.78
374.38
378.79
430.15
444.34
469.42
469.43
488.27
489.32
489.79
509.33
568.44
569.85
580.95
586.2
593.67

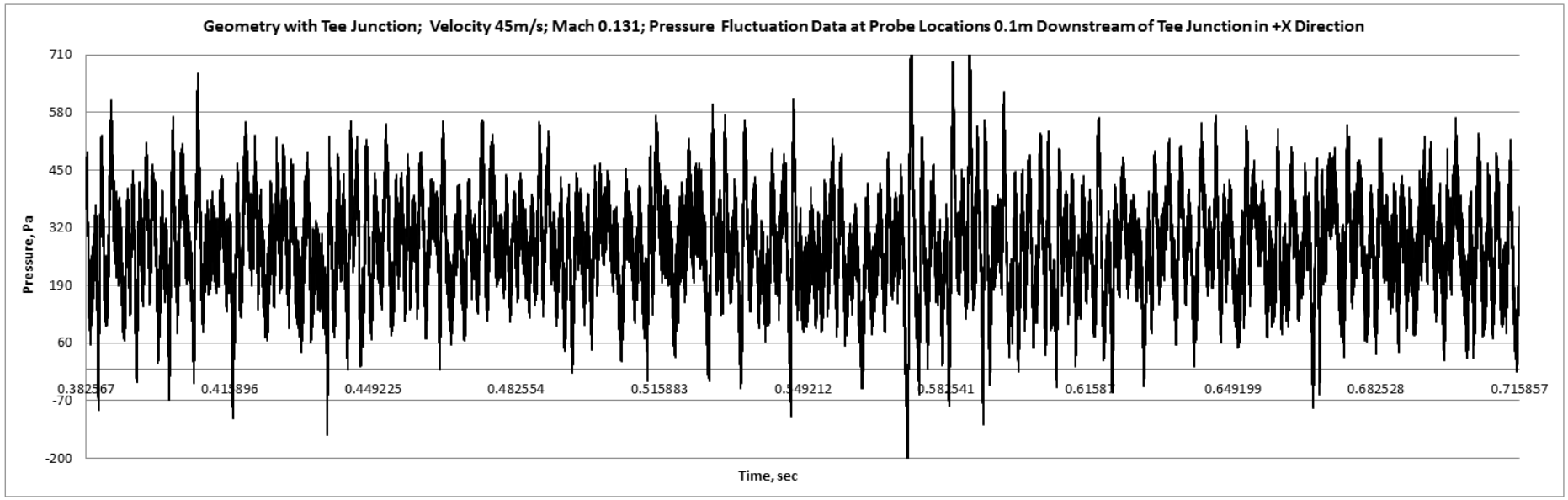
Geometry with Tee Junction; Velocity 45m/s; Mach 0.131; Pressure Fluctuation Data at Probe Locations 0.1m Downstream of Tee Junction in +X Direction
Pressure, Pa
710
580
450
320
190
60
-70
-200
0.382567
0.415896
0.449225
0.482554
0.515883
0.549212
0.582541
0.61587
0.649199
0.682528
0.715857
Time, sec

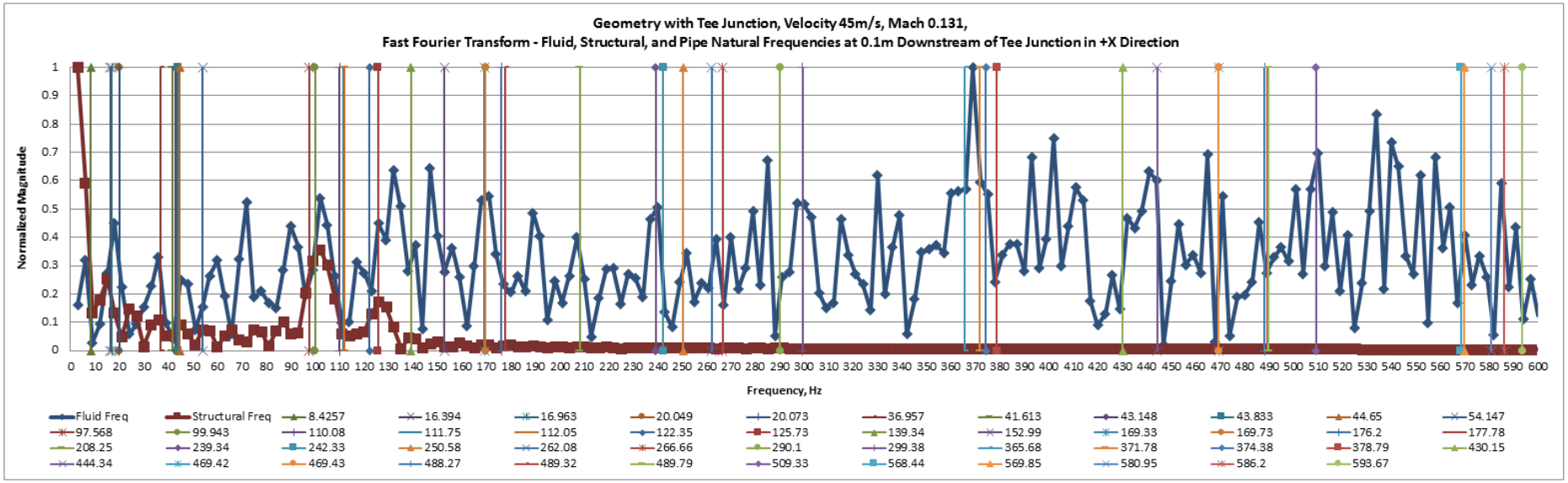
Geometry with Tee Junction, Velocity 45m/s, Mach 0.131,
Fast Fourier Transform - Fluid, Structural, and Pipe Natural Frequencies at 0.1m Downstream of Tee Junction in +X Direction
Normalized Magnitude
Frequency, Hz
Fluid Freq
Structural Freq
8.4257
16.394
16.963
20.049
20.073
36.957
41.613
43.148
43.833
44.65
54.147
97.568
99.943
110.08
111.75
112.05
122.35
125.73
139.34
152.99
169.33
169.73
176.2
177.78
208.25
239.34
242.33
250.58
262.08
266.66
290.1
299.38
365.68
371.78
374.38
378.79
430.15
444.34
469.42
469.43
488.27
489.32
489.79
509.33
568.44
569.85
580.95
586.2
593.67

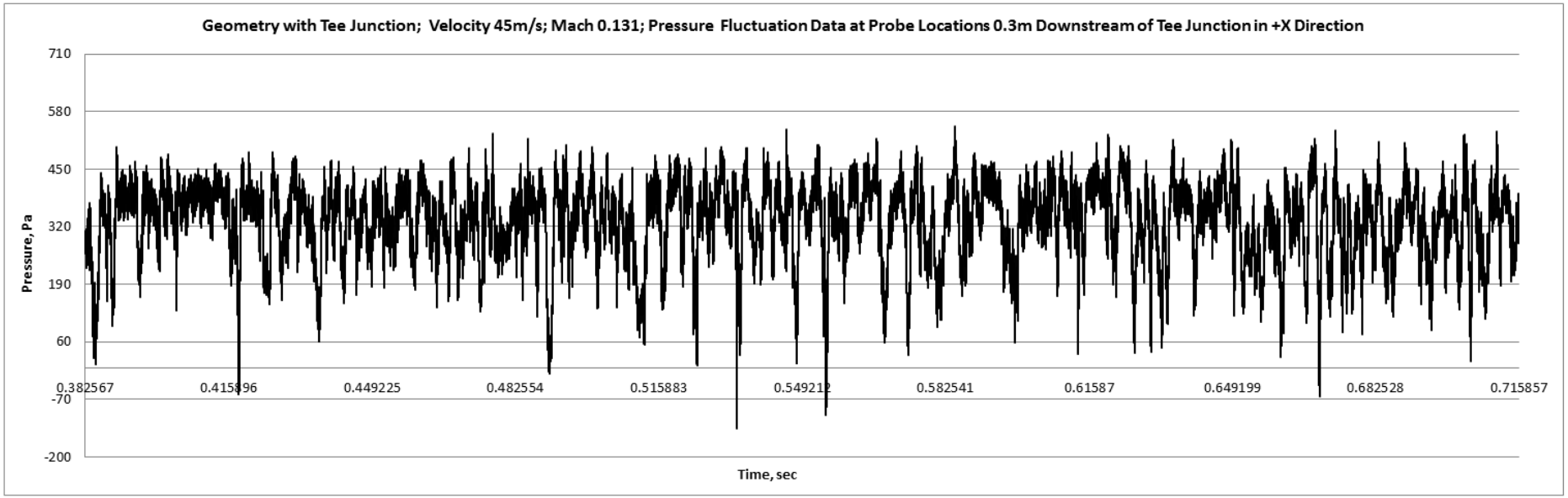
Geometry with Tee Junction; Velocity 45m/s; Mach 0.131; Pressure Fluctuation Data at Probe Locations 0.3m Downstream of Tee Junction in +X Direction
Pressure, Pa
710
580
450
320
190
60
-70
-200
0.382567
0.415896
0.449225
0.482554
0.515883
0.549212
0.582541
0.61587
0.649199
0.682528
0.715857
Time, sec

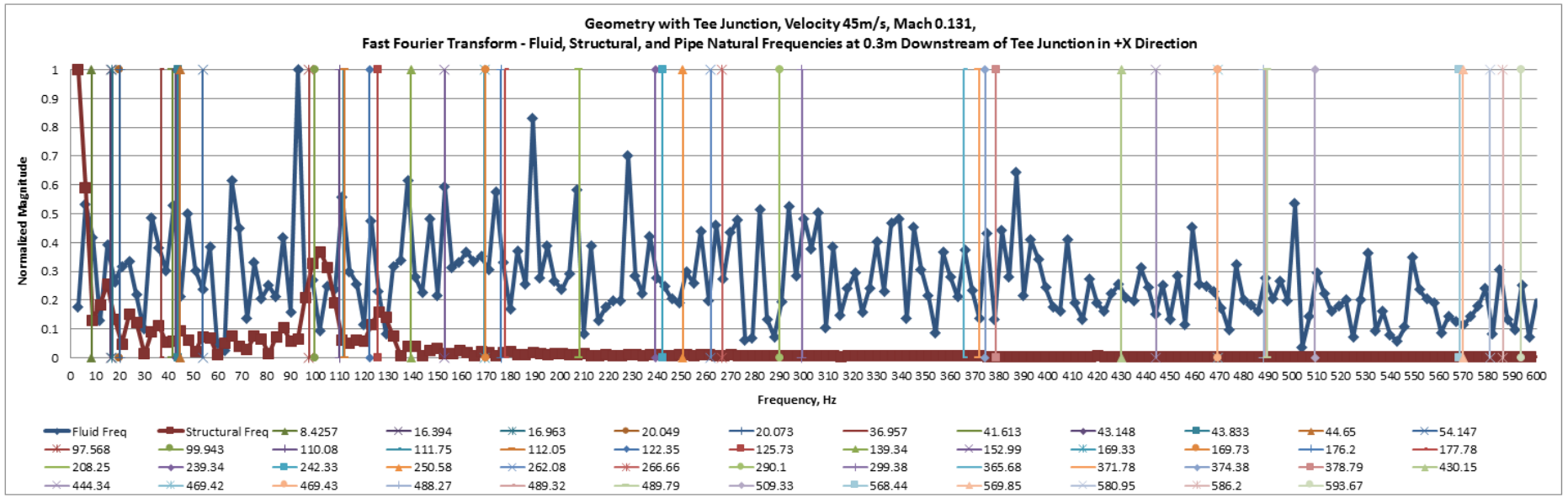
Geometry with Tee Junction, Velocity 45m/s, Mach 0.131,
Fast Fourier Transform - Fluid, Structural, and Pipe Natural Frequencies at 0.3m Downstream of Tee Junction in +X Direction
Normalized Magnitude
Frequency, Hz
Fluid Freq
Structural Freq
8.4257
16.394
16.963
20.049
20.073
36.957
41.613
43.148
43.833
44.65
54.147
97.568
99.943
110.08
111.75
112.05
122.35
125.73
139.34
152.99
169.33
169.73
176.2
177.78
208.25
239.34
242.33
250.58
262.08
266.66
290.1
299.38
365.68
371.78
374.38
378.79
430.15
444.34
469.42
469.43
488.27
489.32
489.79
509.33
568.44
569.85
580.95
586.2
593.67

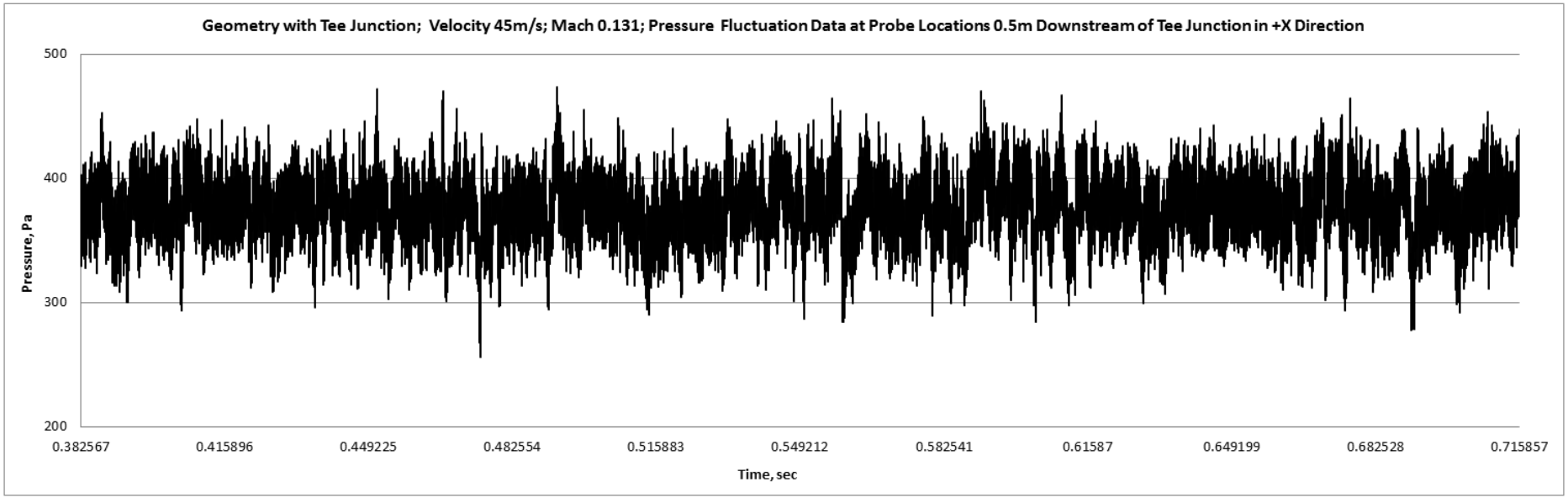
Geometry with Tee Junction; Velocity 45m/s; Mach 0.131; Pressure Fluctuation Data at Probe Locations 0.5m Downstream of Tee Junction in +X Direction
Pressure, Pa
500
400
300
200
0.382567
0.415896
0.449225
0.482554
0.515883
0.549212
0.582541
0.61587
0.649199
0.682528
0.715857
Time, sec

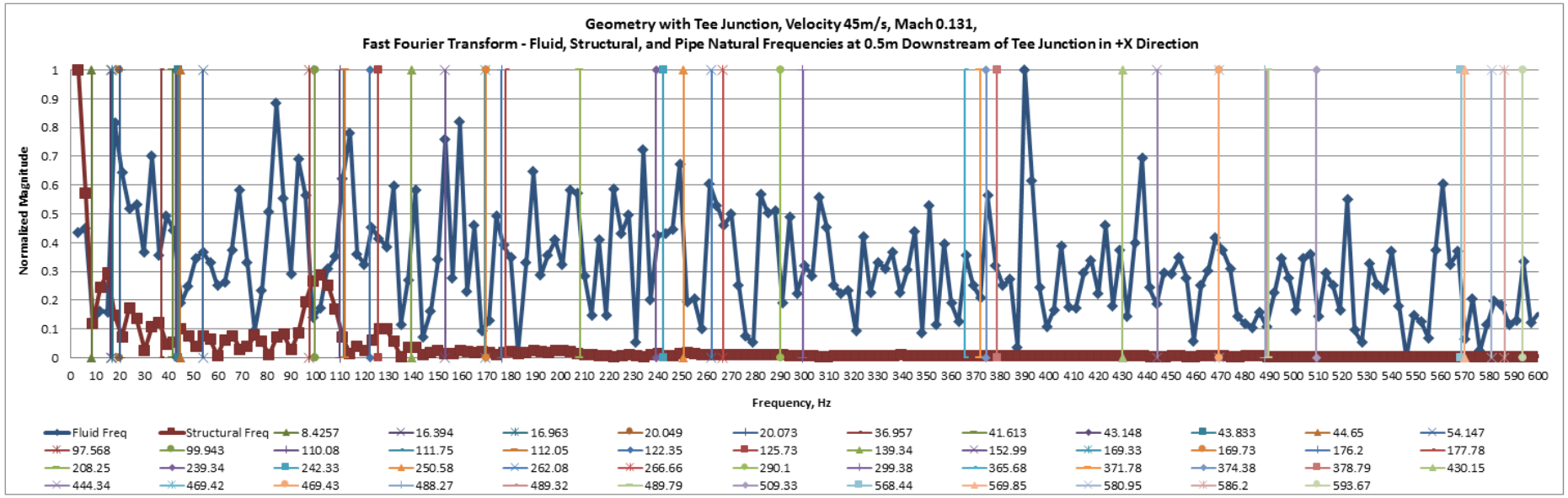
Geometry with Tee Junction, Velocity 45m/s, Mach 0.131,
Fast Fourier Transform - Fluid, Structural, and Pipe Natural Frequencies at 0.5m Downstream of Tee Junction in +X Direction
Normalized Magnitude
Frequency, Hz
Fluid Freq
Structural Freq
8.4257
16.394
16.963
20.049
20.073
36.957
41.613
43.148
43.833
44.65
54.147
97.568
99.943
110.08
111.75
112.05
122.35
125.73
139.34
152.99
169.33
169.73
176.2
177.78
208.25
239.34
242.33
250.58
262.08
266.66
290.1
299.38
365.68
371.78
374.38
378.79
430.15
444.34
469.42
469.43
488.27
489.32
489.79
509.33
568.44
569.85
580.95
586.2
593.67

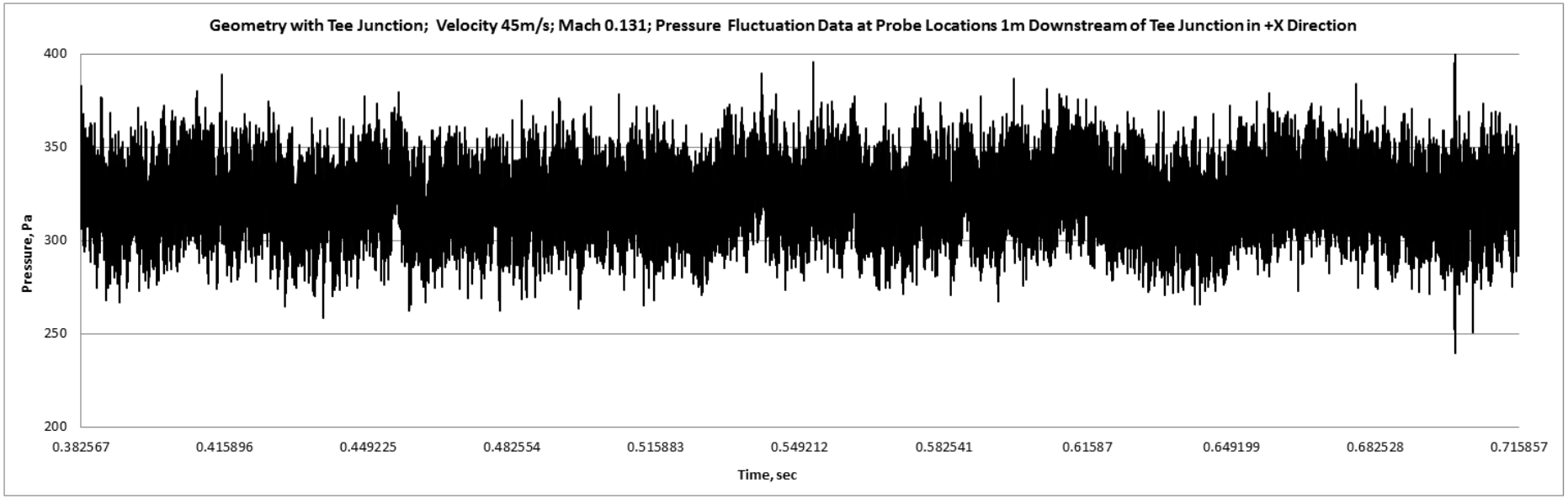
Geometry with Tee Junction; Velocity 45m/s; Mach 0.131; Pressure Fluctuation Data at Probe Locations 1m Downstream of Tee Junction in +X Direction
Pressure, Pa
400
350
300
250
200
0.382567
0.415896
0.449225
0.482554
0.515883
0.549212
0.582541
0.61587
0.649199
0.682528
0.715857
Time, sec

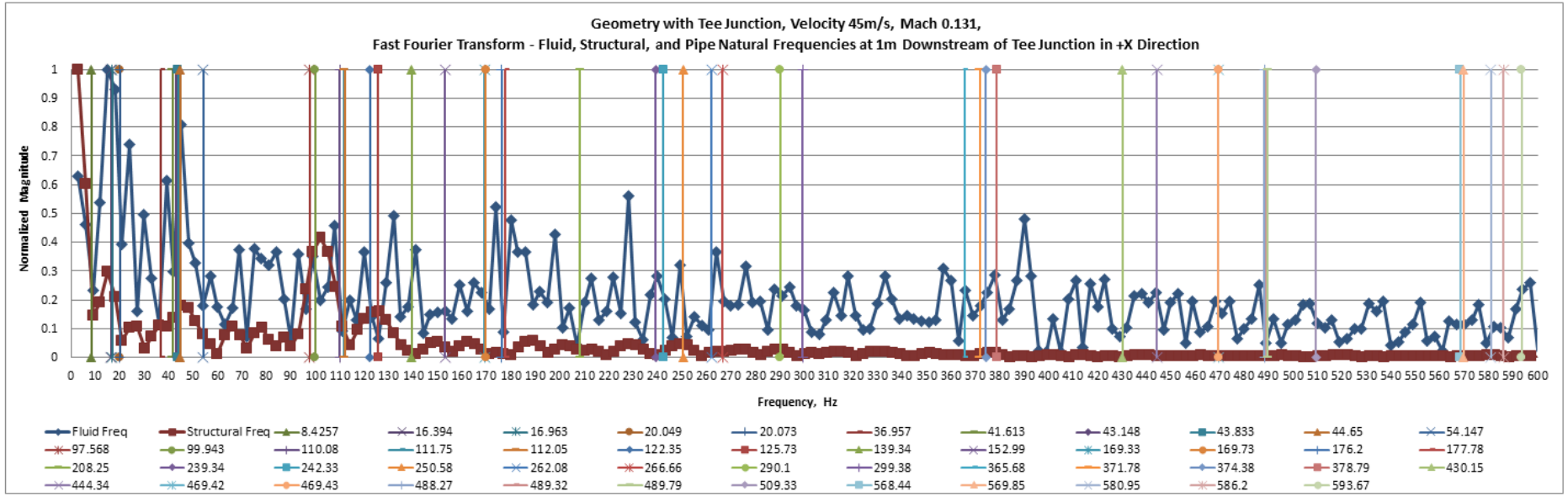
Geometry with Tee Junction, Velocity 45m/s, Mach 0.131,
Fast Fourier Transform - Fluid, Structural, and Pipe Natural Frequencies at 1m Downstream of Tee Junction in +X Direction
Normalized Magnitude
Frequency, Hz
Fluid Freq
Structural Freq
8.4257
16.394
16.963
20.049
20.073
36.957
41.613
43.148
43.833
44.65
54.147
97.568
99.943
110.08
111.75
112.05
122.35
125.73
139.34
152.99
169.33
169.73
176.2
177.78
208.25
239.34
242.33
250.58
262.08
266.66
290.1
299.38
365.68
371.78
374.38
378.79
430.15
444.34
469.42
469.43
488.27
489.32
489.79
509.33
568.44
569.85
580.95
586.2
593.67

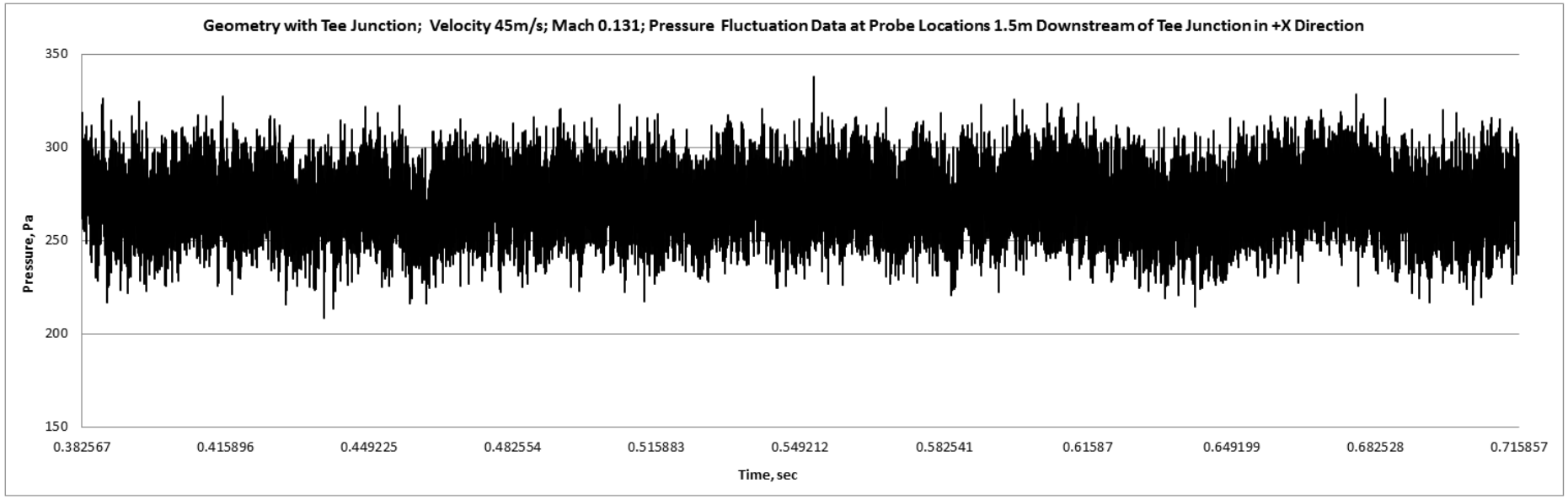
Geometry with Tee Junction; Velocity 45m/s; Mach 0.131; Pressure Fluctuation Data at Probe Locations 1.5m Downstream of Tee Junction in +X Direction
Pressure, Pa
350
300
250
200
150
0.382567
0.415896
0.449225
0.482554
0.515883
0.549212
0.582541
0.61587
0.649199
0.682528
0.715857
Time, sec

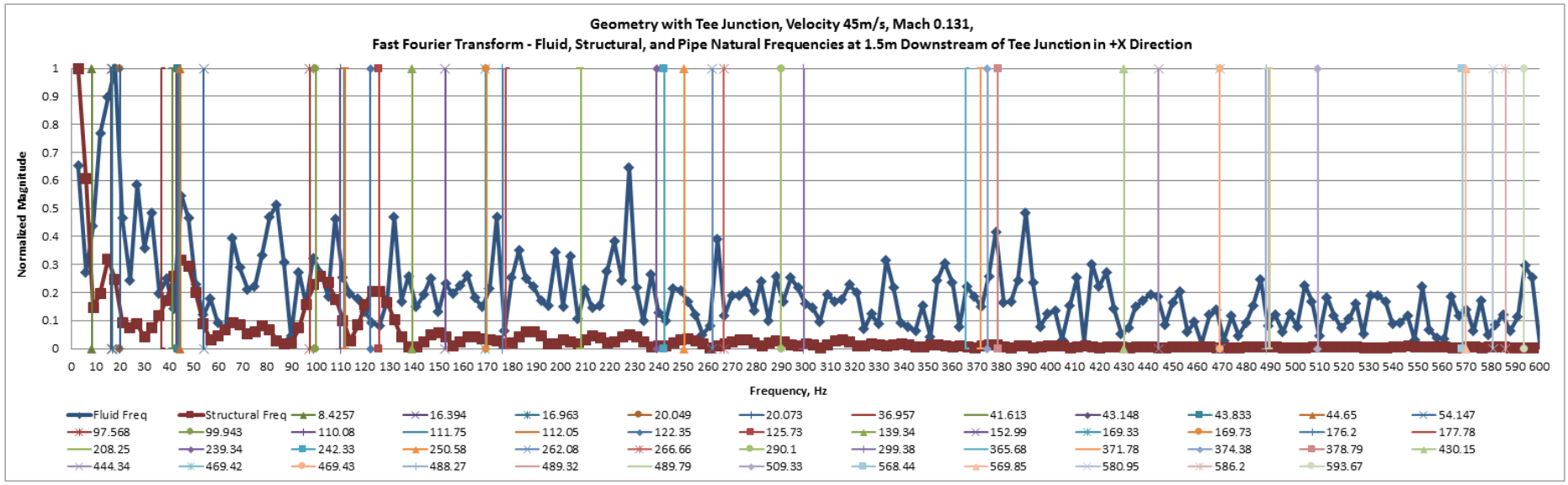
Geometry with Tee Junction, Velocity 45m/s, Mach 0.131,
Fast Fourier Transform - Fluid, Structural, and Pipe Natural Frequencies at 1.5m Downstream of Tee Junction in +X Direction
Normalized Magnitude
Frequency, Hz
Fluid Freq
Structural Freq
8.4257
16.394
16.963
20.049
20.073
36.957
41.613
43.148
43.833
44.65
54.147
97.568
99.943
110.08
111.75
112.05
122.35
125.73
139.34
152.99
169.33
169.73
176.2
177.78
208.25
239.34
242.33
250.58
262.08
266.66
290.1
299.38
365.68
371.78
374.38
378.79
430.15
444.34
469.42
469.43
488.27
489.32
489.79
509.33
568.44
569.85
580.95
586.2
593.67

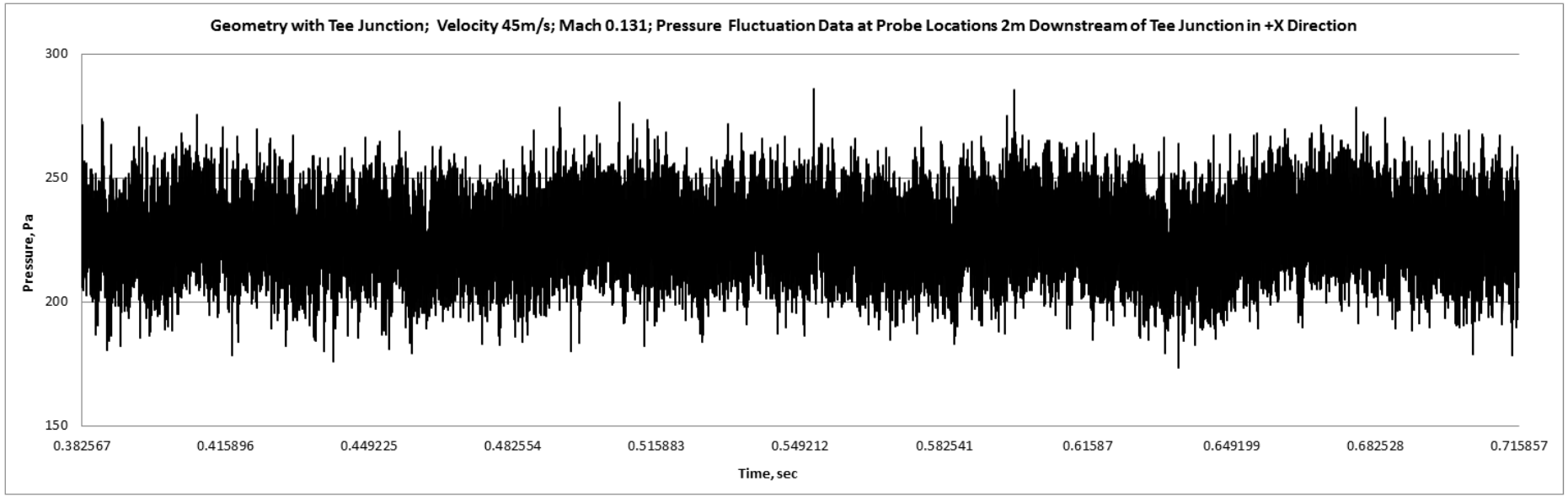
Geometry with Tee Junction; Velocity 45m/s; Mach 0.131; Pressure Fluctuation Data at Probe Locations 2m Downstream of Tee Junction in +X Direction
Pressure, Pa
300
250
200
150
0.382567
0.415896
0.449225
0.482554
0.515883
0.549212
0.582541
0.61587
0.649199
0.682528
0.715857
Time, sec

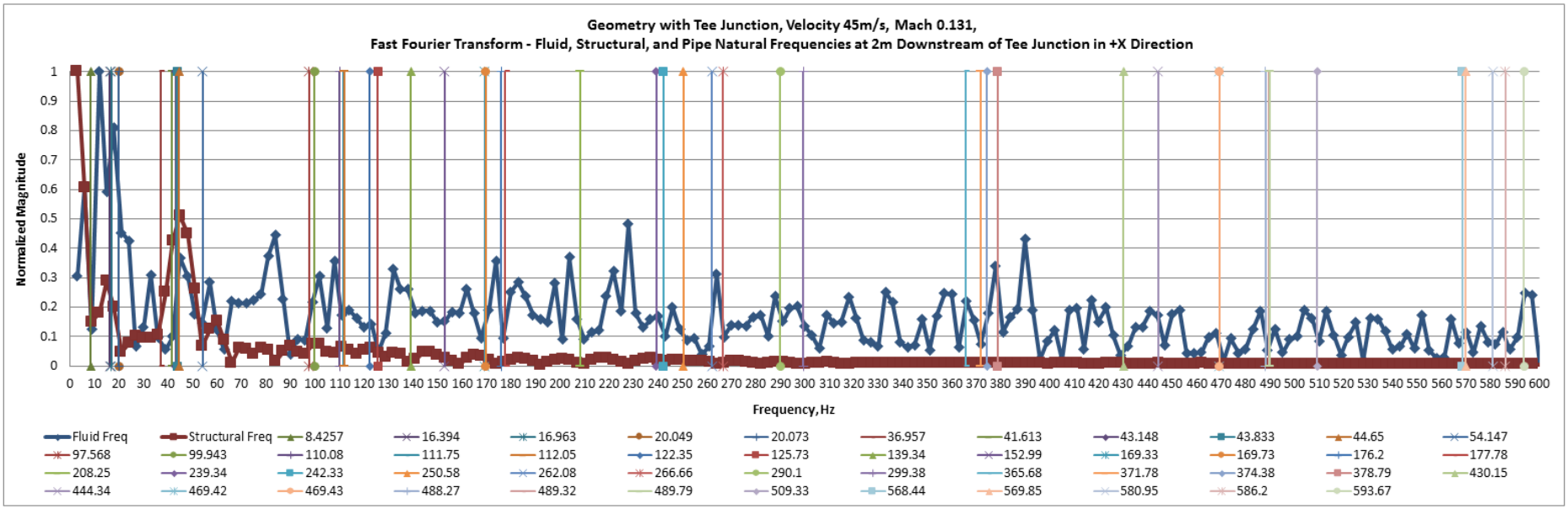
Geometry with Tee Junction, Velocity 45m/s, Mach 0.131,
Fast Fourier Transform - Fluid, Structural, and Pipe Natural Frequencies at 2m Downstream of Tee Junction in +X Direction
Normalized Magnitude
Frequency, Hz
Fluid Freq
Structural Freq
8.4257
16.394
16.963
20.049
20.073
36.957
41.613
43.148
43.833
44.65
54.147
97.568
99.943
110.08
111.75
112.05
122.35
125.73
139.34
152.99
169.33
169.73
176.2
177.78
208.25
239.34
242.33
250.58
262.08
266.66
290.1
299.38
365.68
371.78
374.38
378.79
430.15
444.34
469.42
469.43
488.27
489.32
489.79
509.33
568.44
569.85
580.95
586.2
593.67

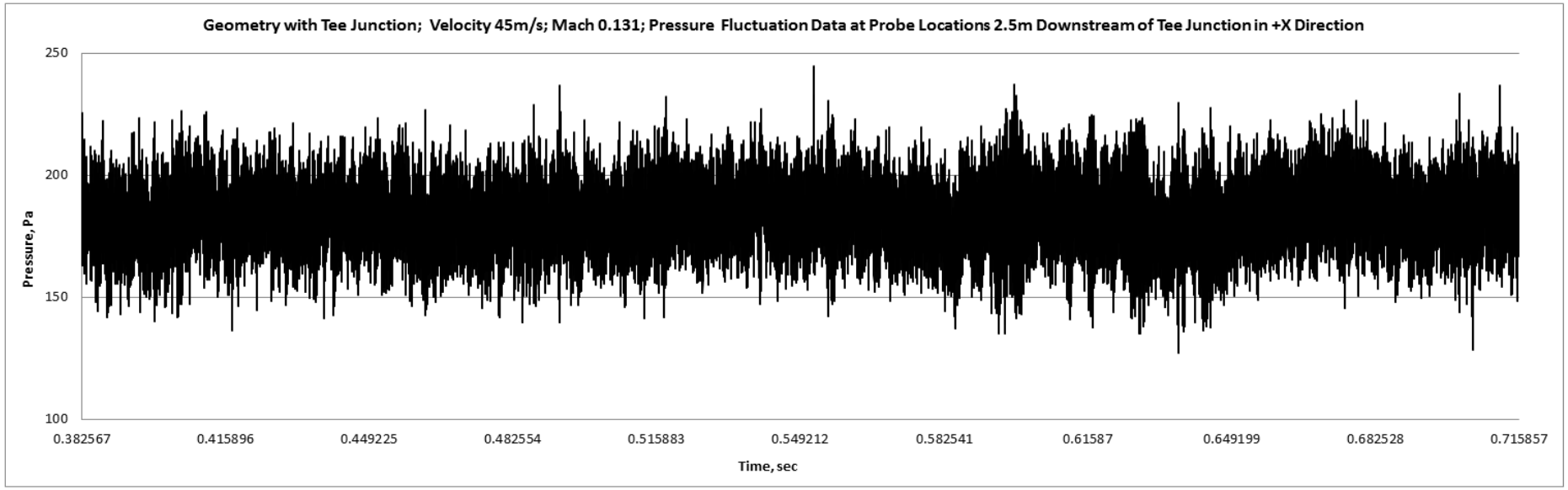
Geometry with Tee Junction; Velocity 45m/s; Mach 0.131; Pressure Fluctuation Data at Probe Locations 2.5m Downstream of Tee Junction in +X Direction
Pressure, Pa
250
200
150
100
0.382567
0.415896
0.449225
0.482554
0.515883
0.549212
0.582541
0.61587
0.649199
0.682528
0.715857
Time, sec

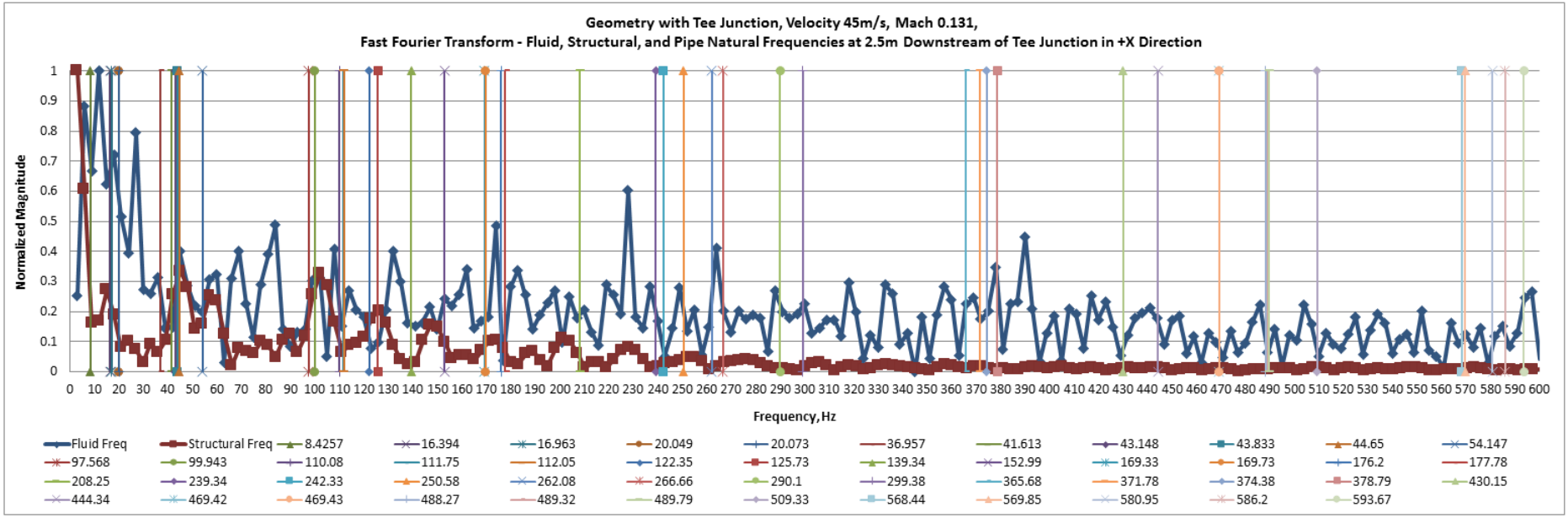
Geometry with Tee Junction, Velocity 45m/s, Mach 0.131,
Fast Fourier Transform - Fluid, Structural, and Pipe Natural Frequencies at 2.5m Downstream of Tee Junction in +X Direction
Normalized Magnitude
Frequency, Hz
Fluid Freq
Structural Freq
8.4257
16.394
16.963
20.049
20.073
36.957
41.613
43.148
43.833
44.65
54.147
97.568
99.943
110.08
111.75
112.05
122.35
125.73
139.34
152.99
169.33
169.73
176.2
177.78
208.25
239.34
242.33
250.58
262.08
266.66
290.1
299.38
365.68
371.78
374.38
378.79
430.15
444.34
469.42
469.43
488.27
489.32
489.79
509.33
568.44
569.85
580.95
586.2
593.67

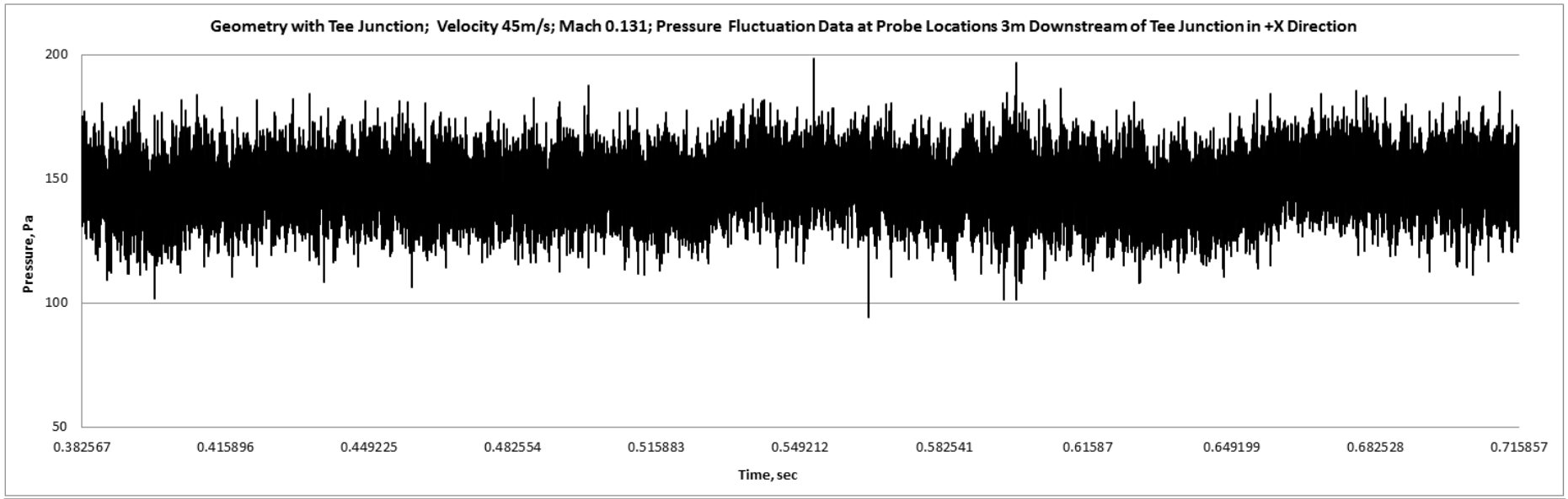
Geometry with Tee Junction; Velocity 45m/s; Mach 0.131; Pressure Fluctuation Data at Probe Locations 3m Downstream of Tee Junction in +X Direction
Pressure, Pa
200
150
100
50
0.382567
0.415896
0.449225
0.482554
0.515883
0.549212
0.582541
0.61587
0.649199
0.682528
0.715857
Time, sec

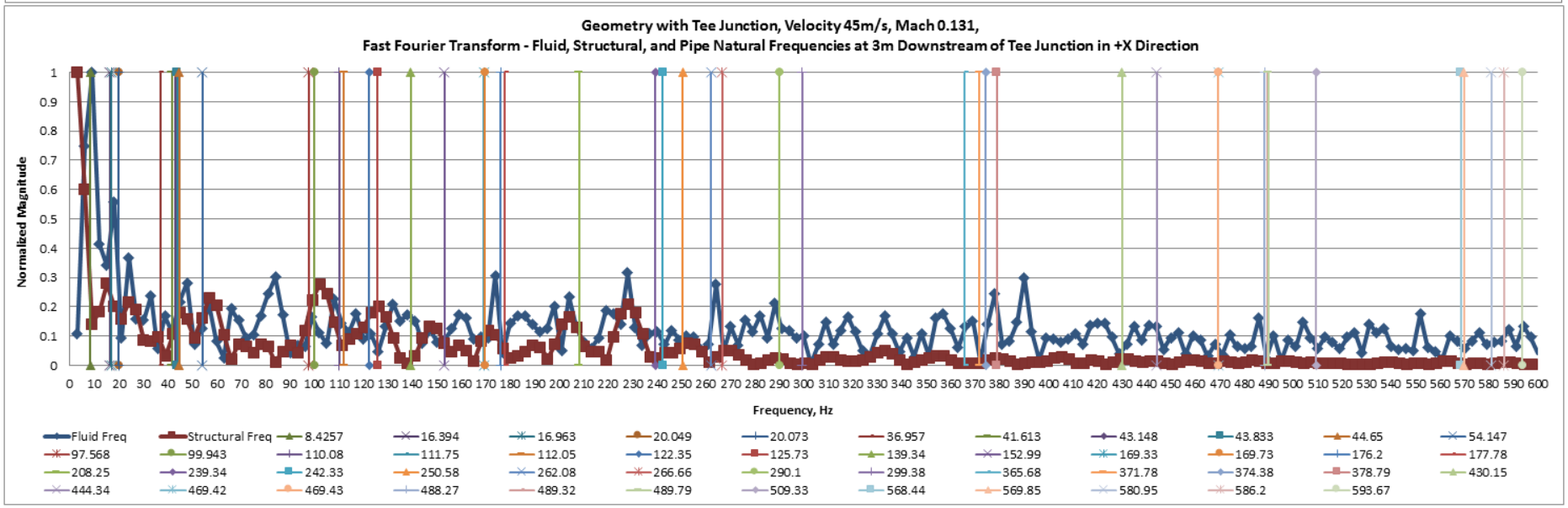
Geometry with Tee Junction, Velocity 45m/s, Mach 0.131,
Fast Fourier Transform - Fluid, Structural, and Pipe Natural Frequencies at 3m Downstream of Tee Junction in +X Direction
Normalized Magnitude
Frequency, Hz
Fluid Freq
Structural Freq
8.4257
16.394
16.963
20.049
20.073
36.957
41.613
43.148
43.833
44.65
54.147
97.568
99.943
110.08
111.75
112.05
122.35
125.73
139.34
152.99
169.33
169.73
176.2
177.78
208.25
239.34
242.33
250.58
262.08
266.66
290.1
299.38
365.68
371.78
374.38
378.79
430.15
444.34
469.42
469.43
488.27
489.32
489.79
509.33
568.44
569.85
580.95
586.2
593.67

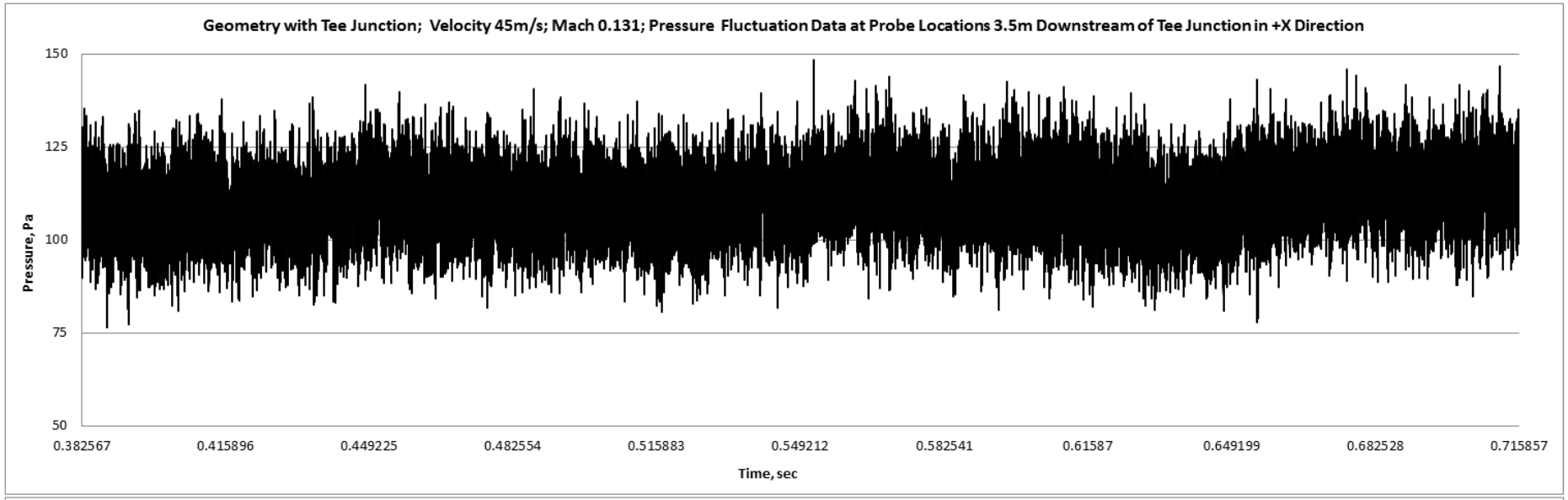
Geometry with Tee Junction; Velocity 45m/s; Mach 0.131; Pressure Fluctuation Data at Probe Locations 3.5m Downstream of Tee Junction in +X Direction
Pressure, Pa
150
125
100
75
50
0.382567
0.415896
0.449225
0.482554
0.515883
0.549212
0.582541
0.61587
0.649199
0.682528
0.715857
Time, sec

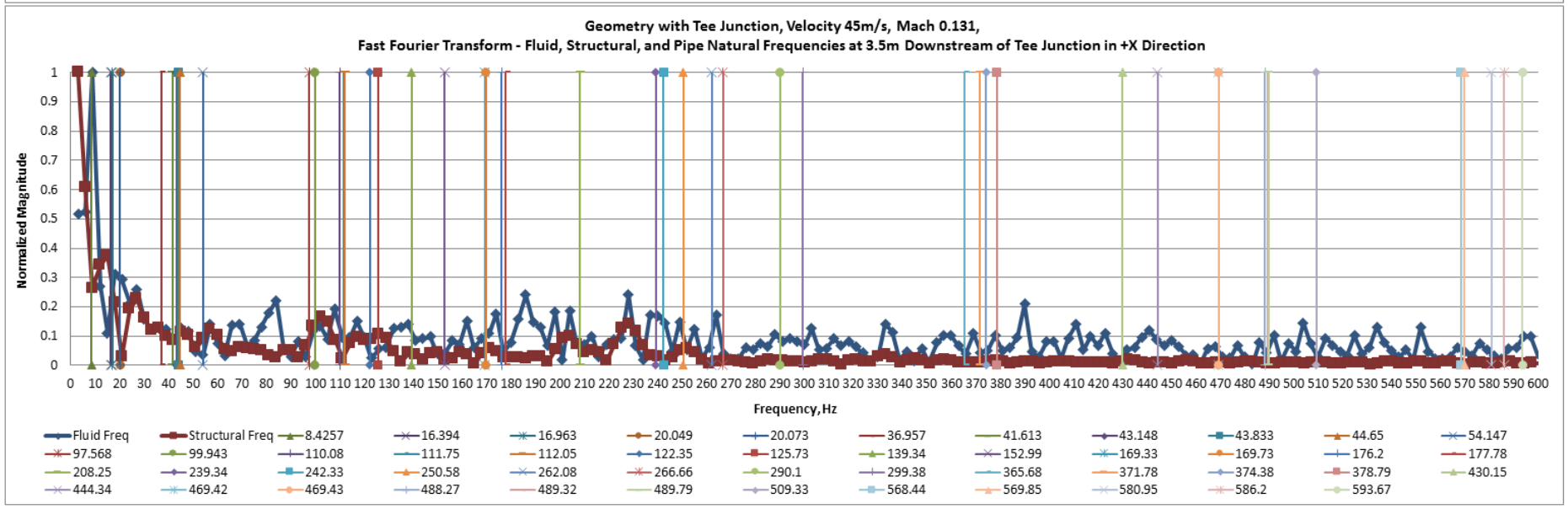
Geometry with Tee Junction, Velocity 45m/s, Mach 0.131,
Fast Fourier Transform - Fluid, Structural, and Pipe Natural Frequencies at 3.5m Downstream of Tee Junction in +X Direction
Normalized Magnitude
Frequency, Hz
Fluid Freq
Structural Freq
8.4257
16.394
16.963
20.049
20.073
36.957
41.613
43.148
43.833
44.65
54.147
97.568
99.943
110.08
111.75
112.05
122.35
125.73
139.34
152.99
169.33
169.73
176.2
177.78
208.25
239.34
242.33
250.58
262.08
266.66
290.1
299.38
365.68
371.78
374.38
378.79
430.15
444.34
469.42
469.43
488.27
489.32
489.79
509.33
568.44
569.85
580.95
586.2
593.67

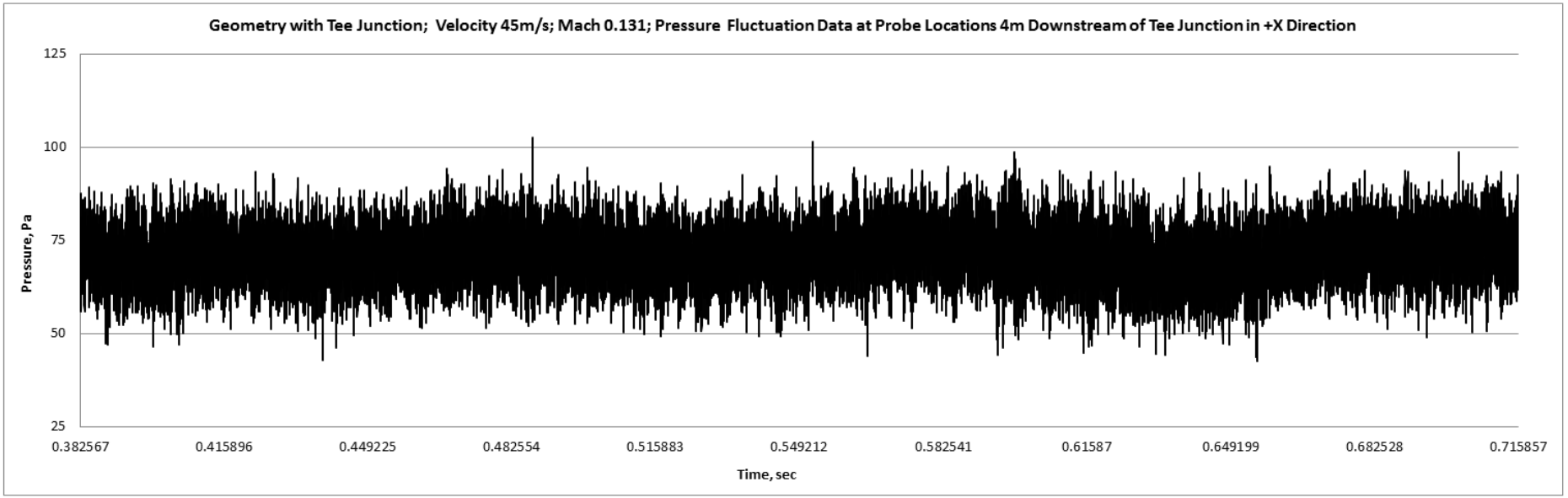
Geometry with Tee Junction; Velocity 45m/s; Mach 0.131; Pressure Fluctuation Data at Probe Locations 4m Downstream of Tee Junction in +X Direction
Pressure, Pa
125
100
75
50
25
0.382567
0.415896
0.449225
0.482554
0.515883
0.549212
0.582541
0.61587
0.649199
0.682528
0.715857
Time, sec

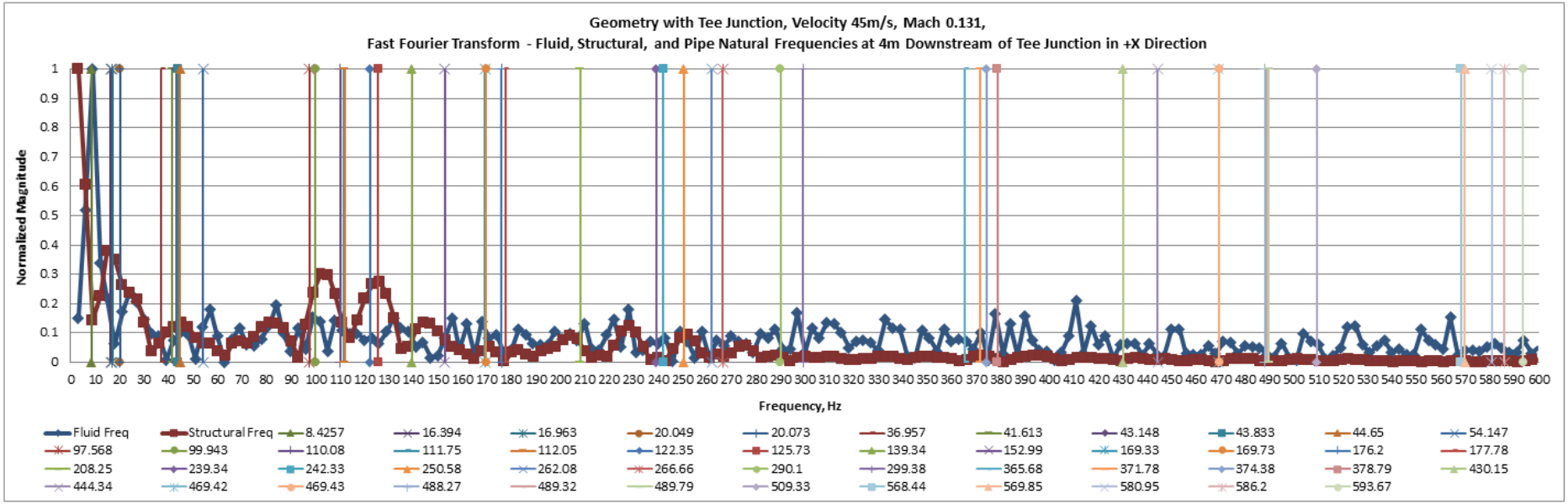
Geometry with Tee Junction, Velocity 45m/s, Mach 0.131,
Fast Fourier Transform - Fluid, Structural, and Pipe Natural Frequencies at 4m Downstream of Tee Junction in +X Direction
Normalized Magnitude
Frequency, Hz
Fluid Freq
Structural Freq
8.4257
16.394
16.963
20.049
20.073
36.957
41.613
43.148
43.833
44.65
54.147
97.568
99.943
110.08
111.75
112.05
122.35
125.73
139.34
152.99
169.33
169.73
176.2
177.78
208.25
239.34
242.33
250.58
262.08
266.66
290.1
299.38
365.68
371.78
374.38
378.79
430.15
444.34
469.42
469.43
488.27
489.32
489.79
509.33
568.44
569.85
580.95
586.2
593.67

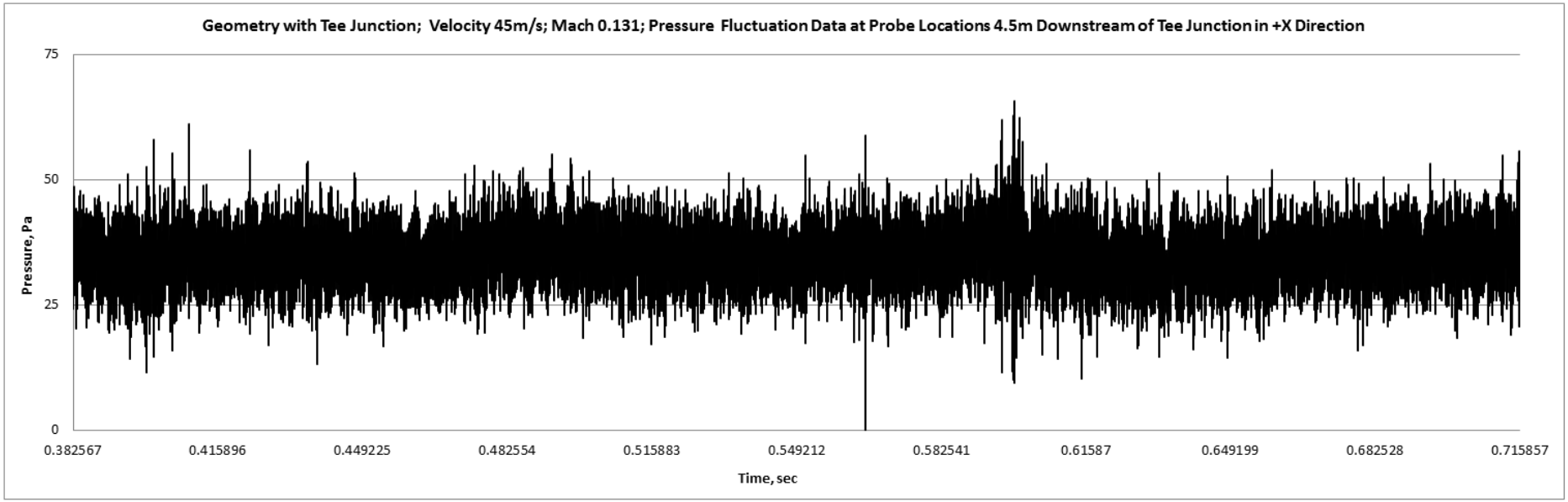
Geometry with Tee Junction; Velocity 45m/s; Mach 0.131; Pressure Fluctuation Data at Probe Locations 4.5m Downstream of Tee Junction in +X Direction
Pressure, Pa
75
50
25
0
0.382567
0.415896
0.449225
0.482554
0.515883
0.549212
0.582541
0.61587
0.649199
0.682528
0.715857
Time, sec

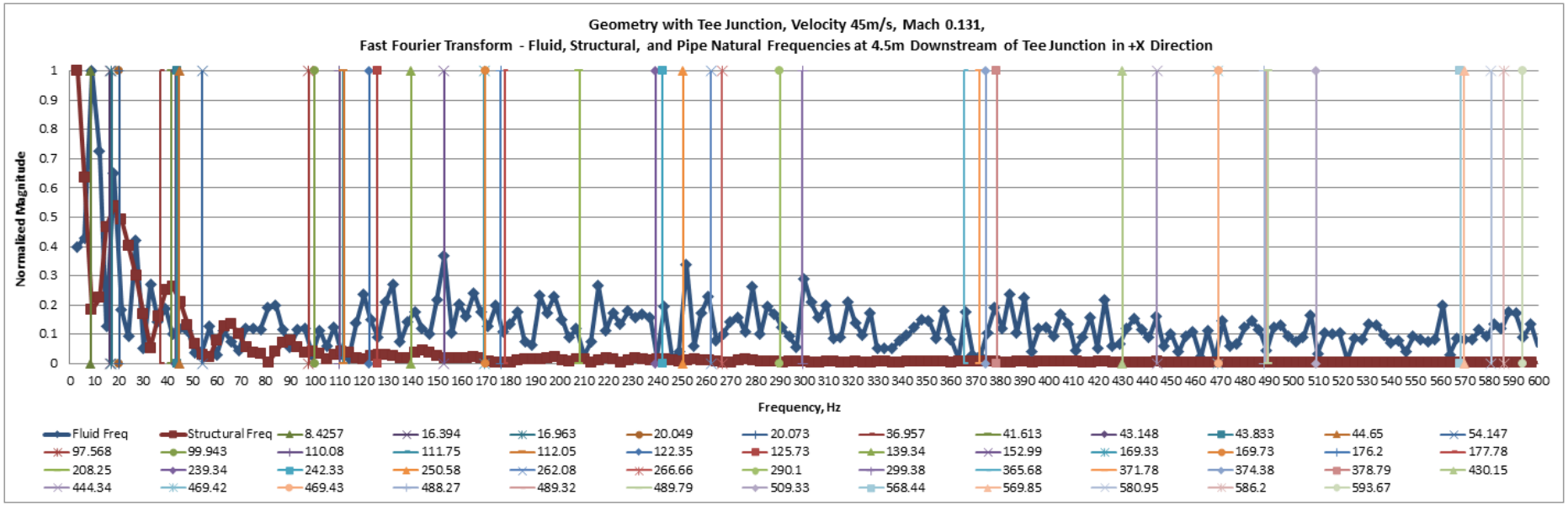
Geometry with Tee Junction, Velocity 45m/s, Mach 0.131,
Fast Fourier Transform - Fluid, Structural, and Pipe Natural Frequencies at 4.5m Downstream of Tee Junction in +X Direction
Normalized Magnitude
Frequency, Hz
Fluid Freq
Structural Freq
8.4257
16.394
16.963
20.049
20.073
36.957
41.613
43.148
43.833
44.65
54.147
97.568
99.943
110.08
111.75
112.05
122.35
125.73
139.34
152.99
169.33
169.73
176.2
177.78
208.25
239.34
242.33
250.58
262.08
266.66
290.1
299.38
365.68
371.78
374.38
378.79
430.15
444.34
469.42
469.43
488.27
489.32
489.79
509.33
568.44
569.85
580.95
586.2
593.67

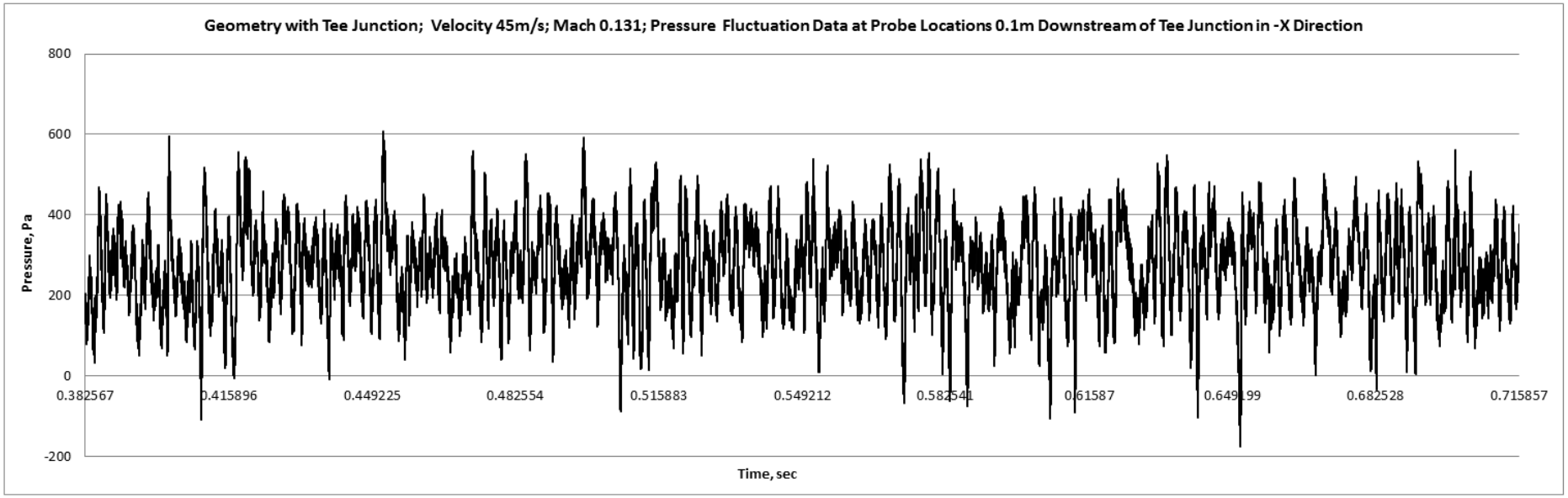
Geometry with Tee Junction; Velocity 45m/s; Mach 0.131; Pressure Fluctuation Data at Probe Locations 0.1m Downstream of Tee Junction in -X Direction
Pressure, Pa
800
600
400
200
0
-200
0.382567
0.415896
0.449225
0.482554
0.515883
0.549212
0.582541
0.61587
0.649199
0.682528
0.715857
Time, sec

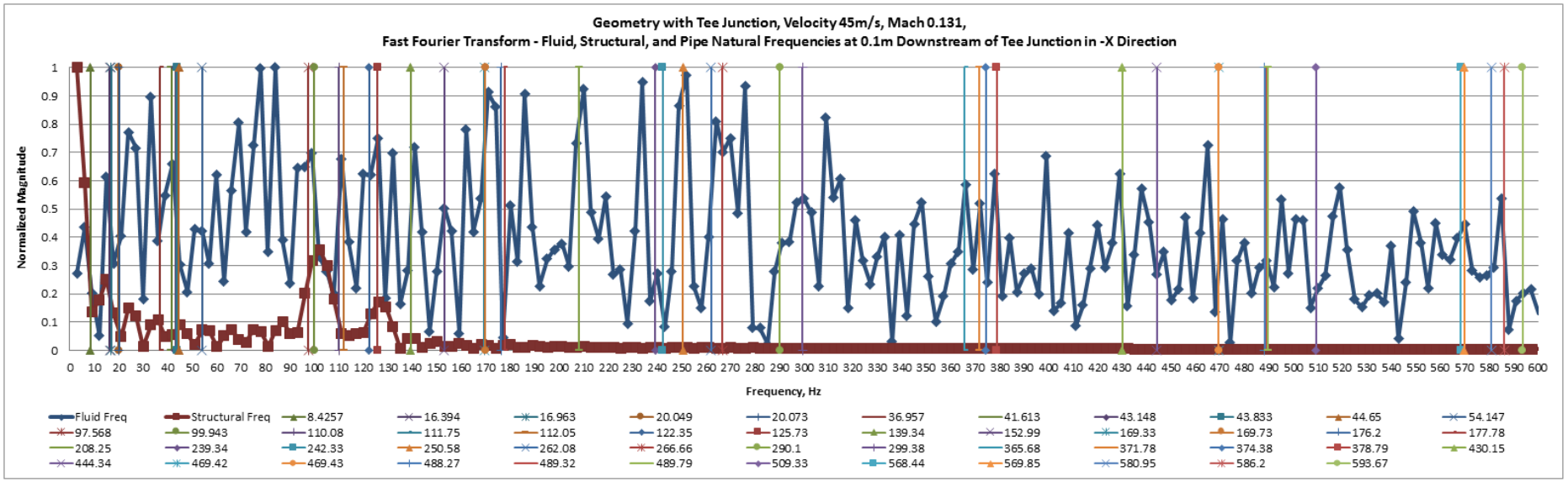
Geometry with Tee Junction, Velocity 45m/s, Mach 0.131,
Fast Fourier Transform - Fluid, Structural, and Pipe Natural Frequencies at 0.1m Downstream of Tee Junction in -X Direction
Normalized Magnitude
Frequency, Hz
Fluid Freq
Structural Freq
8.4257
16.394
16.963
20.049
20.073
36.957
41.613
43.148
43.833
44.65
54.147
97.568
99.943
110.08
111.75
112.05
122.35
125.73
139.34
152.99
169.33
169.73
176.2
177.78
208.25
239.34
242.33
250.58
262.08
266.66
290.1
299.38
365.68
371.78
374.38
378.79
430.15
444.34
469.42
469.43
488.27
489.32
489.79
509.33
568.44
569.85
580.95
586.2
593.67

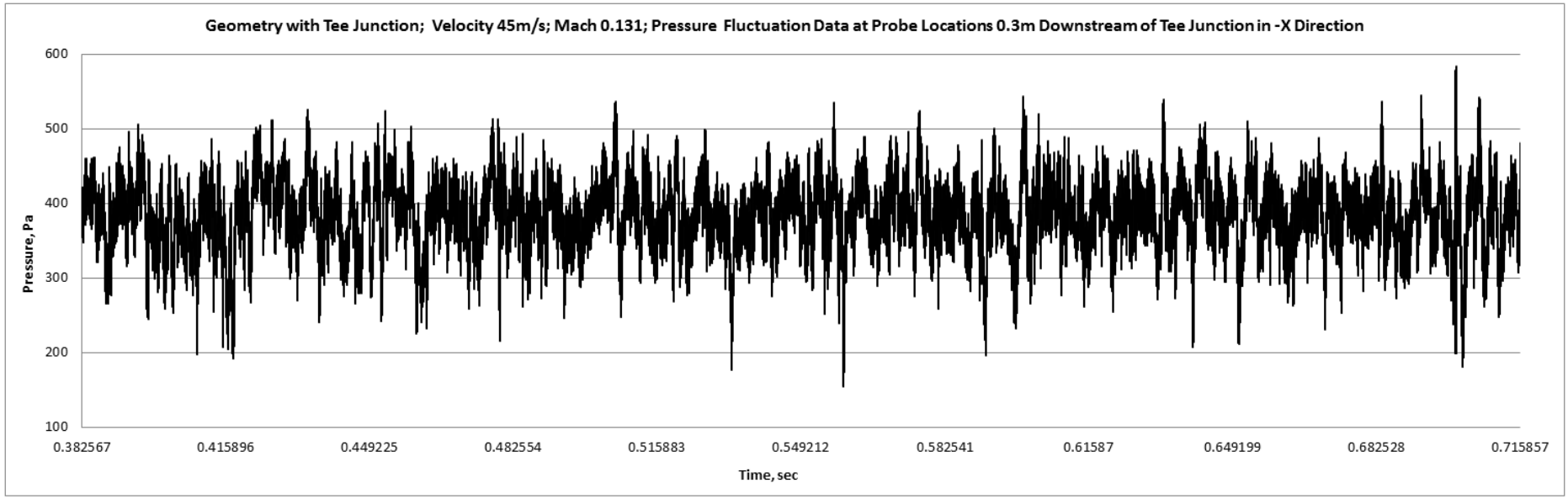
Geometry with Tee Junction; Velocity 45m/s; Mach 0.131; Pressure Fluctuation Data at Probe Locations 0.3m Downstream of Tee Junction in -X Direction
Pressure, Pa
600
500
400
300
200
100
0.382567
0.415896
0.449225
0.482554
0.515883
0.549212
0.582541
0.61587
0.649199
0.682528
0.715857
Time, sec

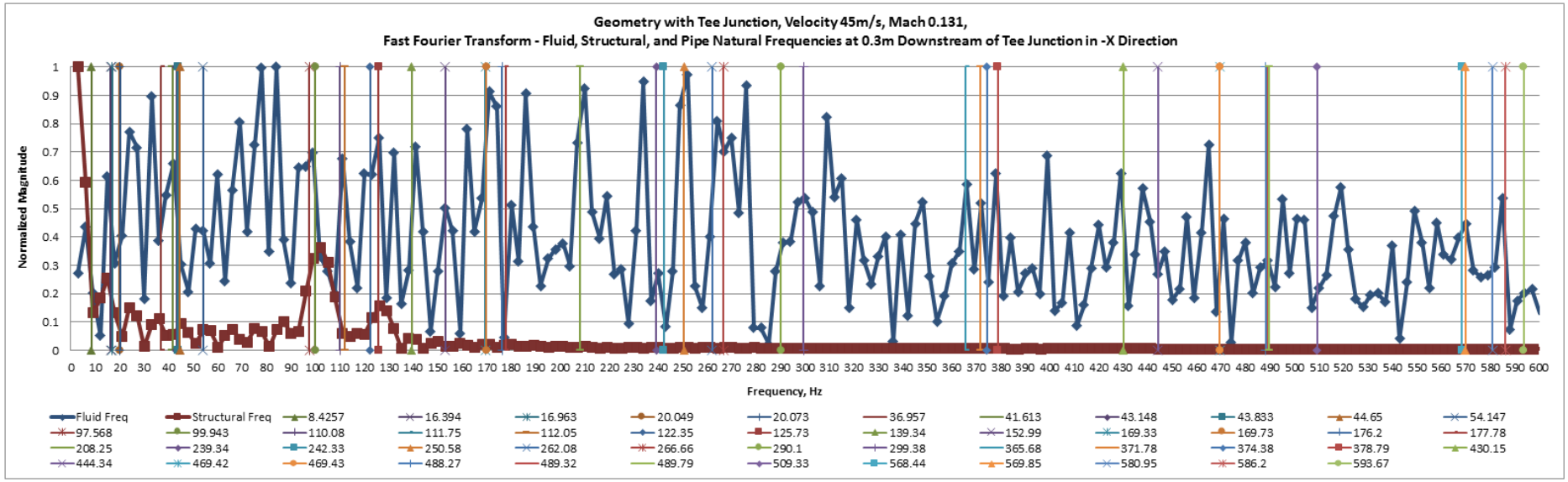
Geometry with Tee Junction, Velocity 45m/s, Mach 0.131,
Fast Fourier Transform - Fluid, Structural, and Pipe Natural Frequencies at 0.3m Downstream of Tee Junction in -X Direction
Normalized Magnitude
Frequency, Hz
Fluid Freq
Structural Freq
8.4257
16.394
16.963
20.049
20.073
36.957
41.613
43.148
43.833
44.65
54.147
97.568
99.943
110.08
111.75
112.05
122.35
125.73
139.34
152.99
169.33
169.73
176.2
177.78
208.25
239.34
242.33
250.58
262.08
266.66
290.1
299.38
365.68
371.78
374.38
378.79
430.15
444.34
469.42
469.43
488.27
489.32
489.79
509.33
568.44
569.85
580.95
586.2
593.67

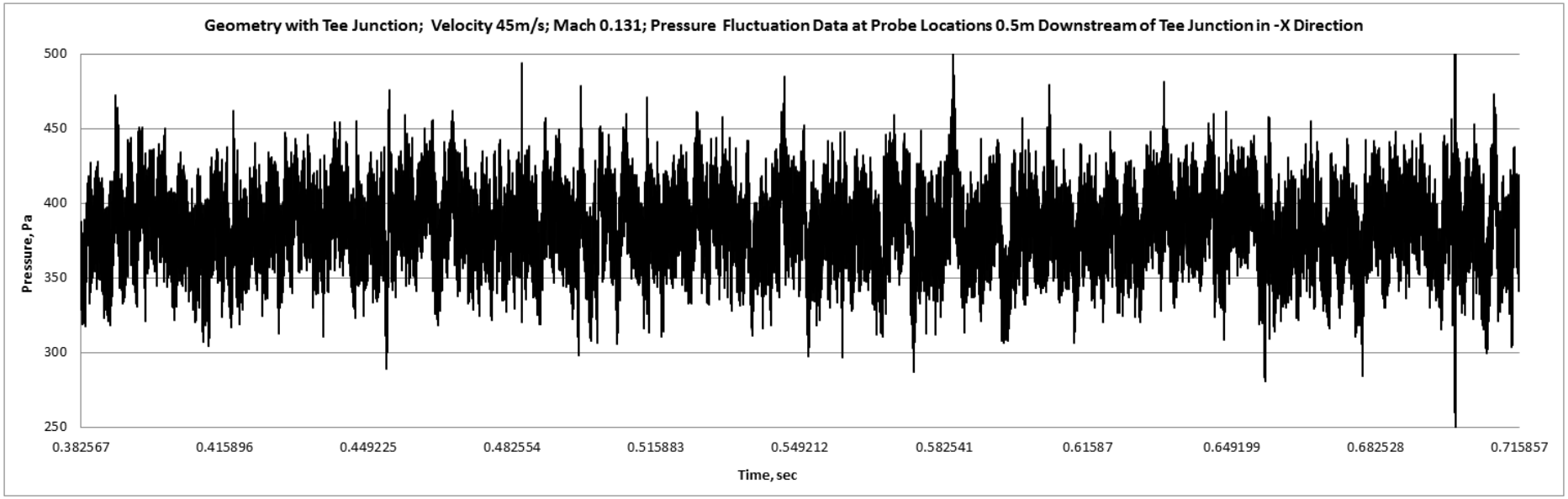
Geometry with Tee Junction; Velocity 45m/s; Mach 0.131; Pressure Fluctuation Data at Probe Locations 0.5m Downstream of Tee Junction in -X Direction
Pressure, Pa
500
450
400
350
300
250
0.382567
0.415896
0.449225
0.482554
0.515883
0.549212
0.582541
0.61587
0.649199
0.682528
0.715857
Time, sec

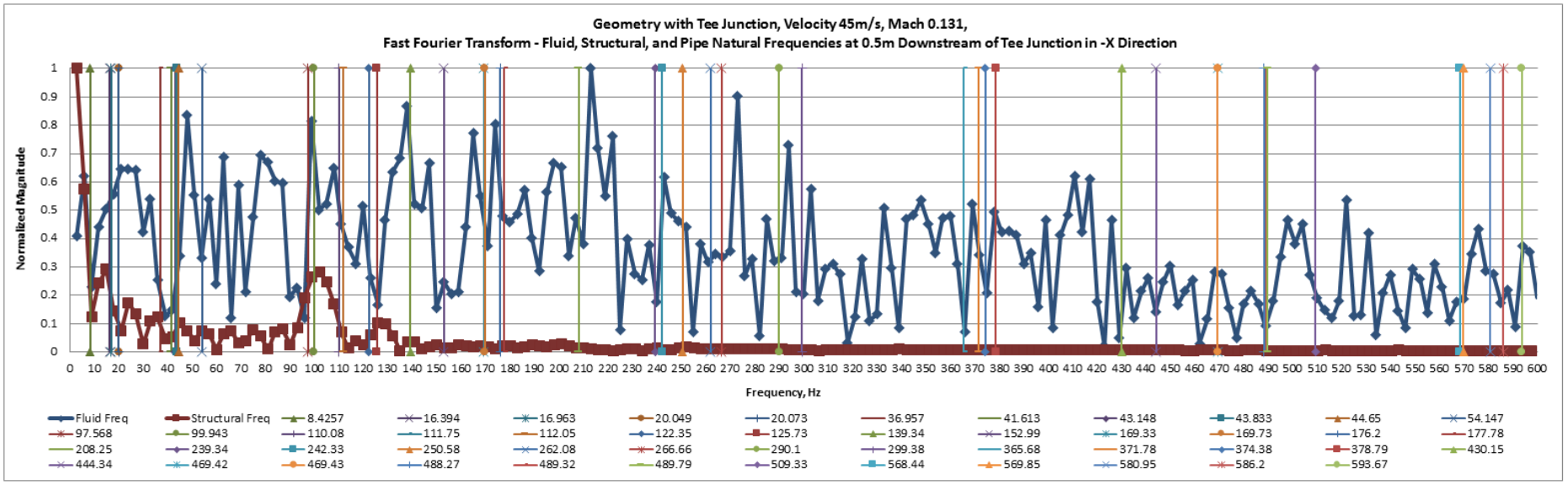
Geometry with Tee Junction, Velocity 45m/s, Mach 0.131,
Fast Fourier Transform - Fluid, Structural, and Pipe Natural Frequencies at 0.5m Downstream of Tee Junction in -X Direction
Normalized Magnitude
Frequency, Hz
Fluid Freq
Structural Freq
8.4257
16.394
16.963
20.049
20.073
36.957
41.613
43.148
43.833
44.65
54.147
97.568
99.943
110.08
111.75
112.05
122.35
125.73
139.34
152.99
169.33
169.73
176.2
177.78
208.25
239.34
242.33
250.58
262.08
266.66
290.1
299.38
365.68
371.78
374.38
378.79
430.15
444.34
469.42
469.43
488.27
489.32
489.79
509.33
568.44
569.85
580.95
586.2
593.67

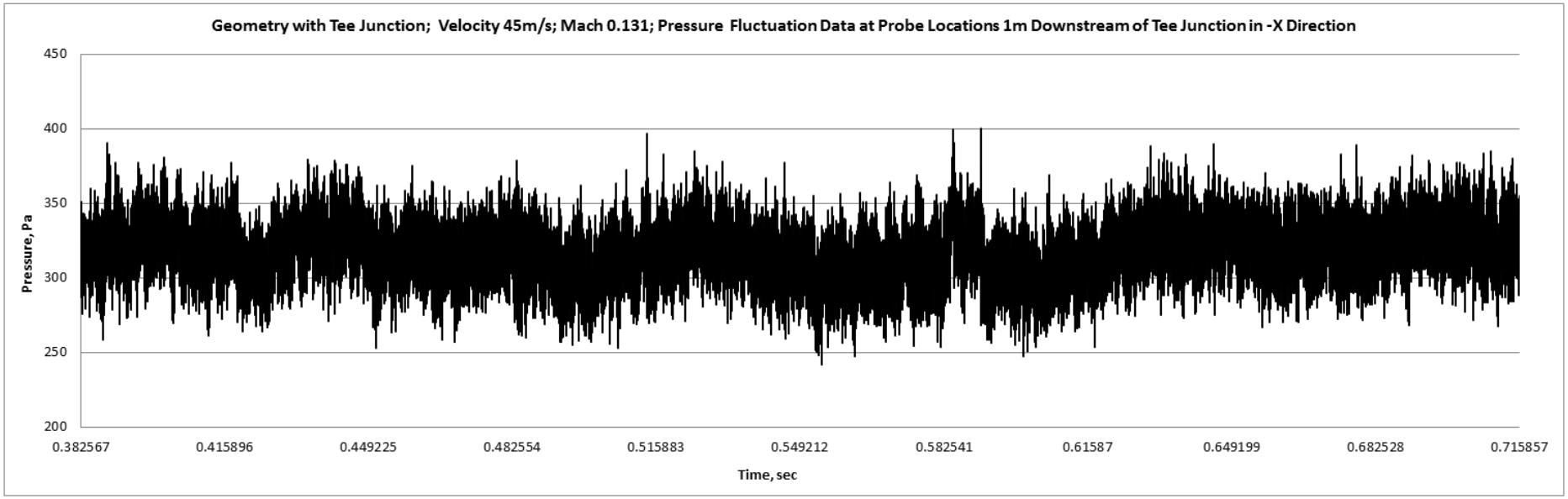
Geometry with Tee Junction; Velocity 45m/s; Mach 0.131; Pressure Fluctuation Data at Probe Locations 1m Downstream of Tee Junction in -X Direction
Pressure, Pa
450
400
350
300
250
200
0.382567
0.415896
0.449225
0.482554
0.515883
0.549212
0.582541
0.61587
0.649199
0.682528
0.715857
Time, sec

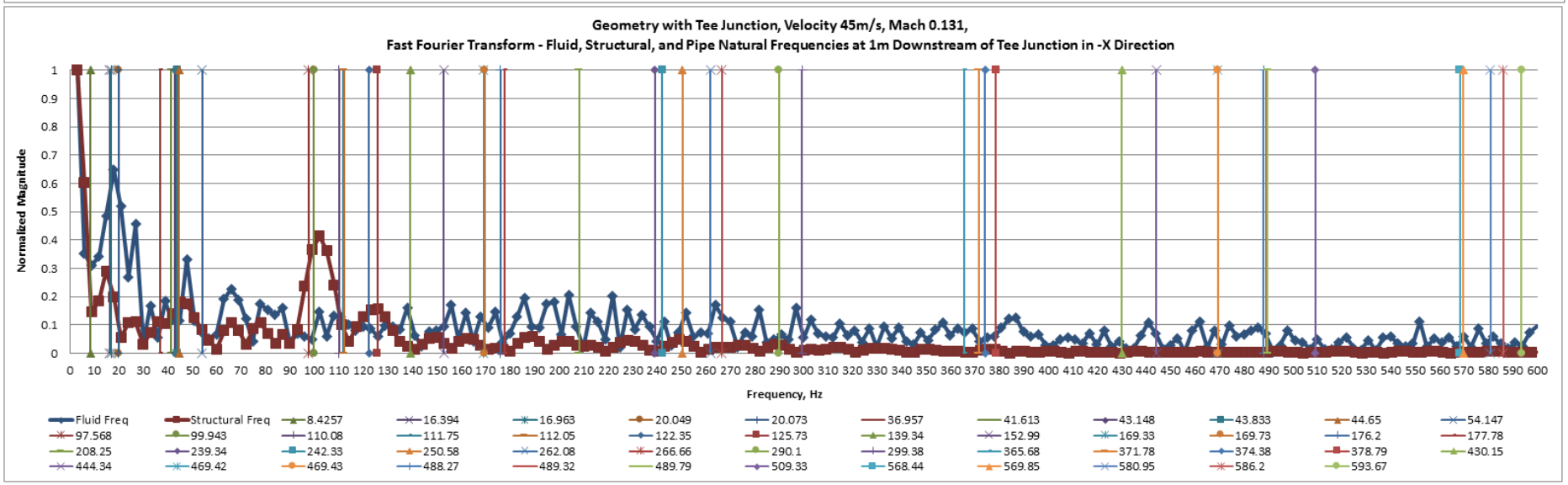
Geometry with Tee Junction, Velocity 45m/s, Mach 0.131,
Fast Fourier Transform - Fluid, Structural, and Pipe Natural Frequencies at 1m Downstream of Tee Junction in -X Direction
Normalized Magnitude
1
0.9
0.8
0.7
0.6
0.5
0.4
0.3
0.2
0.1
0
0 10 20 30 40 50 60 70 80 90 100 110 120 130 140 150 160 170 180 190 200 210 220 230 240 250 260 270 280 290 300 310 320 330 340 350 360 370 380 390 400 410 420 430 440 450 460 470 480 490 500 510 520 530 540 550 560 570 580 590 600
Frequency, Hz
Fluid Freq
Structural Freq
8.4257
16.394
16.963
20.049
20.073
36.957
41.613
43.148
43.833
44.65
54.147
97.568
99.943
110.08
111.75
112.05
122.35
125.73
139.34
152.99
169.33
169.73
176.2
177.78
208.25
239.34
242.33
250.58
262.08
266.66
290.1
299.38
365.68
371.78
374.38
378.79
430.15
444.34
469.42
469.43
488.27
489.32
489.79
509.33
568.44
569.85
580.95
586.2
593.67

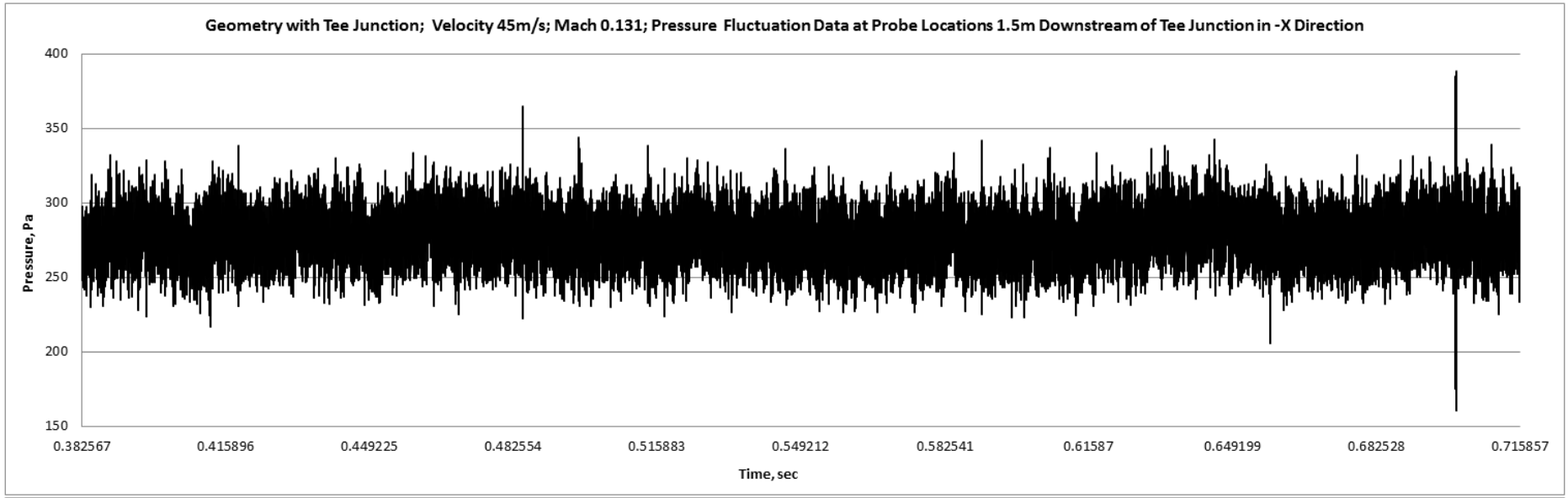
Geometry with Tee Junction; Velocity 45m/s; Mach 0.131; Pressure Fluctuation Data at Probe Locations 1.5m Downstream of Tee Junction in -X Direction
Pressure, Pa
400
350
300
250
200
150
0.382567
0.415896
0.449225
0.482554
0.515883
0.549212
0.582541
0.61587
0.649199
0.682528
0.715857
Time, sec

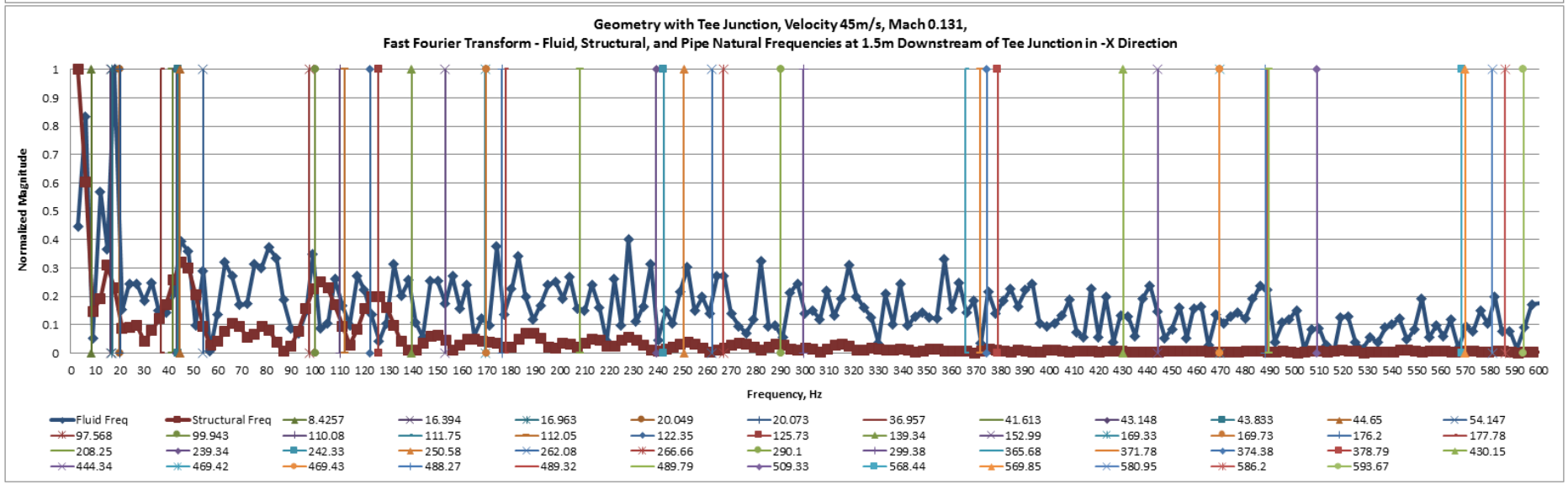
Geometry with Tee Junction, Velocity 45m/s, Mach 0.131,
Fast Fourier Transform - Fluid, Structural, and Pipe Natural Frequencies at 1.5m Downstream of Tee Junction in -X Direction
Normalized Magnitude
Frequency, Hz
Fluid Freq
Structural Freq
8.4257
16.394
16.963
20.049
20.073
36.957
41.613
43.148
43.833
44.65
54.147
97.568
99.943
110.08
111.75
112.05
122.35
125.73
139.34
152.99
169.33
169.73
176.2
177.78
208.25
239.34
242.33
250.58
262.08
266.66
290.1
299.38
365.68
371.78
374.38
378.79
430.15
444.34
469.42
469.43
488.27
489.32
489.79
509.33
568.44
569.85
580.95
586.2
593.67

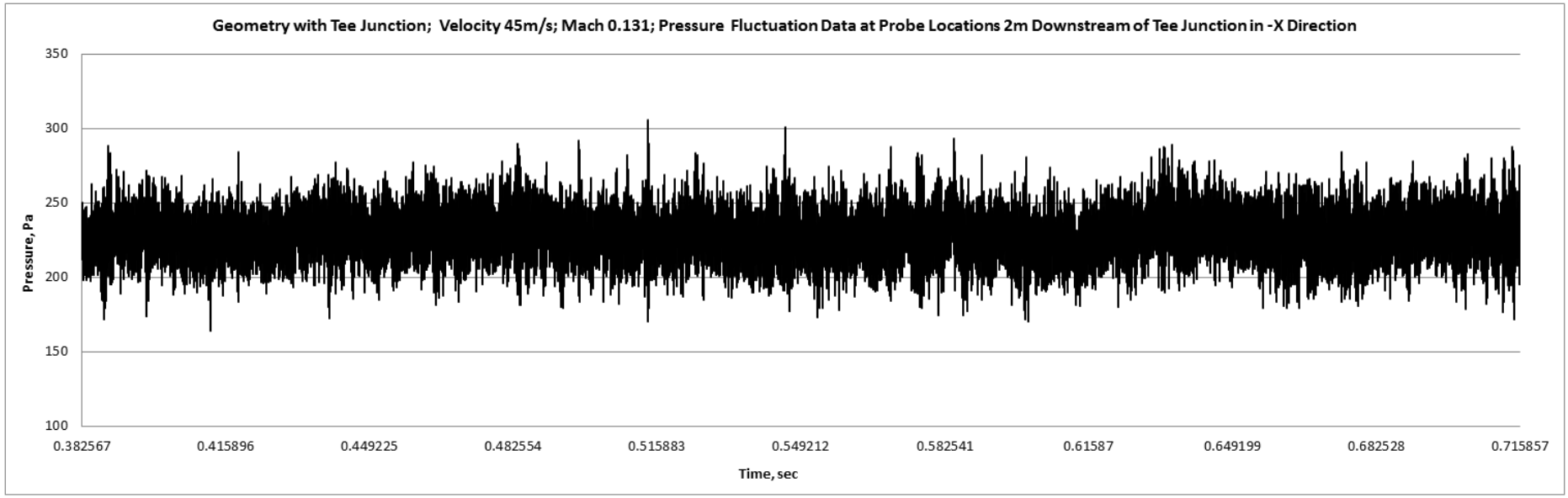
Geometry with Tee Junction; Velocity 45m/s; Mach 0.131; Pressure Fluctuation Data at Probe Locations 2m Downstream of Tee Junction in -X Direction
Pressure, Pa
350
300
250
200
150
100
0.382567
0.415896
0.449225
0.482554
0.515883
0.549212
0.582541
0.61587
0.649199
0.682528
0.715857
Time, sec

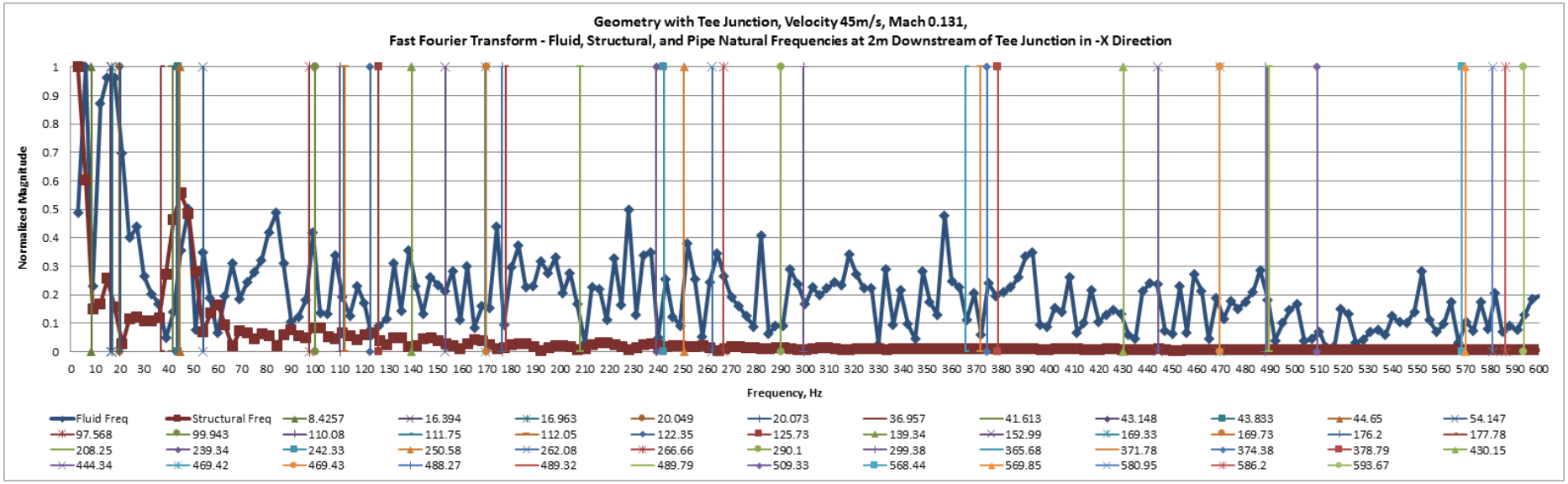
Geometry with Tee Junction, Velocity 45m/s, Mach 0.131,
Fast Fourier Transform - Fluid, Structural, and Pipe Natural Frequencies at 2m Downstream of Tee Junction in -X Direction
Normalized Magnitude
Frequency, Hz
Fluid Freq
Structural Freq
8.4257
16.394
16.963
20.049
20.073
36.957
41.613
43.148
43.833
44.65
54.147
97.568
99.943
110.08
111.75
112.05
122.35
125.73
139.34
152.99
169.33
169.73
176.2
177.78
208.25
239.34
242.33
250.58
262.08
266.66
290.1
299.38
365.68
371.78
374.38
378.79
430.15
444.34
469.42
469.43
488.27
489.32
489.79
509.33
568.44
569.85
580.95
586.2
593.67

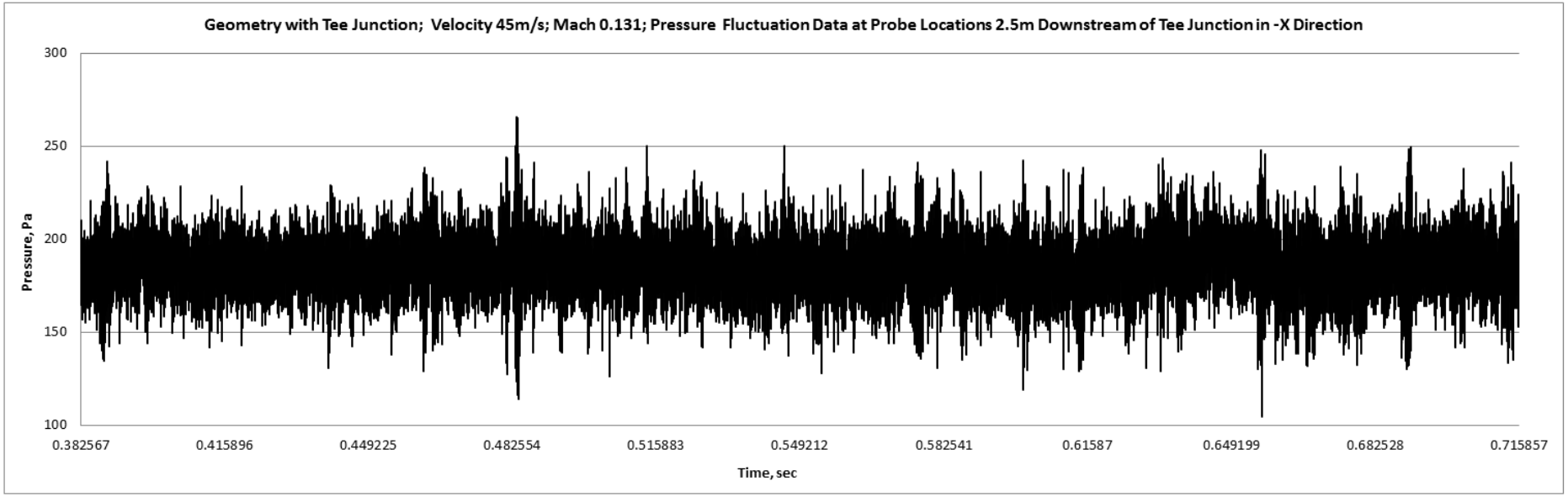
Geometry with Tee Junction; Velocity 45m/s; Mach 0.131; Pressure Fluctuation Data at Probe Locations 2.5m Downstream of Tee Junction in -X Direction
Pressure, Pa
300
250
200
150
100
0.382567
0.415896
0.449225
0.482554
0.515883
0.549212
0.582541
0.61587
0.649199
0.682528
0.715857
Time, sec

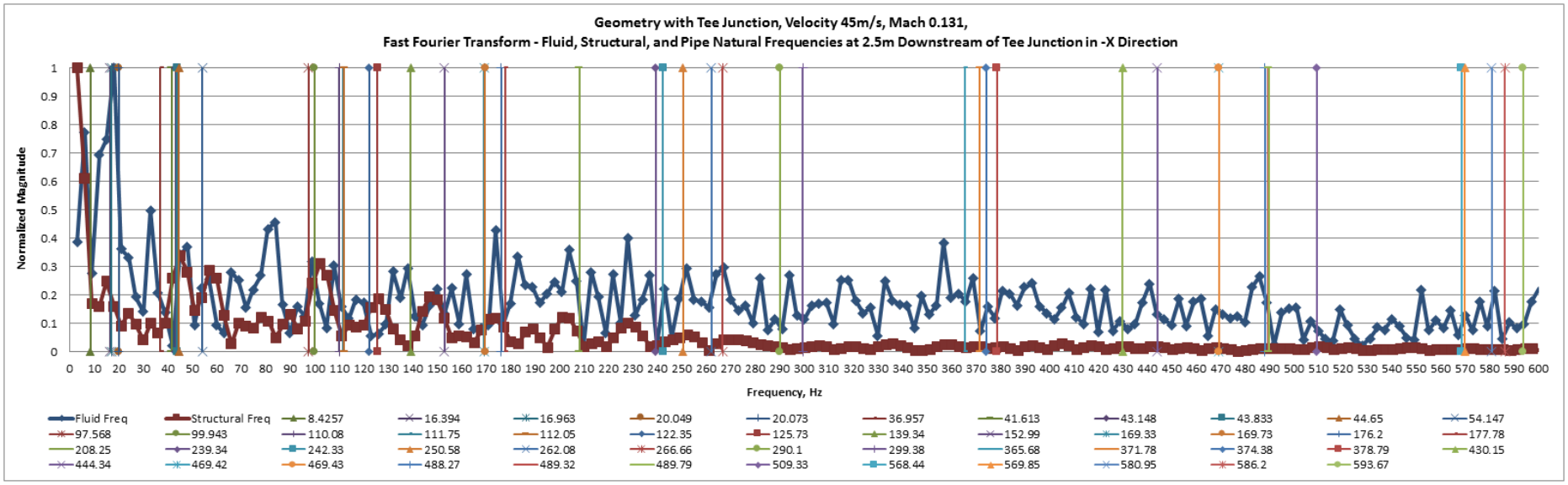
Geometry with Tee Junction, Velocity 45m/s, Mach 0.131,
Fast Fourier Transform - Fluid, Structural, and Pipe Natural Frequencies at 2.5m Downstream of Tee Junction in -X Direction
Normalized Magnitude
Frequency, Hz
Fluid Freq
Structural Freq
8.4257
16.394
16.963
20.049
20.073
36.957
41.613
43.148
43.833
44.65
54.147
97.568
99.943
110.08
111.75
112.05
122.35
125.73
139.34
152.99
169.33
169.73
176.2
177.78
208.25
239.34
242.33
250.58
262.08
266.66
290.1
299.38
365.68
371.78
374.38
378.79
430.15
444.34
469.42
469.43
488.27
489.32
489.79
509.33
568.44
569.85
580.95
586.2
593.67

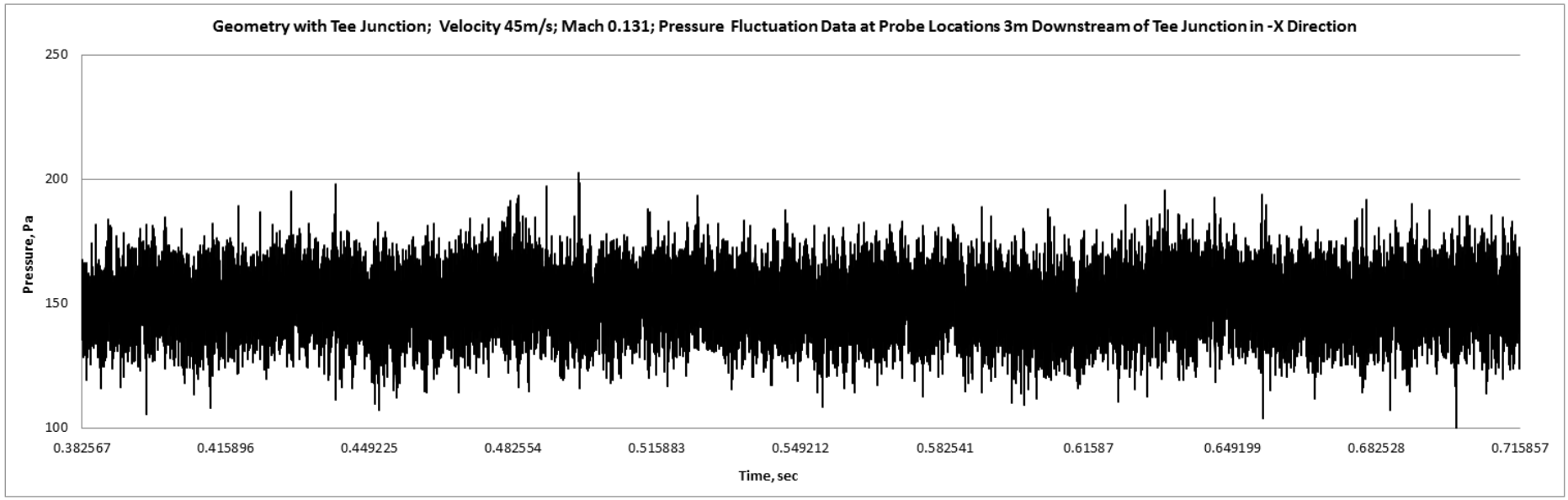
Geometry with Tee Junction; Velocity 45m/s; Mach 0.131; Pressure Fluctuation Data at Probe Locations 3m Downstream of Tee Junction in -X Direction
Pressure, Pa
250
200
150
100
0.382567
0.415896
0.449225
0.482554
0.515883
0.549212
0.582541
0.61587
0.649199
0.682528
0.715857
Time, sec

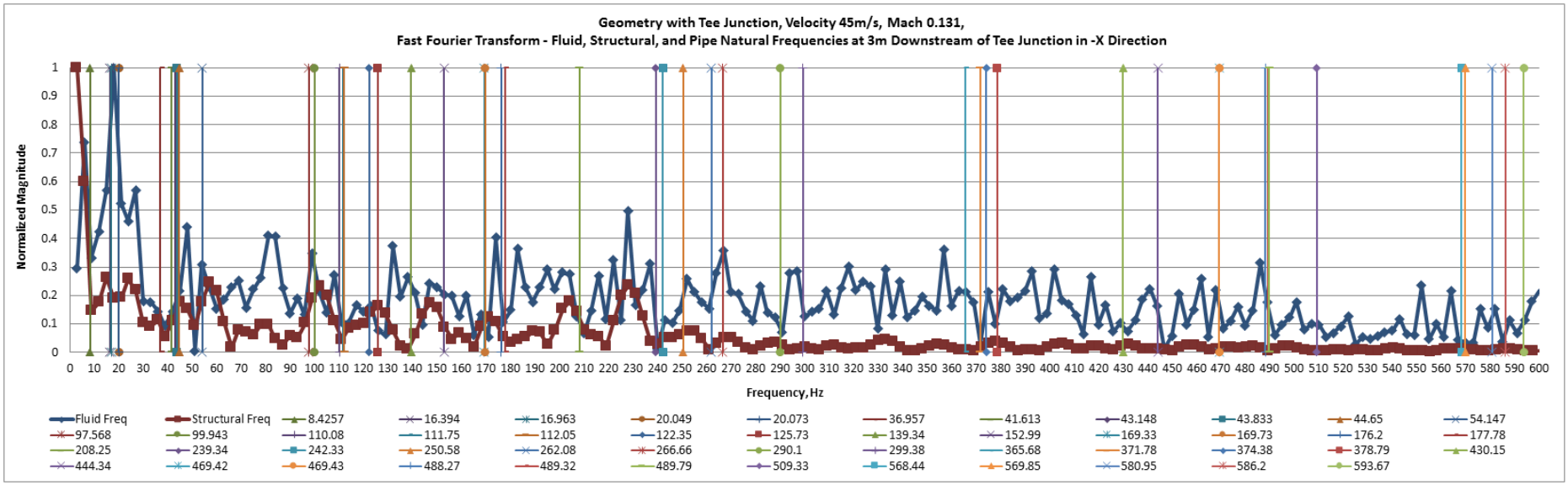
Geometry with Tee Junction, Velocity 45m/s, Mach 0.131,
Fast Fourier Transform - Fluid, Structural, and Pipe Natural Frequencies at 3m Downstream of Tee Junction in -X Direction
Normalized Magnitude
Frequency, Hz
Fluid Freq
Structural Freq
8.4257
16.394
16.963
20.049
20.073
36.957
41.613
43.148
43.833
44.65
54.147
97.568
99.943
110.08
111.75
112.05
122.35
125.73
139.34
152.99
169.33
169.73
176.2
177.78
208.25
239.34
242.33
250.58
262.08
266.66
290.1
299.38
365.68
371.78
374.38
378.79
430.15
444.34
469.42
469.43
488.27
489.32
489.79
509.33
568.44
569.85
580.95
586.2
593.67

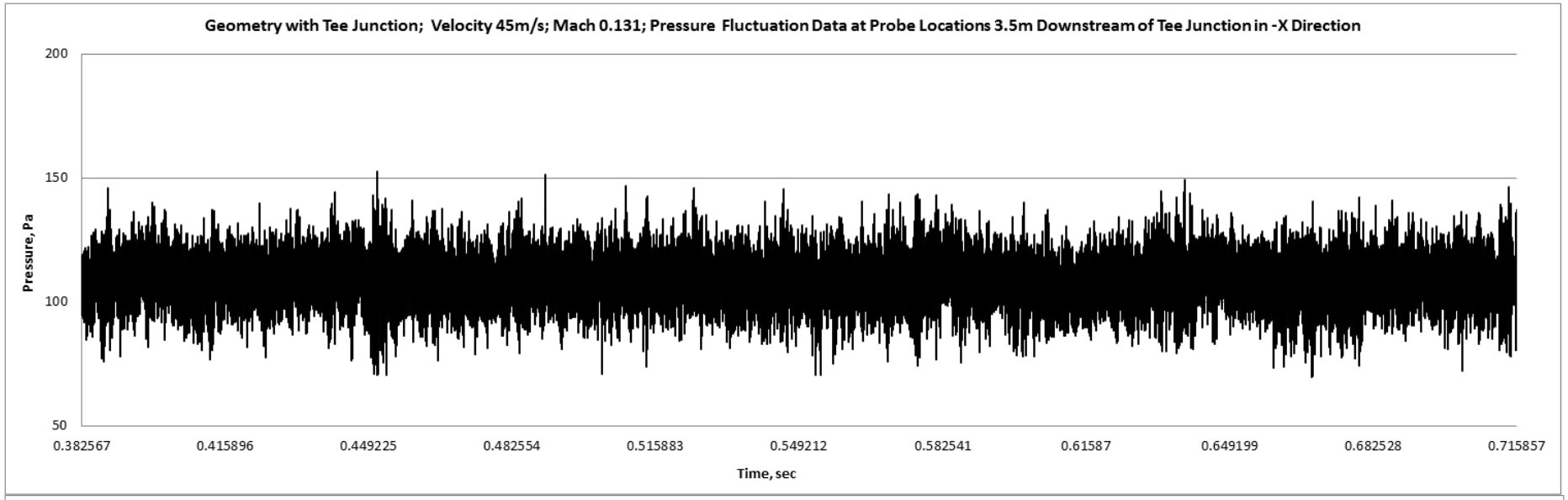
Geometry with Tee Junction; Velocity 45m/s; Mach 0.131; Pressure Fluctuation Data at Probe Locations 3.5m Downstream of Tee Junction in -X Direction
Pressure, Pa
200
150
100
50
0.382567
0.415896
0.449225
0.482554
0.515883
0.549212
0.582541
0.61587
0.649199
0.682528
0.715857
Time, sec

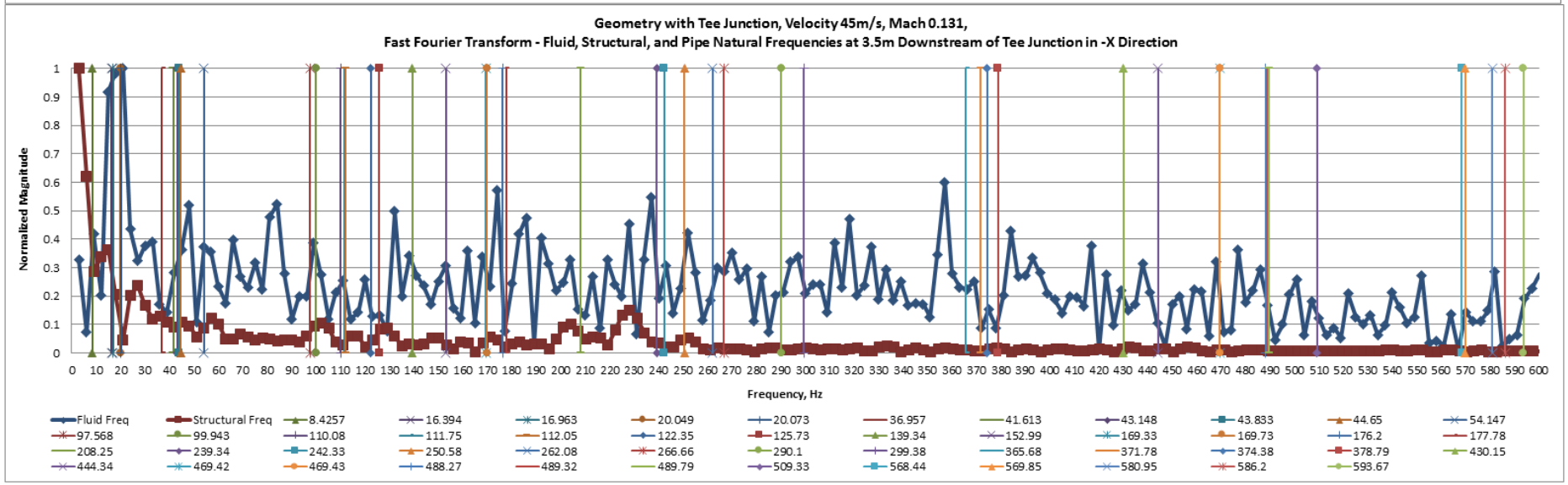
Geometry with Tee Junction, Velocity 45m/s, Mach 0.131,
Fast Fourier Transform - Fluid, Structural, and Pipe Natural Frequencies at 3.5m Downstream of Tee Junction in -X Direction
Normalized Magnitude
Frequency, Hz
Fluid Freq
Structural Freq
8.4257
16.394
16.963
20.049
20.073
36.957
41.613
43.148
43.833
44.65
54.147
97.568
99.943
110.08
111.75
112.05
122.35
125.73
139.34
152.99
169.33
169.73
176.2
177.78
208.25
239.34
242.33
250.58
262.08
266.66
290.1
299.38
365.68
371.78
374.38
378.79
430.15
444.34
469.42
469.43
488.27
489.32
489.79
509.33
568.44
569.85
580.95
586.2
593.67

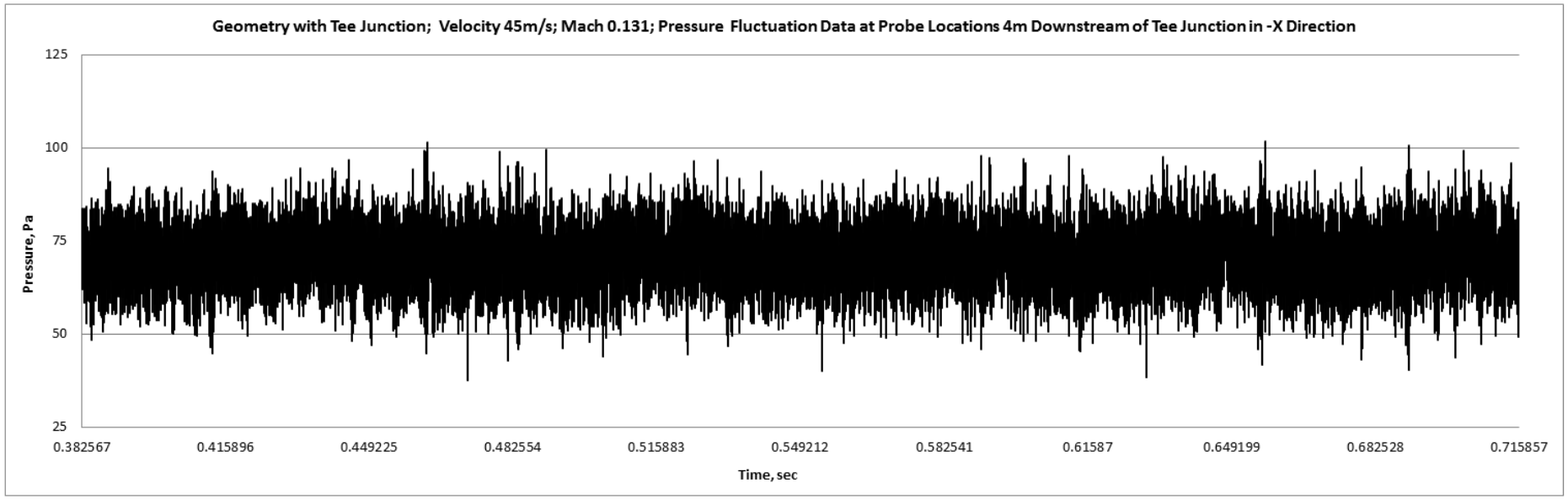
Geometry with Tee Junction; Velocity 45m/s; Mach 0.131; Pressure Fluctuation Data at Probe Locations 4m Downstream of Tee Junction in -X Direction
Pressure, Pa
125
100
75
50
25
0.382567
0.415896
0.449225
0.482554
0.515883
0.549212
0.582541
0.61587
0.649199
0.682528
0.715857
Time, sec

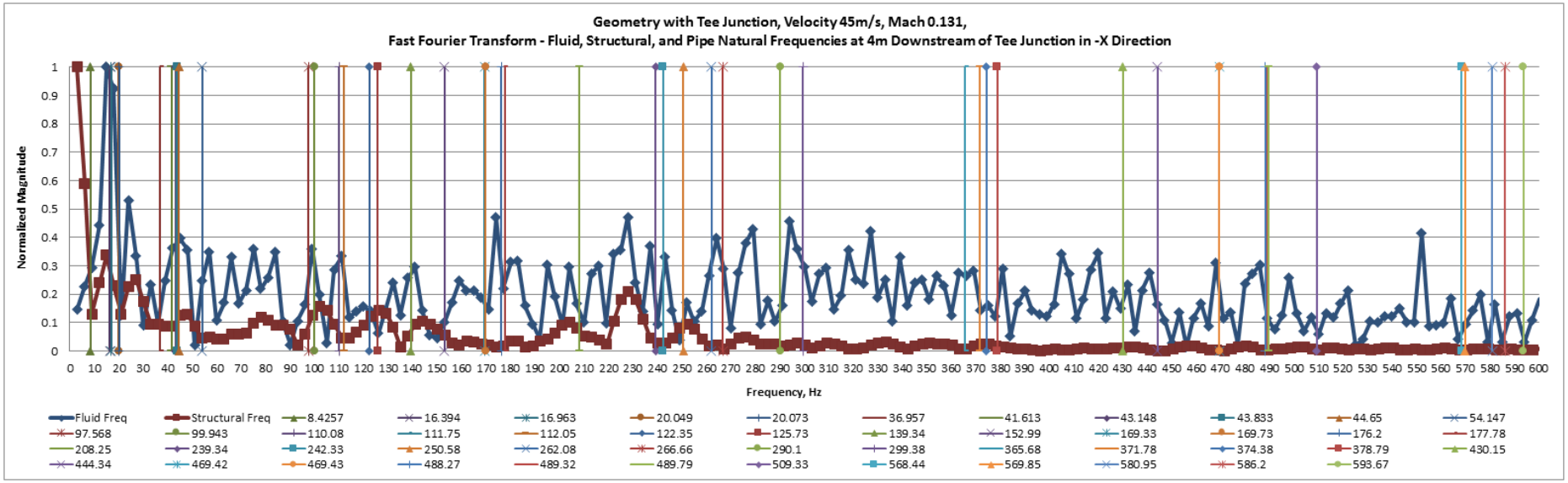
Geometry with Tee Junction, Velocity 45m/s, Mach 0.131,
Fast Fourier Transform - Fluid, Structural, and Pipe Natural Frequencies at 4m Downstream of Tee Junction in -X Direction
Normalized Magnitude
Frequency, Hz
Fluid Freq
Structural Freq
8.4257
16.394
16.963
20.049
20.073
36.957
41.613
43.148
43.833
44.65
54.147
97.568
99.943
110.08
111.75
112.05
122.35
125.73
139.34
152.99
169.33
169.73
176.2
177.78
208.25
239.34
242.33
250.58
262.08
266.66
290.1
299.38
365.68
371.78
374.38
378.79
430.15
444.34
469.42
469.43
488.27
489.32
489.79
509.33
568.44
569.85
580.95
586.2
593.67

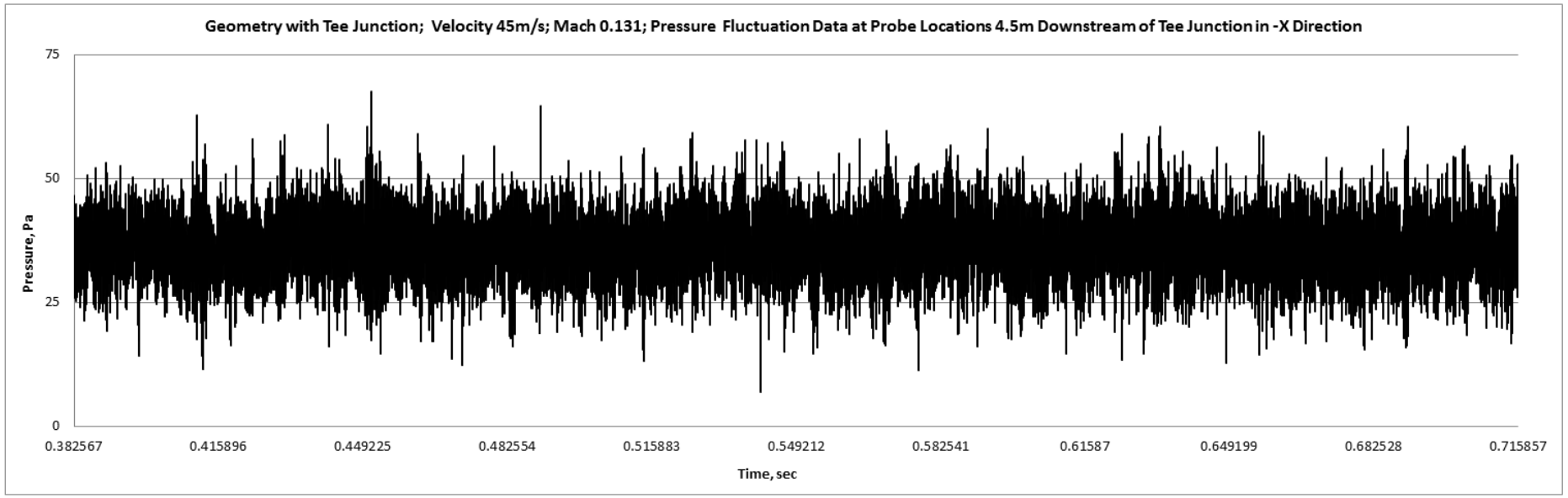
Geometry with Tee Junction; Velocity 45m/s; Mach 0.131; Pressure Fluctuation Data at Probe Locations 4.5m Downstream of Tee Junction in -X Direction
Pressure, Pa
75
50
25
0
0.382567
0.415896
0.449225
0.482554
0.515883
0.549212
0.582541
0.61587
0.649199
0.682528
0.715857
Time, sec

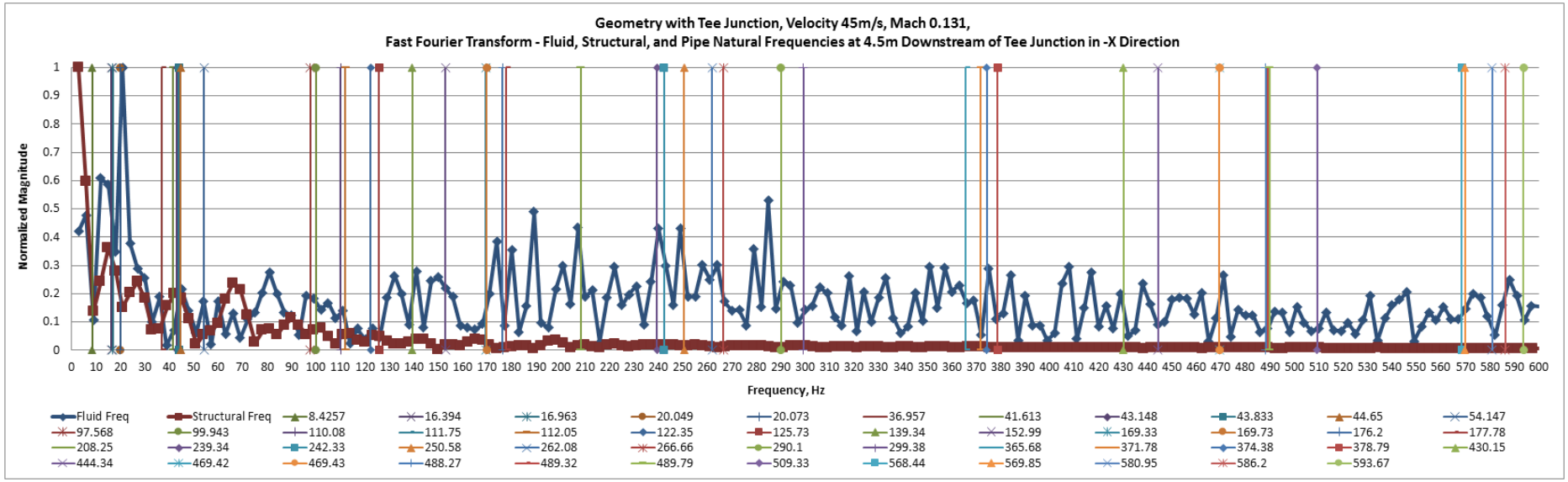
Geometry with Tee Junction, Velocity 45m/s, Mach 0.131,
Fast Fourier Transform - Fluid, Structural, and Pipe Natural Frequencies at 4.5m Downstream of Tee Junction in -X Direction
Normalized Magnitude
1
0.9
0.8
0.7
0.6
0.5
0.4
0.3
0.2
0.1
0
0 10 20 30 40 50 60 70 80 90 100 110 120 130 140 150 160 170 180 190 200 210 220 230 240 250 260 270 280 290 300 310 320 330 340 350 360 370 380 390 400 410 420 430 440 450 460 470 480 490 500 510 520 530 540 550 560 570 580 590 600
Frequency, Hz
Fluid Freq
Structural Freq
8.4257
16.394
16.963
20.049
20.073
36.957
41.613
43.148
43.833
44.65
54.147
97.568
99.943
110.08
111.75
112.05
122.35
125.73
139.34
152.99
169.33
169.73
176.2
177.78
208.25
239.34
242.33
250.58
262.08
266.66
290.1
299.38
365.68
371.78
374.38
378.79
430.15
444.34
469.42
469.43
488.27
489.32
489.79
509.33
568.44
569.85
580.95
586.2
593.67

Appendix I

Frequency Plots for Geometry with Tee Junction for Fluid Velocity modelled at 60m/s, Mach 0.175 at Probe Locations

Distance	Fluid Excited Frequencies Downstream of Tee Junction in +X Direction	Fluid Excited Frequencies Downstream of Tee Junction in -X Direction
0.1	24, 54, 75, 87, 126	15, 36, 66, 102, 159
0.3	54, 102, 138, 150, 180	24, 36, 54, 75, 102, 150, 168
0.5	15, 36, 54, 75, 150	15, 24, 36, 54, 75, 102
1	66, 150	27, 36, 102, 150, 228
1.5	66, 102, 150, 213, 252	102, 150, 165, 213, 228, 252, 315
2	60, 90, 102, 165, 183	60, 69, 90, 102, 123, 165, 183, 237
2.5	24, 90, 102	69, 90, 102, 114, 174, 228, 252
3	90, 102, 159, 333	24, 36, 69, 102, 204, 228, 252, 267
3.5	36, 90, 102, 138	36, 69, 102, 114, 129, 150, 183, 192, 204, 213, 228, 252
4	81, 102, 144, 183, 252	36, 48, 102, 126, 144, 204, 252, 309
4.5	18, 42, 66, 90, 129, 144	42, 90, 102, 114, 144, 165, 198

Table I.1: Fluid excited frequencies downstream of the Tee Junction for 60m/s

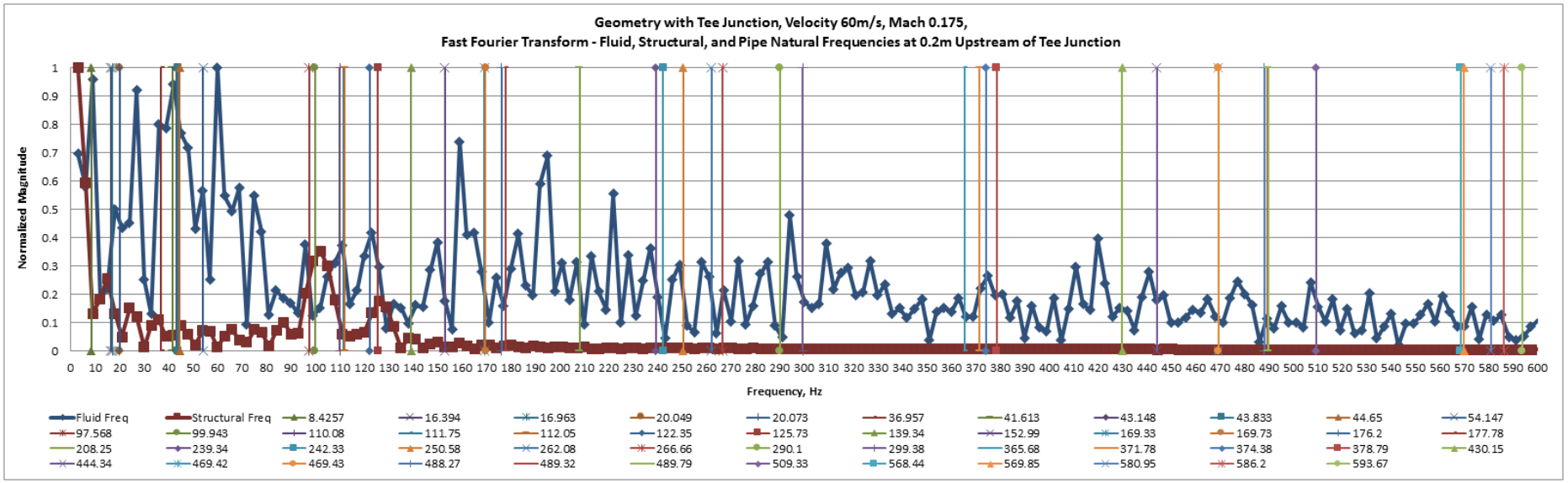
Geometry with Tee Junction, Velocity 60m/s, Mach 0.175,
Fast Fourier Transform - Fluid, Structural, and Pipe Natural Frequencies at 0.2m Upstream of Tee Junction
Normalized Magnitude
Frequency, Hz
Fluid Freq
Structural Freq
8.4257
16.394
16.963
20.049
20.073
36.957
41.613
43.148
43.833
44.65
54.147
97.568
99.943
110.08
111.75
112.05
122.35
125.73
139.34
152.99
169.33
169.73
176.2
177.78
208.25
239.34
242.33
250.58
262.08
266.66
290.1
299.38
365.68
371.78
374.38
378.79
430.15
444.34
469.42
469.43
488.27
489.32
489.79
509.33
568.44
569.85
580.95
586.2
593.67

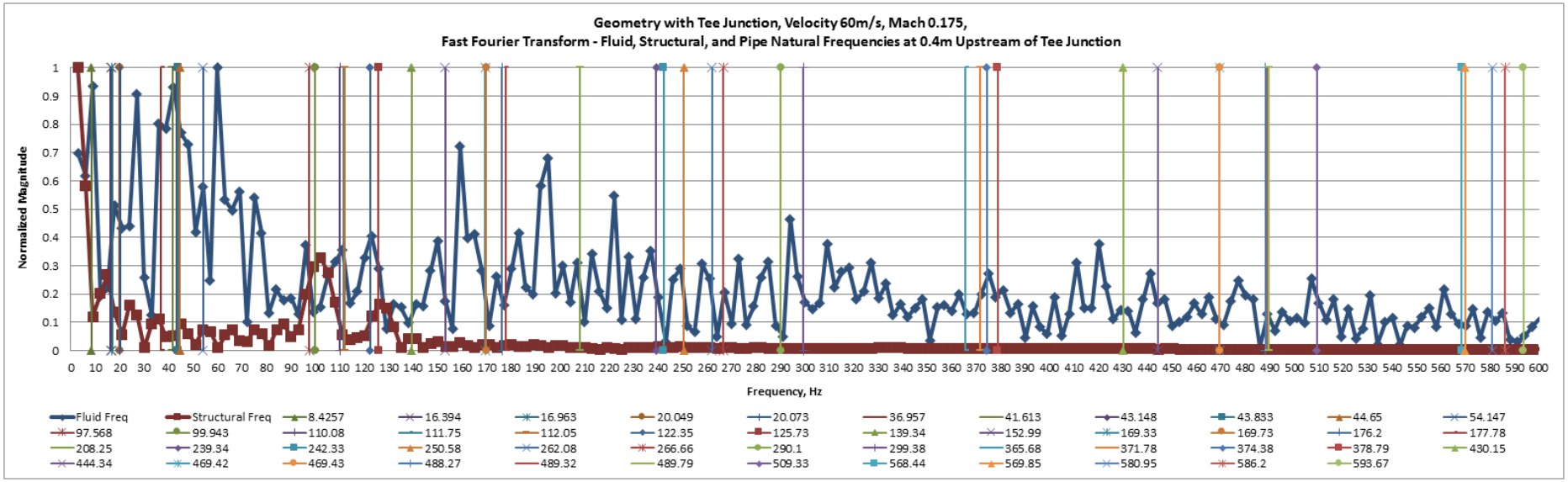
Geometry with Tee Junction, Velocity 60m/s, Mach 0.175,
Fast Fourier Transform - Fluid, Structural, and Pipe Natural Frequencies at 0.4m Upstream of Tee Junction
Normalized Magnitude
Frequency, Hz
Fluid Freq
Structural Freq
8.4257
16.394
16.963
20.049
20.073
36.957
41.613
43.148
43.833
44.65
54.147
97.568
99.943
110.08
111.75
112.05
122.35
125.73
139.34
152.99
169.33
169.73
176.2
177.78
208.25
239.34
242.33
250.58
262.08
266.66
290.1
299.38
365.68
371.78
374.38
378.79
430.15
444.34
469.42
469.43
488.27
489.32
489.79
509.33
568.44
569.85
580.95
586.2
593.67

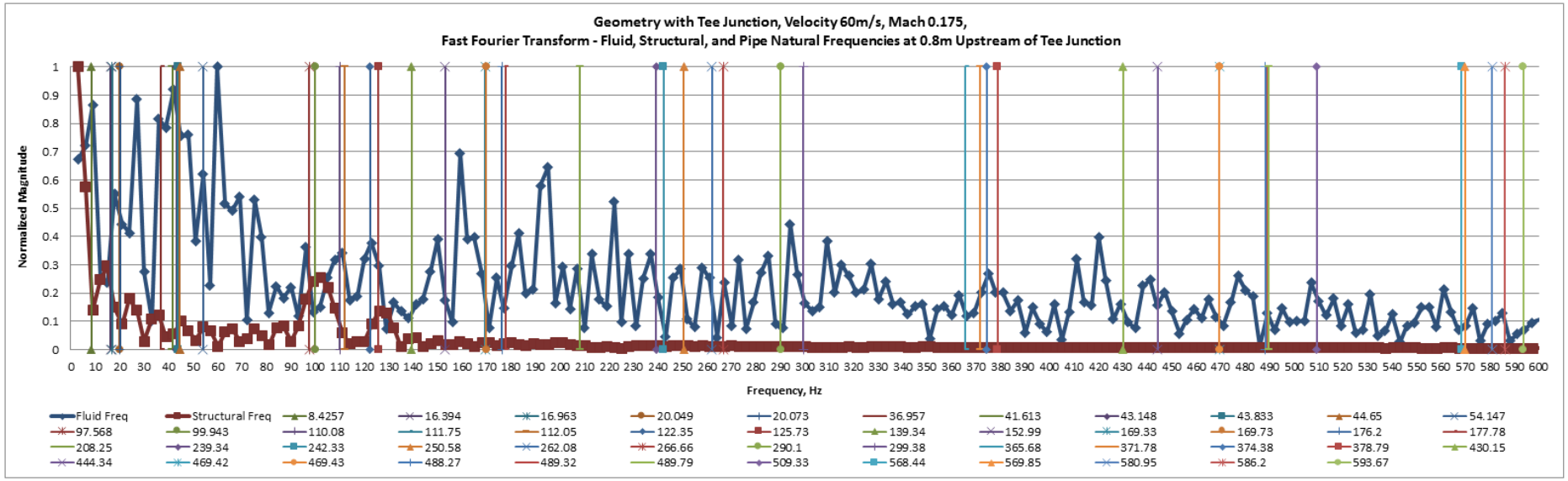
Geometry with Tee Junction, Velocity 60m/s, Mach 0.175,
Fast Fourier Transform - Fluid, Structural, and Pipe Natural Frequencies at 0.8m Upstream of Tee Junction
Normalized Magnitude
Frequency, Hz
Fluid Freq
Structural Freq
8.4257
16.394
16.963
20.049
20.073
36.957
41.613
43.148
43.833
44.65
54.147
97.568
99.943
110.08
111.75
112.05
122.35
125.73
139.34
152.99
169.33
169.73
176.2
177.78
208.25
239.34
242.33
250.58
262.08
266.66
290.1
299.38
365.68
371.78
374.38
378.79
430.15
444.34
469.42
469.43
488.27
489.32
489.79
509.33
568.44
569.85
580.95
586.2
593.67

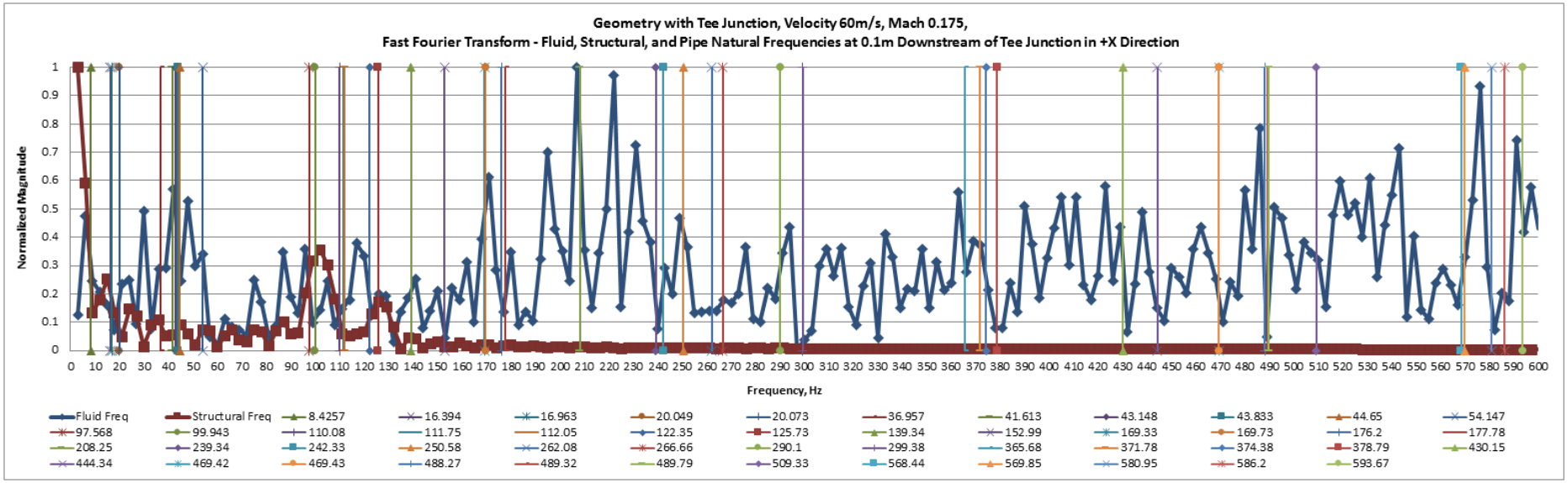
Geometry with Tee Junction, Velocity 60m/s, Mach 0.175,
Fast Fourier Transform - Fluid, Structural, and Pipe Natural Frequencies at 0.1m Downstream of Tee Junction in +X Direction
Normalized Magnitude
Frequency, Hz
Fluid Freq
Structural Freq
8.4257
16.394
16.963
20.049
20.073
36.957
41.613
43.148
43.833
44.65
54.147
97.568
99.943
110.08
111.75
112.05
122.35
125.73
139.34
152.99
169.33
169.73
176.2
177.78
208.25
239.34
242.33
250.58
262.08
266.66
290.1
299.38
365.68
371.78
374.38
378.79
430.15
444.34
469.42
469.43
488.27
489.32
489.79
509.33
568.44
569.85
580.95
586.2
593.67

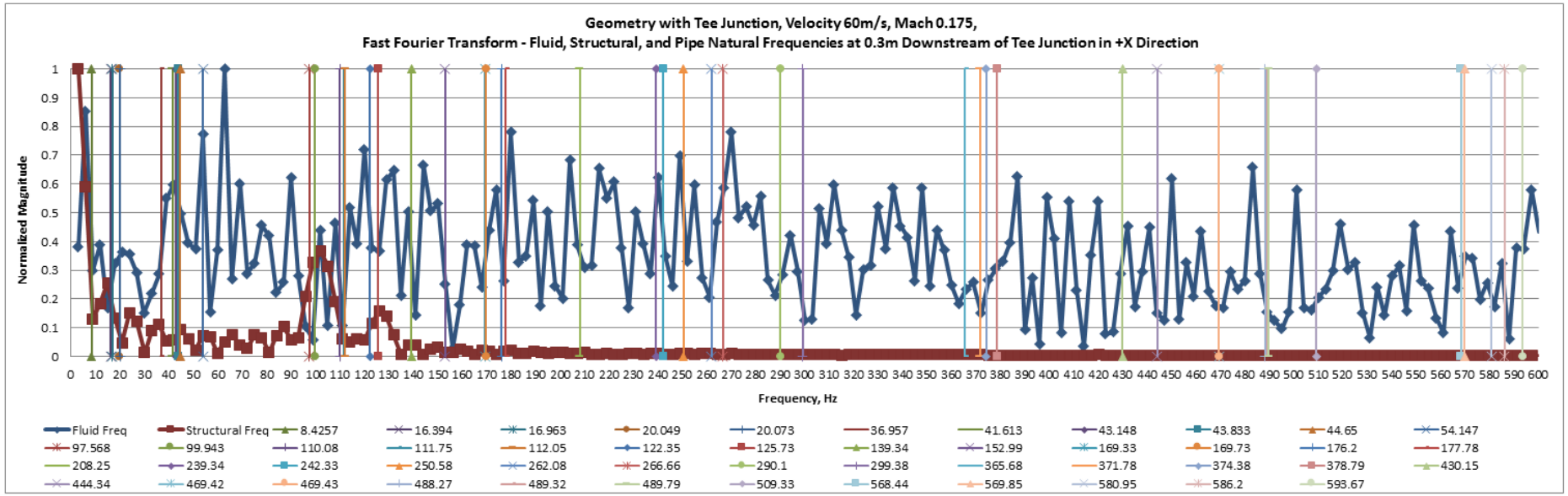
Geometry with Tee Junction, Velocity 60m/s, Mach 0.175,
Fast Fourier Transform - Fluid, Structural, and Pipe Natural Frequencies at 0.3m Downstream of Tee Junction in +X Direction
Normalized Magnitude
Frequency, Hz
Fluid Freq
Structural Freq
8.4257
16.394
16.963
20.049
20.073
36.957
41.613
43.148
43.833
44.65
54.147
97.568
99.943
110.08
111.75
112.05
122.35
125.73
139.34
152.99
169.33
169.73
176.2
177.78
208.25
239.34
242.33
250.58
262.08
266.66
290.1
299.38
365.68
371.78
374.38
378.79
430.15
444.34
469.42
469.43
488.27
489.32
489.79
509.33
568.44
569.85
580.95
586.2
593.67

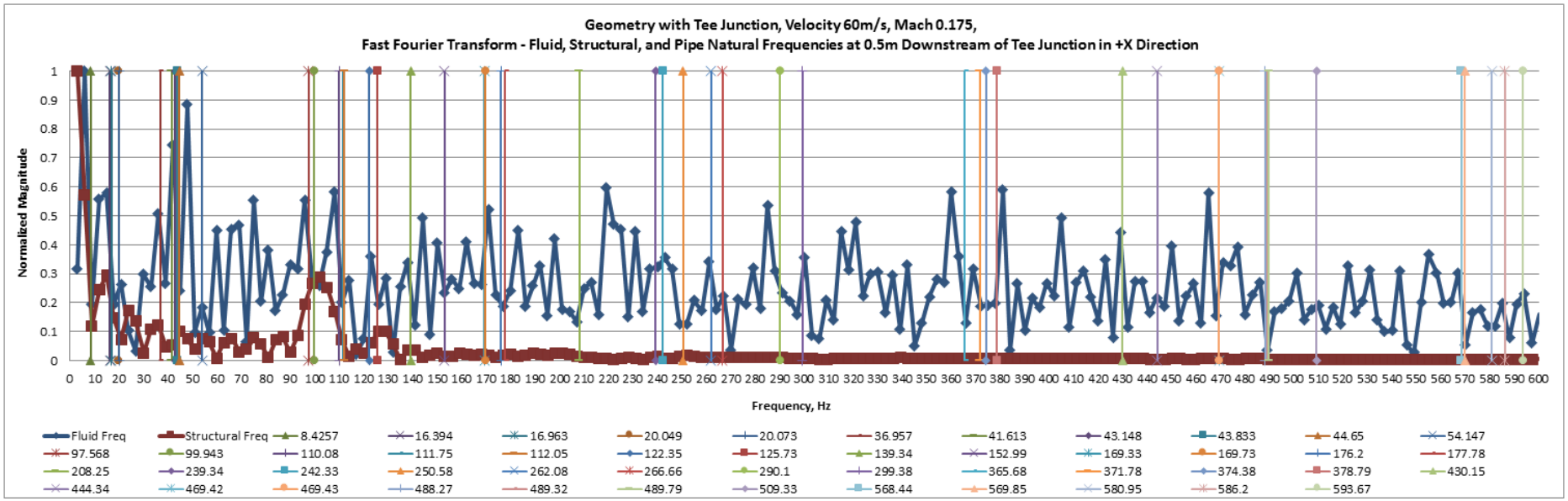
Geometry with Tee Junction, Velocity 60m/s, Mach 0.175,
Fast Fourier Transform - Fluid, Structural, and Pipe Natural Frequencies at 0.5m Downstream of Tee Junction in +X Direction
Normalized Magnitude
Frequency, Hz
Fluid Freq
Structural Freq
8.4257
16.394
16.963
20.049
20.073
36.957
41.613
43.148
43.833
44.65
54.147
97.568
99.943
110.08
111.75
112.05
122.35
125.73
139.34
152.99
169.33
169.73
176.2
177.78
208.25
239.34
242.33
250.58
262.08
266.66
290.1
299.38
365.68
371.78
374.38
378.79
430.15
444.34
469.42
469.43
488.27
489.32
489.79
509.33
568.44
569.85
580.95
586.2
593.67

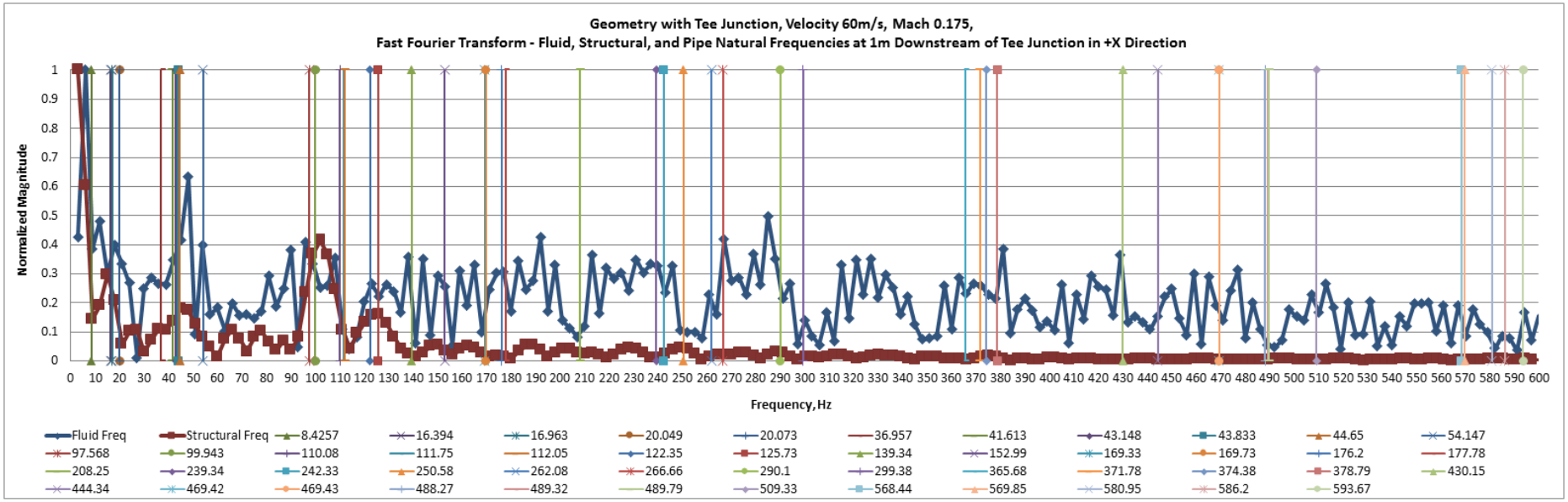
Geometry with Tee Junction, Velocity 60m/s, Mach 0.175,
Fast Fourier Transform - Fluid, Structural, and Pipe Natural Frequencies at 1m Downstream of Tee Junction in +X Direction
Normalized Magnitude
Frequency, Hz
Fluid Freq
Structural Freq
8.4257
16.394
16.963
20.049
20.073
36.957
41.613
43.148
43.833
44.65
54.147
97.568
99.943
110.08
111.75
112.05
122.35
125.73
139.34
152.99
169.33
169.73
176.2
177.78
208.25
239.34
242.33
250.58
262.08
266.66
290.1
299.38
365.68
371.78
374.38
378.79
430.15
444.34
469.42
469.43
488.27
489.32
489.79
509.33
568.44
569.85
580.95
586.2
593.67

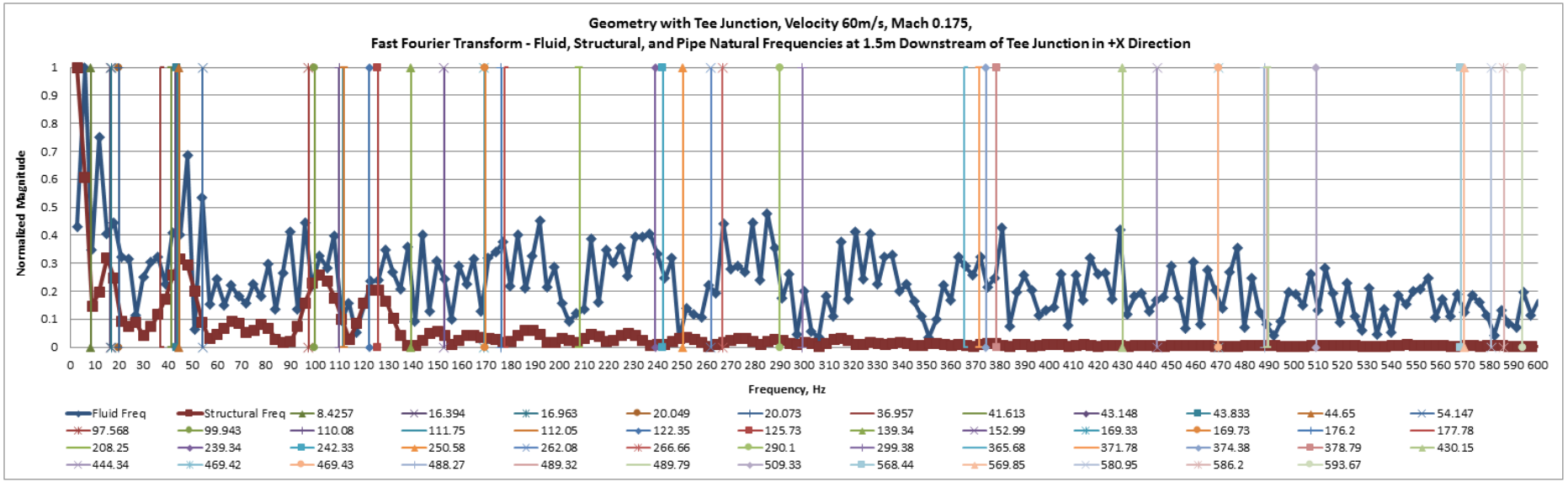
Geometry with Tee Junction, Velocity 60m/s, Mach 0.175,
Fast Fourier Transform - Fluid, Structural, and Pipe Natural Frequencies at 1.5m Downstream of Tee Junction in +X Direction
Normalized Magnitude
Frequency, Hz
Fluid Freq
Structural Freq
8.4257
16.394
16.963
20.049
20.073
36.957
41.613
43.148
43.833
44.65
54.147
97.568
99.943
110.08
111.75
112.05
122.35
125.73
139.34
152.99
169.33
169.73
176.2
177.78
208.25
239.34
242.33
250.58
262.08
266.66
290.1
299.38
365.68
371.78
374.38
378.79
430.15
444.34
469.42
469.43
488.27
489.32
489.79
509.33
568.44
569.85
580.95
586.2
593.67

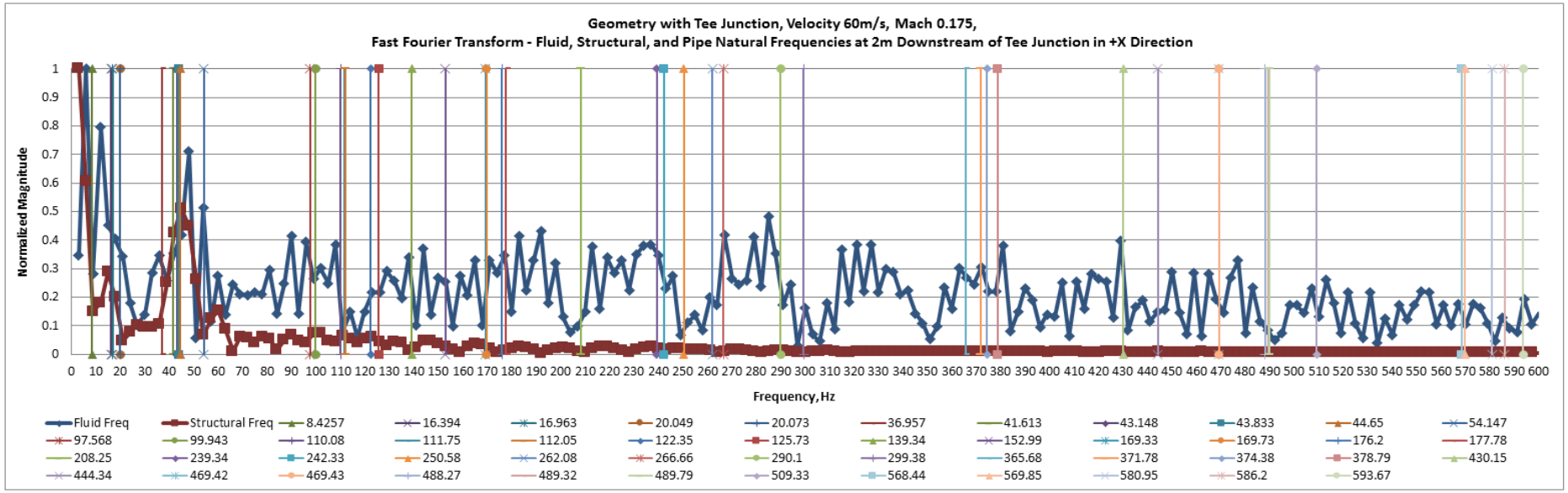
Geometry with Tee Junction, Velocity 60m/s, Mach 0.175,
Fast Fourier Transform - Fluid, Structural, and Pipe Natural Frequencies at 2m Downstream of Tee Junction in +X Direction
Normalized Magnitude
Frequency, Hz
Fluid Freq
Structural Freq
8.4257
16.394
16.963
20.049
20.073
36.957
41.613
43.148
43.833
44.65
54.147
97.568
99.943
110.08
111.75
112.05
122.35
125.73
139.34
152.99
169.33
169.73
176.2
177.78
208.25
239.34
242.33
250.58
262.08
266.66
290.1
299.38
365.68
371.78
374.38
378.79
430.15
444.34
469.42
469.43
488.27
489.32
489.79
509.33
568.44
569.85
580.95
586.2
593.67

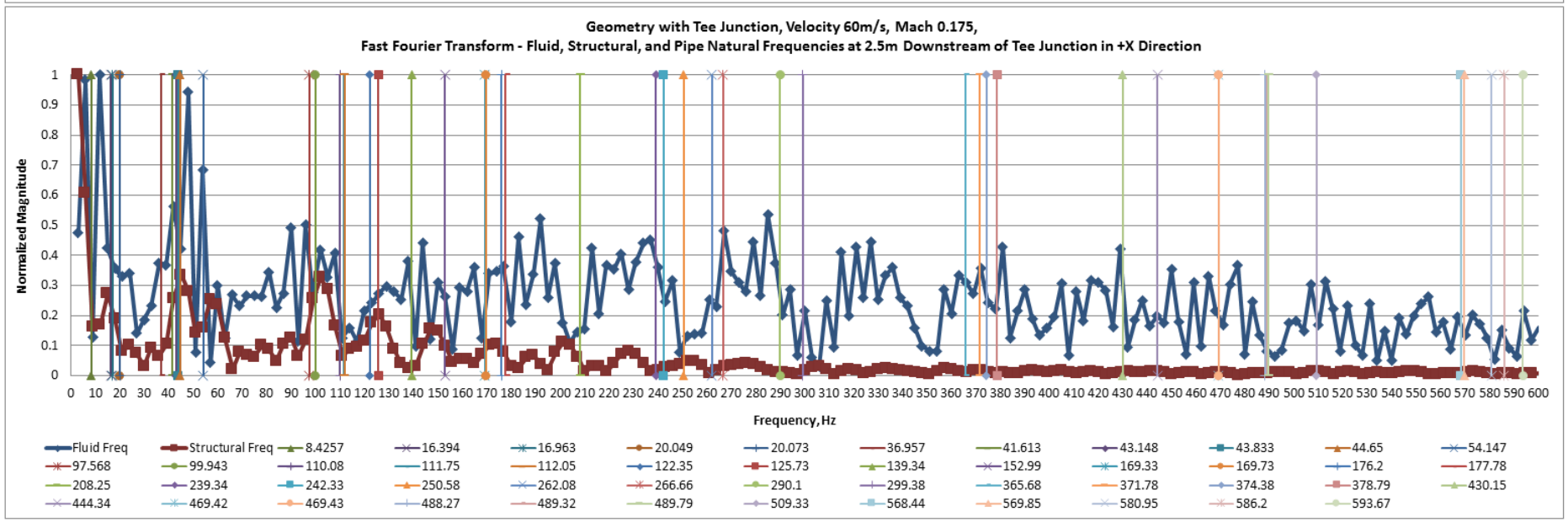
Geometry with Tee Junction, Velocity 60m/s, Mach 0.175,
Fast Fourier Transform - Fluid, Structural, and Pipe Natural Frequencies at 2.5m Downstream of Tee Junction in +X Direction
Normalized Magnitude
Frequency, Hz
Fluid Freq
Structural Freq
8.4257
16.394
16.963
20.049
20.073
36.957
41.613
43.148
43.833
44.65
54.147
97.568
99.943
110.08
111.75
112.05
122.35
125.73
139.34
152.99
169.33
169.73
176.2
177.78
208.25
239.34
242.33
250.58
262.08
266.66
290.1
299.38
365.68
371.78
374.38
378.79
430.15
444.34
469.42
469.43
488.27
489.32
489.79
509.33
568.44
569.85
580.95
586.2
593.67

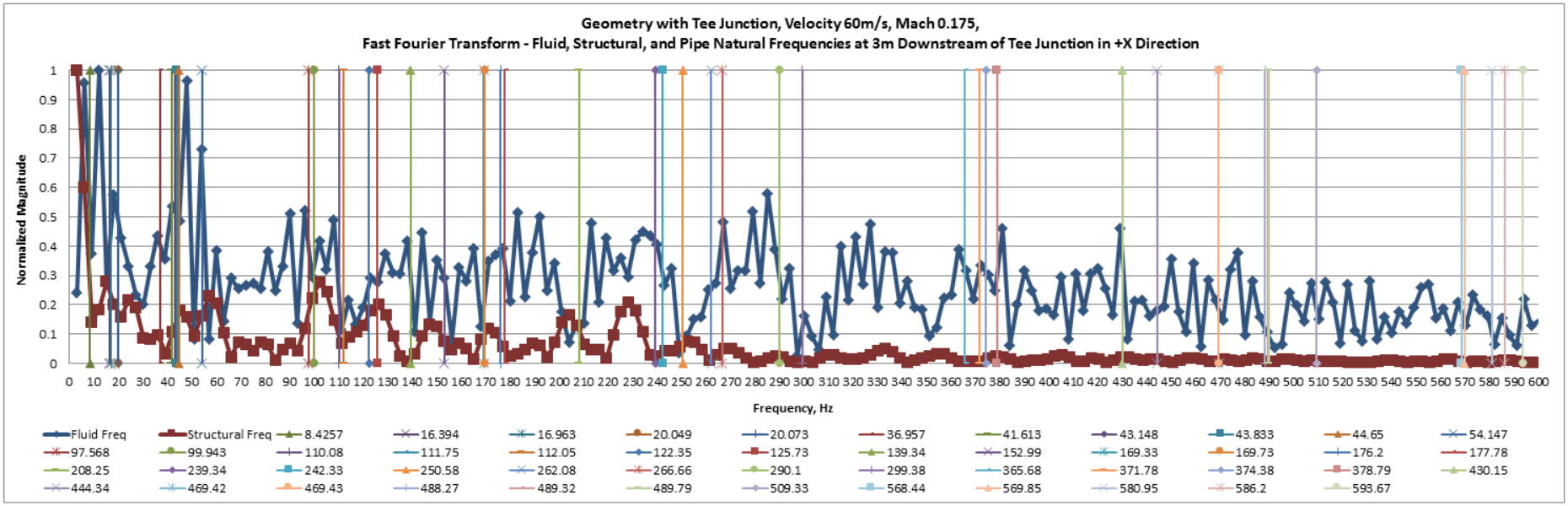
Geometry with Tee Junction, Velocity 60m/s, Mach 0.175,
Fast Fourier Transform - Fluid, Structural, and Pipe Natural Frequencies at 3m Downstream of Tee Junction in +X Direction
Normalized Magnitude
Frequency, Hz
Fluid Freq
Structural Freq
8.4257
16.394
16.963
20.049
20.073
36.957
41.613
43.148
43.833
44.65
54.147
97.568
99.943
110.08
111.75
112.05
122.35
125.73
139.34
152.99
169.33
169.73
176.2
177.78
208.25
239.34
242.33
250.58
262.08
266.66
290.1
299.38
365.68
371.78
374.38
378.79
430.15
444.34
469.42
469.43
488.27
489.32
489.79
509.33
568.44
569.85
580.95
586.2
593.67

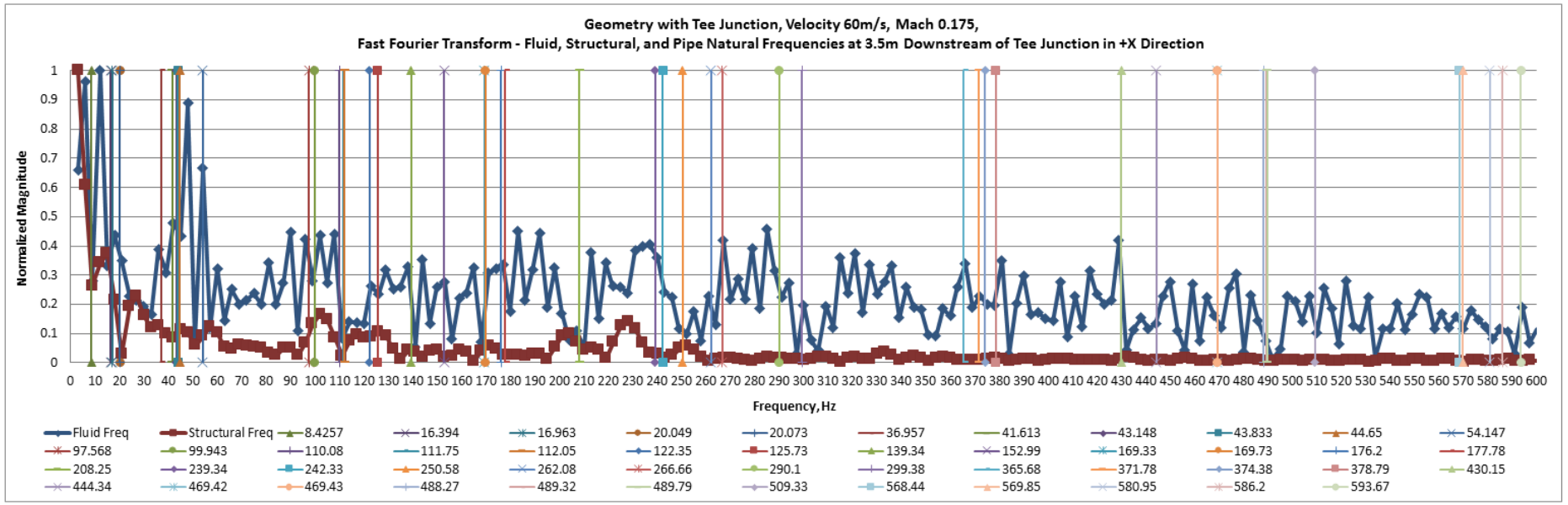
Geometry with Tee Junction, Velocity 60m/s, Mach 0.175,
Fast Fourier Transform - Fluid, Structural, and Pipe Natural Frequencies at 3.5m Downstream of Tee Junction in +X Direction
Normalized Magnitude
Frequency, Hz
Fluid Freq
Structural Freq
8.4257
16.394
16.963
20.049
20.073
36.957
41.613
43.148
43.833
44.65
54.147
97.568
99.943
110.08
111.75
112.05
122.35
125.73
139.34
152.99
169.33
169.73
176.2
177.78
208.25
239.34
242.33
250.58
262.08
266.66
290.1
299.38
365.68
371.78
374.38
378.79
430.15
444.34
469.42
469.43
488.27
489.32
489.79
509.33
568.44
569.85
580.95
586.2
593.67

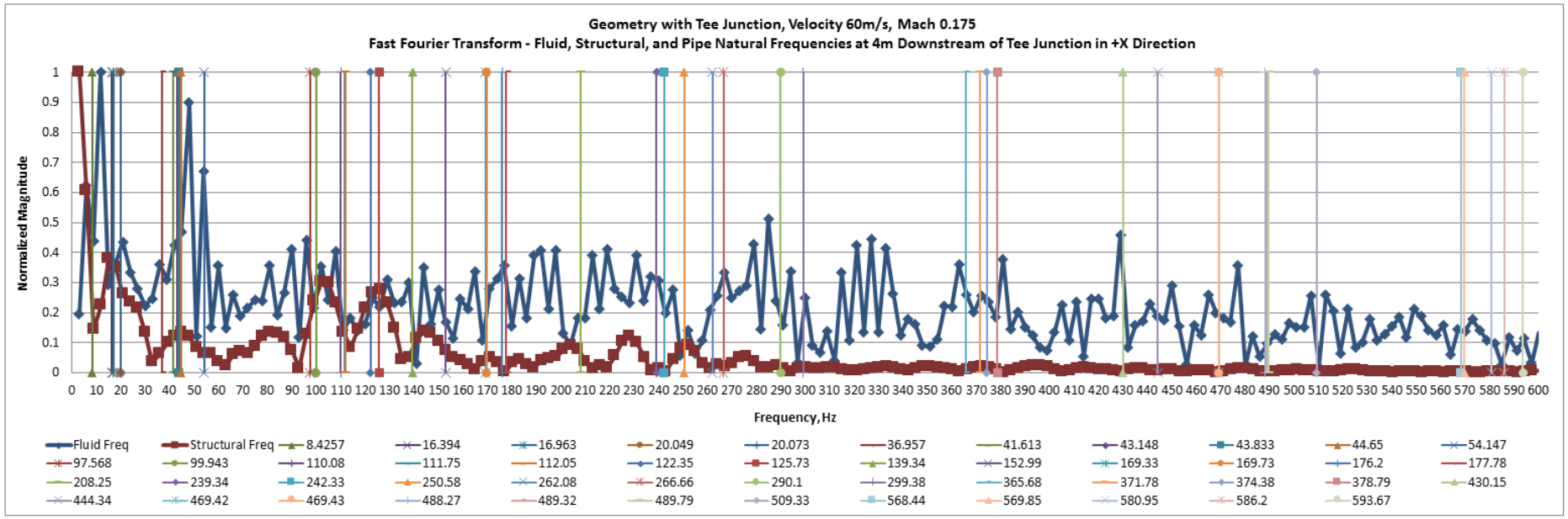
Geometry with Tee Junction, Velocity 60m/s, Mach 0.175
Fast Fourier Transform - Fluid, Structural, and Pipe Natural Frequencies at 4m Downstream of Tee Junction in +X Direction
Normalized Magnitude
Frequency, Hz
Fluid Freq
Structural Freq
8.4257
16.394
16.963
20.049
20.073
36.957
41.613
43.148
43.833
44.65
54.147
97.568
99.943
110.08
111.75
112.05
122.35
125.73
139.34
152.99
169.33
169.73
176.2
177.78
208.25
239.34
242.33
250.58
262.08
266.66
290.1
299.38
365.68
371.78
374.38
378.79
430.15
444.34
469.42
469.43
488.27
489.32
489.79
509.33
568.44
569.85
580.95
586.2
593.67

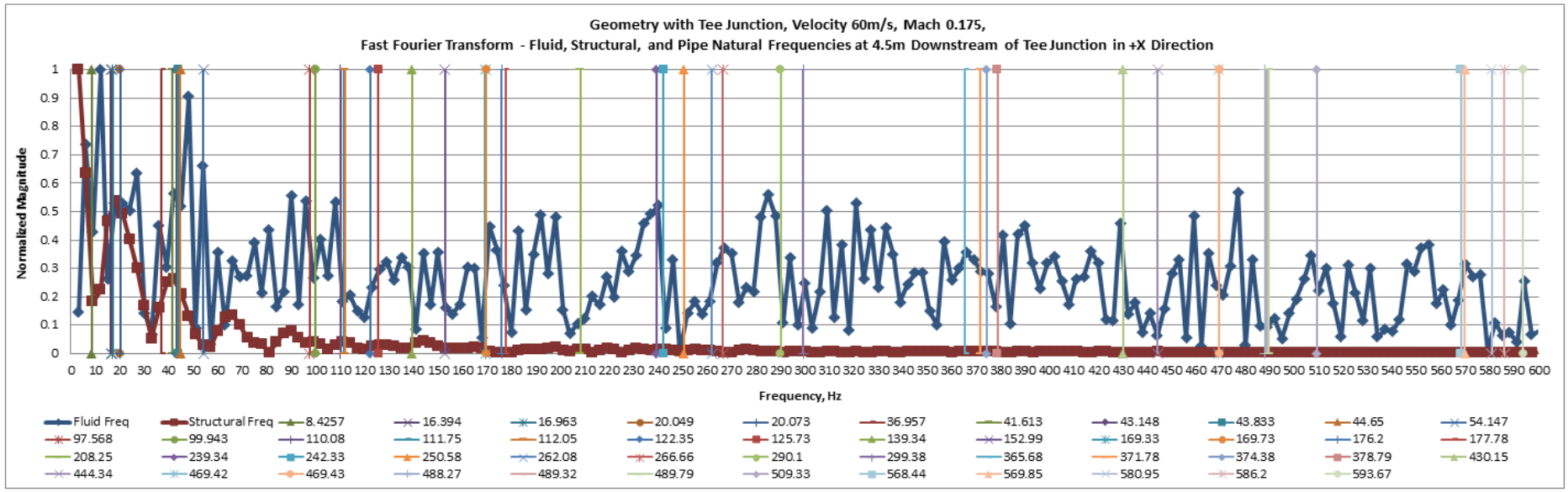
Geometry with Tee Junction, Velocity 60m/s, Mach 0.175,
Fast Fourier Transform - Fluid, Structural, and Pipe Natural Frequencies at 4.5m Downstream of Tee Junction in +X Direction
Normalized Magnitude
Frequency, Hz
Fluid Freq
Structural Freq
8.4257
16.394
16.963
20.049
20.073
36.957
41.613
43.148
43.833
44.65
54.147
97.568
99.943
110.08
111.75
112.05
122.35
125.73
139.34
152.99
169.33
169.73
176.2
177.78
208.25
239.34
242.33
250.58
262.08
266.66
290.1
299.38
365.68
371.78
374.38
378.79
430.15
444.34
469.42
469.43
488.27
489.32
489.79
509.33
568.44
569.85
580.95
586.2
593.67

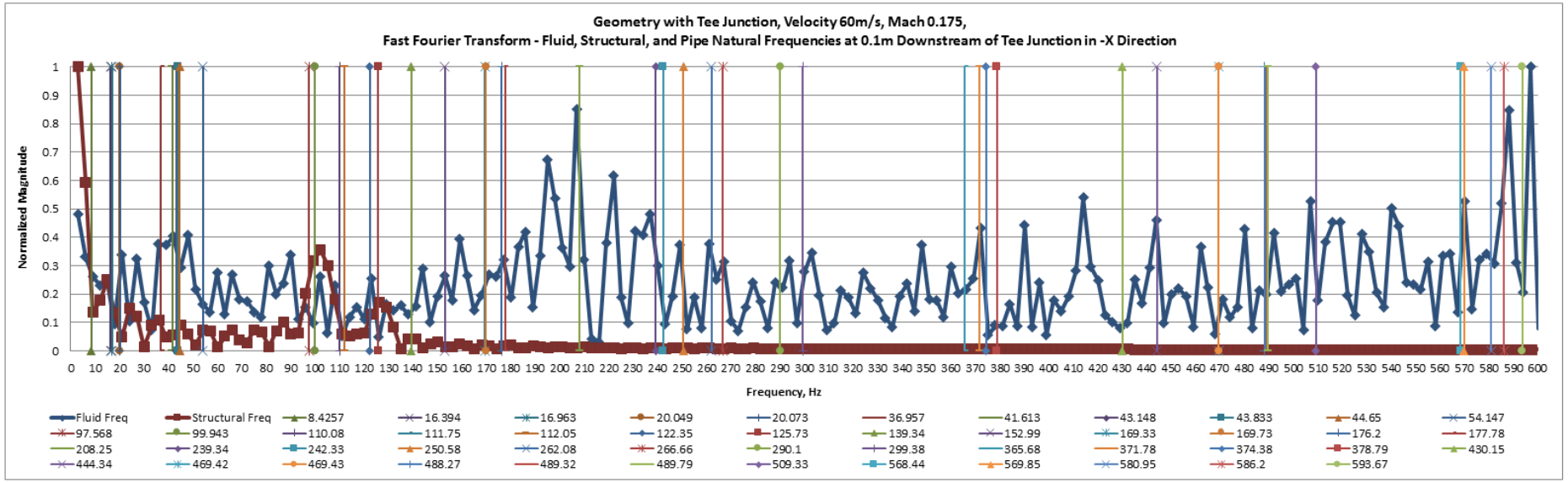
Geometry with Tee Junction, Velocity 60m/s, Mach 0.175,
Fast Fourier Transform - Fluid, Structural, and Pipe Natural Frequencies at 0.1m Downstream of Tee Junction in -X Direction
Normalized Magnitude
Frequency, Hz
Fluid Freq
Structural Freq
8.4257
16.394
16.963
20.049
20.073
36.957
41.613
43.148
43.833
44.65
54.147
97.568
99.943
110.08
111.75
112.05
122.35
125.73
139.34
152.99
169.33
169.73
176.2
177.78
208.25
239.34
242.33
250.58
262.08
266.66
290.1
299.38
365.68
371.78
374.38
378.79
430.15
444.34
469.42
469.43
488.27
489.32
489.79
509.33
568.44
569.85
580.95
586.2
593.67

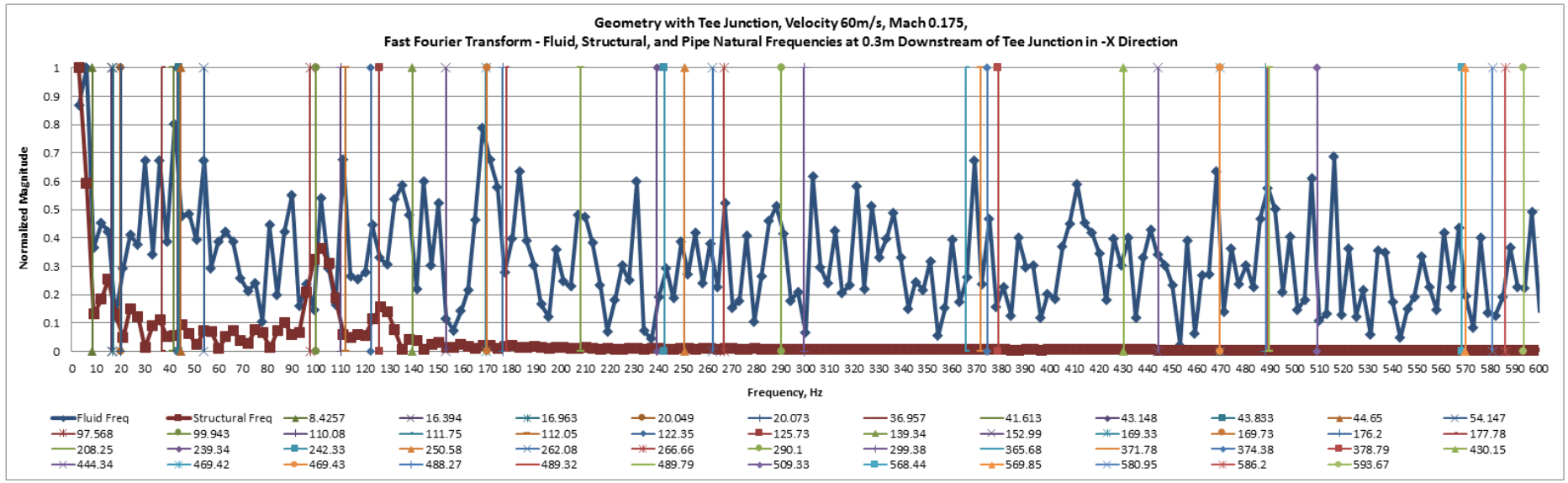
Geometry with Tee Junction, Velocity 60m/s, Mach 0.175,
Fast Fourier Transform - Fluid, Structural, and Pipe Natural Frequencies at 0.3m Downstream of Tee Junction in -X Direction
Normalized Magnitude
Frequency, Hz
Fluid Freq
Structural Freq
8.4257
16.394
16.963
20.049
20.073
36.957
41.613
43.148
43.833
44.65
54.147
97.568
99.943
110.08
111.75
112.05
122.35
125.73
139.34
152.99
169.33
169.73
176.2
177.78
208.25
239.34
242.33
250.58
262.08
266.66
290.1
299.38
365.68
371.78
374.38
378.79
430.15
444.34
469.42
469.43
488.27
489.32
489.79
509.33
568.44
569.85
580.95
586.2
593.67

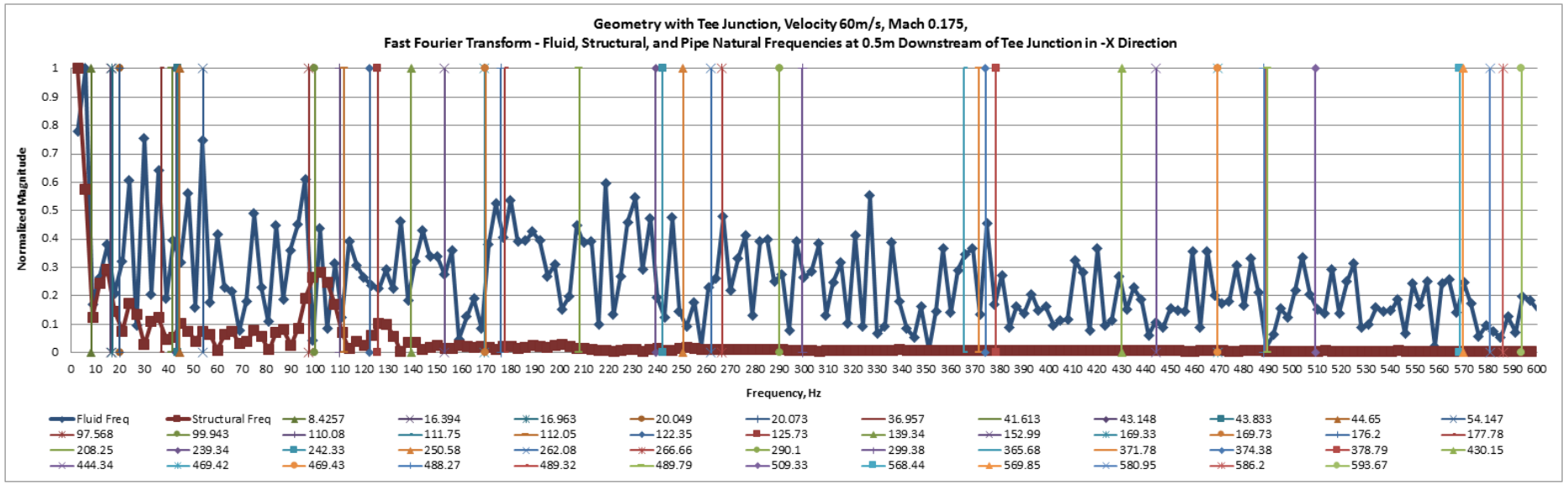
Geometry with Tee Junction, Velocity 60m/s, Mach 0.175,
Fast Fourier Transform - Fluid, Structural, and Pipe Natural Frequencies at 0.5m Downstream of Tee Junction in -X Direction
Normalized Magnitude
Frequency, Hz
Fluid Freq
Structural Freq
8.4257
16.394
16.963
20.049
20.073
36.957
41.613
43.148
43.833
44.65
54.147
97.568
99.943
110.08
111.75
112.05
122.35
125.73
139.34
152.99
169.33
169.73
176.2
177.78
208.25
239.34
242.33
250.58
262.08
266.66
290.1
299.38
365.68
371.78
374.38
378.79
430.15
444.34
469.42
469.43
488.27
489.32
489.79
509.33
568.44
569.85
580.95
586.2
593.67

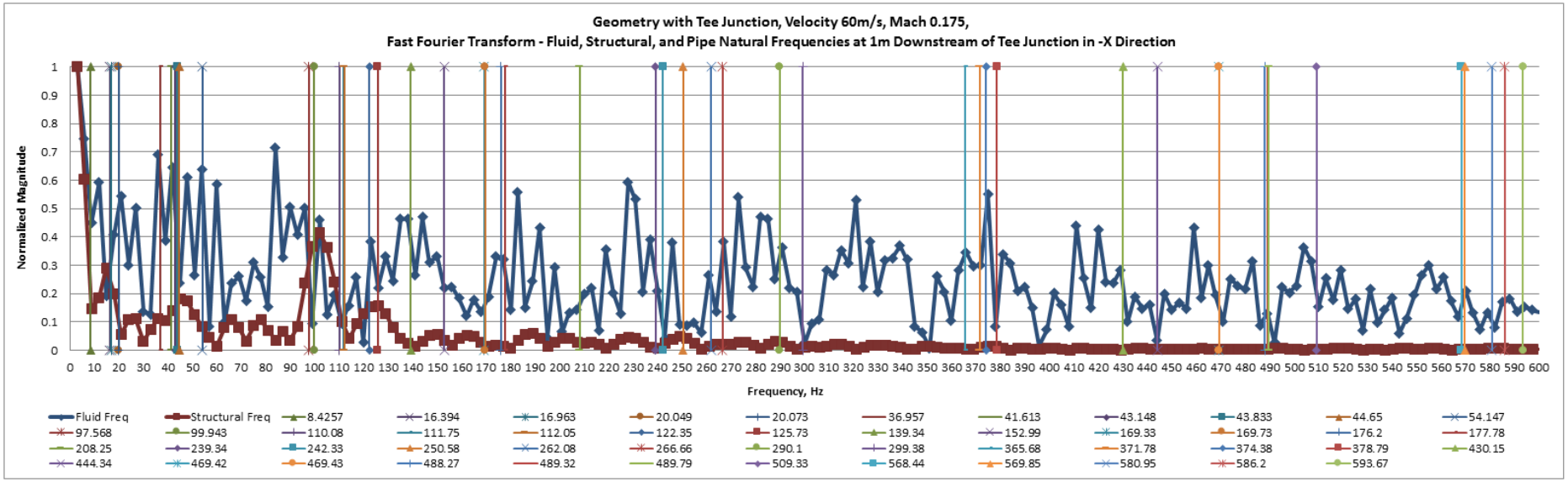
Geometry with Tee Junction, Velocity 60m/s, Mach 0.175,
Fast Fourier Transform - Fluid, Structural, and Pipe Natural Frequencies at 1m Downstream of Tee Junction in -X Direction
Normalized Magnitude
Frequency, Hz
Fluid Freq
Structural Freq
8.4257
16.394
16.963
20.049
20.073
36.957
41.613
43.148
43.833
44.65
54.147
97.568
99.943
110.08
111.75
112.05
122.35
125.73
139.34
152.99
169.33
169.73
176.2
177.78
208.25
239.34
242.33
250.58
262.08
266.66
290.1
299.38
365.68
371.78
374.38
378.79
430.15
444.34
469.42
469.43
488.27
489.32
489.79
509.33
568.44
569.85
580.95
586.2
593.67

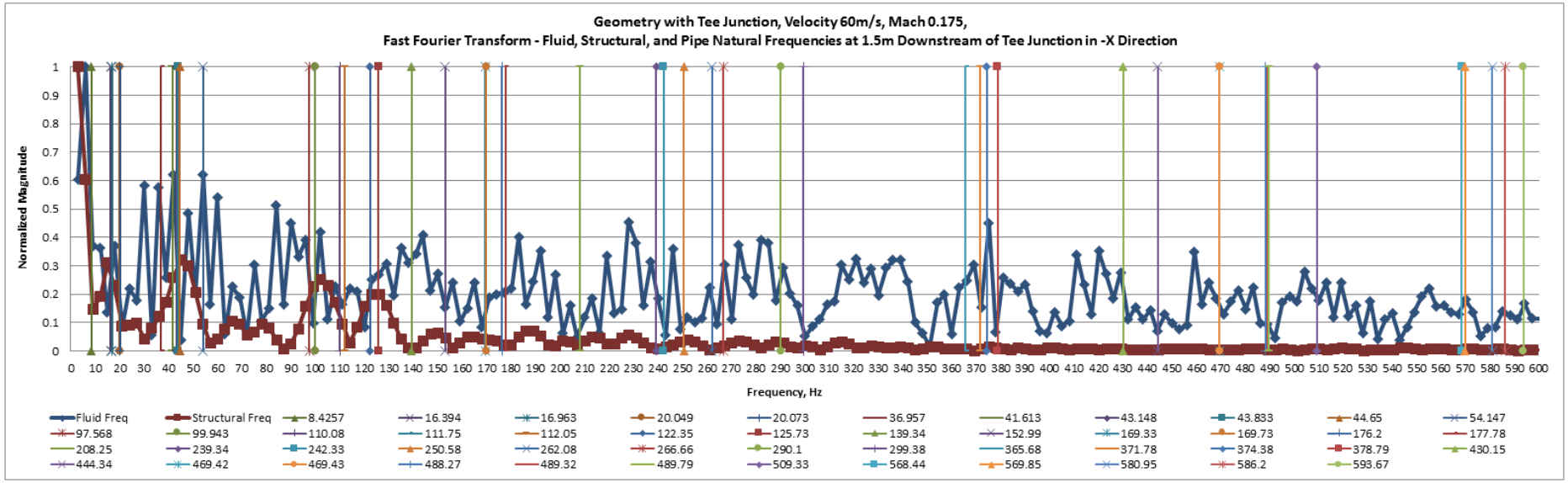
Geometry with Tee Junction, Velocity 60m/s, Mach 0.175,
Fast Fourier Transform - Fluid, Structural, and Pipe Natural Frequencies at 1.5m Downstream of Tee Junction in -X Direction
Normalized Magnitude
Frequency, Hz
Fluid Freq
Structural Freq
8.4257
16.394
16.963
20.049
20.073
36.957
41.613
43.148
43.833
44.65
54.147
97.568
99.943
110.08
111.75
112.05
122.35
125.73
139.34
152.99
169.33
169.73
176.2
177.78
208.25
239.34
242.33
250.58
262.08
266.66
290.1
299.38
365.68
371.78
374.38
378.79
430.15
444.34
469.42
469.43
488.27
489.32
489.79
509.33
568.44
569.85
580.95
586.2
593.67

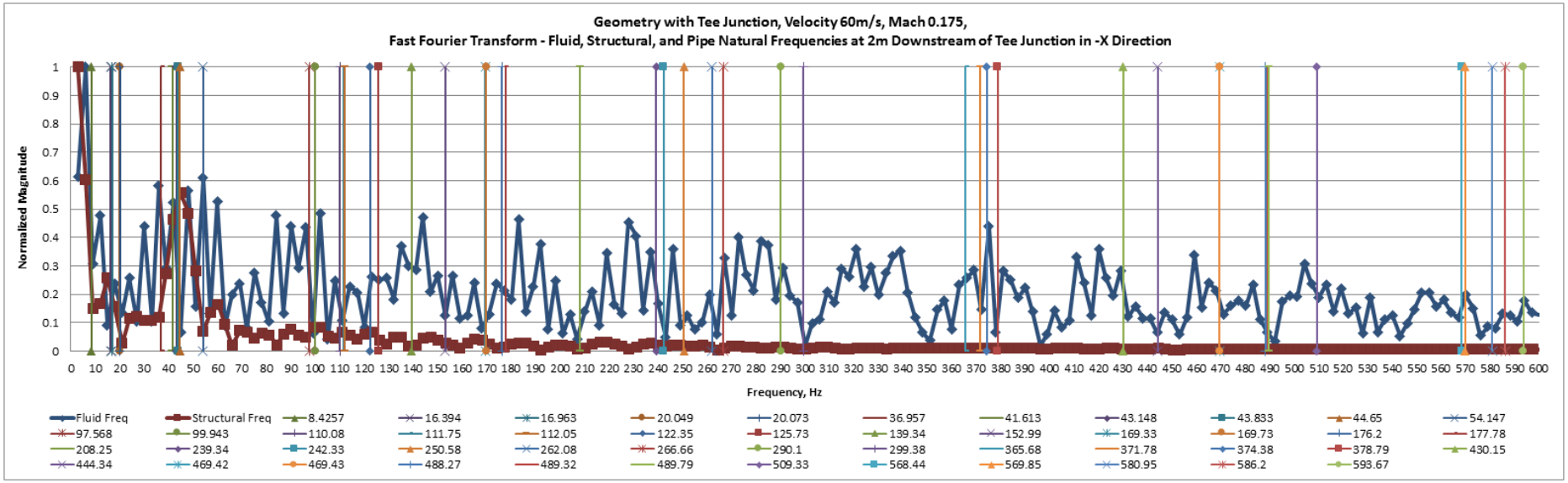
Geometry with Tee Junction, Velocity 60m/s, Mach 0.175,
Fast Fourier Transform - Fluid, Structural, and Pipe Natural Frequencies at 2m Downstream of Tee Junction in -X Direction
Normalized Magnitude
Frequency, Hz
Fluid Freq
Structural Freq
8.4257
16.394
16.963
20.049
20.073
36.957
41.613
43.148
43.833
44.65
54.147
97.568
99.943
110.08
111.75
112.05
122.35
125.73
139.34
152.99
169.33
169.73
176.2
177.78
208.25
239.34
242.33
250.58
262.08
266.66
290.1
299.38
365.68
371.78
374.38
378.79
430.15
444.34
469.42
469.43
488.27
489.32
489.79
509.33
568.44
569.85
580.95
586.2
593.67

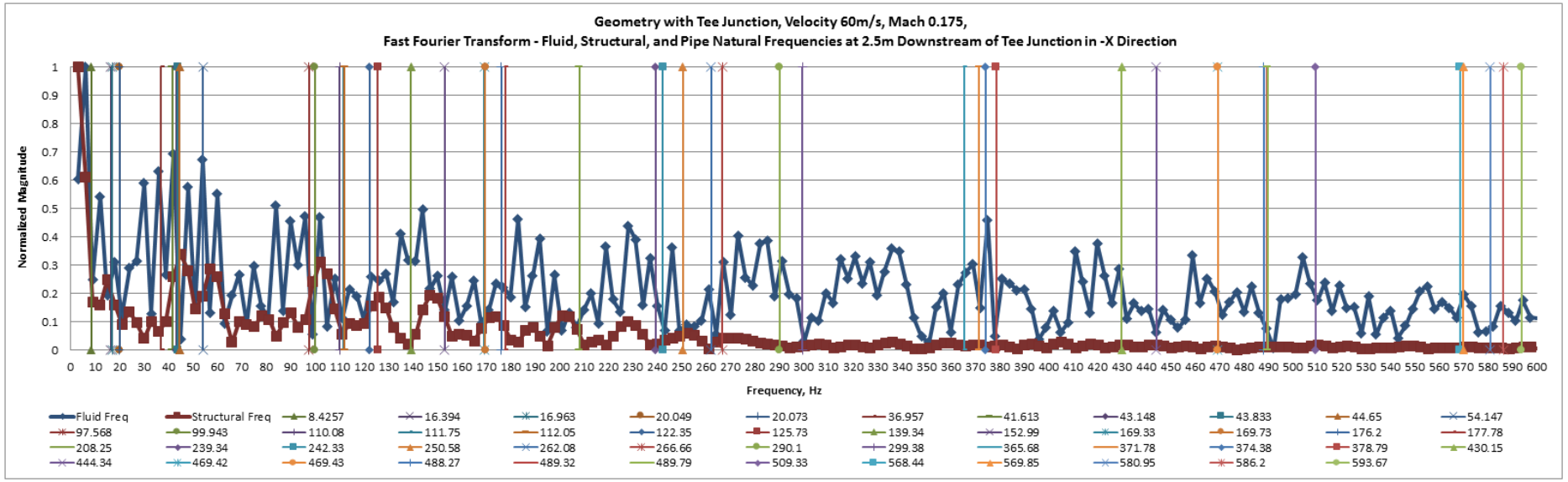
Geometry with Tee Junction, Velocity 60m/s, Mach 0.175,
Fast Fourier Transform - Fluid, Structural, and Pipe Natural Frequencies at 2.5m Downstream of Tee Junction in -X Direction
Normalized Magnitude
Frequency, Hz
Fluid Freq
Structural Freq
8.4257
16.394
16.963
20.049
20.073
36.957
41.613
43.148
43.833
44.65
54.147
97.568
99.943
110.08
111.75
112.05
122.35
125.73
139.34
152.99
169.33
169.73
176.2
177.78
208.25
239.34
242.33
250.58
262.08
266.66
290.1
299.38
365.68
371.78
374.38
378.79
430.15
444.34
469.42
469.43
488.27
489.32
489.79
509.33
568.44
569.85
580.95
586.2
593.67

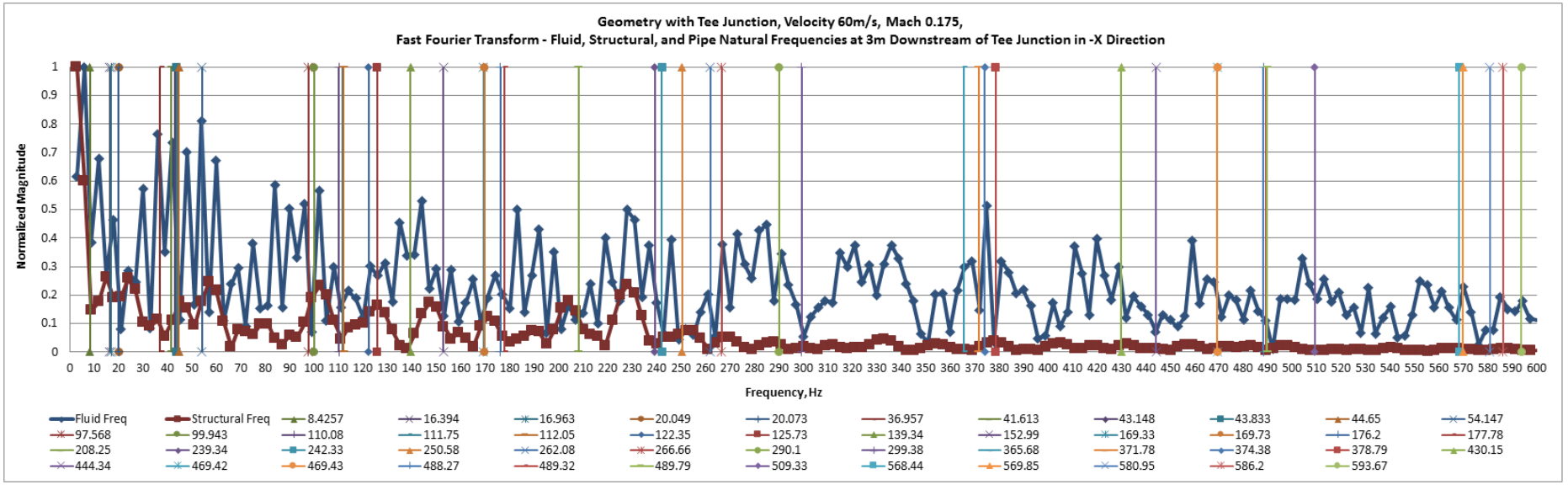
Geometry with Tee Junction, Velocity 60m/s, Mach 0.175,
Fast Fourier Transform - Fluid, Structural, and Pipe Natural Frequencies at 3m Downstream of Tee Junction in -X Direction
Normalized Magnitude
Frequency, Hz
Fluid Freq
Structural Freq
8.4257
16.394
16.963
20.049
20.073
36.957
41.613
43.148
43.833
44.65
54.147
97.568
99.943
110.08
111.75
112.05
122.35
125.73
139.34
152.99
169.33
169.73
176.2
177.78
208.25
239.34
242.33
250.58
262.08
266.66
290.1
299.38
365.68
371.78
374.38
378.79
430.15
444.34
469.42
469.43
488.27
489.32
489.79
509.33
568.44
569.85
580.95
586.2
593.67

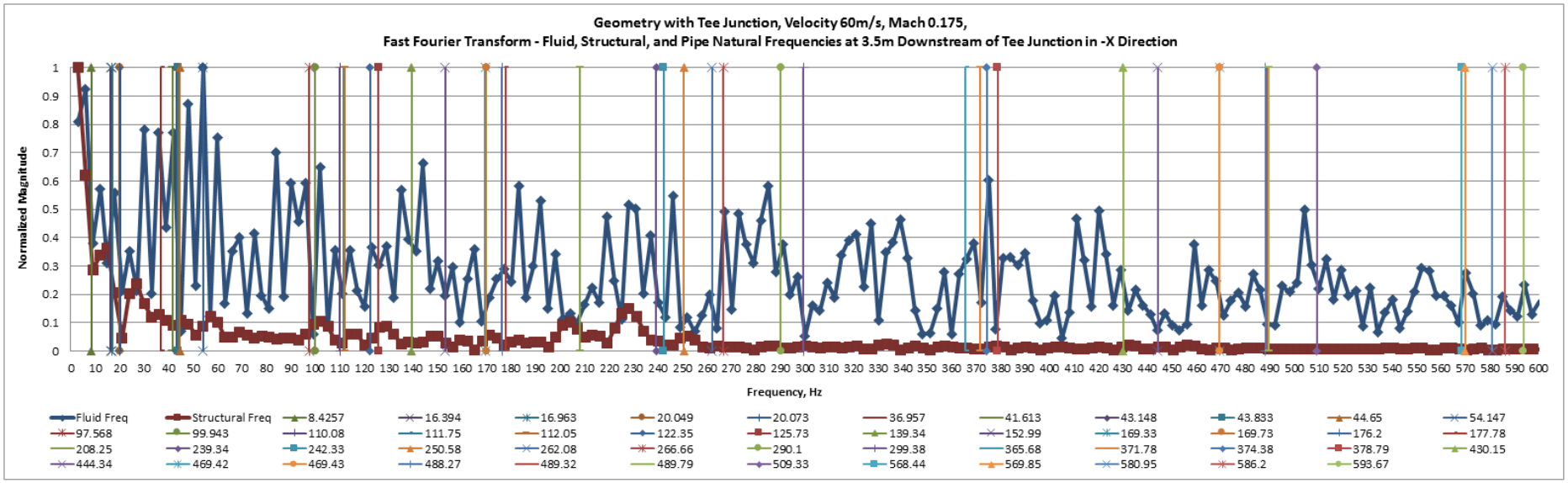
Geometry with Tee Junction, Velocity 60m/s, Mach 0.175,
Fast Fourier Transform - Fluid, Structural, and Pipe Natural Frequencies at 3.5m Downstream of Tee Junction in -X Direction
Normalized Magnitude
Frequency, Hz
Fluid Freq
Structural Freq
8.4257
16.394
16.963
20.049
20.073
36.957
41.613
43.148
43.833
44.65
54.147
97.568
99.943
110.08
111.75
112.05
122.35
125.73
139.34
152.99
169.33
169.73
176.2
177.78
208.25
239.34
242.33
250.58
262.08
266.66
290.1
299.38
365.68
371.78
374.38
378.79
430.15
444.34
469.42
469.43
488.27
489.32
489.79
509.33
568.44
569.85
580.95
586.2
593.67

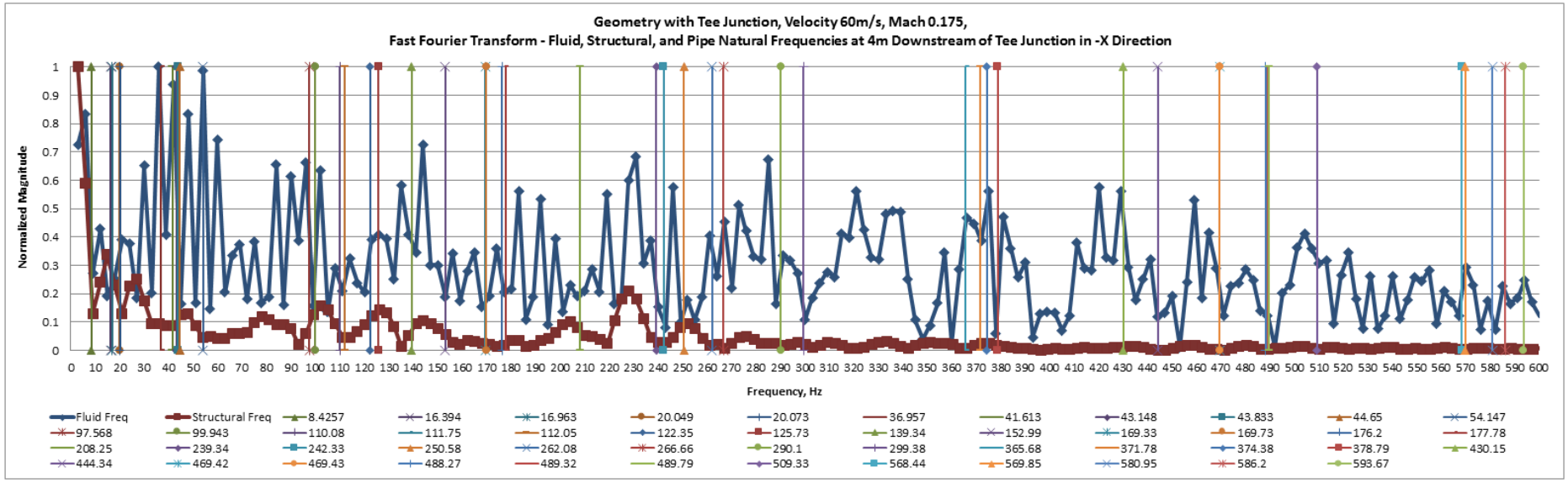
Geometry with Tee Junction, Velocity 60m/s, Mach 0.175,
Fast Fourier Transform - Fluid, Structural, and Pipe Natural Frequencies at 4m Downstream of Tee Junction in -X Direction
Normalized Magnitude
Frequency, Hz
Fluid Freq
Structural Freq
8.4257
16.394
16.963
20.049
20.073
36.957
41.613
43.148
43.833
44.65
54.147
97.568
99.943
110.08
111.75
112.05
122.35
125.73
139.34
152.99
169.33
169.73
176.2
177.78
208.25
239.34
242.33
250.58
262.08
266.66
290.1
299.38
365.68
371.78
374.38
378.79
430.15
444.34
469.42
469.43
488.27
489.32
489.79
509.33
568.44
569.85
580.95
586.2
593.67

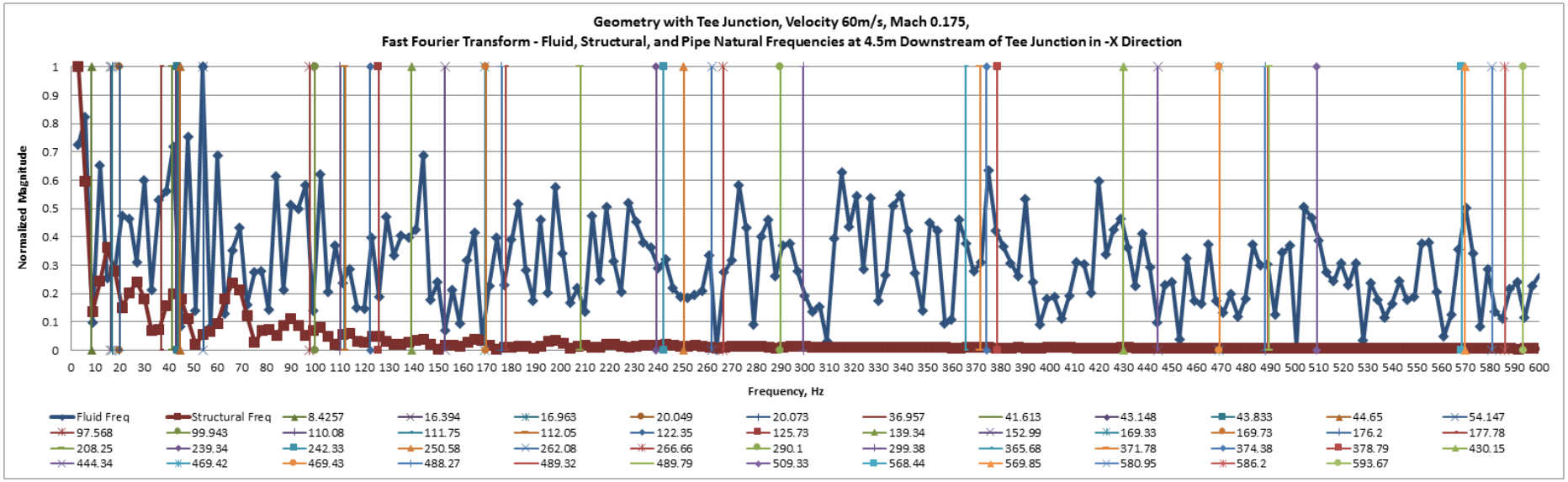
Geometry with Tee Junction, Velocity 60m/s, Mach 0.175,
Fast Fourier Transform - Fluid, Structural, and Pipe Natural Frequencies at 4.5m Downstream of Tee Junction in -X Direction
Normalized Magnitude
Frequency, Hz
Fluid Freq
Structural Freq
8.4257
16.394
16.963
20.049
20.073
36.957
41.613
43.148
43.833
44.65
54.147
97.568
99.943
110.08
111.75
112.05
122.35
125.73
139.34
152.99
169.33
169.73
176.2
177.78
208.25
239.34
242.33
250.58
262.08
266.66
290.1
299.38
365.68
371.78
374.38
378.79
430.15
444.34
469.42
469.43
488.27
489.32
489.79
509.33
568.44
569.85
580.95
586.2
593.67

Appendix J

Frequency Plots for Geometry with Tee Junction for Fluid Velocity modelled at 75m/s, Mach 0.218 at Probe Locations

Distance	Fluid Excited Frequencies Downstream of Tee Junction in +X Direction	Fluid Excited Frequencies Downstream of Tee Junction in -X Direction
0.1	3, 24, 45	3, 15, 66, 90, 150
0.3	3, 15, 102, 150, 159	3, 15, 24, 45, 75, 102, 126, 138, 159, 189
0.5	75, 129	3, 15, 45, 75, 150, 159, 189, 201
1	66, 150, 189, 249, 288	45, 150, 189, 249, 264, 288
1.5	66, 150, 189, 213, 288	3, 15, 66, 150, 189, 288
2	90, 183	3, 90
2.5	33, 90, 189, 255, 276, 306	3, 33, 90, 159, 189
3	15, 159, 189	3, 15, 189, 288, 312, 333
3.5	15, 90, 150, 159, 183, 189	3, 15, 45, 90, 129, 159, 333
4	144, 183, 264, 276	3, 15, 48, 144, 276, 333
4.5	66, 90, 99, 129, 144, 198, 243, 255, 276	15, 66, 90, 144, 198, 210

Table J.1: Fluid excited frequencies downstream of the Tee Junction for 75m/s

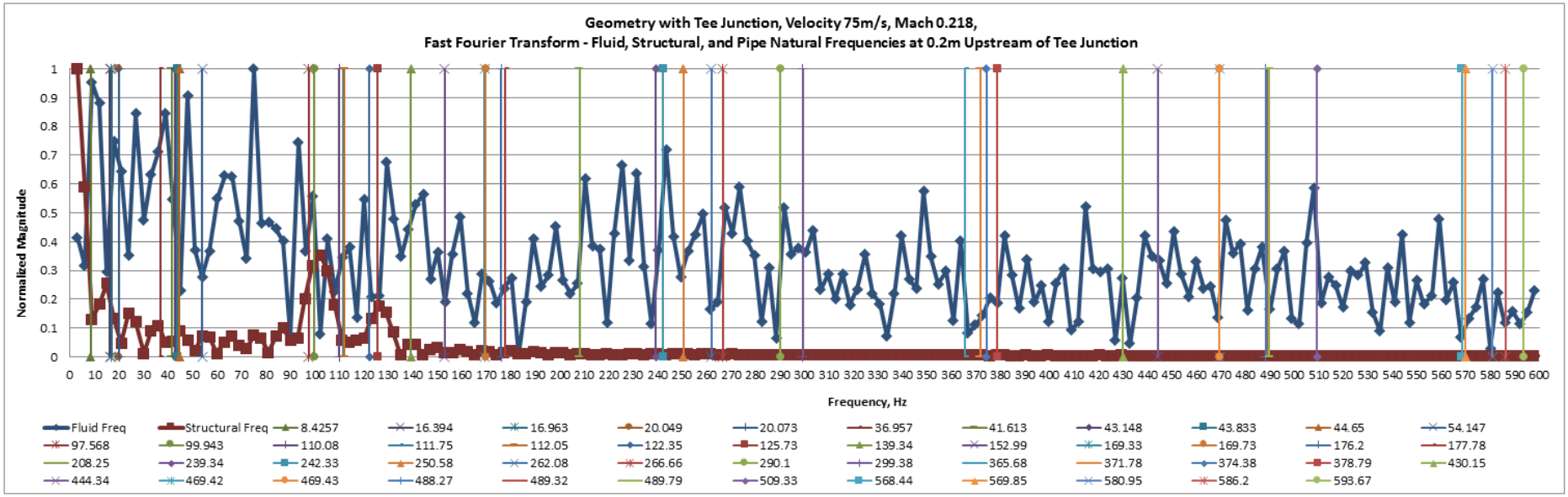
Geometry with Tee Junction, Velocity 75m/s, Mach 0.218,
Fast Fourier Transform - Fluid, Structural, and Pipe Natural Frequencies at 0.2m Upstream of Tee Junction
Normalized Magnitude
Frequency, Hz
Fluid Freq
Structural Freq
8.4257
16.394
16.963
20.049
20.073
36.957
41.613
43.148
43.833
44.65
54.147
97.568
99.943
110.08
111.75
112.05
122.35
125.73
139.34
152.99
169.33
169.73
176.2
177.78
208.25
239.34
242.33
250.58
262.08
266.66
290.1
299.38
365.68
371.78
374.38
378.79
430.15
444.34
469.42
469.43
488.27
489.32
489.79
509.33
568.44
569.85
580.95
586.2
593.67

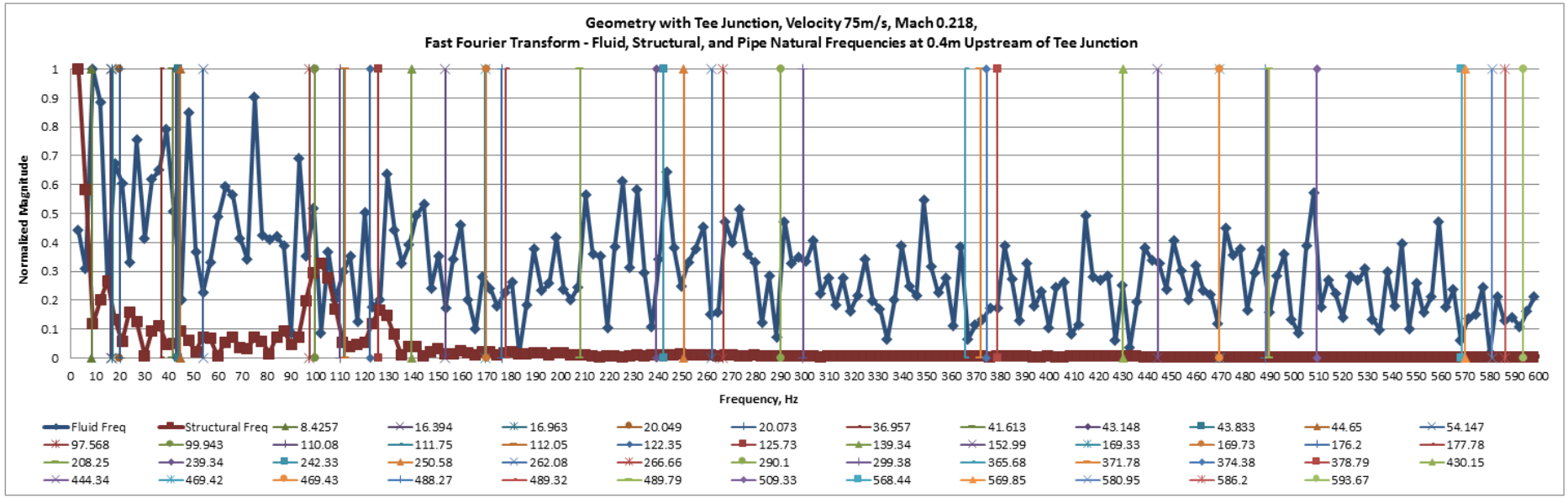
Geometry with Tee Junction, Velocity 75m/s, Mach 0.218,
Fast Fourier Transform - Fluid, Structural, and Pipe Natural Frequencies at 0.4m Upstream of Tee Junction
Normalized Magnitude
Frequency, Hz
Fluid Freq
Structural Freq
8.4257
16.394
16.963
20.049
20.073
36.957
41.613
43.148
43.833
44.65
54.147
97.568
99.943
110.08
111.75
112.05
122.35
125.73
139.34
152.99
169.33
169.73
176.2
177.78
208.25
239.34
242.33
250.58
262.08
266.66
290.1
299.38
365.68
371.78
374.38
378.79
430.15
444.34
469.42
469.43
488.27
489.32
489.79
509.33
568.44
569.85
580.95
586.2
593.67

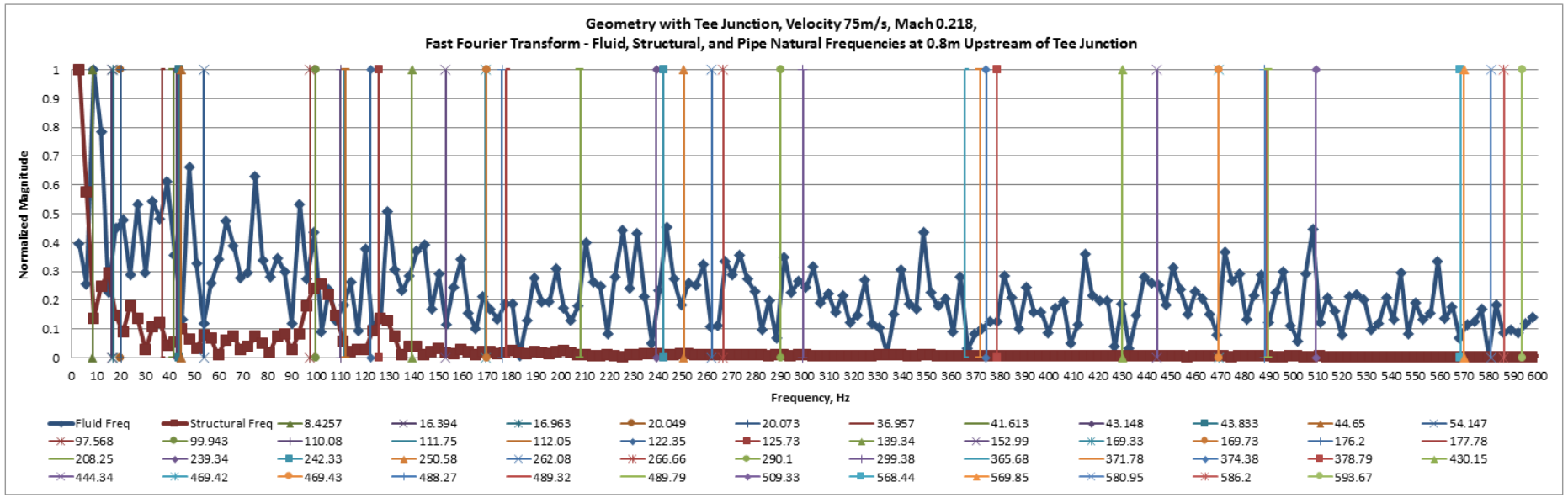
Geometry with Tee Junction, Velocity 75m/s, Mach 0.218,
Fast Fourier Transform - Fluid, Structural, and Pipe Natural Frequencies at 0.8m Upstream of Tee Junction
Normalized Magnitude
Frequency, Hz
Fluid Freq
Structural Freq
8.4257
16.394
16.963
20.049
20.073
36.957
41.613
43.148
43.833
44.65
54.147
97.568
99.943
110.08
111.75
112.05
122.35
125.73
139.34
152.99
169.33
169.73
176.2
177.78
208.25
239.34
242.33
250.58
262.08
266.66
290.1
299.38
365.68
371.78
374.38
378.79
430.15
444.34
469.42
469.43
488.27
489.32
489.79
509.33
568.44
569.85
580.95
586.2
593.67

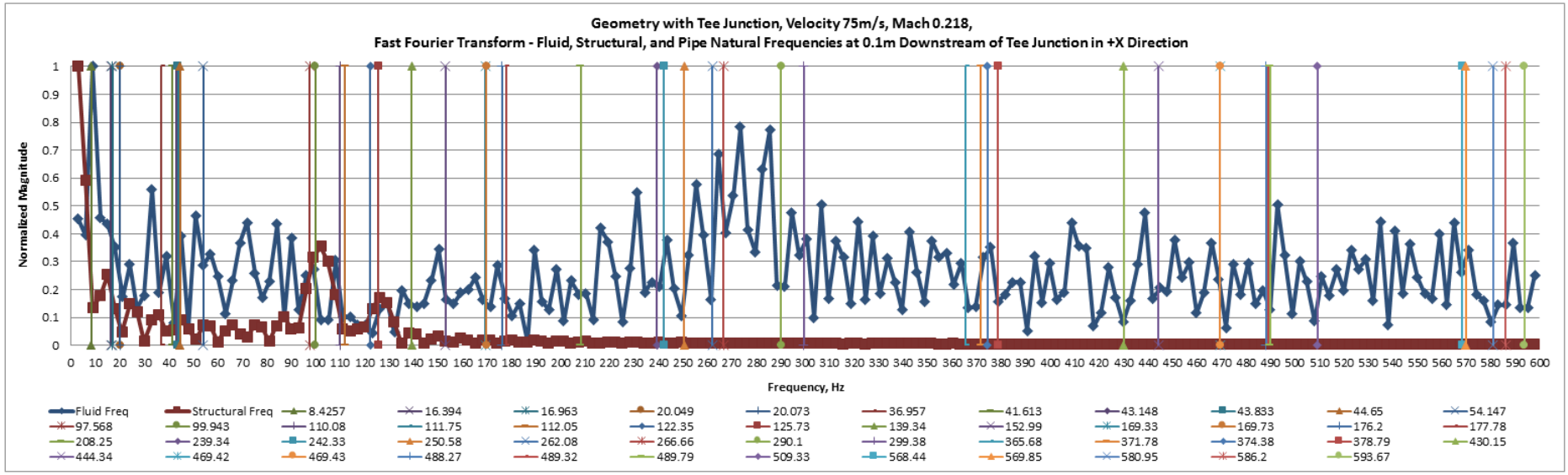
Geometry with Tee Junction, Velocity 75m/s, Mach 0.218,
Fast Fourier Transform - Fluid, Structural, and Pipe Natural Frequencies at 0.1m Downstream of Tee Junction in +X Direction
Normalized Magnitude
Frequency, Hz
Fluid Freq
Structural Freq
8.4257
16.394
16.963
20.049
20.073
36.957
41.613
43.148
43.833
44.65
54.147
97.568
99.943
110.08
111.75
112.05
122.35
125.73
139.34
152.99
169.33
169.73
176.2
177.78
208.25
239.34
242.33
250.58
262.08
266.66
290.1
299.38
365.68
371.78
374.38
378.79
430.15
444.34
469.42
469.43
488.27
489.32
489.79
509.33
568.44
569.85
580.95
586.2
593.67

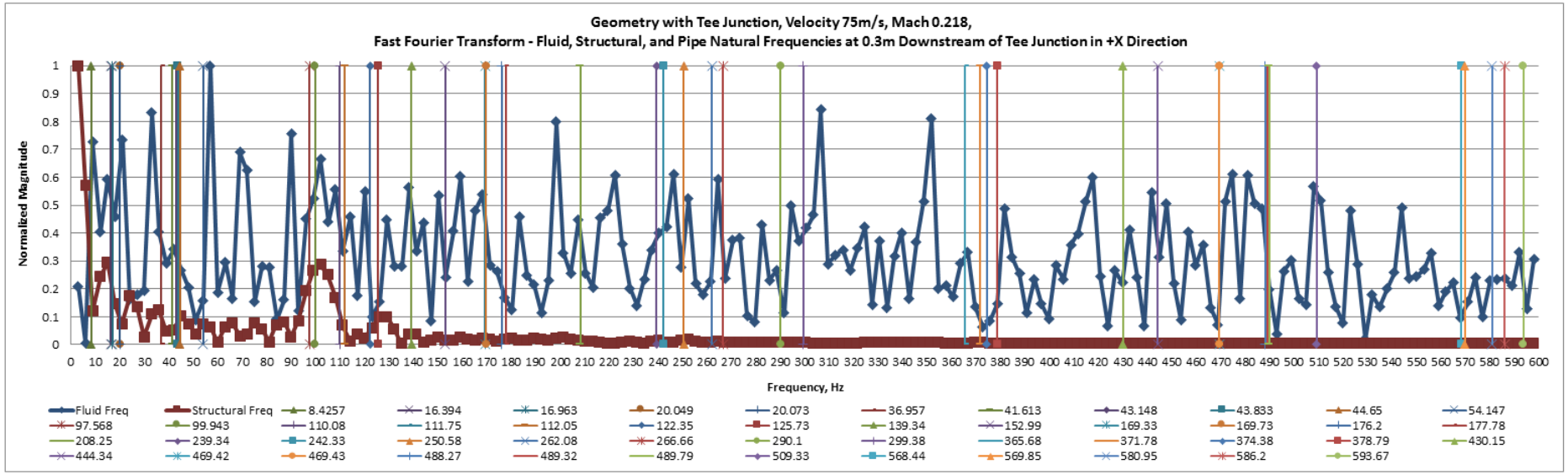
Geometry with Tee Junction, Velocity 75m/s, Mach 0.218,
Fast Fourier Transform - Fluid, Structural, and Pipe Natural Frequencies at 0.3m Downstream of Tee Junction in +X Direction
Normalized Magnitude
Frequency, Hz
Fluid Freq
Structural Freq
8.4257
16.394
16.963
20.049
20.073
36.957
41.613
43.148
43.833
44.65
54.147
97.568
99.943
110.08
111.75
112.05
122.35
125.73
139.34
152.99
169.33
169.73
176.2
177.78
208.25
239.34
242.33
250.58
262.08
266.66
290.1
299.38
365.68
371.78
374.38
378.79
430.15
444.34
469.42
469.43
488.27
489.32
489.79
509.33
568.44
569.85
580.95
586.2
593.67

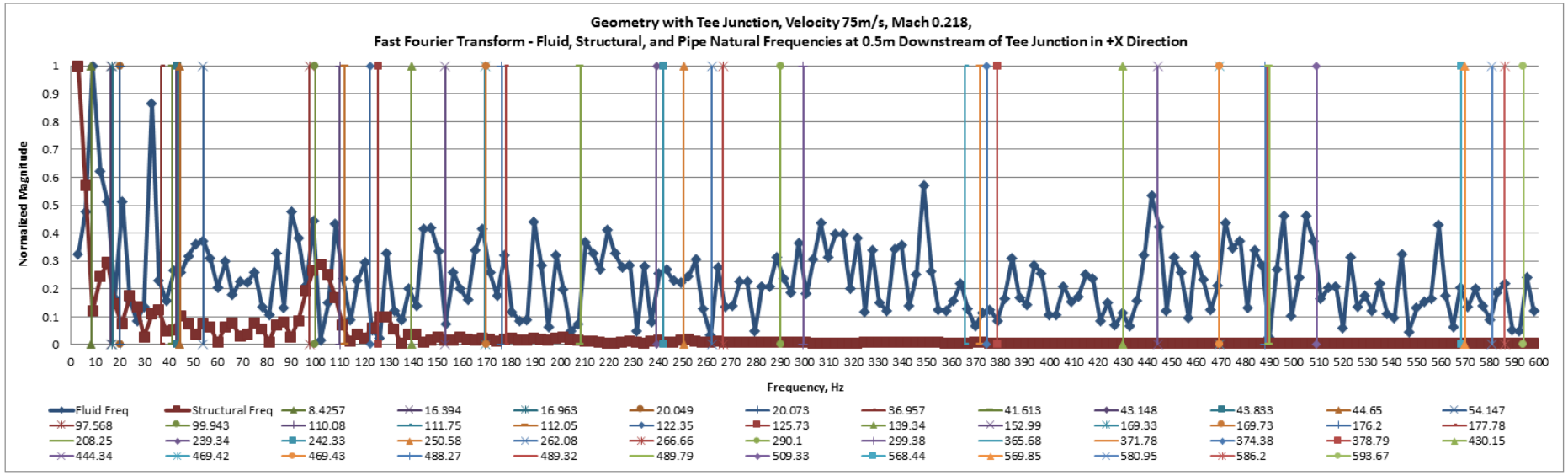
Geometry with Tee Junction, Velocity 75m/s, Mach 0.218,
Fast Fourier Transform - Fluid, Structural, and Pipe Natural Frequencies at 0.5m Downstream of Tee Junction in +X Direction
Normalized Magnitude
Frequency, Hz
Fluid Freq
Structural Freq
8.4257
16.394
16.963
20.049
20.073
36.957
41.613
43.148
43.833
44.65
54.147
97.568
99.943
110.08
111.75
112.05
122.35
125.73
139.34
152.99
169.33
169.73
176.2
177.78
208.25
239.34
242.33
250.58
262.08
266.66
290.1
299.38
365.68
371.78
374.38
378.79
430.15
444.34
469.42
469.43
488.27
489.32
489.79
509.33
568.44
569.85
580.95
586.2
593.67

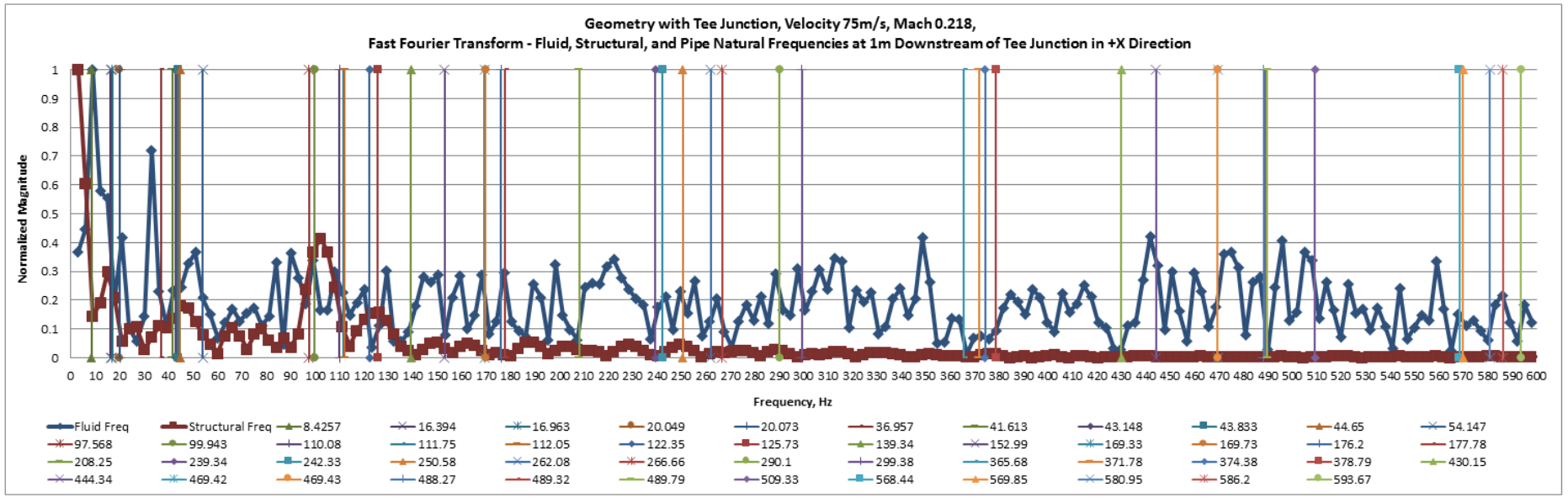
Geometry with Tee Junction, Velocity 75m/s, Mach 0.218,
Fast Fourier Transform - Fluid, Structural, and Pipe Natural Frequencies at 1m Downstream of Tee Junction in +X Direction
Normalized Magnitude
Frequency, Hz
Fluid Freq
Structural Freq
8.4257
16.394
16.963
20.049
20.073
36.957
41.613
43.148
43.833
44.65
54.147
97.568
99.943
110.08
111.75
112.05
122.35
125.73
139.34
152.99
169.33
169.73
176.2
177.78
208.25
239.34
242.33
250.58
262.08
266.66
290.1
299.38
365.68
371.78
374.38
378.79
430.15
444.34
469.42
469.43
488.27
489.32
489.79
509.33
568.44
569.85
580.95
586.2
593.67

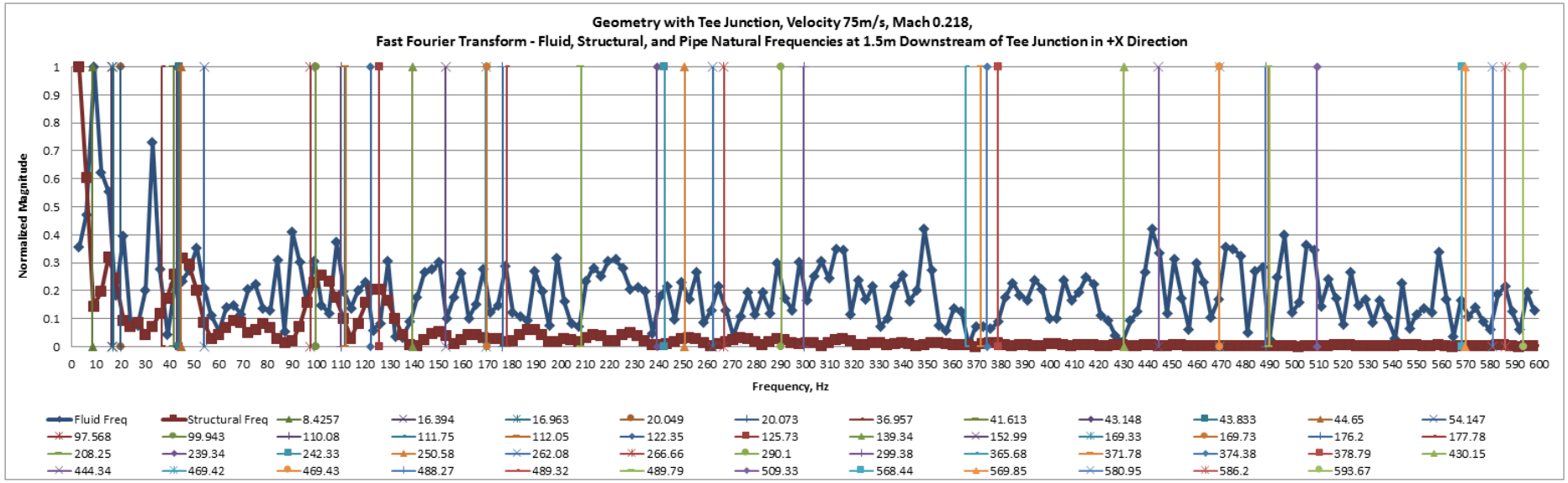
Geometry with Tee Junction, Velocity 75m/s, Mach 0.218,
Fast Fourier Transform - Fluid, Structural, and Pipe Natural Frequencies at 1.5m Downstream of Tee Junction in +X Direction
Normalized Magnitude
Frequency, Hz
Fluid Freq
Structural Freq
8.4257
16.394
16.963
20.049
20.073
36.957
41.613
43.148
43.833
44.65
54.147
97.568
99.943
110.08
111.75
112.05
122.35
125.73
139.34
152.99
169.33
169.73
176.2
177.78
208.25
239.34
242.33
250.58
262.08
266.66
290.1
299.38
365.68
371.78
374.38
378.79
430.15
444.34
469.42
469.43
488.27
489.32
489.79
509.33
568.44
569.85
580.95
586.2
593.67

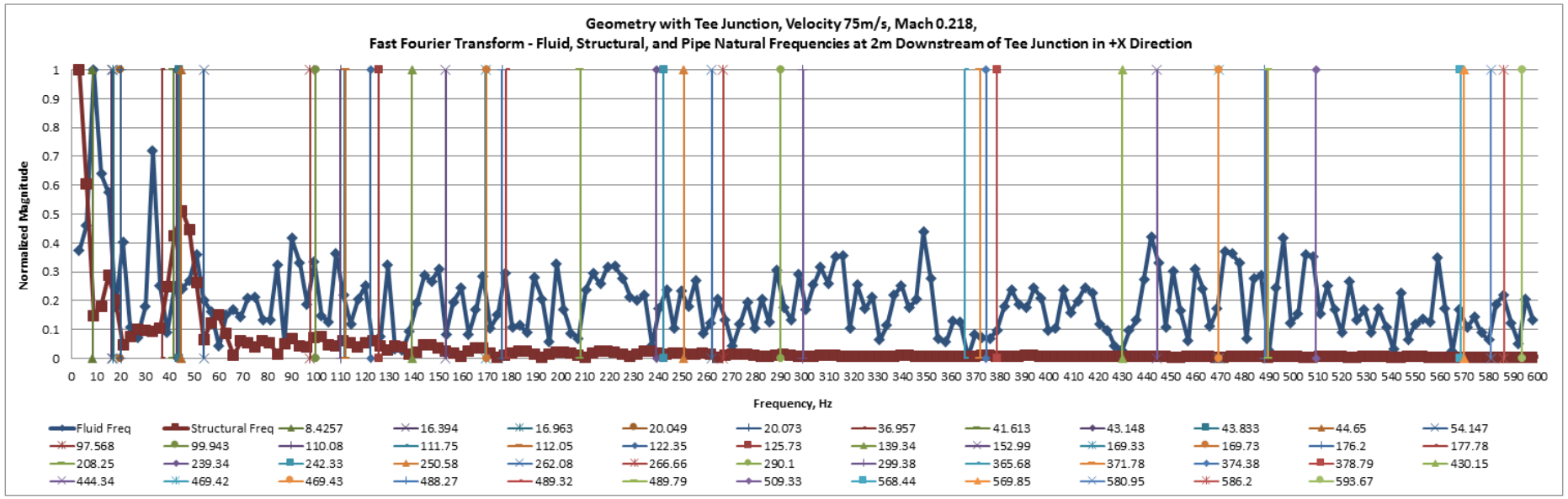
Geometry with Tee Junction, Velocity 75m/s, Mach 0.218,
Fast Fourier Transform - Fluid, Structural, and Pipe Natural Frequencies at 2m Downstream of Tee Junction in +X Direction
Normalized Magnitude
Frequency, Hz
Fluid Freq
Structural Freq
8.4257
16.394
16.963
20.049
20.073
36.957
41.613
43.148
43.833
44.65
54.147
97.568
99.943
110.08
111.75
112.05
122.35
125.73
139.34
152.99
169.33
169.73
176.2
177.78
208.25
239.34
242.33
250.58
262.08
266.66
290.1
299.38
365.68
371.78
374.38
378.79
430.15
444.34
469.42
469.43
488.27
489.32
489.79
509.33
568.44
569.85
580.95
586.2
593.67

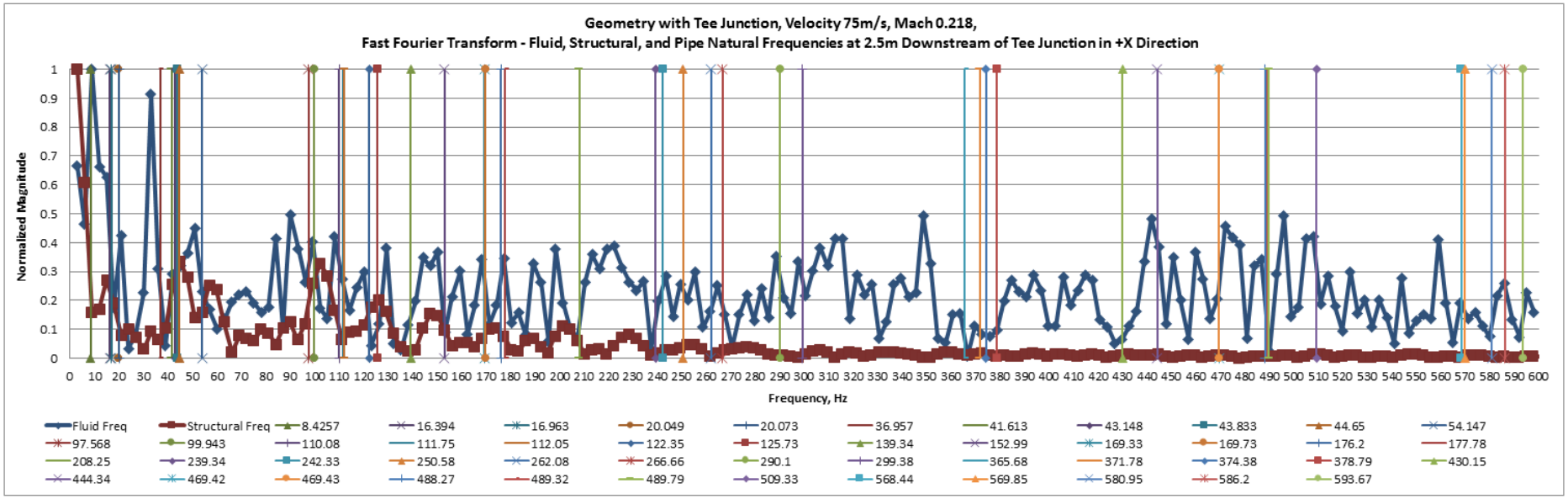
Geometry with Tee Junction, Velocity 75m/s, Mach 0.218,
Fast Fourier Transform - Fluid, Structural, and Pipe Natural Frequencies at 2.5m Downstream of Tee Junction in +X Direction
Normalized Magnitude
Frequency, Hz
Fluid Freq
Structural Freq
8.4257
16.394
16.963
20.049
20.073
36.957
41.613
43.148
43.833
44.65
54.147
97.568
99.943
110.08
111.75
112.05
122.35
125.73
139.34
152.99
169.33
169.73
176.2
177.78
208.25
239.34
242.33
250.58
262.08
266.66
290.1
299.38
365.68
371.78
374.38
378.79
430.15
444.34
469.42
469.43
488.27
489.32
489.79
509.33
568.44
569.85
580.95
586.2
593.67

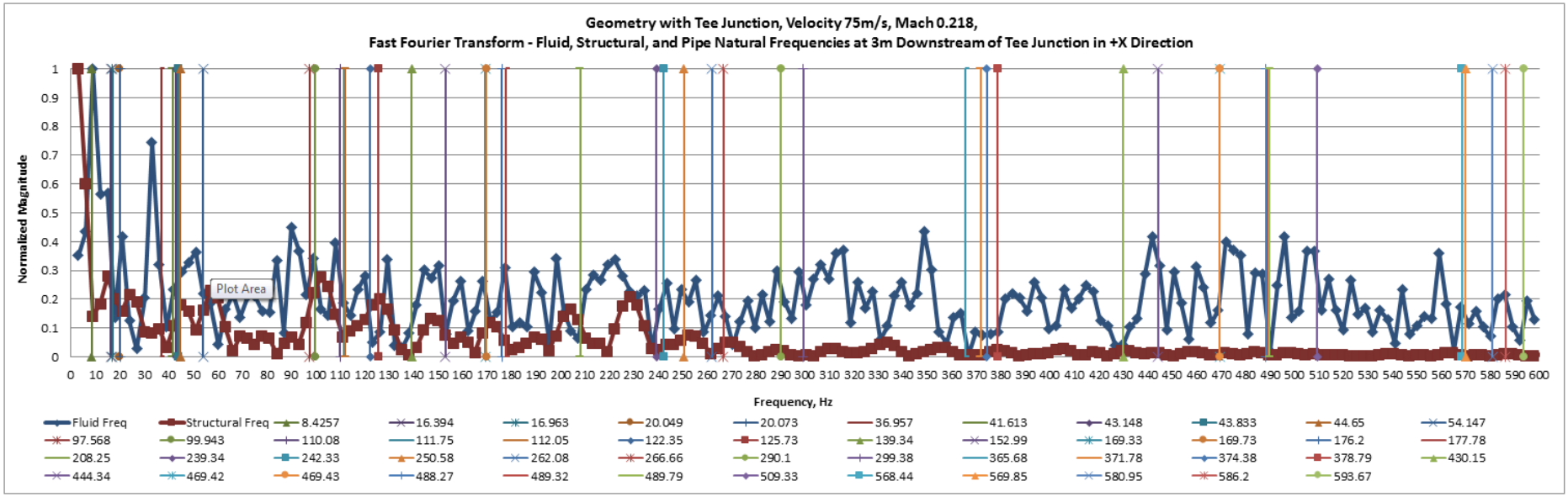
Geometry with Tee Junction, Velocity 75m/s, Mach 0.218,
Fast Fourier Transform - Fluid, Structural, and Pipe Natural Frequencies at 3m Downstream of Tee Junction in +X Direction
Normalized Magnitude
Plot Area
Frequency, Hz
Fluid Freq
Structural Freq
8.4257
16.394
16.963
20.049
20.073
36.957
41.613
43.148
43.833
44.65
54.147
97.568
99.943
110.08
111.75
112.05
122.35
125.73
139.34
152.99
169.33
169.73
176.2
177.78
208.25
239.34
242.33
250.58
262.08
266.66
290.1
299.38
365.68
371.78
374.38
378.79
430.15
444.34
469.42
469.43
488.27
489.32
489.79
509.33
568.44
569.85
580.95
586.2
593.67

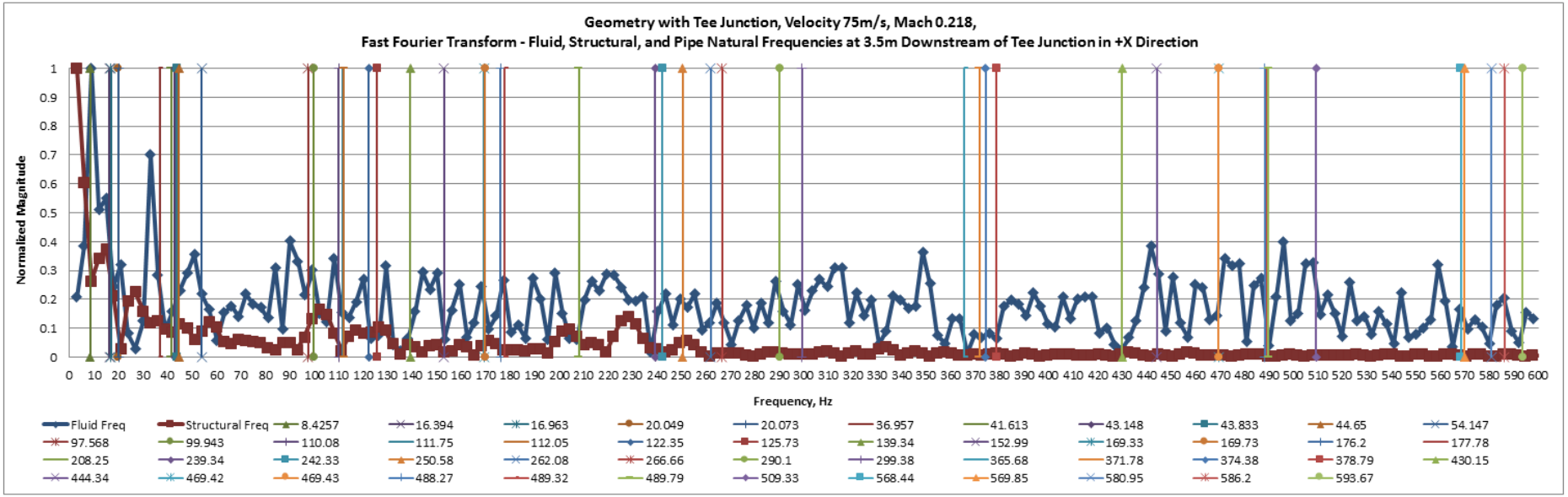
Geometry with Tee Junction, Velocity 75m/s, Mach 0.218,
Fast Fourier Transform - Fluid, Structural, and Pipe Natural Frequencies at 3.5m Downstream of Tee Junction in +X Direction
Normalized Magnitude
Frequency, Hz
Fluid Freq
Structural Freq
8.4257
16.394
16.963
20.049
20.073
36.957
41.613
43.148
43.833
44.65
54.147
97.568
99.943
110.08
111.75
112.05
122.35
125.73
139.34
152.99
169.33
169.73
176.2
177.78
208.25
239.34
242.33
250.58
262.08
266.66
290.1
299.38
365.68
371.78
374.38
378.79
430.15
444.34
469.42
469.43
488.27
489.32
489.79
509.33
568.44
569.85
580.95
586.2
593.67

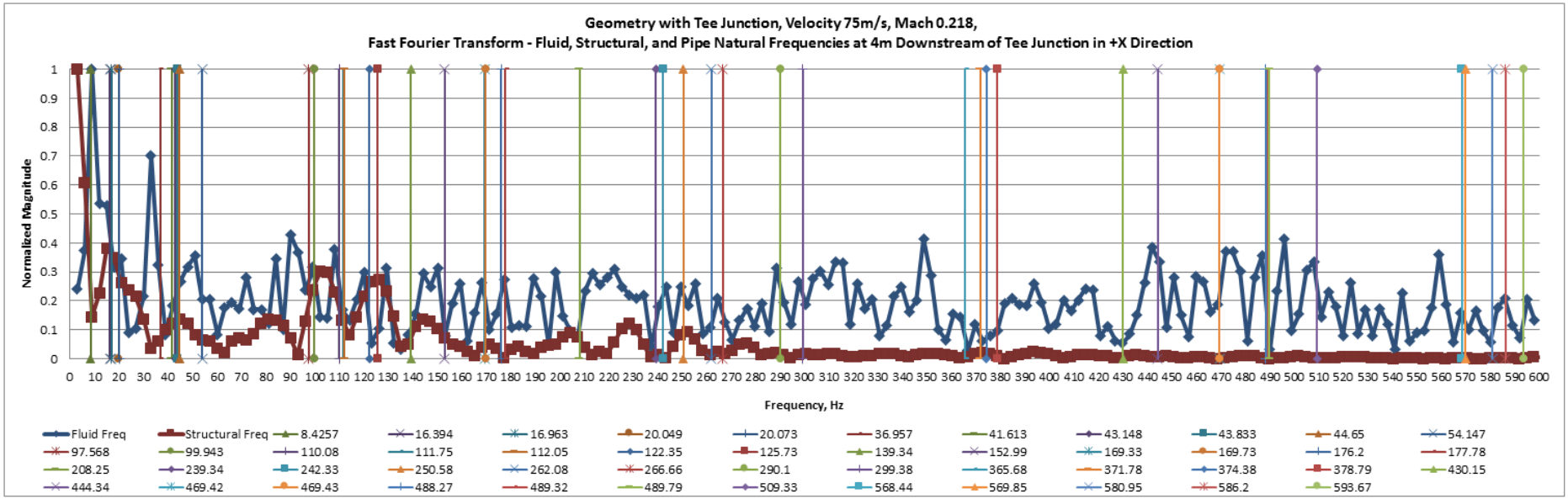
Geometry with Tee Junction, Velocity 75m/s, Mach 0.218,
Fast Fourier Transform - Fluid, Structural, and Pipe Natural Frequencies at 4m Downstream of Tee Junction in +X Direction
Normalized Magnitude
Frequency, Hz
Fluid Freq
Structural Freq
8.4257
16.394
16.963
20.049
20.073
36.957
41.613
43.148
43.833
44.65
54.147
97.568
99.943
110.08
111.75
112.05
122.35
125.73
139.34
152.99
169.33
169.73
176.2
177.78
208.25
239.34
242.33
250.58
262.08
266.66
290.1
299.38
365.68
371.78
374.38
378.79
430.15
444.34
469.42
469.43
488.27
489.32
489.79
509.33
568.44
569.85
580.95
586.2
593.67

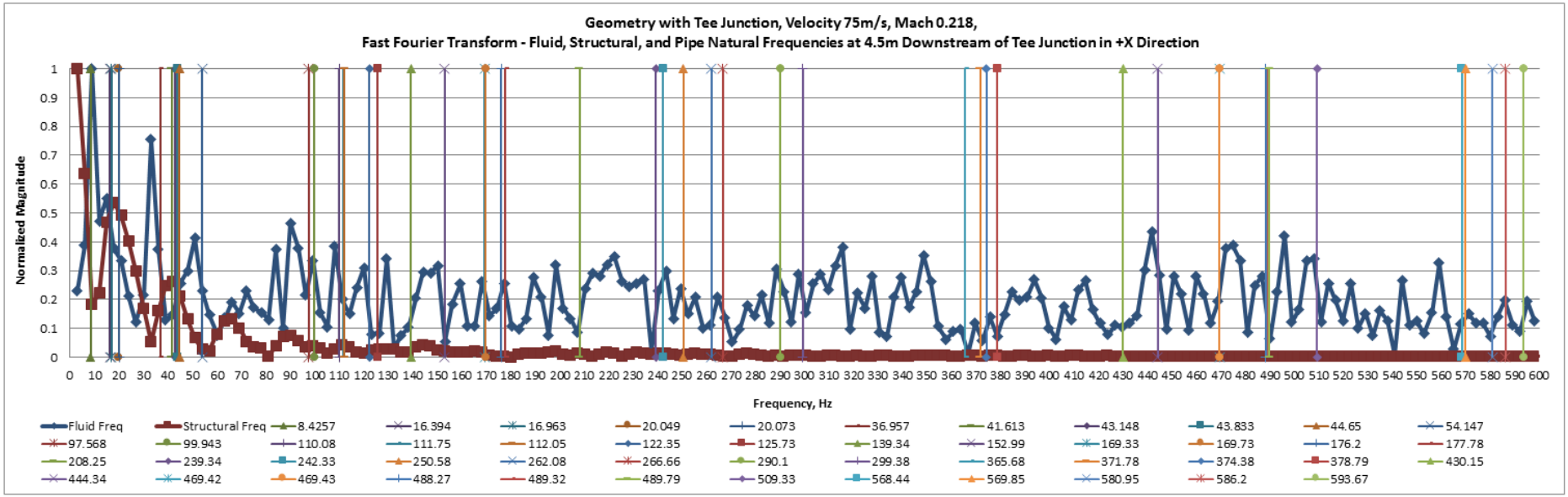
Geometry with Tee Junction, Velocity 75m/s, Mach 0.218,
Fast Fourier Transform - Fluid, Structural, and Pipe Natural Frequencies at 4.5m Downstream of Tee Junction in +X Direction
Normalized Magnitude
Frequency, Hz
Fluid Freq
Structural Freq
8.4257
16.394
16.963
20.049
20.073
36.957
41.613
43.148
43.833
44.65
54.147
97.568
99.943
110.08
111.75
112.05
122.35
125.73
139.34
152.99
169.33
169.73
176.2
177.78
208.25
239.34
242.33
250.58
262.08
266.66
290.1
299.38
365.68
371.78
374.38
378.79
430.15
444.34
469.42
469.43
488.27
489.32
489.79
509.33
568.44
569.85
580.95
586.2
593.67

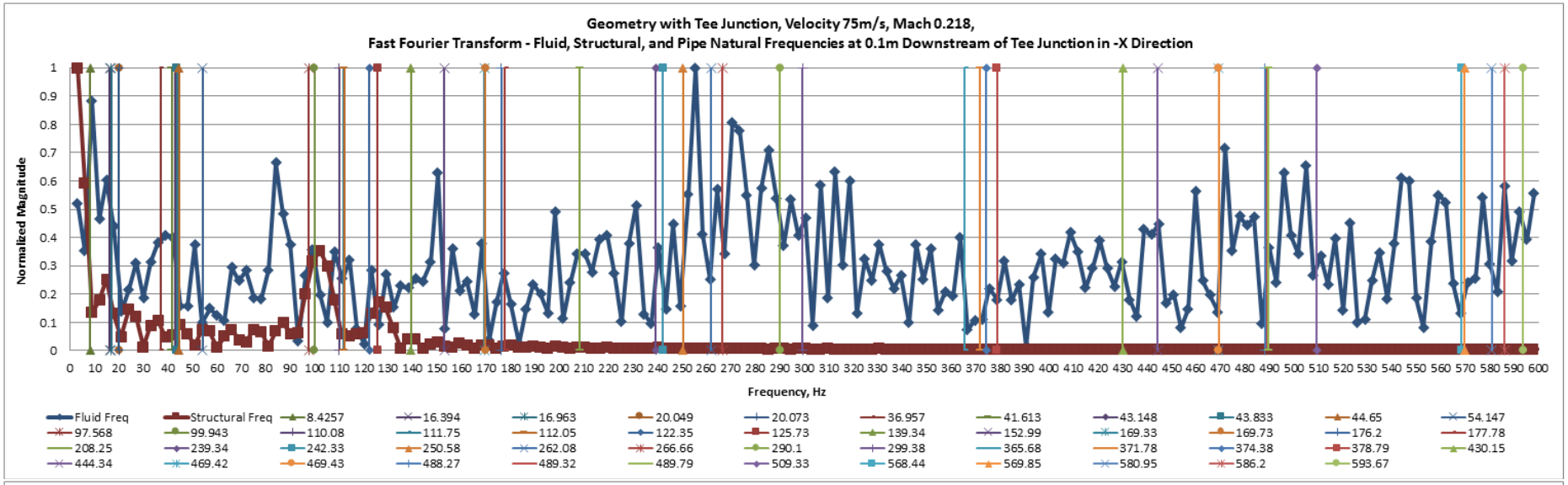
Geometry with Tee Junction, Velocity 75m/s, Mach 0.218,
Fast Fourier Transform - Fluid, Structural, and Pipe Natural Frequencies at 0.1m Downstream of Tee Junction in -X Direction
Normalized Magnitude
Frequency, Hz
Fluid Freq
Structural Freq
8.4257
16.394
16.963
20.049
20.073
36.957
41.613
43.148
43.833
44.65
54.147
97.568
99.943
110.08
111.75
112.05
122.35
125.73
139.34
152.99
169.33
169.73
176.2
177.78
208.25
239.34
242.33
250.58
262.08
266.66
290.1
299.38
365.68
371.78
374.38
378.79
430.15
444.34
469.42
469.43
488.27
489.32
489.79
509.33
568.44
569.85
580.95
586.2
593.67

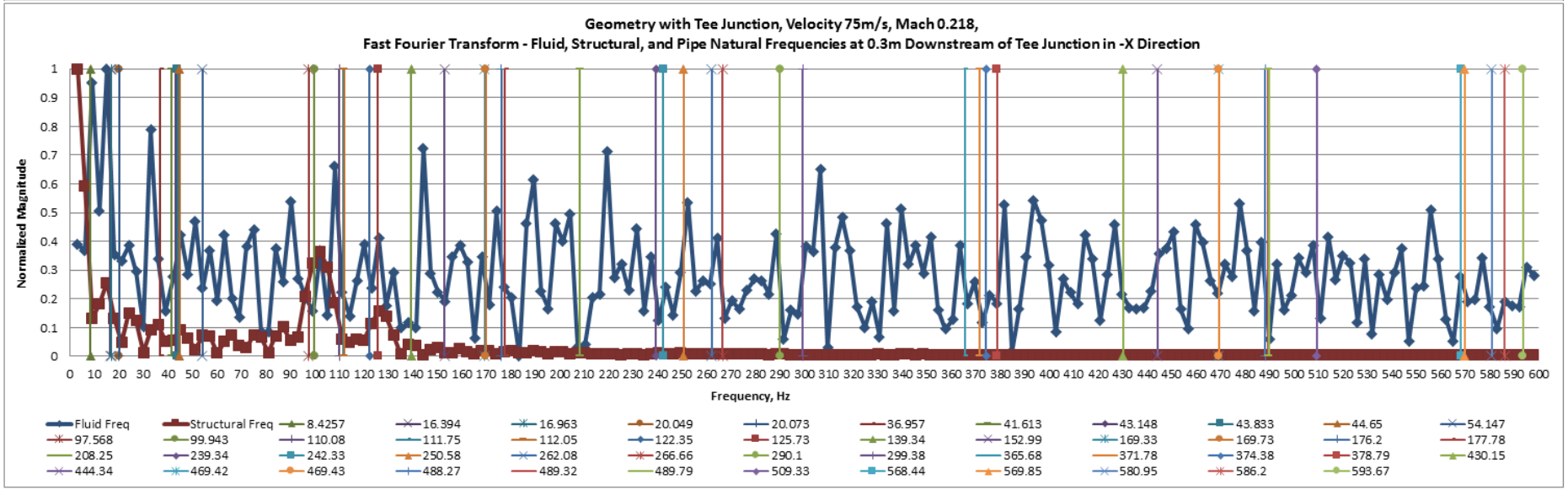
Geometry with Tee Junction, Velocity 75m/s, Mach 0.218,
Fast Fourier Transform - Fluid, Structural, and Pipe Natural Frequencies at 0.3m Downstream of Tee Junction in -X Direction
Normalized Magnitude
Frequency, Hz
Fluid Freq
Structural Freq
8.4257
16.394
16.963
20.049
20.073
36.957
41.613
43.148
43.833
44.65
54.147
97.568
99.943
110.08
111.75
112.05
122.35
125.73
139.34
152.99
169.33
169.73
176.2
177.78
208.25
239.34
242.33
250.58
262.08
266.66
290.1
299.38
365.68
371.78
374.38
378.79
430.15
444.34
469.42
469.43
488.27
489.32
489.79
509.33
568.44
569.85
580.95
586.2
593.67

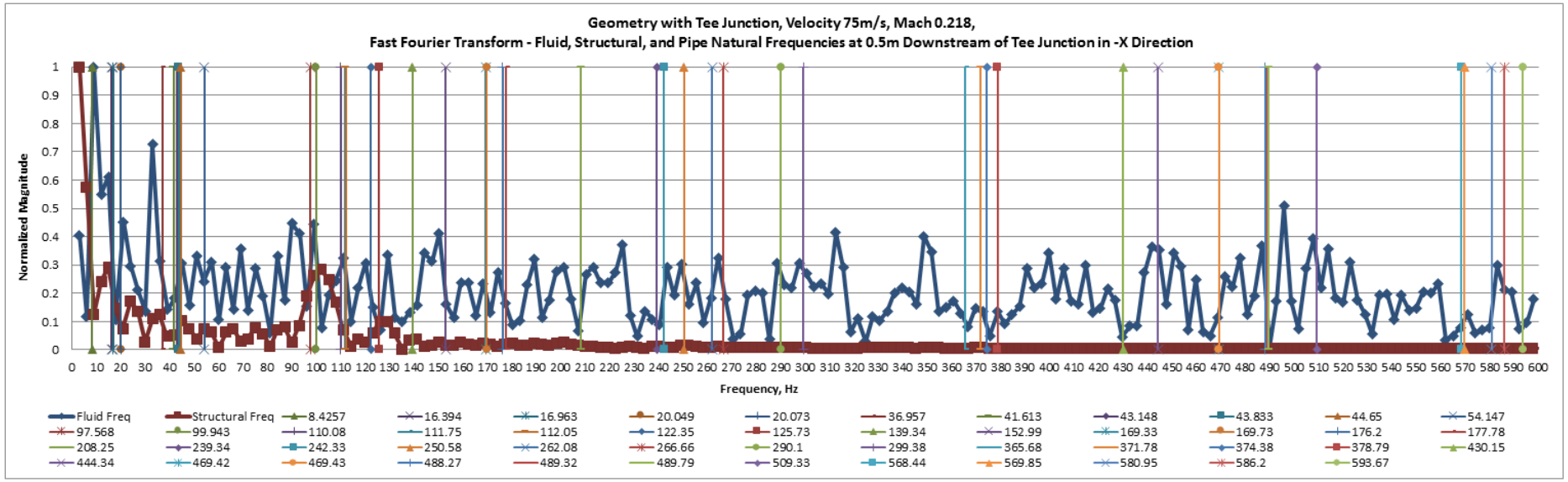
Geometry with Tee Junction, Velocity 75m/s, Mach 0.218,
Fast Fourier Transform - Fluid, Structural, and Pipe Natural Frequencies at 0.5m Downstream of Tee Junction in -X Direction
Normalized Magnitude
Frequency, Hz
Fluid Freq
Structural Freq
8.4257
16.394
16.963
20.049
20.073
36.957
41.613
43.148
43.833
44.65
54.147
97.568
99.943
110.08
111.75
112.05
122.35
125.73
139.34
152.99
169.33
169.73
176.2
177.78
208.25
239.34
242.33
250.58
262.08
266.66
290.1
299.38
365.68
371.78
374.38
378.79
430.15
444.34
469.42
469.43
488.27
489.32
489.79
509.33
568.44
569.85
580.95
586.2
593.67

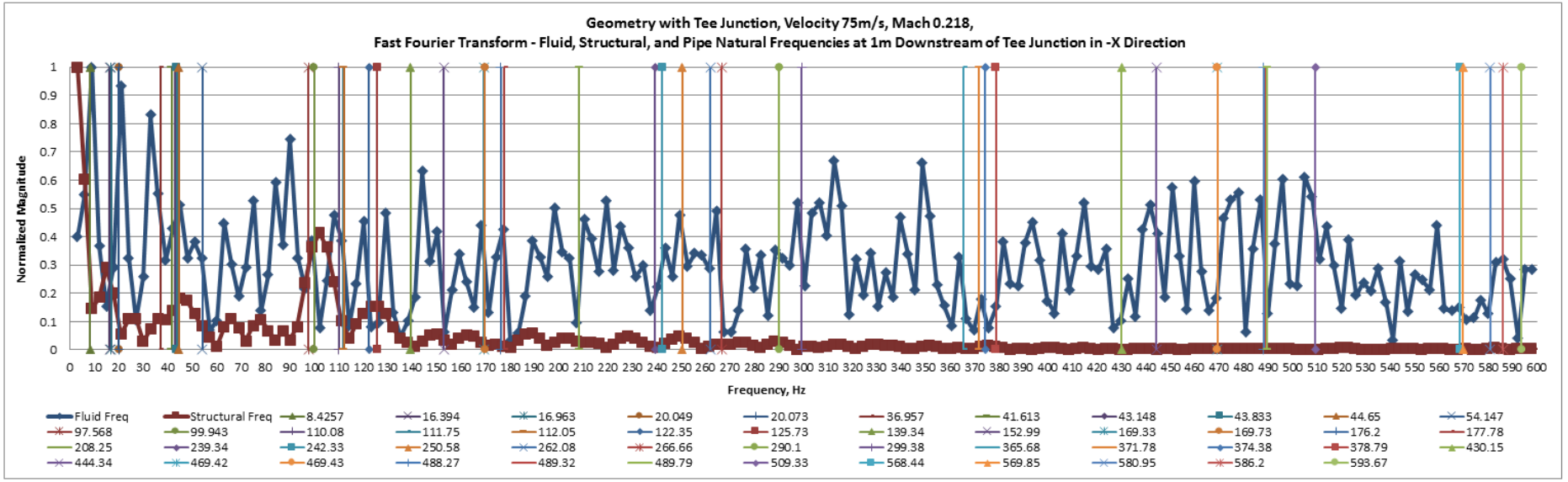
Geometry with Tee Junction, Velocity 75m/s, Mach 0.218,
Fast Fourier Transform - Fluid, Structural, and Pipe Natural Frequencies at 1m Downstream of Tee Junction in -X Direction
Normalized Magnitude
Frequency, Hz
Fluid Freq
Structural Freq
8.4257
16.394
16.963
20.049
20.073
36.957
41.613
43.148
43.833
44.65
54.147
97.568
99.943
110.08
111.75
112.05
122.35
125.73
139.34
152.99
169.33
169.73
176.2
177.78
208.25
239.34
242.33
250.58
262.08
266.66
290.1
299.38
365.68
371.78
374.38
378.79
430.15
444.34
469.42
469.43
488.27
489.32
489.79
509.33
568.44
569.85
580.95
586.2
593.67

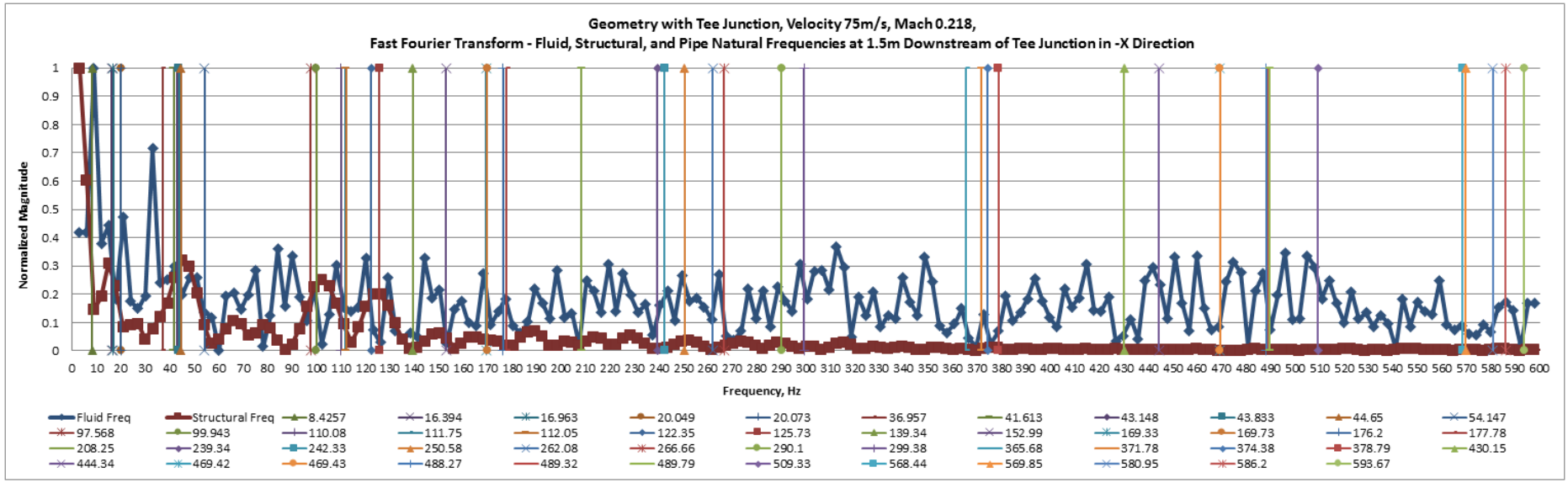
Geometry with Tee Junction, Velocity 75m/s, Mach 0.218,
Fast Fourier Transform - Fluid, Structural, and Pipe Natural Frequencies at 1.5m Downstream of Tee Junction in -X Direction
Normalized Magnitude
Frequency, Hz
Fluid Freq
Structural Freq
8.4257
16.394
16.963
20.049
20.073
36.957
41.613
43.148
43.833
44.65
54.147
97.568
99.943
110.08
111.75
112.05
122.35
125.73
139.34
152.99
169.33
169.73
176.2
177.78
208.25
239.34
242.33
250.58
262.08
266.66
290.1
299.38
365.68
371.78
374.38
378.79
430.15
444.34
469.42
469.43
488.27
489.32
489.79
509.33
568.44
569.85
580.95
586.2
593.67

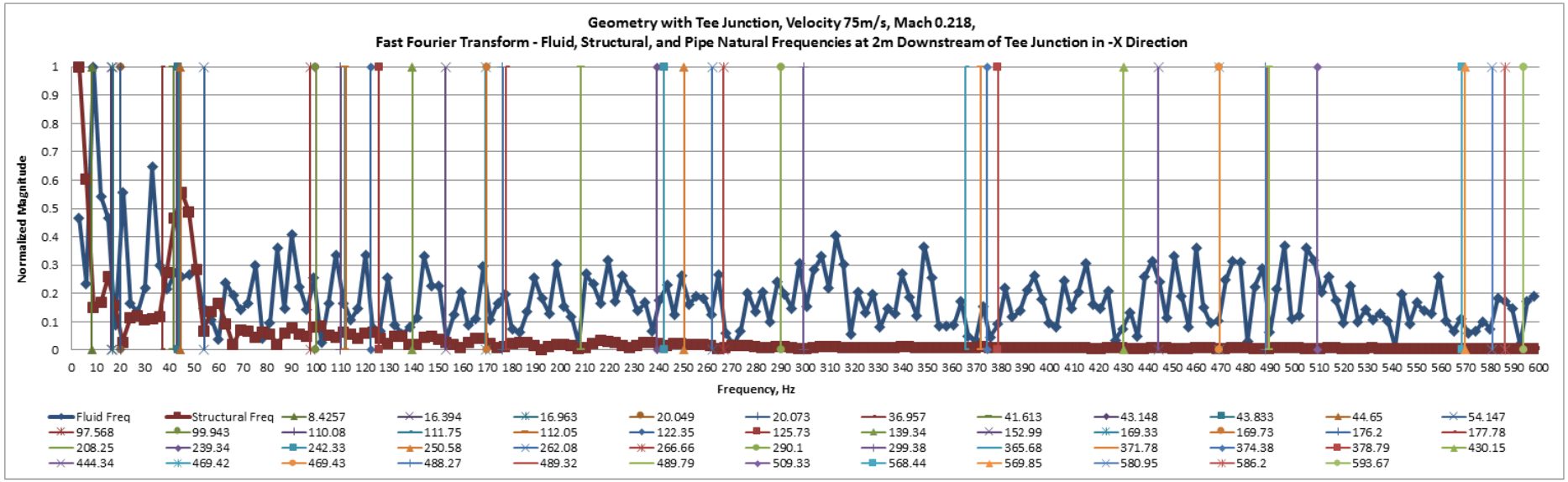
Geometry with Tee Junction, Velocity 75m/s, Mach 0.218,
Fast Fourier Transform - Fluid, Structural, and Pipe Natural Frequencies at 2m Downstream of Tee Junction in -X Direction
Normalized Magnitude
Frequency, Hz
Fluid Freq
Structural Freq
8.4257
16.394
16.963
20.049
20.073
36.957
41.613
43.148
43.833
44.65
54.147
97.568
99.943
110.08
111.75
112.05
122.35
125.73
139.34
152.99
169.33
169.73
176.2
177.78
208.25
239.34
242.33
250.58
262.08
266.66
290.1
299.38
365.68
371.78
374.38
378.79
430.15
444.34
469.42
469.43
488.27
489.32
489.79
509.33
568.44
569.85
580.95
586.2
593.67

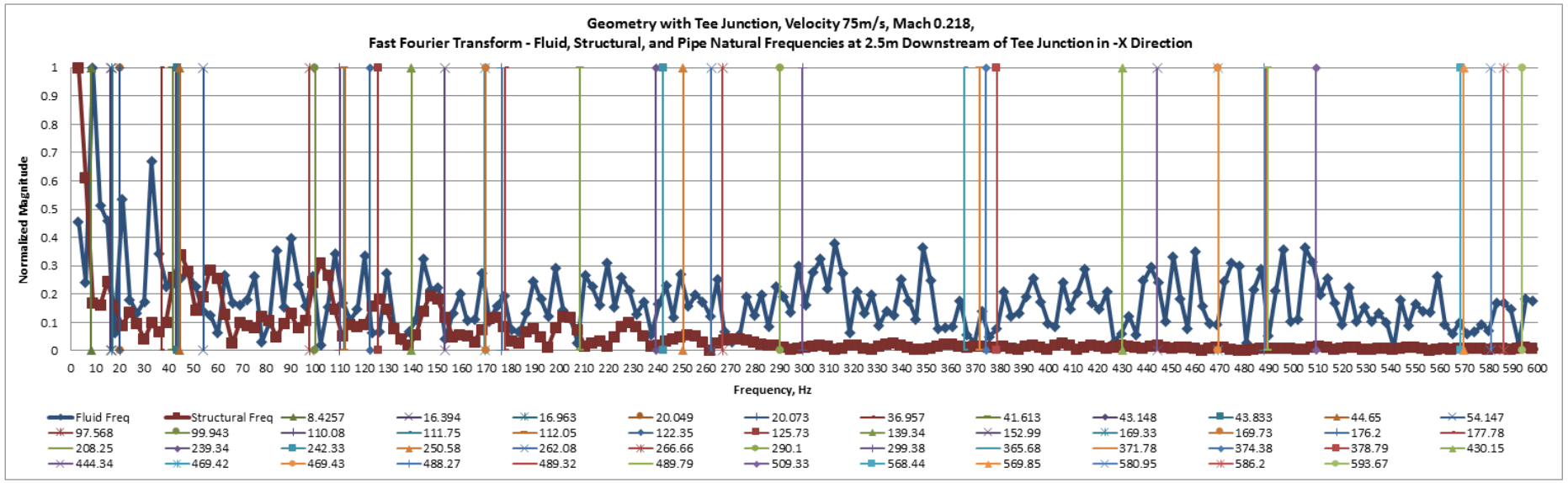
Geometry with Tee Junction, Velocity 75m/s, Mach 0.218,
Fast Fourier Transform - Fluid, Structural, and Pipe Natural Frequencies at 2.5m Downstream of Tee Junction in -X Direction
Normalized Magnitude
Frequency, Hz
Fluid Freq
Structural Freq
8.4257
16.394
16.963
20.049
20.073
36.957
41.613
43.148
43.833
44.65
54.147
97.568
99.943
110.08
111.75
112.05
122.35
125.73
139.34
152.99
169.33
169.73
176.2
177.78
208.25
239.34
242.33
250.58
262.08
266.66
290.1
299.38
365.68
371.78
374.38
378.79
430.15
444.34
469.42
469.43
488.27
489.32
489.79
509.33
568.44
569.85
580.95
586.2
593.67

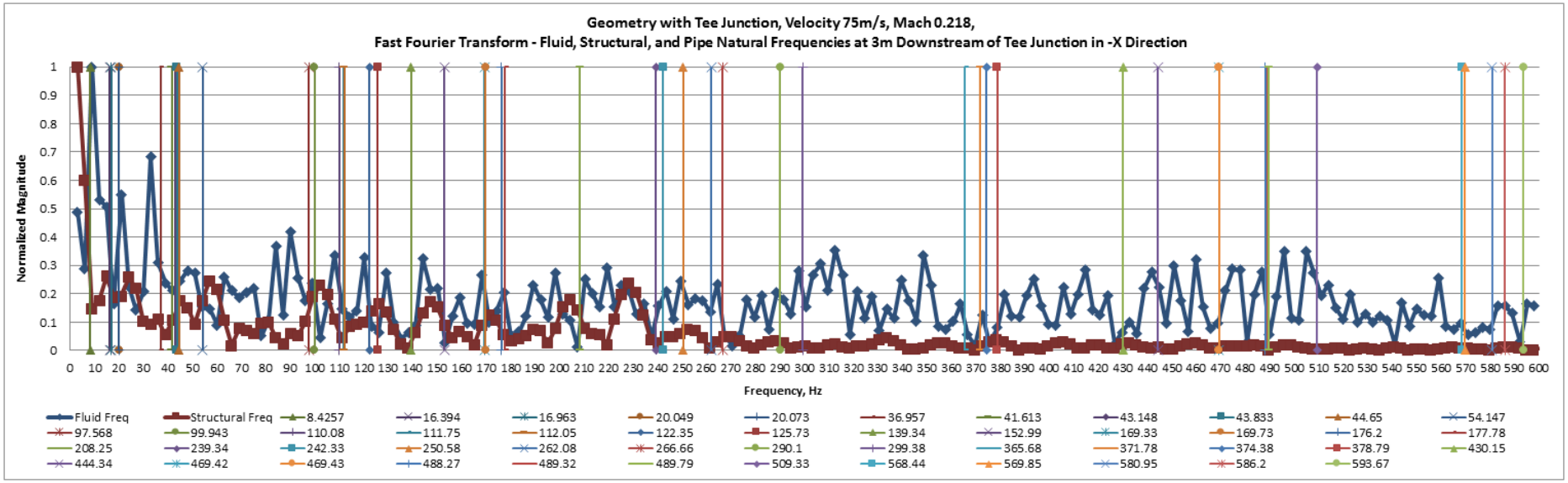
Geometry with Tee Junction, Velocity 75m/s, Mach 0.218,
Fast Fourier Transform - Fluid, Structural, and Pipe Natural Frequencies at 3m Downstream of Tee Junction in -X Direction
Normalized Magnitude
Frequency, Hz
Fluid Freq
Structural Freq
8.4257
16.394
16.963
20.049
20.073
36.957
41.613
43.148
43.833
44.65
54.147
97.568
99.943
110.08
111.75
112.05
122.35
125.73
139.34
152.99
169.33
169.73
176.2
177.78
208.25
239.34
242.33
250.58
262.08
266.66
290.1
299.38
365.68
371.78
374.38
378.79
430.15
444.34
469.42
469.43
488.27
489.32
489.79
509.33
568.44
569.85
580.95
586.2
593.67

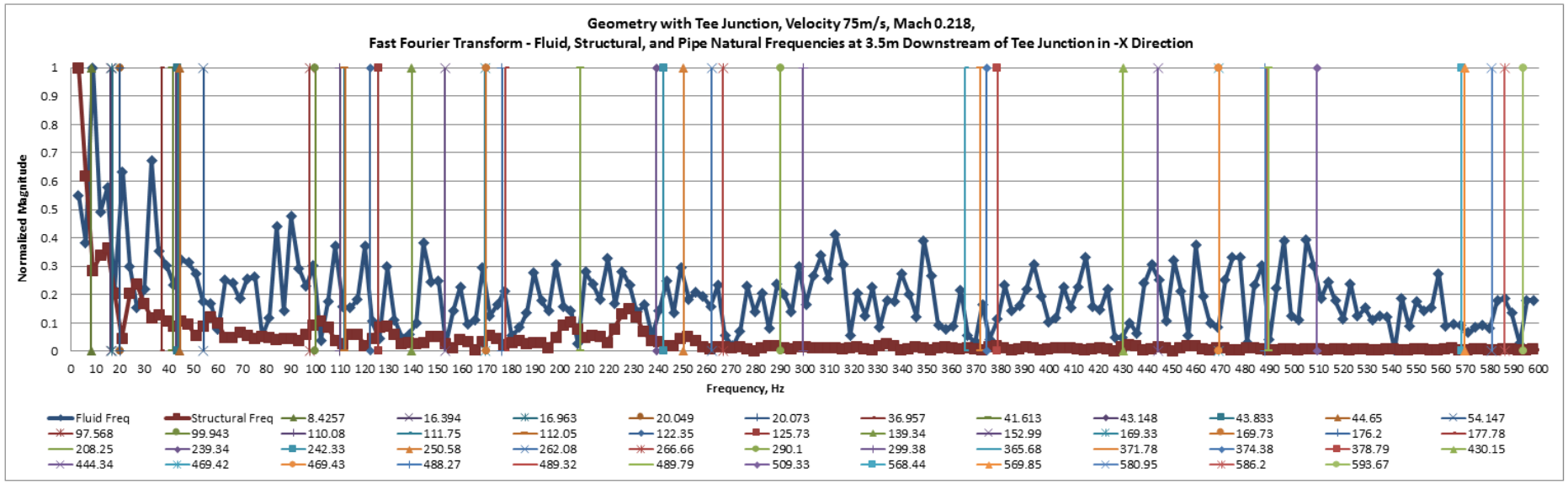
Geometry with Tee Junction, Velocity 75m/s, Mach 0.218,
Fast Fourier Transform - Fluid, Structural, and Pipe Natural Frequencies at 3.5m Downstream of Tee Junction in -X Direction
Normalized Magnitude
Frequency, Hz
Fluid Freq
Structural Freq
8.4257
16.394
16.963
20.049
20.073
36.957
41.613
43.148
43.833
44.65
54.147
97.568
99.943
110.08
111.75
112.05
122.35
125.73
139.34
152.99
169.33
169.73
176.2
177.78
208.25
239.34
242.33
250.58
262.08
266.66
290.1
299.38
365.68
371.78
374.38
378.79
430.15
444.34
469.42
469.43
488.27
489.32
489.79
509.33
568.44
569.85
580.95
586.2
593.67

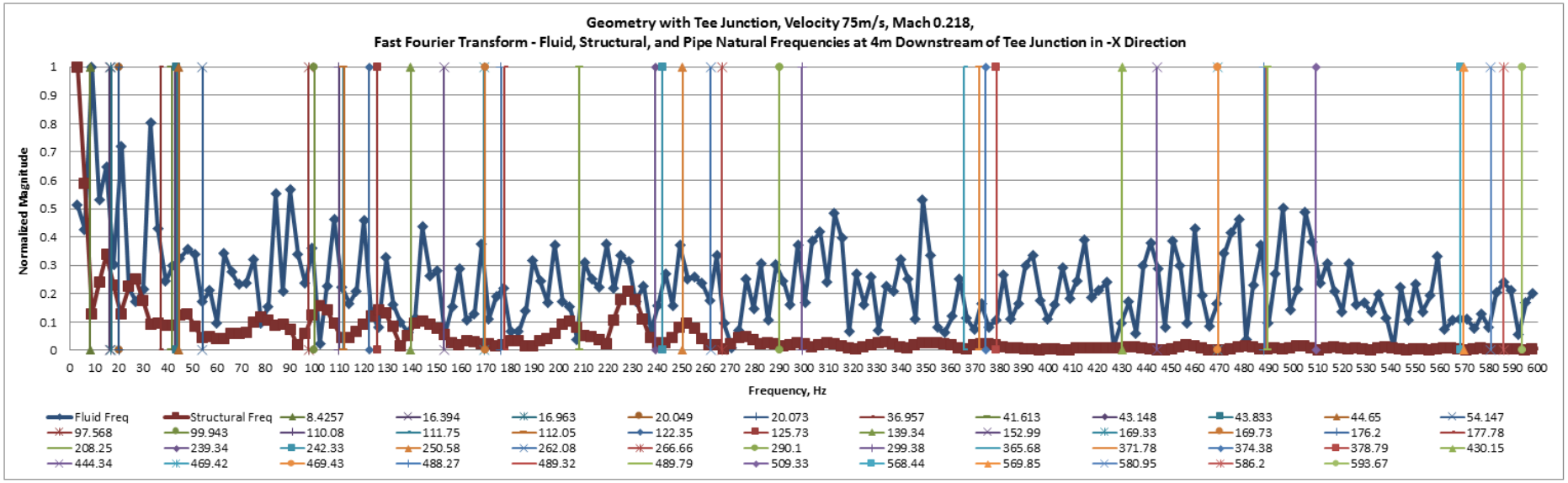
Geometry with Tee Junction, Velocity 75m/s, Mach 0.218,
Fast Fourier Transform - Fluid, Structural, and Pipe Natural Frequencies at 4m Downstream of Tee Junction in -X Direction
Normalized Magnitude
Frequency, Hz
Fluid Freq
Structural Freq
8.4257
16.394
16.963
20.049
20.073
36.957
41.613
43.148
43.833
44.65
54.147
97.568
99.943
110.08
111.75
112.05
122.35
125.73
139.34
152.99
169.33
169.73
176.2
177.78
208.25
239.34
242.33
250.58
262.08
266.66
290.1
299.38
365.68
371.78
374.38
378.79
430.15
444.34
469.42
469.43
488.27
489.32
489.79
509.33
568.44
569.85
580.95
586.2
593.67

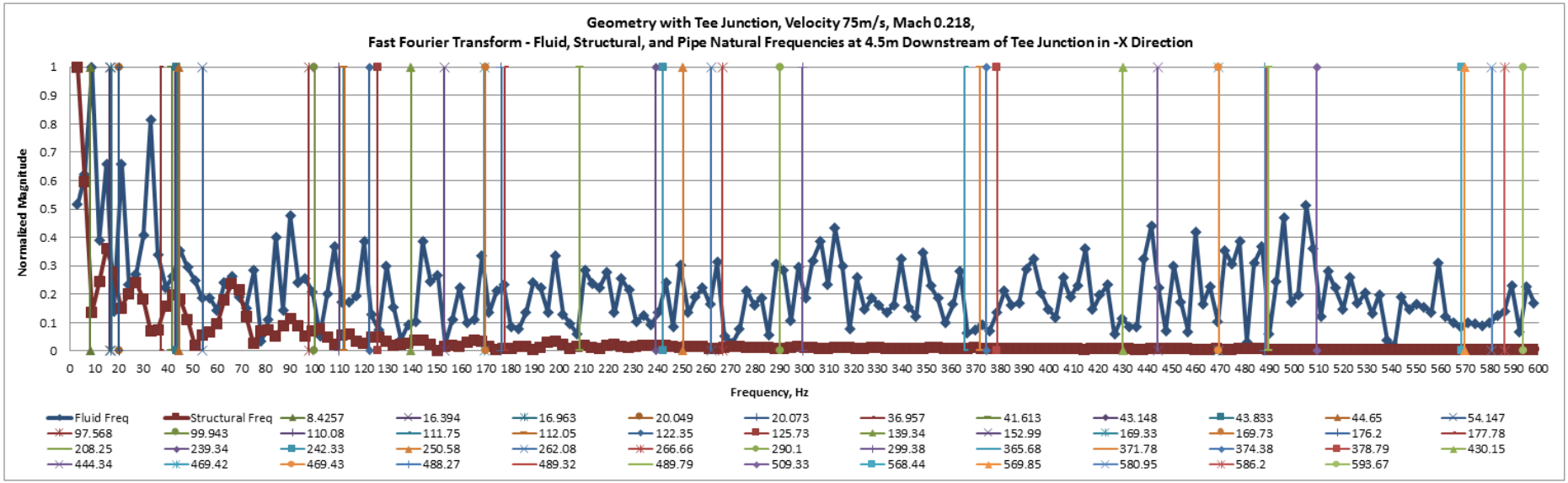
Geometry with Tee Junction, Velocity 75m/s, Mach 0.218,
Fast Fourier Transform - Fluid, Structural, and Pipe Natural Frequencies at 4.5m Downstream of Tee Junction in -X Direction
Normalized Magnitude
Frequency, Hz
Fluid Freq
Structural Freq
8.4257
16.394
16.963
20.049
20.073
36.957
41.613
43.148
43.833
44.65
54.147
97.568
99.943
110.08
111.75
112.05
122.35
125.73
139.34
152.99
169.33
169.73
176.2
177.78
208.25
239.34
242.33
250.58
262.08
266.66
290.1
299.38
365.68
371.78
374.38
378.79
430.15
444.34
469.42
469.43
488.27
489.32
489.79
509.33
568.44
569.85
580.95
586.2
593.67